Human-induced Lateral Excitation of Public Assembly Structures

S Nhleko

A thesis submitted for the degree of

Doctor of Philosophy

at the University of Oxford

Trinity Term 2011

ABSTRACT
Human-induced Lateral Excitation of Assembly Structures

A thesis submitted for the degree of Doctor of Philosophy

Sifiso Nhleko
New College, Oxford, Trinity Term 2011

Excessive human-induced vibrations of assembly structures have been reported more frequently over the past two decades. In the automotive industry, the evaluation of the response of the human body to vibration is an important and active research area due to its significance in design safety. For example, the results of on-going research has led to the establishment of a number of models for predicting the effects of sitting posture, vibration magnitude and direction on the response of the human body when it is exposed to different types of vibration motion. However, research focusing on structural engineering applications remains scarce, leading to inadequate design standards. For example, current structural design guidelines focus on human-induced vertical forces and assume linear structural behaviour, however, the most widely publicized problems have involved horizontal vibrations and many real-life structures are characterized by nonlinear behaviour. Following a brief investigation of vibration perception and comfort for subjects occupying a vibrating rig-structure, this dissertation focuses on human-induced horizontal forces and examines the effect of nonlinear structural behaviour.

Dynamic horizontal loads of individuals performing predefined manoeuvres such as swaying and vertical jumping were measured in a laboratory setting. The fundamental force due to swaying occurred at the activity frequency. By contrast, the fundamental horizontal force due to vertical jumping did not always occur at the activity frequency. Furthermore, tests conducted for swaying were used to establish the relationship between the side-to-side force and the velocity of the subject's centre of mass. A customized footswitch system was also developed to monitor synchronization among individuals performing as a group in order to form a crowd loading model.

Models of analytic forces were derived based on measured data and used to evaluate structural response by focusing on a finite element model of a demountable grandstand characterized by nonlinear structural behaviour. The frequency spectra of displacement and acceleration responses showed clear peaks at the fundamental and the third harmonic of the swaying force, demonstrating the capability of the horizontal force to excite resonance. The resonant frequency decreased at higher levels of excitation, indicating a reduction in the stiffness due to the onset of nonlinear behaviour. Finally, load cases assuming synchronized and perfectly periodic group forces produced a significantly higher response compared to unsynchronized and imperfect group loads.

ACKNOWLEDGEMENTS

I am very grateful to my supervisors, Prof. Anthony Blakeborough and Prof. Martin Williams for their engaging discussions and invaluable guidance during the production of this work, including their assistance and support during the funding application process.

I would also like to acknowledge the informative discussions held with Paul Godwin, Paul Baglin and Joe O'Neill of Arena Seating® and to thank them for providing industrial collaboration and their permission to conduct dynamic tests on the demountable grandstand structure described in Chapter 7 of this dissertation.

Other thanks go to several experts who shared data, communicated important suggestions, shared their experience on the measurement and significance of human-induced forces; and/or lent additional equipment used for this study at no charge. They are: Pat Dallard (Arup), Michael Griffin (University of Southampton), Julie Stebbins and her colleagues (Nuffield Orthopaedic Centre), Vito Racic and James Brownjohn (University of Sheffield).

The work reported here would not have been possible without the financial support received from the South African National Nuclear Regulator, the National Research Foundation of South Africa and the help and dedication of friends and colleagues who volunteered to take part as test subjects. The laboratory assistance of Clive Baker is also gratefully acknowledged.

Last but not least, I would like to thank my parents, family and friends for their encouraging support during my studies and to Naomi Robertson and Janice Henderson for their proof reading comments.

LIST OF CONTENTS

LIST OF FIGURES

LIST OF TABLES

Chapter 1

1. Introduction

1.1. The problem of excessive human-induced vibrations

Public structures have been subject to the problem of excessive human-induced vibrations. In the United Kingdom and elsewhere, predicting the structural response due to crowd-induced vibrations is now recognised as an important aspect in the design and/or performance assessment of pedestrian footbridges, stadium structures, assembly halls and entertainment venues (Dallard *et al.* 2001; Reynolds *et al.* 2004, Macdonald 2008). Dynamic testing techniques whereby human subjects deliberately induce structural excitation have also become an essential part of the design and structural performance assessment process (Dallard *et al.* 2001; Ji *et al.* 2003; Brownjohn *et al.* 2004; Caetano *et al.* 2010). This thesis examines the problem of human-induced vibrations in sports grandstands, focusing on lateral excitation.

Unexpected structural vibrations caused by crowds are not a new phenomenon. In 1978, Greimann & Klaiber (1978) presented a case study in which excessive vertical vibrations due to spectator motion were observed and measured on the upper deck of the Iowa State University's long-span stadium. However, in the past two decades there have been an increasing number of reports of excessive vibration levels in public structures from many different countries of the world. Some examples are given below to demonstrate the problem:

- In Brazil, two incidents of high vibration levels have been reported. In 1993, excessive deflections led to the development of visible cracks in the cantilever

beams of the Maracaña football stadium (Batista & Magluta 1993). The lowest frequency of the affected stand when empty was reported to be 4.6 Hz. In another report, the Morumbi football stadium was retrofitted with vibration mitigation dampers after persistent crowd complaints (Almeida & Rodrigues 1998). The affected stand had frequencies between 2 and 4 Hz when empty.

- In the Netherlands, excessive vibrations were reported on the upper tier of the Feyenoord Stadium (Staalduinen & Courage 1994). The problem occurred mainly during pop concert events. The grandstand had natural frequencies of 2.3, 4.6 and 5.8 Hz.

- The United Kingdom has had the highest number of reported cases, all involving football stadiums, such as Old Trafford, Highbury, Anfield and the Millennium Stadium. At the Old Trafford Stadium the problem became apparent during a pop concert in 1996 on the third tier deck and, in order to mitigate vibrations, this deck is now only used for football matches (Rogers 2000). Highbury stadium was retrofitted with tuned mass dampers to reduce excessive vibrations in its top deck (Rogers 2000) and three additional steel columns were installed to support the newly constructed upper deck of the Anfield Stadium to raise its natural frequency after excessive motion was reported (Rogers & Thompson 2000). Similarly, excessive motion was also observed in the middle tier of the Millenium Stadium, Cardiff resulting in retrofitting with temporary metal struts (Glackin 2000).

There are several factors contributing to excessive crowd-induced vibrations. Firstly, modern assembly venues are generally designed with a large open space for two main reasons (i) it allows a better view for spectator enjoyment and (ii) it accommodates a large seating capacity that maximises revenue. This results in a structural system with a low stiffness or natural frequencies. When these structures are occupied by crowds, the problem is compounded by further reductions of structural frequencies confirmed by the studies of Ellis & Ji (1997), Littler (1998, 1999) and Reynolds *et al.* (2004). Secondly, there is also an increasing trend to use the venues as multifunctional facilities. For example, many football stadiums in the UK are frequently used to host pop concert events. Therefore, there is a high probability that they will be subjected to loads that were not considered in the original design. Finally, the live music at pop concert events promotes coordinated spectator activity leading to more intense forces.

The resulting excessive vibrations are a concern for serviceability and safety because they can cause discomfort or result in crowd panic and, under extreme conditions, structural failures also can occur. Consequently, existing design codes and guidelines, for example, the National Building Code of Canada (NBC) guideline on human-induced vibration of floors and footbridges (NRCC 1995), the 'Green Guide' (HMSO 1997), BS 6399 (British Standards Institution 1996), and the recommendations published by IStructE/ODPM/DCMS Working Group (2008, 2007, 2001), specify particular structural frequencies as threshold values for different types of assembly structures. The standards make provision for a detailed dynamic analysis of the structure to be conducted in the vertical and two horizontal directions (side-to-side and front-to-back) for structures which fail to meet the natural frequency criteria. However, as shown below, there are some serious limitations in this guidance.

- Whilst establishing the limits for the maximum level of vibration deemed acceptable for spectator safety is a fundamental principle in grandstand design, there is a paucity of research data to determine spectator tolerance of vibration motion to inform current guidelines and design standards.

- By giving guidance that is based on compliance with certain frequency criteria, the current standards and guidelines assume that most structures will exhibit linear behaviour. However, the dynamic response of some structures, particularly demountable structures, is characterized by nonlinear behaviour. For these structures there are concerns about the relevance of complying with the recommended frequency criteria which is strictly applicable only to linear structural behaviour.

- The current standards and guidelines emphasise vertical forces including the techniques for the analysis of a structure's vertical vibration behaviour and give very little guidance on the techniques for the analysis of horizontal vibrations. Whilst the view that vertical excitation will normally be the controlling influence in the design is adequate for permanent structures, horizontal excitation is the controlling influence in the design of demountable grandstand structures. Consequently, there have been a few recent studies (Yu 2004; Yao *et al*. 2005) that have investigated human-induced horizontal forces (front-to-back and side-to-side). However, these have not, as yet, found application in design standards.

- In order to fully describe loads that can be produced by a specific crowd motion on a structure, it is necessary to know firstly what forces a single individual is capable of producing and secondly, the maximum level of synchronization or degree of coordination that is likely to occur during the activity. At the present time, there are no methods for measuring the likely degree of crowd synchronization.

These limitations in the guidance require resolution and, in so doing, the problem of human-structure interaction will lead to greater safety and comfort for the public in grandstand type entertainment venues.

1.2. Aims and objectives

This research is aimed at understanding and modelling horizontal dynamic forces due to human motion and their effects on assembly structures. This will be accomplished by performing a range of studies with specific objectives addressing the paucity of research data in the areas identified in Section 1.1, namely:

1) Investigation of human tolerance of vibration motion in the context of grandstand structures

2) Measurement of human-induced horizontal forces generated by swaying and jumping movements

3) Development of a footswitch method for estimating the likely degree of synchronization for groups of people and collection of foot-timing synchronization data

4) Analytical modelling of human-induced horizontal forces for single individuals and groups or crowds

5) Modelling of the horizontal response of a structure characterized by nonlinear behaviour when it is excited by human-induced horizontal forces

1.3. Brief outline of research in this thesis

A literature review focusing on the nature of human-structure interaction problems and recent research relating to this topic is presented in Chapter 2. The review summarises factors contributing to human-induced vibrations, current models of human-structure interaction, design guidance used to assess human-induced vibrations as well as human perception of vibration and comfort levels. The main finding is that previous research relating to human-induced vibrations in grandstands has been heavily biased towards dealing with vertical vibrations and there is very little reference to horizontal vibrations. The latter point and other issues arising from the literature review are addressed by performing a range of tasks with specific objectives. The tasks performed are discussed in detail in subsequent chapters and a brief outline is given below.

Research to determine the tolerance of vertical vibration motion for human subjects, in both seated and standing positions when occupying a vibrating grandstand rig, is presented in Chapter 3. The reported serviceability data lies below the recommended limits for transportation structures but above the recommended limits for most classes of

buildings. This suggests that the serviceability limit state for grandstand design lies somewhere between the recommended limits of the two standards. Changes in bobbing forces as a result of structural vibration are also presented. These changes indicate different postures or stance and consequently different human-structure interaction mechanisms.

Chapter 4 deals with experimental work conducted to characterize horizontal forces for the dynamic analysis of assembly structures. The measurements show that significant horizontal loads can be induced by spectators performing swaying or vertical jumping movements. The fundamental force due to swaying occurred at the swaying frequency. However, the fundamental horizontal force due to jumping did not always occur at the jumping frequency. This means that a load model similar to the one used for vertical loading due to jumping is not always appropriate for horizontal loading due to jumping. The measurements were also used to establish the relationship between the side-to-side force and the velocity of the subject's centre of mass.

The development and validation of an inexpensive footswitch system that was used to monitor group synchronization in order to derive a crowd loading model from the data of individual subjects is detailed in Chapter 5. The validated footswitch was used successfully for measuring essential parameters required for the development of the lateral human loading model for single individuals and groups of subjects swaying from side-to-side. Foot-timing data for individuals and groups of subjects are presented.

In Chapter 6 a horizontal load model is developed by fitting mathematical analytic expressions to the experimental results reported in Chapters 4 and 5. Two load models are dealt with, namely a load model for single individuals and a load model for a crowd.

For individual loads, the positive and negative parts of the force pulse were each modelled using a Fourier series of a rectangular pulse which were shifted and added together to form a total pulse. The Fourier series was reduced to a simple formula for side-to-side forces. The results simulated using the analytic model compared very well with the corresponding laboratory-measured data. A group model for swaying was formed by summing up simulated individual forces due to side-to-side swaying as a severe load case scenario.

The analytic horizontal load model presented in Chapter 6 is used to conduct numerical and finite element simulations (Chapter 7). For numerical studies, the forces were applied to an idealized single-degree-of-freedom system in order to validate the theoretical model for horizontal forces. For finite element simulations, the forces were applied to a model of a grandstand system at a prototype stage of development for the purpose of predicting its structural response in the presence of non-linear behaviour. Field tests conducted to determine the structural properties of this system and the type of nonlinear behaviour used to describe the finite element model are presented briefly in this chapter. Simulation results showed that the resonant frequency of the structural model decreased at higher excitation levels due to the onset of nonlinear behaviour. In addition, load cases assuming synchronized and perfectly periodic group forces led to higher responses compared to unsynchronized and imperfect group loads. Finally, conclusions and recommendations for future work are presented (Chapter 8).

Chapter 2

2. Review of the Literature

Factors which affect problematic interactions between a structure and a crowd are discussed with reference to published experimental work and case studies (Sections 2.1 and 2.2). This is followed by a discussion of theoretical models designed to analyse the effects of passive and active humans (Section 2.3). In addition, the problem of human-induced vibrations has required the formulation of national guidelines and design models that are examined in Section 2.4. Finally, the analysis of the literature highlights areas requiring further research, some of which are addressed in the specific objectives of this project (Section 2.5).

2.1. Factors exacerbating human-induced vibrations on a structure

2.1.1. Design practice

Due to the availability of improved materials, there is an increasing tendency to build modern stadium structures using slender structural members. There is also a trend to provide for large seating capacities and better sight lines for spectators. This combination has led to the use of cantilevered structural systems with open and column-free spaces or long-span structural systems (Blakeborough &Williams, 2005). Systems of this type are characterized by a low stiffness or natural frequency. Consequently, in some cases, the structural natural frequencies are low to the point that crowd movement may produce excessive structural vibrations that are uncomfortable for some occupants.

This problem is compounded by further reductions of structural frequencies or the development of new structural frequencies which are observed when structures are

occupied by crowds compared with when the structure is unoccupied. For example, modal tests conducted on the Twickenham Stadium (Ellis & Ji 1997) showed that the structure had a natural frequency of 7.32 Hz when unoccupied. However, when occupied the lowest frequency recorded was 5.41 Hz.

2.1.2. Use of sports stadia

Owners of modern sports stadia have the opportunity to increase revenue by using sports stadia for forms of entertainment other than sporting events, for example hosting musical concerts is common in the United Kingdom (Blakeborough & Williams 2005). In other countries also, sports stadia are used to host local and international rock, pop and other musical concerts. For example, Soccer City Stadium, South Africa (one of the largest football stadiums in South Africa and host to the 2010 FIFA World Cup) hosts a wide variety of activities on a regular basis in addition to football games (personal communication from the Logistics Manger by email). These activities include musical concerts, political, religious, funeral service and cultural gatherings. Thus there is a high probability that the majority of modern assembly structures will be subjected to additional load types that should have been considered during design. Another adverse effect occurs when the movement of a crowd in a structure is coordinated (such as during live musical concerts) creating synchronised 'dance-type' loads.

2.1.3. Spectator behaviour

Prior to the game and during the half-time interval, spectators often engage in entertainment such as listening and dancing to recorded or live music. Furthermore, chanting and singing occur frequently throughout the game in addition to the celebration

of goal events. The effect of music is to stimulate the crowd and synchronize crowd activity which leads to synchronous 'dance type' loads. This results in the load on the structure being applied for a much longer duration. Therefore, any pre-existing vibration problem in the structure will be exacerbated.

Spectator behaviour can also be unpredictable in crowd panic situations. Helbing *et al.* (2003), report that since 1945 thirty large crowd panics have occurred resulting in stampedes causing 1,000 deaths and 3,400 serious injuries. The majority of these disasters occurred in soccer stadia. Although none of the accidents were caused by structural vibration, crowd panic can also occur as a result of excessive structural vibrations and lead to injuries or loss of lives. For example, preliminary reports of the investigation into the stampede in Phnom Penh, Cambodia on 22 November 2010 that resulted in 456 fatalities found that the stampede had been triggered by the swaying of a pedestrian footbridge causing panic among many of those on it (http://www.bbc.co.uk/news/world-asia-pacific-11827313, 24th November, 2010).

2.1.4. Summary

Firstly, modern design practice can result in a structure which has low natural frequencies with the potential to fall into the range where excitation by humans is possible. Secondly, the use of modern football stadia as multi-functional facilities means that these structures are subjected to other load types that were not considered during the design stage. Thirdly, there is a demand for musical entertainment in sports stadia which results in loads applied for much longer durations than anticipated for sports events alone. The additional effect of music is to synchronize human activity

such as dancing and create other types of loads on the structure. Finally, human activity can be unpredictable in crowd panic situations and may lead to fatal stampedes.

2.2. Human-structure interaction and experimental research

In general, human occupants can affect the dynamic behaviour of structures by various activities such as sitting, standing, walking, jumping, dancing, or even hand clapping (Bachman 1992). The effect on the structure depends on the type of activity by human occupants. There are broadly two categories, namely, the effects of 'passive humans' and the effects of 'active humans'. The effects on a structure due to active humans that are documented in the literature predate reports on the effects due to passive humans. A brief chronology is given below.

2.2.1. Effects of active humans

2.2.1.1. Early studies from 1905 to the early 1990s

It has long been known that a human engaged in some form of activity whilst occupying a structure will induce a dynamic force on the structure. Tuan & Saul (1986) presented a historical review on this subject and will be briefly reviewed here. The earliest references were Moreland (1905) and Tilden (1913). Moreland measured vertical loads due to 90 subjects jumping on a 10 ton weigh-bridge. In contrast, Tilden (1913) highlighted the importance of accounting for the horizontal forces and, more importantly, when subjects engaged in synchronous activity, there was a high probability of exciting the natural frequencies of a structure. From 1920-30, the use of a

portable or temporary grandstand was a catalyst to the development of standards for the design of buildings and stadia. This was because there were frequent collapses of these temporary grandstands which became such a serious threat to the lives of spectators that rules and regulations governing the erection and use of portable steel and wood grandstands were necessary. Both Ries (1928) and Serby (1930) suggested safety guidelines for the design of grandstands. During this period, safety organizations were founded and also codes of practice such as the Building Officials of America (BOCA) and Uniform Building Code (UBC) were implemented.

About 30 years later, a study by Harper *et al.* (1961) reported comprehensive data for force measurements of individual footfalls during walking. Consideration of different speeds led to a more detailed model. The load-time history of a single footfall during walking was shown to have two peaks or single peak depending on the walking speed (see Figure 2.1 as an example).

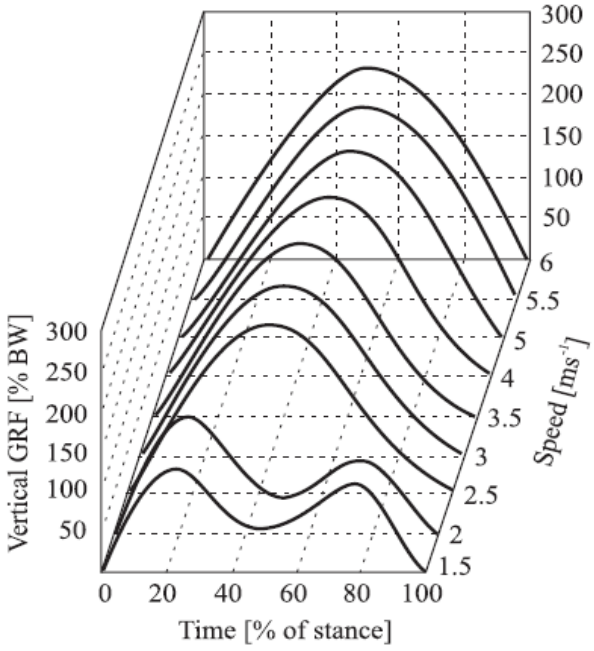

Figure 2.1: Typical profile of vertical forces during walking at different speeds after Keller *et al.* (1996) – the vertical axis shows the force as a percentage of body weight. The short horizontal axis shows the time as a percentage of the period when the foot is on the ground.

Since that time similar measurements for walking have been obtained and reported (e.g. Rainer *et al.* 1986; Bachmann & Ammann 1987; Keller *et al.* 1996; Brownjohn *et al.* 2004) and a review on the characterization of forces induced by walking was published recently by Racic *et al.* (2009).

Excessive vertical vibrations due to spectator motion during a football game in the late 1970s were measured and reported by Greimann & Klaiber (1978) in the upper deck of the long-span stadium of Iowa State University. The data were analysed to identify the relationship between spectator activity and the observed vertical vibrations. A large structural response was recorded during a goal event and it was concluded that the structural response depended on the dominant mode of spectator activity. Recently, techniques for remote monitoring of the source of the vibration and affected structural components in stadium structures during live matches have been established and analysis of the resulting data has shown that the dynamic properties of a structure are affected by the presence of a crowd (Reynolds *et al*. 2004).

Tuan & Saul (1985) measured horizontal forces for 22 individuals swaying from side-to-side or front-to-back in both seated and standing positions. These measurements included vertical forces due to jumping. This research was significant because it took into account forces in all three directions. However, their measurements focused on a single rhythm. The rhythm or tempo of the music used in all their simulations was 132 beats/min. Thus only the horizontal load magnitude for swaying at this single frequency can be deduced from their measurements (Table 2.1).

Tuan & Saul (1985) presented their measurements in Imperial units of the pound-force (lbf). In Table 2.1 their data have been converted to units of Newtons and percentage of

body weight (shown in brackets). The symbols SS and FB stand for side-to-side and front-to-back (respectively) for each category of swaying activity the subjects were asked to perform. Note that each force can act either in the positive (+ve) or negative (-ve) direction. Positive forces were defined as acting to the right for side-to-side swaying and to the front for front-to-back swaying while negative forces acted to the left for side-to-side swaying and to the back for front-to-back swaying. The mean and peak forces data were used as estimates for 'live loads per person' in the design of assembly structures. Their data showed that in the case of swaying front-to-back, forwards forces are slightly different from backwards forces. This implied the presence of a small asymmetry in the force. The magnitudes of the horizontal force at higher harmonics (i.e. at frequencies that are multiples of the fundamental swaying frequency) were not presented in this study.

Table 2.1: Horizontal forces data from Tuan and Saul (1985)

Activity	Peak +ve N(%BW)	Peak -ve N(%BW)	Mean +ve N(%BW)	Mean -ve N(%BW)	Std. dev. N(%BW)
SS stand	138(20)	129(19)	79(11)	79(11)	26(4)
SS sit	116(17)	120(17)	79(12)	85(12)	19(3)
FB stand	120(17)	142(21)	67(10)	78(11)	32(5)
FB sit	151(22)	187(27)	103(15)	119(17)	38(5)

Subsequent measurements for vertical forces due to jumping were improved by taking into account a range of achievable jumping frequencies instead of focusing on a single frequency (Pernica 1990; Rainer *et al.* 1986). The latter study also involved groups of subjects jumping at the same time (up to 4 subjects), rather than obtaining

measurements for a single individual. In addition, force measurements of walking and running activities were included. This study was the first to report the magnitude of the force for all of these activities at higher harmonics. Bachmann & Ammann (1987) and Ebrahimmpour & Sack (1989) also measured forces due both to individuals jumping and to the same individuals jumping as a group (2-4 subjects). Ebrahimmpour & Sack (1989) then manipulated load-time histories for individual jumping by random time phase lags and superimposed the results until these matched closely the directly measured load time histories for the same individuals jumping as a group to obtain a group or crowd load model. Before this successful manipulation they admitted having tried another manipulation strategy which was based on aligning a single person's loads by a prompt (beep) signal and summing up the individual contributions to form a group model. This is equivalent to assuming that individuals in a crowd only follow the beep and ignore any possible interference from other members. However this procedure failed to give loads that were similar to the measured loads. They concluded that crowd coherency is governed by auditory and visual effects. In a later study, they conducted similar experiments using a force platform built to accommodate up to 40 people (Ebrahimmpour & Sack 1992).

These studies simply confirmed earlier measurements which showed that jumping forces consisted of a sequence of isolated pulses separated by a period of zero force. The maximum force of this single peak pulse, which was defined as the magnitude of the force at the jumping frequency or fundamental harmonic, lay between 1.6-2 times the bodyweight. The data when plotted as a Fourier spectrum of the jumping force also consisted of higher harmonic components with lower force magnitudes compared with the component at the fundamental frequency. In addition, the relative load per person

reduced with increasing group size due to a lack of synchronization when individuals jumped as a group. Higher forces were recorded for frequencies between 2-3 Hz which demonstrated that people were most synchronized when jumping within this frequency range (Pernica 1990).

2.2.1.2 Recent studies (1993-2010)

Work on the measurements of human-induced forces has continued to the present with the aim of improving data gathered from earlier studies by utilizing the latest available technology. Whilst early studies focused on jumping as the only critical design case for grandstands, recently, another form of body movement called bobbing (a type of body movement that involves moving the body up and down but with feet on the floor all the time) has also been considered. Few studies have dealt with horizontal forces. Studies published over the past two decades are summarized below.

Research work on the measurement of vertical forces due to jumping and/or bobbing have been undertaken by among others, Ji & Ellis (1994), Ellis & Ji (2004), Sim *et al*. (2005), Kasperski & Agu (2005), Yao *et al.* (2003), Yao *et al.* (2006), Parkhouse & Ewins (2006), Comer *et al*. (2007), Harrison (2008), Hoath (2009), Racic *et al*. (2010) and Racic & Pavic (2010).

Ji & Ellis (1994) performed tests involving a single subject jumping on a precast reinforced beam. The fundamental frequency of the bare beam was measured at 18.68 Hz. They concluded that a jumping person only acts as a load on the structure with no significant human-structure interaction. However the structure they used was very rigid (18.68 Hz) compared to typical frequencies of structures where human induced

vibration are a concern. By contrast Yao *et al*. (2003, 2006) designed an experiment to account for jumping on a perceptibly moving structure (with an adjustable natural frequency) and showed that jumping force levels were frequency dependent for low structural frequencies. In particular, they discovered that the level of the force that can be generated by a human subject when jumping reduces significantly ('drop out' of force) when the structure response increases in the resonant region (see Figure 2.2). This result means that using force results from a rigid platform and ignoring human-structure interaction effects is conservative for perceptibly moving structures. They also showed that it was near impossible to jump at the frequency of the structure.

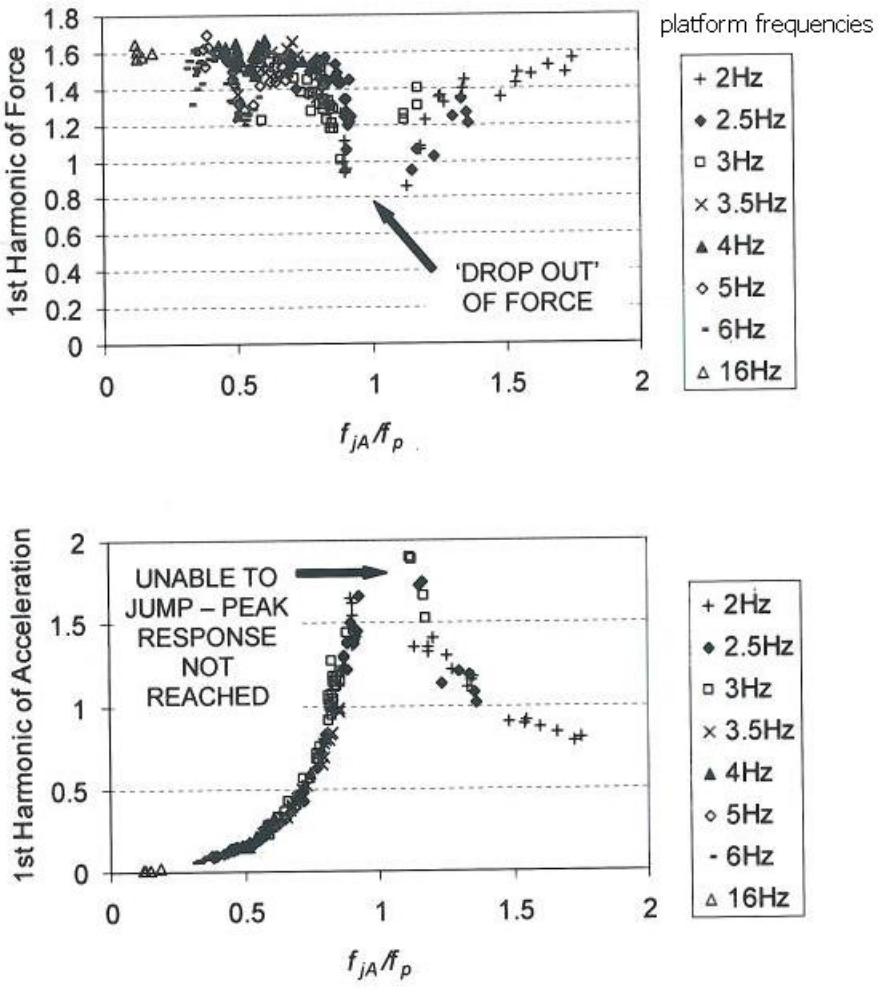

Figure 2.2: Variation of first harmonics of applied jumping force and platform acceleration for different jumping frequency to platform frequency ratios (after Yao *et al.* 2006)

Yao *et al*. (2005) and Yu (2004) extended the previous work to include a single subject swaying between 1-3.5 Hz and considered both the horizontal response and applied horizontal forces. Their results showed that the first harmonic of the swaying force lies between 12 and 20 percent of subject body weight. Like the previous study, they also found significant reduction in the swaying force levels when the structure vibrated in the resonant region. However, this study (Yao *et al*. 2005) only involved a single individual. They found that swaying at frequencies beyond 2 Hz was not possible.

In the study of Yu (2004) the effect of front-to-back forces resulting from jumping on a perceptibly moving structure was investigated and clear reductions of front-to-back forces when the ratio of the jumping frequency and the frequency of the structure is close to either 1.0 or 0.5 were found.

Recently, the work of Yao *et al.* (2006) has been continued by Harrison (2008) who extended it to include bobbing. He also, found that the force levels due to bobbing were frequency dependent for platform frequencies less than 6 Hz and subsequently developed a design model for human bobbing based on the model by Dougill *et al*. (2006).

Parkhouse & Ewins (2006) performed tests which involved over 100 subjects performing jumping or bobbing as single individuals in response to a metronome beat. Their measurements constitute the most extensive database of jumping and bobbing forces currently available and were also supplemented and used by Sim *et al*. (2005) who managed to publish their findings one year earlier than Parkhouse & Ewins (2006).

Jumping frequencies generally reported in the literature start from 2 Hz. However, Sim *et al.* (2005) considered jumping frequencies as low as 1 Hz. They showed also that the graph of the force impulse has two peaks that can be either symmetrical or non-symmetrical when a subject jumps at frequencies below 2 Hz. As will be discussed in Section 2.3 this observation has important implications for the model representing forces due to jumping as this model is based on the assumption that the load impulse will always have a single peak.

The studies mentioned above focused on single individuals and did not investigate possible interaction effects caused by proximity to other crowd members and the spatial constraints of a grandstand venue, including any vibration of the supporting structure. In order to address these aspects, Comer *et al*. (2010) designed a grandstand rig with a motion simulator that could be programmed. The rig had a capacity of 15 subjects and was designed to resemble a grandstand as realistically as possible. For tests conducted on a stationary rig they found that over 90% of the subjects were synchronized when the jumping frequency was 2.25 Hz. This figure reduced to about 30% for jumping frequencies beyond 3 Hz. It was noticed that all subjects located behind the front row achieved better synchronization because the subjects in front of them provided another stimulation type (visual stimulation) in addition to the beat (aural stimulation).

More recent studies have focused on reproducing forces from position time-history data recorded from the movement of specific parts of the body. When a sophisticated motion capture system (of the standard found in clinical gait laboratories) is used and several body parts are monitored in order to achieve a high level of accuracy, a good correlation between the human induced force and the movement of the specific body part has been

reported (Harrison 2008; Hoath 2009; Racic *et al*. 2010). The work of Harrison (2008) and Racic *et al*. (2010) dealt with a single individual while the work of Hoath (2009) dealt with a group of up to 15 subjects.

The majority of the studies conducted over the past two decades also dealt with vertical forces and horizontal force components were ignored during data collection. Apart from the work of Yao *et al*. (2005) and Yu (2004) reviewed previously, two studies (Kim *et al*. 2009, and Pavic *et al*. 2002) dealing with horizontal forces were found. Kim *et al*. (2009) measured forces due to a single swaying subject. However, like Tuan & Saul (1985) they also focused on a single frequency (1.4 and 1.0 Hz for swaying front-to-back and side-to-side, respectively). Swaying in a sitting position was not considered. Pavic *et al*. (2002) undertook measurement of horizontal forces due to vertical jumping and confirmed their significance for structural engineering design probably as a result of the incident involving the lateral sway vibration of the Millennium Bridge in London in the UK in June 2000 (see Section 2.2.1.3). Their study also focused on a single jumping frequency, namely 2 Hz. They found the magnitude of the front-to-back force to be approximately 20 percent of the vertical force due to jumping at this frequency. The side-to-side force was found to be a negligible fraction of the front-to-back force. They attributed the existence of horizontal forces due to vertical jumping to the inability of humans to perfectly jump from and land on the same spot.

2.2.1.3 Negative damping, synchronization and tests on real-life structures

In addition to laboratory studies, the effect of active humans on structures has been observed in real-life structures. A widely publicized example is that of the lateral swaying when crowds were on the London Millenium Footbridge in 2000 (Dallard *et al.*

2001). The vibration behaviour of the bridge was attributed to a negative damping phenomenon. A footbridge structure experiences negative damping when the pedestrian-induced lateral force becomes greater than the inherent damping forces in the structure, and this lateral force has been demonstrated to be proportional to the velocity of the structure (Dallard *et al.* 2001). Recently, there have been a number of studies reporting the same phenomenon for different footbridges in other countries (Brownjohn *et al*. 2004; Macdonald 2008; Caetano *et al*. 2010). Crowd synchronization is thought to be the main cause of the negative damping phenomenon but a recent study on pedestrian induced vibrations (Clifton Suspension Bridge, UK) reported negative damping with no significant synchronization (Macdonald 2008). As a result of the London Millennium Footbridge incident and the controversy regarding the probability for a crowd to synchronize, the use of human subjects to induce deliberate structural excitation as a form of dynamic testing of public structures has increased dramatically over the last decade (Ji *et al*. 2003; Brownjohn *et al*. 2004; Macdonal 2008; Caetano *et al*. 2010).

In summary, studies conducted during the early period (1905-1992) showed that jumping forces consist of a sequence of isolated pulses separated by a section of zero force. The maximum force of this single peak pulse defined the force at the jumping frequency or fundamental harmonic as lying between 1.6 and 2 times body weight. The Fourier spectrum of the force also consisted of higher harmonic components with lower force magnitudes compared to the component at the fundamental frequency. The studies showed that the relative load per person reduced with increasing group sizes, because of a lack of synchronization when individuals jump as a group. Higher forces were recorded for frequencies between 2 and 3 Hz which showed that people were most synchronized when jumping within this frequency range. Finally, only one study (Tuan

& Saul 1985) dealt with the measurements of horizontal forces during this research period.

In the later period (1993-2010), research on the measurements of vertical forces continued but utilizing the latest available technology. Apart from jumping, another form of body movement called bobbing was introduced as a design case scenario for grandstands. However, the tendency to ignore horizontal forces continued despite the incident involving the lateral swaying of the London Millennium Footbridge. On the other hand this incident led to the establishment of a dynamic testing technique in which human subjects are used to induce deliberate structural excitation on a public structure.

Finally, perfect synchronization of vertical forces due to jumping is considered impossible for the design of grandstands. Divided opinions were found regarding the likelihood of the occurrence of perfect synchronization of lateral forces due to walking for the design of footbridges. However, large structural vibrations are thought to lead to synchronization. This suggests that it is necessary to consider (i) synchronization between the motion of the crowd and the structure, and (ii) synchronization among the forces applied by individual members of the crowd for a meaningful interpretation of results in human-structure interaction research.

2.2.2. Effects of passive humans

In the past, structural engineers have considered passive human occupants simply to be an additional mass on the structure. However, recent measurements conducted on full scale structures suggested that passive human occupants also affect other properties of

the structure such as natural frequencies and damping in a manner that cannot be explained by treating the human occupant simply as an additional mass on the primary structure. This is consistent with the field of biomechanics where the human body is conventionally treated as a complex system with its own stiffness and damping properties in addition to its mass. The following research highlights some of the effects passive humans are reported to have on a structure.

Modal tests conducted on the Twickenham Stadium showed that a truss substructure of the stadium had a natural frequency of 7.32 Hz when empty, and frequencies of 5.41 Hz and 7.91 Hz when occupied (Ellis & Ji 1997). A retractable grandstand with natural frequencies 3.05, 3.66, and 13.6 Hz in the front-to-back, side-to-side and vertical directions respectively, had frequencies of 3.3, 3.54 and 9.16 Hz when occupants were standing and frequencies of 1.71, 1.83 and 9.03 Hz when occupants were seated (Littler 2000). The latter findings were important because they indicated that not only vertical but also horizontal modes were affected by passive humans.

Tests involving an individual person instead of a crowd have also been performed. Experimental tests conducted on a platform occupied by a standing person (Harrison & Wright 2004) showed that there was a reduction in the natural frequency of the occupied structure and an increase in damping. However, a vibration test on an 18.68 Hz beam (Ellis & Ji 1997) showed that there was an increase in the natural frequency when a person was seated or standing on the beam while no changes were recorded when the person was jumping or walking on the beam. Rainer & Pernica (1981) and Lenzen (1996) had earlier showed that the damping capacity of a structure could be increased by people on it.

Prompted by the observations noted above, Sachse *et al.* (2004) calculated the modal properties of damped 2-degree-of-freedom representations of crowd-occupied civil engineering structures and showed that a damped 2-d.o.f. model of a crowd–structure system can explain: damping increases, additional modes of vibration and increases as well as decreases of natural frequencies observed on real-life grandstand structures due to crowd occupation.

2.3. Human-structure interaction and analytical models

This section deals with analytical models used for the design of structures against human-induced vibrations. Design engineers use approximate analytical models to represent the effects of humans on the vibration behaviour of structures. Consistent with the previous section, these models can also be discussed broadly under two categories, namely, models describing the effects of passive humans and those describing effects of active humans. However, in most practical situations there will be a group of passive and active people at the same time. In recognition of this situation, models for describing the combined effects of active and passive humans have also been developed.

2.3.1. Models for the effect of active humans

Focusing on grandstand design, there are a number of different dancing and jumping activities accompanied by a wide range of rhythms or frequencies that need to be accommodated for design purposes. However, for analytical purposes, they are conveniently grouped into two categories (Ji & Ellis 1994) and limited to a particular range of frequencies. The first category is when the human occupant is always in contact with the floor (structure). An example of this is swaying, dancing, bobbing

where one's body moves side-to-side, front-to-back or up and down but maintaining contact with the floor or structure all the time. In the second category, the human occupant is intermittently in contact with the structure. An example of this is repeated jumping. This literature review focuses on the model for vertical forces due to jumping because it is the only analytical model available which is featured in design standards. As may be expected the modelling approach would differ depending on whether a single human or a crowd is involved.

2.3.1.1 Individual loads

The load-time history of a single human subject engaged in rhythmic jumping can be described by a high contact force for a certain time t_c (contact phase duration) followed by a zero force when the feet leave the floor for a certain time t_f (flight or free fall phase duration). Bachmann & Ammann (1987) suggested that the load time function describing this can be expressed by a sequence of semi-sinusoidal pulses as shown in Figure 2.3.

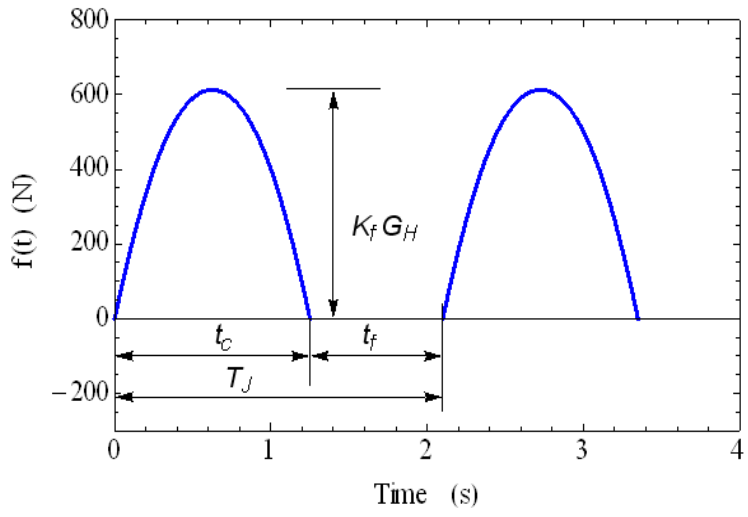

Figure 2.3: Half-sinusoidal model of idealized load impulses due to periodic jumping.

Considering a single jump or one period of jumping (T_J), the function describing the load impulse in the vertical direction as shown in Figure 2.3 is given as (Bachmann & Ammann 1987; Ji & Ellis 1994):

$$f_H(t) = K_f G_H \sin\left(\frac{\pi t}{t_c}\right) \qquad 0 \le t \le t_c \qquad (2.1a)$$

$$f_H(t) = 0 \qquad t_c \le t \le T_J \qquad (2.1b)$$

where: $K_f = f_{\max} / G_H$, impact or load amplitude factor

$f_{\max}$ = the peak dynamic load

G_H = the weight of the jumper

t_c = the contact phase duration in seconds

T_J = the period of a single jump in seconds

In addition two useful parameters can be defined in terms of the parameters already presented above, namely the contact ratio $\alpha = t_c / T_J$ and the jumping frequency $f_J = 1/T_J$. The jumping frequencies, f_J, that need to be considered for design purposes have been suggested or implied by a number of researchers, namely, 0 – 4 Hz (Taun & Saul 1985), 1.5 – 3.5 Hz (Ji & Ellis 1994), 1.5-2.8 Hz (Reid *et al*. 1997), 1.0 – 3.5 Hz (Yao *et al*. 2006; Sim *et al*. 2005).

The most useful form of Equation 2.1 is its Fourier series equivalent (Equation 2.2) which has been used in several references (Ji & Ellis 1994; Ellis & Ji 2004; Nhleko *et al.* 2008).

$$\left.\begin{aligned} f_H(t) &= G_H\left[a_0 + \sum_{n=1}^{\infty} a_n \cos\left(\frac{2\pi n}{T_J}t\right) + \sum_{n=1}^{\infty} b_n \sin\left(\frac{2\pi n}{T_J}t\right)\right] \\ f_H(t) &= G_H\left[a_0 + \sum_{n=1}^{\infty} r_n \sin\left(\frac{2\pi n}{T_J}t + \varphi_n\right)\right] \end{aligned}\right\} \qquad (2.2a)$$

where the Fourier coefficients and phase lags are determined as follows;

$$a_0 = \frac{2K_f\alpha}{\pi} \qquad r_n = \sqrt{a_n^2 + b_n^2} \qquad \varphi_n = \tan^{-1}\left(\frac{a_n}{b_n}\right)$$

when $2n\alpha = 1$ $n = 1,2,3,.....$

then $a_n = 0$ $b_n = \alpha K_f$

otherwise

$$\left.\begin{aligned} a_n &= \frac{K_f\alpha}{\pi}\left[\frac{\pi\cos(2n\alpha - 1) - 1}{2n\alpha - 1} - \frac{\pi\cos(2n\alpha + 1) - 1}{2n\alpha + 1}\right] \\ b_n &= \frac{K_f\alpha}{\pi}\left[\frac{\pi\sin(2n\alpha - 1)}{2n\alpha - 1} - \frac{\pi\sin(2n\alpha + 1)}{2n\alpha + 1}\right] \end{aligned}\right\} \qquad (2.2b)$$

It has been observed and verified empirically that the mean value of the time history of a vertical load $f_H(t)$ corresponding to rhythmic jumping is always equal to the weight of the jumping subject (Taun & Saul 1985; Ji & Ellis 1994). In expressing this observation analytically, Ji & Ellis (1994) formed the equation shown below:

$$\frac{1}{T_J}\int_0^{tc} f_H(t)dt = G_H \qquad (2.3a)$$

Upon substituting Equation 2.1a, into Equation 2.3a, Ji & Ellis (1994) obtained the equation:

$$\frac{1}{T_J}\int_0^{tc} K_f G_H \sin\left(\frac{\pi t}{t_c}\right)dt = G_H \qquad (2.3b)$$

When evaluated, Equation 2.3b was reduced to Equation 2.4, shown below:

$$K_f = \frac{\pi}{2\alpha} \qquad (2.4)$$

Equation 2.4 describes the relationship between the load amplitude factor and the contact ratio. Plotting of this equation, leads to the curve shown in Figure 2.4a. Contact ratios measured experimentally typically lie between 0.3 and 0.6 for jumping at 2 Hz on a rigid platform and rarely lie below 0.5 for jumping on a flexible platform (Yao *et al*. 2006). This means that the amplitude factor is not likely to exceed a value of 5; alternatively, the force due to jumping is not likely to exceed five times the body weight.

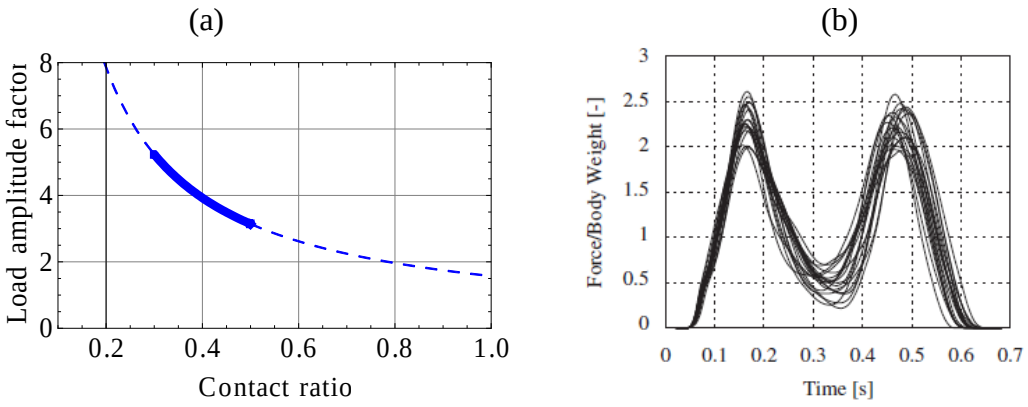

Figure 2.4: Graphs showing (a) the load amplitude factor as a function of the contact ratio, (b) impulse with twin peaks for jumping at 1.5 Hz (after Racic & Pavic 2010)

By substituting Equation 2.4 into Equation 2.2, Ji & Ellis (1994) eliminated the load amplitude factor in Equations 2.2. Thus they were able to express the Fourier series representation of the jumping load model as a function of the contact ratio and the jumping frequency or period, as shown in Equation 2.5.

$$\left.\begin{aligned} f_H(t) &= G_H\left[1.0+\sum_{n=1}^{\infty} a_n \cos\left(\frac{2\pi n}{T_J}t\right)+\sum_{n=1}^{\infty} b_n \sin\left(\frac{2\pi n}{T_J}t\right)\right] \\ f_H(t) &= G_H\left[1.0+\sum_{n=1}^{\infty} r_n \sin\left(\frac{2\pi n}{T_J}t+\varphi_n\right)\right] \end{aligned}\right\} \qquad (2.5a)$$

where the Fourier coefficients and phase lags are:

$$r_n = \sqrt{a_n^2 + b_n^2} \qquad \varphi_n = \tan^{-1}\left(\frac{a_n}{b_n}\right)$$

when $2n\alpha = 1$ $n = 1,2,3,.....$

then $a_n = 0$ $b_n = \pi/2$

otherwise

$$\left.\begin{aligned} a_n &= 0.5\left[\frac{\pi\cos(2n\alpha-1)-1}{2n\alpha-1} - \frac{\pi\cos(2n\alpha+1)-1}{2n\alpha+1}\right] \\ b_n &= 0.5\left[\frac{\pi\sin(2n\alpha-1)}{2n\alpha-1} - \frac{\pi\sin(2n\alpha+1)}{2n\alpha+1}\right] \end{aligned}\right\} \quad (2.5b)$$

Other variants of the basic model (Equation 2.1) have been explored by Sim *et al*. (2006), Nhleko *et al*. (2008), and Racic & Pavic (2010). In the work of Sim *et al*. (2008) the half-sinusoid function (Equation 2.1) was replaced by a cosine-squared function fitted to experimental data. This was a modest improvement from the basic model as it meant that the impact factor and the contact ratio were constrained by experimental data instead of being mere theoretical expressions. However, both the basic model and the model of Sim *et al*. (2008) do not accommodate jumping at frequencies less than 2 Hz because the force impulse has two peaks (see Figure 2.4b) for jumping at low frequencies as reported in the work of Sim *et al*. (2005), Harrisson (2008) and Racic & Pavic (2010). For this reason Sim *et al*. (2008) did not include test records with twin impulse shape in their statistical model. To address this, Nhleko *et al*. (2008) adopted an approach where impulse shape factors were incorporated to accommodate different impulse shapes. Similarly, Racic & Pavic (2010) used a sum of Gaussian functions to simulate twin peak behaviour of impulses.

It is also important to highlight that the Fourier series of the half-sine model cannot produce the jump-by-jump variation of peak forces as observed in normal jumping. However, it is still possible to use it in a repeated fashion or cycle-by-cycle to reproduce

the variation observed in normal jumping as explained in the work of Ellis & Ji (2004). This involves appending the jumping force time history from cycle to cycle based on statistical foreknowledge of cycle-by-cycle variations of the contact ratio and the jumping frequency for a particular subject.

Recent models address the cycle-by-cycle variation by assuming a particular distribution of the variation of the magnitude of the peak force and the jumping frequency from one jump to the next. This procedure relies on the availability of an existing database of experimental force measurements for different subjects (Sim 2006; Parkhouse & Ewins 2006; Racic & Pavic 2010). These models also involve treating each jumping cycle separately and appending the cycles to form a total time history record. The statistical distributions parameters and other techniques used to achieve the jump-by-jump variation of the force (as observed when forces due to jumping are measured in real life) in these recent models are a significant departure from the original model proposed by Ji & Ellis (1994). The latter is now considered over-conservative as it overestimates the structural response by significant margins when used in structural calculations. It is important to highlight that the new generation of models cannot be used without a sophisticated computer algebra system and the generating algorithms are always published in a flow chart format. An extensive database of experimentally measured forces also needs to be available to draw parameters for the various statistical distributions used in these models.

Finally, it is important to emphasize that the load models discussed here were derived from test data collected using rigid force platforms and the dependence of applied forces on platform frequencies as reported in the work of Yao *et al.* (2003), Yu (2004), Yao *et*

al. (2006) and Harrison (2008) were ignored. Therefore the models are likely to over-estimate the response for structures with low frequencies.

2.3.1.2 Crowd loads for jumping

Here the general approach is to collect data for a small group of people, introduce certain statistical parameters to quantify the main characteristics and use the Monte Carlo method of sampling (based on some fitted probability distributions) to generate the loads for a large crowd from a suitably modified version of Equation 2.5. This procedure was first adopted by Ebrahimpour & Sack (1989). Further developments have been made by Willford (2001), Ellis & Ji (2004), Parkhouse & Ewins (2006), Kasperski & Agu (2005), Sim (2006) and Hoath (2009). It is important to note that the range of possible jumping frequencies to take into account when dealing with group loads is different from that for single individuals. For example, the British design standard, BS 6399, recommends a frequency range of 1.5–2.8 Hz for group jumping because at higher frequencies it is difficult for a large group to maintain a coordinated rhythm.

When group loads are considered, the main parameter to focus on is the inter-subject phase lag between the forces of different individuals in a group and this was the focus of earlier work (Ebrahimpour & Sack 1989, Ellis & Ji 1993, Willford 2001). However, as mentioned in the previous section, recent work has also included intra-subject variability (cycle-by-cycle variations) during group jumping as no individual can jump in a perfectly periodic manner. For example Kasperski & Agu (2005) and Ellis & Ji (2004) took into account the slight variation between each jump by modelling the statistical parameters of the jumping frequency and contact ratio.

Parkhouse & Ewins (2006) presented a model in which group loads were formed by combining two components of the loads measured for individuals, namely, a synchronized component and a stochastic component. The force time histories were first segmented into individual impulses by the time histories of the beeps which had been simultaneously recorded with the force. They then added together the individual time-histories to derive group loads. They showed that the synchronized component is proportional to crowd size while the stochastic component is proportional to the square root of the crowd size. In addition they introduced a new parameter called the synchronization factor defined as:

$$f_{syn} = \frac{P_{sync}}{P_{tot}} \qquad (2.6)$$

where P_{sync} is the power of the synchronized component and P_{tot} is the total power. These parameters were calculated from the power spectral distribution of the force time history signal.

Sim (2006) modelled the time delay, $t_{delay} = t_d$ between the time of the beep, $t_{beep} = t_b$, and the effective timing, t_{eff}, of each impulse (see Figure 2.5 and Equations 2.7). The effective impulse timing was calculated at the centroid of the impulse using Equation 2.7b.

$$t_{d,k} = t_{b,k} - t_{eff,k} \qquad (2.7a)$$

$$t_{eff,k} = \frac{\sum_{i}^{n} F_i t_i}{\sum_{i}^{n} F_i} \qquad (2.7b)$$

where t_{eff} is the k^{th} impulse centroid, F is the force digitized at discrete time values t to form a total sample size n.

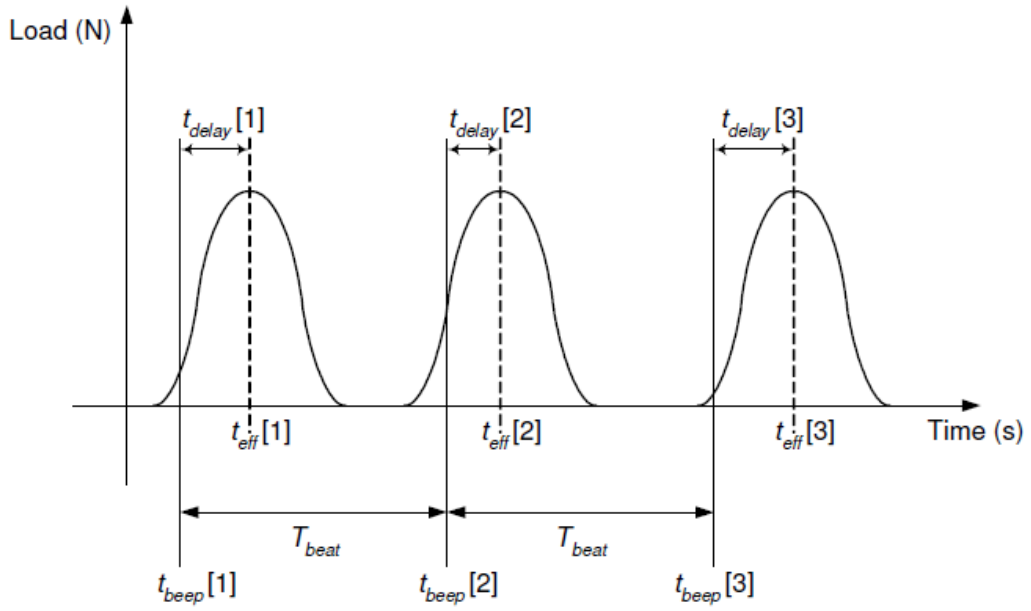

Figure 2.5: Schematic description of impulse timing parameters used by Sim (2006)

A further relationship (Equation 2.8) between the impulse size (i_k) and impulse timing was derived.

$$i_k = \frac{1}{2}(t_{eff,k+1} - t_{eff,k-1}) \qquad (2.8)$$

However, by her own admission she did not get a good fit to the experimental data when verifying this relationship for some of the jumping frequencies investigated. Nevertheless, both equations were used in the simulation of group jumping loads.

Instead of impulse timing, Racic & Pavic (2010) modelled the period and derived a relationship between the impulse size normalized by subject weight and the period. They backed up the relationship with a good experimental fit, although the experimental

measurements were made at one frequency only. The integral of the impulse size relationship used by both Sim (2009) and Racic & Pavic (2010) is the same relationship used in the model of Ji & Ellis (1994) except that Sim (2009) replaced the half-sinusoid force function (refer to Equation 2.3b) by a cosine-squared function while Racic *et al*. (2010) used a digitized force function (measured data) instead.

The crowd models of both Parkhouse & Ewins (2006) and Sim (2006) are based on aligning a single person's loads by a prompt (beep) signal and summing up the individual contributions to form a group model. This is equivalent to assuming that individuals in a crowd only follow the beep and ignore any possible interference from other members. As mentioned in Section 2.2.1, decades earlier Ebrahimpour & Sack (1989) had adopted the same approach and observed that it gave loads that did not resemble the measured group loads, leading them to conclude that crowd coherency is governed by auditory and visual effects. Consequently, Hoath (2009) took account of neighbouring crowd members when formulating a crowd model. Thus the time delay of individual subjects was a function of the beep, the timing of each impulse and an effect produced by their three immediate neighbours' landing times. Apart from this modification, her model used variables similar to those of the model developed by Sim (2009).

Finally, when a group of people jump in perfect unison the crowd model reduces to that of a single person with a force magnitude that depends on the number of jumpers. However, perfect unison among crowd members is considered impossible and an unrealistic case for grandstand design.

2.3.2. Modelling the effect of passive humans

Mathematical models used by structural engineers to represent the effect of passive humans on structures have been adapted from biomechanics research where extensive research on the dynamic properties of the human body has been carried out. Predictably, the modelling approach differs depending on whether a single individual or a crowd is involved. It is important to emphasize that these models are for the vertical direction as no model has been suggested for the horizontal directions.

2.3.2.1 Passive individual

Sachse (2002) and Sim (2006) conducted separate investigations on the suitability of human body models found in biomechanics literature for structural engineering applications. Based on simplicity and good fit to experimental data, Sim (2006) concluded that the models proposed by Wei & Griffin (1998) and Matsumoto & Griffin (2003) were adequate for structural engineering applications. The seated and standing human models are shown in Figure 2.6a and b, respectively.

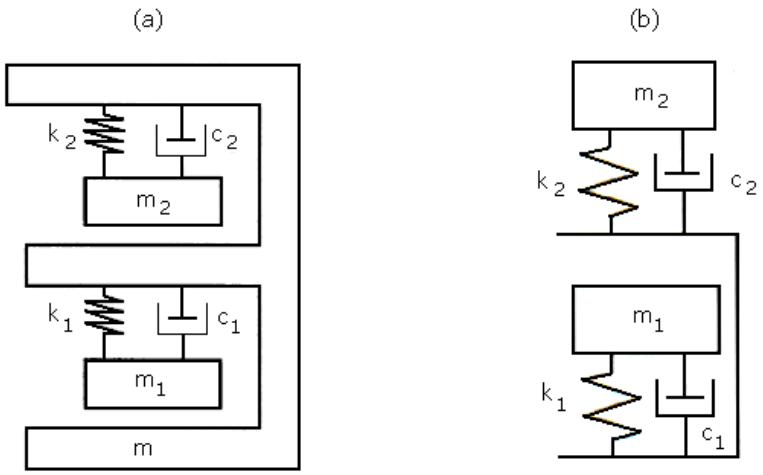

Figure 2.6: (a) Seated human model, (b) Standing human model

The models shown are 2-DOF (two-degrees-of-freedom) systems consisting of masses, *m*, springs, *k*, and dampers, *c*, which represent the mass, stiffness and energy dissipation property of the human body. Each model has two modes of vibrations at approximately 5Hz and 10Hz in agreement with the measured apparent mass data from which each model was derived.

2.3.2.2 Passive crowd

The models by Wei and Griffin (1998) only represent a seated or a standing individual but not a group. Sim (2006) developed a passive crowd model from the individual human model so as to model the effects of a group of people. This was achieved by fitting a fourth order rational polynomial to the apparent mass experimental data (for a group of seated and standing subjects) presented by Wei & Griffin (1998). Curves that were fitted are shown in Figure 2.7. She concluded that the agreement of the fit with measured data indicated that the crowd can be successfully modelled as a 2-DOF system with a 4th order Laplace transfer function of the form:

$$m^*_{app}(s) = \frac{a_4 s^4 + a_3 s^3 + a_2 s^2 + a_1 s + a_0}{b_4 s^4 + b_3 s^3 + b_2 s^2 + b_1 s + b_0} \tag{2.9}$$

where $m^*_{app}(s)$ is the normalized apparent mass for each group which is defined as:

$$m^*_{app} = \frac{total \quad apparent \quad mass \quad of \quad all \quad subjects}{total \quad apparent \quad mass \quad of \quad each \quad group} \tag{2.10}$$

and apparent mass $m_{app}(s) = \frac{F(s)}{\ddot{x}_g(s)}$ (2.11)

$F(s)$ = the force transmitted across the human-structure interface

$\ddot{x}_g$ = the acceleration at the interface

a_n and b_n are coefficients for $n = 0$ to 4 with different values in each group

s = the Laplace transform variable

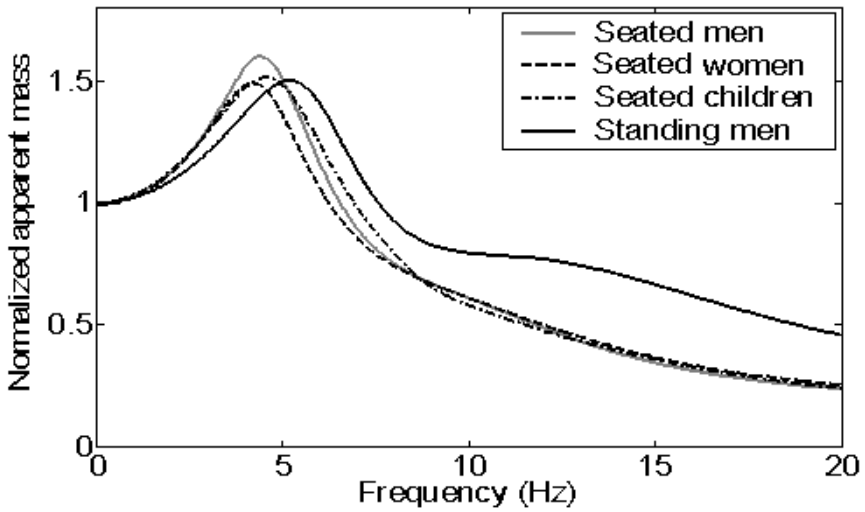

Figure 2.7: Curves fitted to represent normalized apparent mass data (Sim 2006)

Figure 2.7 shows that the standing posture led to slightly higher natural frequency than the seated posture. This occurs because on a low natural frequency platform, the crowd acts mainly as a mass since there is little relative movement between the human and the support. The movement becomes greatest at the frequency range of 4 to 6Hz. It reduces at high platform frequencies as the human system behaves like damper and the body mass remains still. All the motion is absorbed by the equivalent spring and damper. The increase in mass at low frequencies and the rise in damping at high frequencies both lead to a reduction in the natural frequency of the structure. These results agree with the studies by Littler (1998) and Reynolds *et al*. (2004).

2.3.3. Modelling the combined effect of active and passive humans

In practical situations, such as with grandstands, the crowd consists of both the passive and active audience. In this case the effects of the passive and active elements must be combined in a specific fashion to obtain the total effect. Sim (2006) used a feedback model featuring the active and passive models she developed to represent the total effect. Another model based on a different approach was proposed by Dougill *et al.* 2006. Due to its simplicity and agreement with empirical data this model has been incorporated in the latest guidelines for dynamic assessment of permanent grandstands (see IStructE 2008). The model is illustrated in Figure 2.8 and the guidelines provide different parameters for this model for different design scenarios.

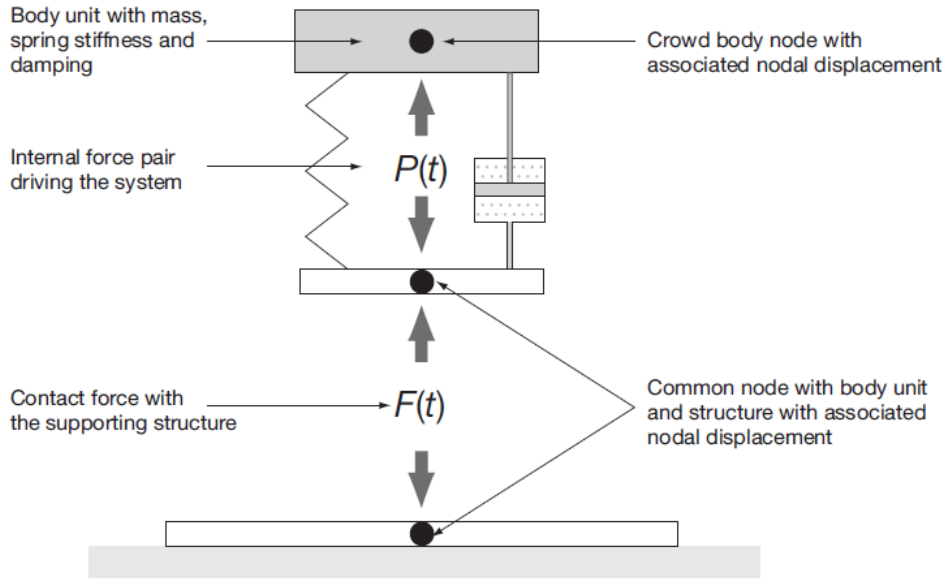

Figure 2.8: Model for the combined effect of active and passive humans on a structure (IStructE 2008)

The attractive feature of the model shown in Figure 2.8 is that both the passive (mass, damping and stiffness properties of the crowd) and active (driving force) elements are neatly represented in a single-degree-of-freedom human system in addition to the

structural system. For example, the passive and active models discussed previously become special cases of this model when the driving force or passive properties are assumed to vanish, respectively.

Finally, because the model is based on force data gathered from subjects performing on rigid force platforms, the principal assumption of this model is that the internal forces, $P(t)$, used by groups of people to move on a flexible platform will be the same as would be involved when undertaking the same activity on a rigid base.

2.4. Human-structure interaction and design guidance

There are several standards and guidelines in the UK and other countries which provide guidance for the design of vibration environments or structures. Although some of these guidelines have a long history and have undergone many updates in the past, the recent occurrence of persistent and troublesome vibrations serves as a testimony that some of the guidelines are inadequate and cannot be applied to all vibration problems. The following sections will illustrate the content of these guidelines and briefly highlight important areas. The focus is on local standards.

2.4.1. Guidance specific to sports stadia

Guidance specifically dealing with permanent and temporary grandstand structures can be found in documents such as BS6399 (1996), Guide to safety at sports grounds (1997) (also called the Green Guide) and IStructE Interim Guidance (2001; 2007 & 2008). The guidelines make a distinction between different uses of a structure. For instance the design criterion for structures where viewing sport only is expected is different to those

where music and dancing may be expected. For permanent grandstands solely used for normal viewing with non-rhythmic loading, the recommended limit for a structure's vertical frequencies is 3.5 Hz (IStructE 2001; 2007; 2008). For grandstands used for pop concerts with crowd rhythmic movements, 6 Hz is the suggested threshold for vertical frequencies. A minimum horizontal frequency of 3 Hz is considered acceptable (Department of National Heritage and Scottish offices, 1997). For temporary grandstands the limits for vertical and horizontal frequencies are higher at 8.4 Hz and 4Hz respectively (IStructE 2007).

The natural frequency criteria are intended to facilitate design for engineers who do not have enough background in structural dynamics and human-induced dynamic loading. They do not necessarily lead to an economic design. Due to this limitation BS6399 makes allowance for a performance based dynamic design if the designer does not wish to obey the frequency criteria. Designers are also permitted to make their own estimates of dynamic loading based on available data. Recent guidelines produced by the Institution of Structural Engineers also permit the use of a two degree of freedom model of the crowd-structure system that is treated by modal analysis design principles to ensure that the maximum root-mean-square of the acceleration is below a threshold (IStructE 2008).

Finally, it is important to highlight that a design approach based on compliance with certain frequency criteria is strictly applicable only to linear structural behaviour. Thus these standards assume that most structures will exhibit linear behaviour. However, the dynamic response of some structures such as demountable structures is characterized by nonlinear behaviour (Nhleko *et al.* 2010). For these structures the importance of

complying with the recommended frequency criteria lacks a theoretical justification and has been questioned (Nhleko *et al.* 2010).

2.4.2. Previous research on human perception of vibration and comfort levels

A fundamental basis in the design of facilities or environments that involve human exposure to vibrations requires establishing the limits for the maximum level of vibration that is acceptable to occupants based on perception, comfort, safety or health thresholds. Whilst, there is a paucity of published research specific to grandstands (see for example Kasperski 2001 and Kasperski 1996 discussed in Section 3.3.3 of Chapter 3), there is abundant literature in the area of human responses to vibration (referenced in Griffin 1990). Studies have also been performed to understand human perception thresholds and to examine human comfort levels during exposure to different vibration levels (Lenzen 1966; Murray 1979; Allen & Rainer 1976; Allen *et al.* 1985). Some of this research has resulted in a number of local and international standards such as BS6472 (1992, 2008), BS6841 (1987), BS7085 (1987), ISO2631-2 (2003) and ISO10137 (2007).

The previous standards were developed to deal with specific vibration environments and may not be suitable to be used in relation to grandstands. For example BS6472 (1992) (subsequently replaced by the 2008 edition) provides acceleration (serviceability) limits recommended for different classes of buildings such as residential buildings, offices and industrial buildings. In ISO10137 (2007), the criteria for acceptable vibrations for stadiums and assembly halls under coordinated crowd action are given in terms of a

specific curve referred to as the base curve. The standard also specifies maximum vibration levels which should not be exceeded to avoid panic situations.

BS6841 (1987) provides guidance on human response to mechanical vibration and repeated shock. Its specific focus is mainly on vibrations encountered on transportation structures or vessels and industrial environments. It gives methods for quantifying vibration and repeated shocks in relation to human health, interference with activities, discomfort, the probability of vibration perception and the incidence of motion sickness. BS7085 (1987) contains similar provisions but its aim is directed at the protection of human subject participating in experiments involving vibrating machinery. ISO2631-2 (2003) deals with the evaluation of human exposure to whole body vibration in buildings but also makes no reference to grandstands. Finally, since human response to vibration is a function of the frequency of vibration, it is customary to "weight" measured data to give greater prominence to frequencies where humans are most sensitive. Consequently, these standards also provide frequency weightings to modify measured response for different frequencies so that the relative effects of different vibration frequencies on human health, comfort, perception, etc, can be approximately quantified and compared.

2.5. Literature review summary

The literature review showed that there is a need for specific research to address human tolerance of vibration motion in the context of grandstand structures. Past research in human-structure interaction has also been heavily biased towards dealing with human-induced vibrations in the vertical direction. Consequently, there is currently a lack of experimental data and corresponding mathematical models for representing human

induced forces in the horizontal directions. This includes experimental data and mathematical models for representing the dynamic properties of the human body in the horizontal directions in the structural model. Finally, no method exists for measuring crowd synchronization which is an important aspect of the loading mechanism. As a result, recent investigators (Sim 2006; Parkhouse & Ewins 2006) have derived crowd models by aligning a person's loads by a beep (music) signal. Two decades ago Ebrahimpour & Sack (1989) demonstrated that whilst this procedure accounts for single individuals; it does not suffice for a crowd because coherency of a crowd is governed by two effects: auditory (music) and visual (other crowd members). Finally, complying with the frequency criteria recommended in various design guidelines and standards is inappropriate for structures which exhibit nonlinear behaviour.

2.6. Problem areas to address

In order to address the challenges highlighted above the specific objectives of the proposed work are:

(1) To investigate vibration perception and comfort levels of human subjects occupying a vibrating structure driven by a motion simulator

(2) To measure and characterize horizontal forces due to typical spectator movements

(3) To develop an economical method for measuring synchronization between individual subjects performing as a group and to collect foot-timing data in order to form a group load model

(4) To determine mathematical models to describe horizontal loads for design

(5) To conduct numerical parametric studies and finite element simulations as part of validating the developed models

Chapter 3

3. Assessment of comfort levels on a vibrating grandstand rig

A fundamental basis in grandstand design requires establishing the limits for the maximum level of vibration that is acceptable to spectators. This chapter reports controlled laboratory investigations on human vibration perception and comfort states when vibration levels in an occupied grandstand rig attached to a motion simulator are changed. This was an introductory study undertaken at the beginning of the project.

Students were recruited to participate as either a seated or a standing audience and then to provide feedback on the state of their comfort and vibration perception during exposure to different vibration levels. The data collected was compared with (and/or analysed using techniques and) provisions specified in standards relevant to this area of research, namely, BS6472 (1992), BS6841 (1987), BS7085 (1987) and ISO2631-2 (2003). These standards were introduced in Section 2.4.2. The data collected are presented in graphical form where each graph describes the vibration perception and comfort levels of the subjects for a specific movement of the structure. Finally, the effects of structural vibration on the forces exerted by the subjects on the structure are presented.

3.1. Background on the assessment of the human response to vibration

Vibration environments, in terms of human sensation of vibration levels, need to be quantified in order to establish baseline values that can be used in the design of grandstands. Therefore, it is necessary to conduct a psychophysical experiment or

survey by means of a category judgment method (Guilford 1954). This method requires subjects to select their subjective perception and/or levels of comfort during exposure to vibration from a range of text descriptors written in natural (ordinary spoken) language. The general principles of this method are illustrated in the flow chart (Figure 3.1). In this study, the vibration source was a vertically oscillating grandstand rig platform moved by four electric motors. Figure 3.1 shows the two categories of subjective responses or output that were requested from the participants after a brief period of exposure to a vibration input, namely, the level of vibration perception and the level of comfort together. The text descriptors shown in the flow chart are modified from BS6472 (1992). Five instead of the six descriptor used in BS6472 (1992) were adopted and the double negation form 'not uncomfortable' was paraphrased to 'comfortable'.

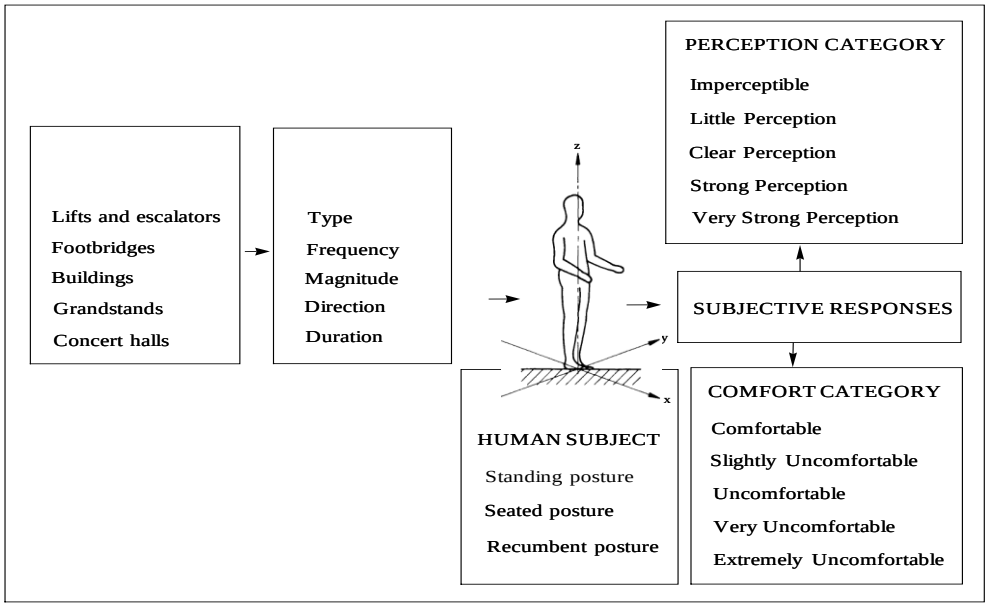

Figure 3.1 Flow chart of the category judgment method

3.2. Description of test structure, participants and methodology

The tests were undertaken using a suitably designed and fully-instrumented grandstand rig which had been constructed by the Department of Engineering, University of Oxford

for a similar project (Figure 3.2). The design of the rig is described in detail by Comer *et al*. (2007; 2010) and others. The essential features of the rig are that firstly, it was designed to resemble a real grandstand, including the raking; therefore human movement could be expected to be limited by the same spatial constraints of a normal grandstand structure (see Figure 3.2). Secondly, it could accommodate 15 individual subjects to allow group or crowd effects to be investigated.

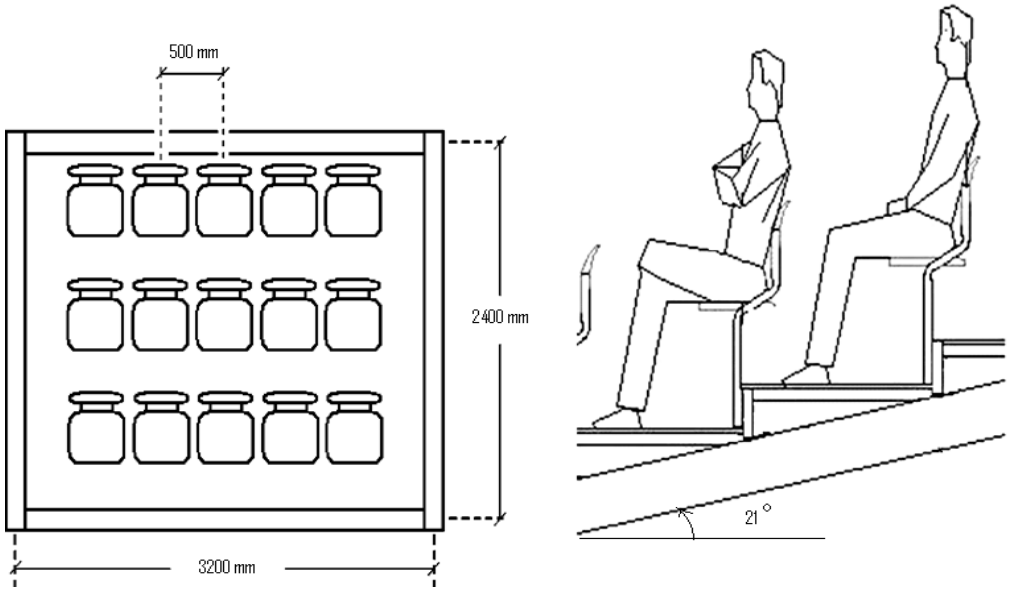

Figure 3.2: Overall geometry of grandstand rig (Comer *et al*. 2010)

Thirdly, the rig was attached to a motion simulator to allow vertical vibration motion of a real-life structure to be simulated. The simulator consisted of four linear electro-magnetic motors that supported the deck of the rig and controlled its vertical motion (Figure 3.3).

The rig was also instrumented with fifteen force plates to measure forces due to jumping and bobbing. These were positioned on the floor of the rig, in front of each seat. The force plates were fabricated from aluminium alloy and slotted between the cross beams which supported the seat rows (Figure 3.4).

Figure 3.3: Test structure showing one of four motors located on each corner (Comer *et al*. 2010)

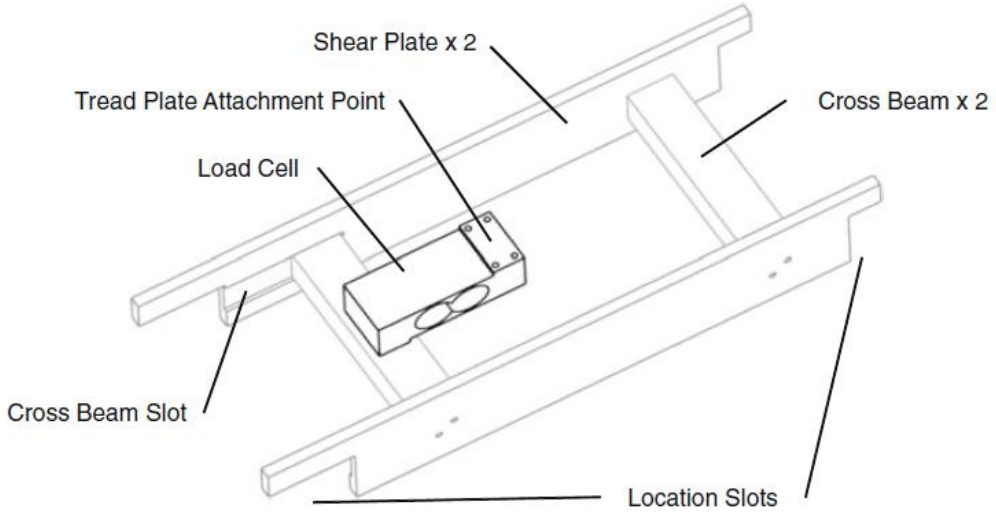

Figure 3.4: Load plate general assembly beneath the tread plate (Comer *et al*. 2010)

Finally, displacement transducers monitored the movement (or vibration level) to which occupants were subjected by recording the motion of the deck. To ensure that dangerous vibration levels were not approached during testing, the monitoring mechanism allowed for the automatic shut down and abortion of such a test, allowing the test structure to come immediately to rest, thus ensuring the safety of the occupants.

Post-graduate students were recruited to participate as either a seated or a standing spectator audience (Figure 3.5). The age range of the recruited audience was 25-30

years. The availability of postgraduate students allowed the same individuals and roughly the same number (12-15) of participants to take part in all test sessions. At the beginning of each test session, the participants were given specific instructions on the test procedure, the objective of the test, completion of a test questionnaire, and the emergency procedure applicable to the tests venue as well as during any abnormal operation of the rig.

For sitting tests, the participants were asked to remain seated for the duration of the vibration. No specific posture (such as maintaining a straight back) was prescribed and all subjects sat freely without the use of any restraint mechanism (e.g. seatbelts). Similarly, for standing tests the participants were requested to remain standing for the duration of the vibration but not asked to adopt a specific posture. However, the subjects were asked to stand freely (e.g. without leaning against a seats while standing).

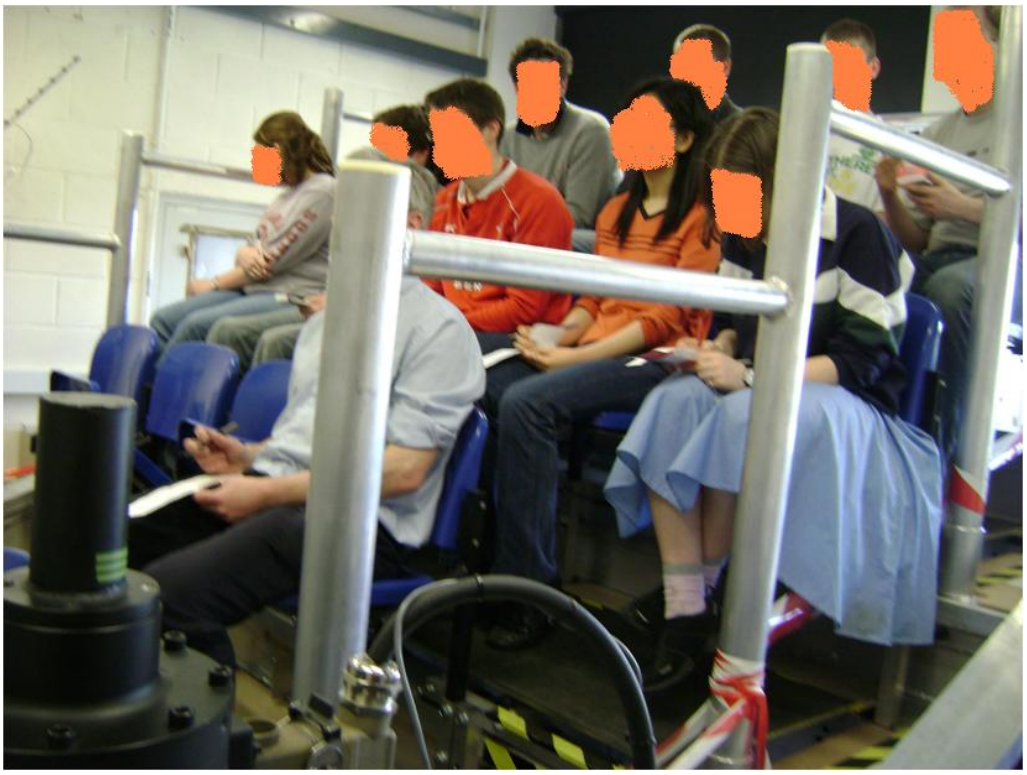

Figure 3.5 Sitting participants on a vibrating grandstand rig

Following exposure to a vibration level of a minute duration, the participants were required to provide feedback on the state of their comfort and vibration perception during the exposure period by selecting one option from the list of subjective responses shown in Figure 3.1. For each test, the vertical vibration (displacement) of the deck was recorded for a period of 60 seconds at a sampling rate of 1000 samples per second. The recorded data were digitally filtered to minimize the effect of background noise and to ensure that only motion with a frequency content up to 80 Hz was retained as required by the use of weighting filters in further analysis (see Figure 3.9).

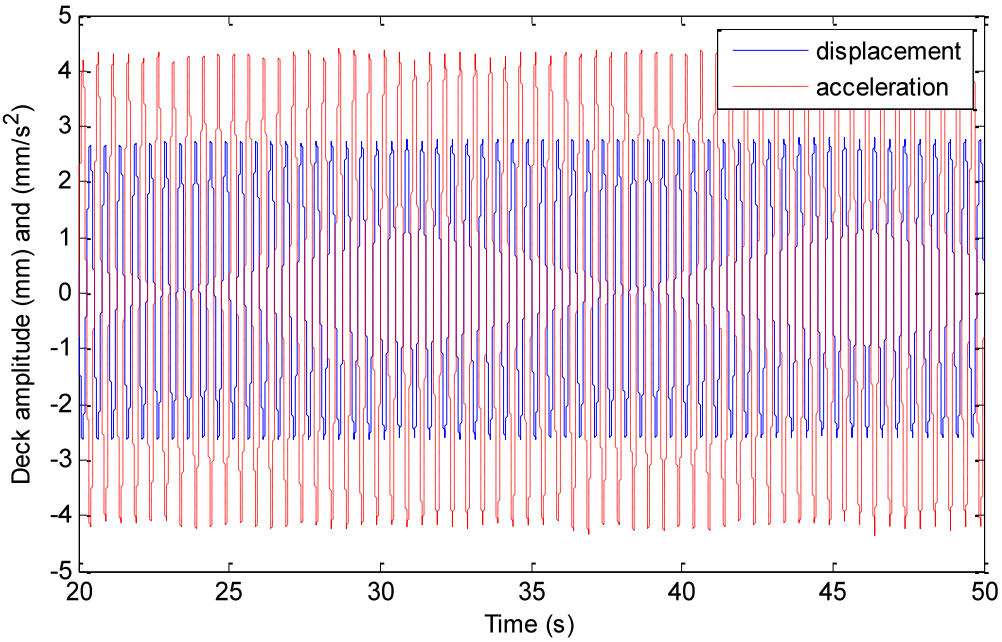

Figure 3.6: Typical vertical motion of the rig deck

The mean vertical motion of the grandstand deck recorded during a sitting test is shown as an example in Figure 3.6. A complete description of grandstand motion during each test is indicated by the acceleration root mean square (RMS) value which is a measure used by most standards to quantify vibration levels.

The RMS value of an acceleration time-history *a(t)* recorded over the time interval $0 \leq t \leq T$ is given by Equation 3.1.

$$RMS = \sqrt{\int_0^T a^2(t)dt} \qquad [\text{m/s}^2] \qquad (3.1)$$

Note that the RMS measure (see Equation 3.1) is only applicable to the assessment of exposure to continuous sinusoidal or random mechanical vibrations which are statistically stationary. The RMS measure cannot be used to evaluate exposure to mechanical vibrations whose characteristics vary over time. Thus other standards such as BS7085 (1989), ISO10137 and the most recent revision of BS6472 (i.e. BS6472 2008) provide for the use of an additional measure (Equation 3.2) called the vibration dose value (VDV) for dealing with mechanical vibrations whose characteristics vary over time.

$$VDV = \sqrt[4]{\int_0^T a^4(t)dt} \qquad [\text{m/s}^{1.75}] \qquad (3.2)$$

However, for mechanical vibrations which are statistically stationary (such as the sinusoidal vibrations investigated in the tests described in this chapter), the use of either measure (RMS or VDV) is acceptable and Equation 3.3 gives an approximate relationship between the two measures (see BS7085 1989).

$$VDV \approx 1.4 \times RMS \times \sqrt[4]{T} \qquad (3.3)$$

Data describing the mean vertical motion for both standing and sitting experiments are presented in Tables 3.1 and 3.2 in terms of the RMS measure (column 5). Each RMS value was obtained by numerically evaluating the derivative of the deck displacement time-history record (twice). For the analysis presented in Section 3.3, weighting filters were first applied to the time-history records before evaluating the RMS. The filters used will be discussed in Section 3.3.

Table 3.1: Grandstand vibration motion used for standing tests

Test Description	Frequency (Hz)	Vertical displacement (mm)	Target acceleration R.M.S (%g)	Measured acceleration R.M.S (%g)
2Hz/1.5mm		1.5	1.707	1.571
2Hz/3.5mm	2	3.5	3.984	3.616
2.67Hz/1.5mm		1.5	3.036	2.784
2.67Hz/3.5mm	2.67	3.5	7.084	6.506
3.3Hz/1mm		1	3.161	2.971
3.3Hz/1.5mm	3.33	1.5	4.742	4.472
3.3Hz/2mm		2	6.222	5.879
4Hz/0.5mm		0.5	2.276	2.205
4Hz/1.5mm	4	1.5	6.829	6.643
4Hz/1.5mm		1.5	6.829	6.722
4Hz/2.5mm		2.5	11.382	11.294
6Hz/1mm	6	1	10.244	13.983

Tables 3.1 and 3.2 show that there was a very small difference between the target acceleration and measured acceleration motion of the structure. Note that there were more data points collected for the sitting tests than for the standing tests. This is because current legislation in the UK (Football Spectators Act 1989) requires all clubs in the Premiership and the Championship to provide all-seater accommodation (that is, no standing accommodation) for spectators attending football games. The legislation resulted from Lord Justice Taylor's Report (1990) of the inquiry into the Hillsborough Stadium Disaster and took effect from August 1994.

Table 3.2: Grandstand vibration motion used for sitting tests

Test Description	Frequency (Hz)	Vertical displacement (mm)	Target acceleration R.M.S (%g)	Measured acceleration R.M.S (%g)
2Hz/1mm		1	1.138	1.001
2Hz/1.5mm		1.5	1.707	1.516
2Hz/2mm		2	2.276	2.032
2Hz/2.5mm	2	2.5	2.846	2.552
2Hz/3mm		3	3.415	3.055
2Hz/4mm		4	4.553	4.102
2Hz/5mm		5	5.691	5.026
3.3Hz/0.5mm		0.5	1.581	1.52
3.3Hz/0.5mm		0.5	1.581	1.632
3.3Hz/0.75mm	3.3	0.75	2.371	2.49
3.3Hz/1mm		1	3.161	3.294
3.3Hz/2mm		2	6.322	6.579
4Hz/0.15mm		0.15	0.683	0.776
4Hz/0.15mm		0.15	0.683	0.781
4Hz/0.15mm		0.15	0.683	0.744
4Hz/0.25mm		0.25	1.138	1.278
4Hz/0.5mm	4	0.5	2.276	2.51
4Hz/1mm		1	4.553	4.621
4Hz/1.5mm		1.5	6.829	6.838
4Hz/1.5mm		1.5	6.829	6.871
4Hz/2.5mm		2.5	11.382	10.802
6Hz/0.15mm		0.1	1.024	0.978
6Hz/0.25mm		0.25	2.561	2.536
6Hz/0.5mm	6	0.5	5.122	5.244
6Hz/0.5mm		0.5	5.122	5.444
6Hz/0.75mm		0.75	7.683	8.449
6Hz/1mm		1	10.244	10.911

3.3. Test results and analysis

3.3.1. Sitting tests data

Participant responses for sitting tests are shown in Figures 3.7 and 3.8. The horizontal axis represents responses obtained from the participants as a percentage of the total number of participants with each vibration level shown on the vertical axis.

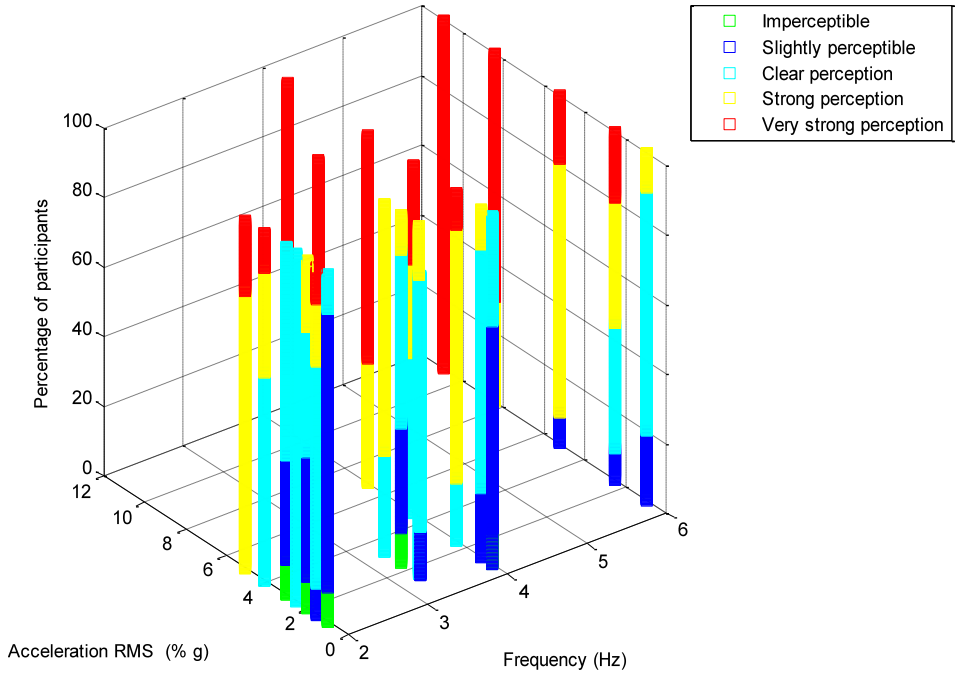

Figure 3.7: Sitting perception data

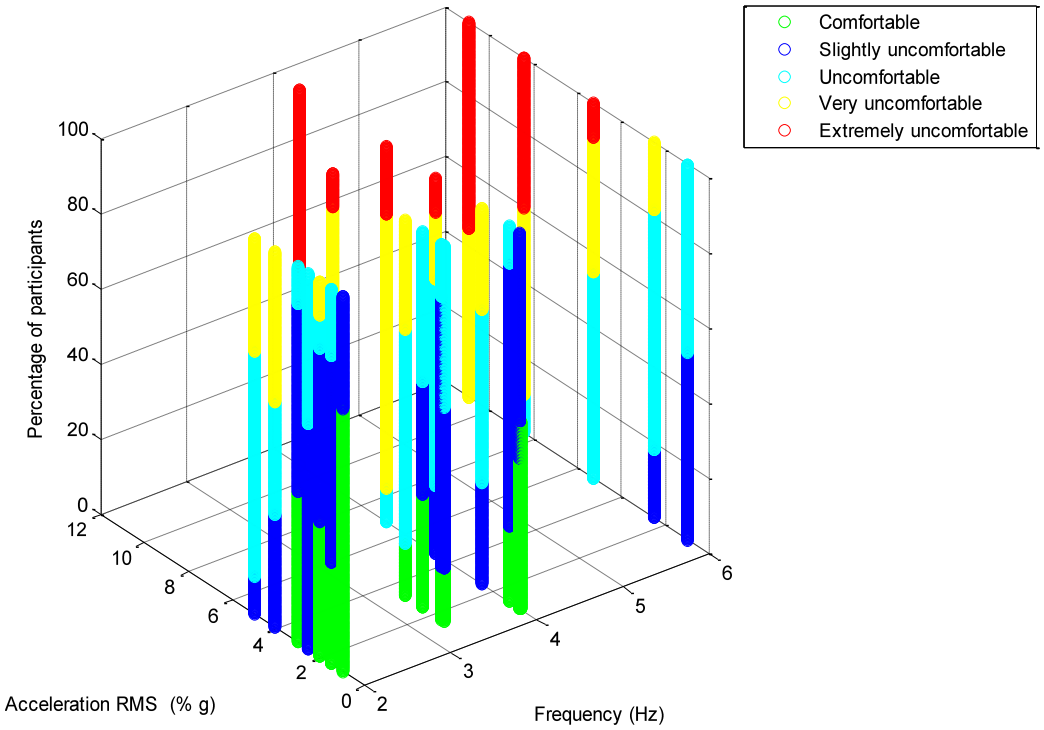

Figure 3.8: Sitting comfort data

Note that because some tests had acceleration RMS values very close to each other (refer to Table 3.1) some data points are co-incident. Nevertheless, it is clear from both figures that the responses from the participants are dependent on the measured acceleration RMS value.

Since human response to vibration is a function of the frequency of vibration, it is customary to "weight" measured data by applying a frequency weighting filter or factor (Rimell & Mansfield 2007). The aim of this is to give greater prominence to frequencies where humans are most sensitive to vibration. Therefore, data points recorded at frequencies where humans are more sensitive are multiplied by a higher factor and vice versa. In this research it was decided to "weight" the data using frequency weighting filters specified in three different legislative standards (Figure 3.9).

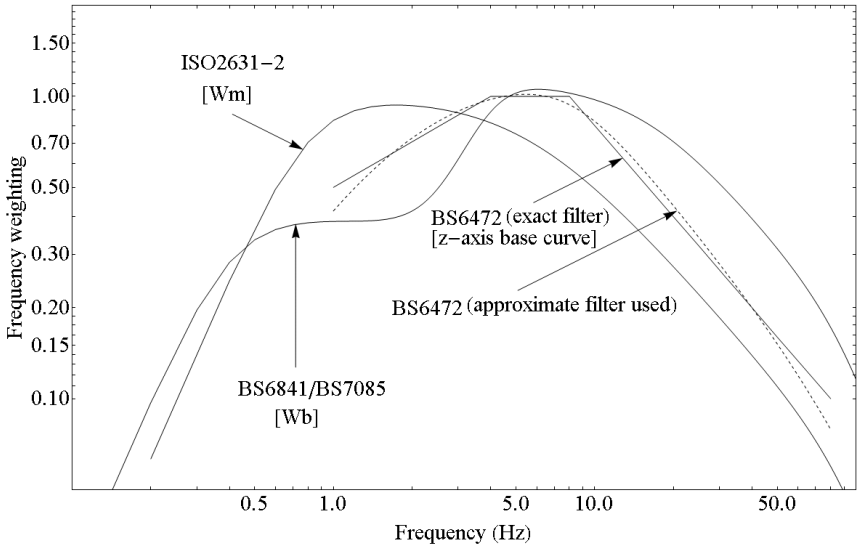

Figure 3.9: Frequency weighting filters relevant to whole body vibration

Derivation and guidance on the use of the filters shown in Figure 3.9 is reported in the research of other investigators, for example Rimell & Mansfield (2007). The effects of applying frequency weighting filters to the perception and comfort data for sitting is shown in Figures 3.10 to 3.12.

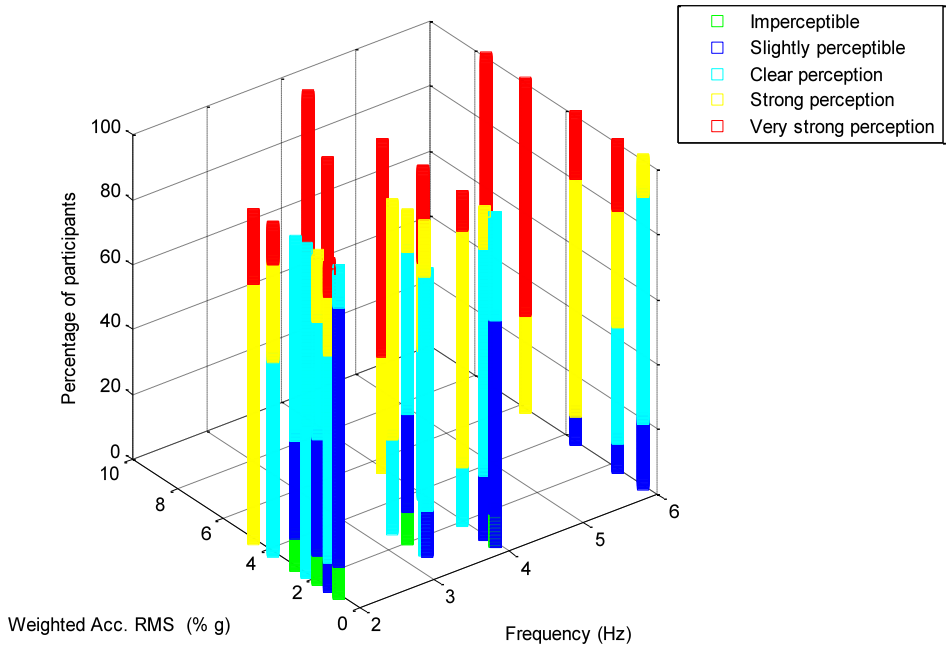

Figure 3.10(a): Sitting vibration perception data after applying weighting filter of ISO 2631-2

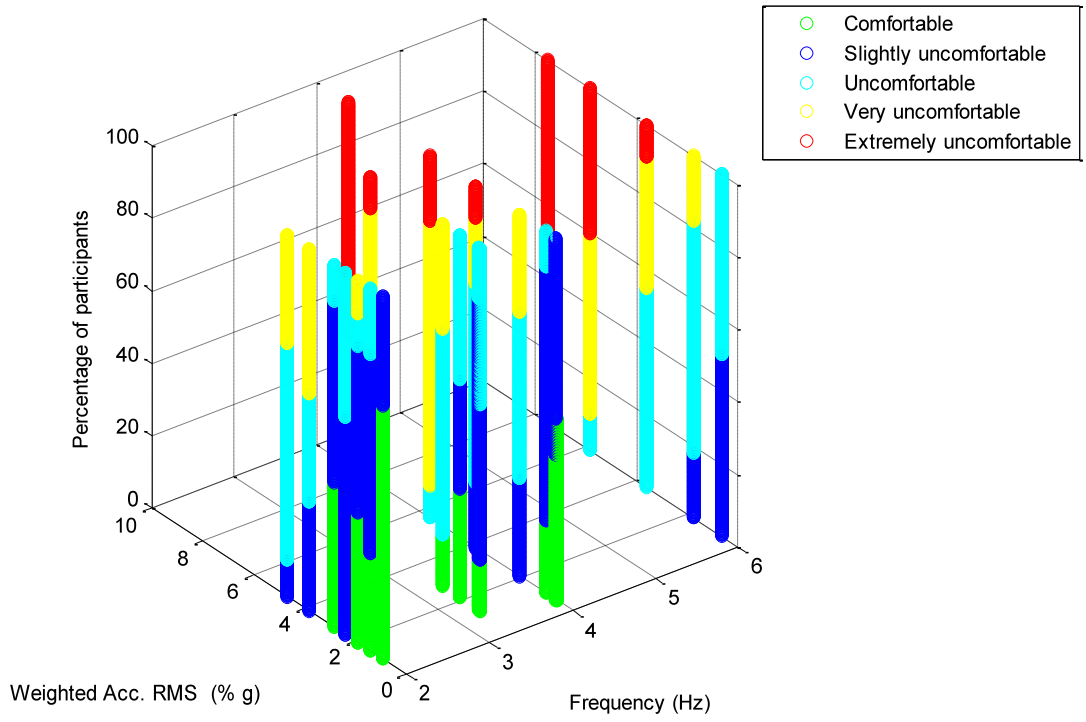

Figure 3.10(b): Sitting vibration comfort data after applying weighting filter of ISO 2631-2

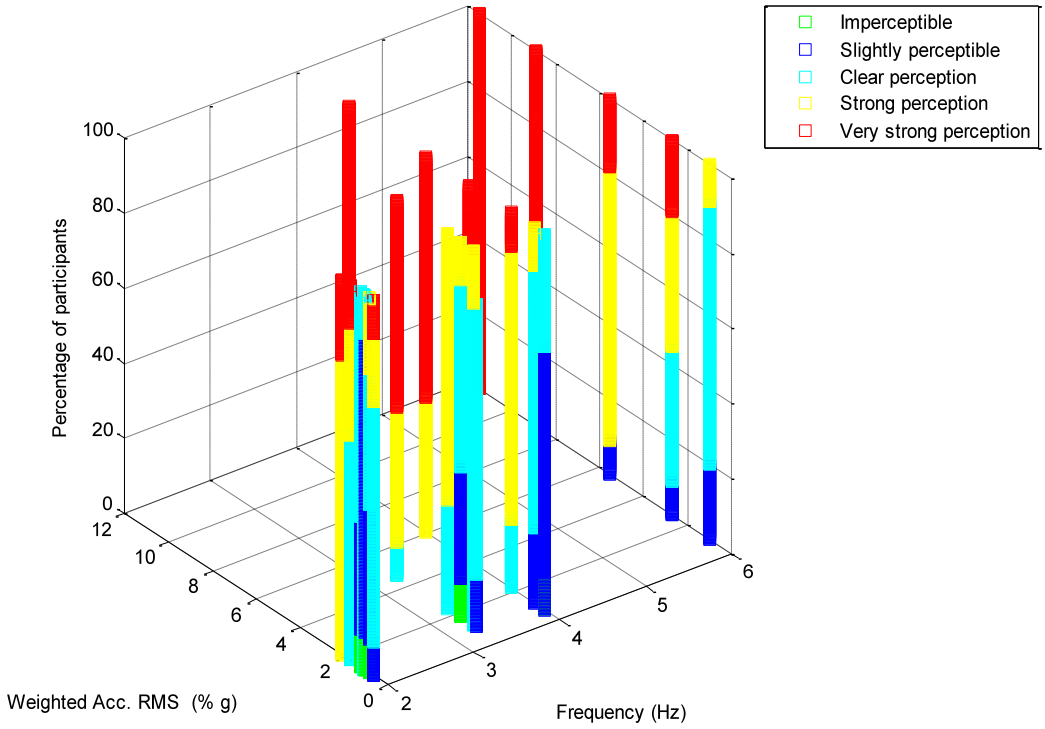

Figure 3.11(a): Sitting vibration perception data after applying weighting filter of BS6841

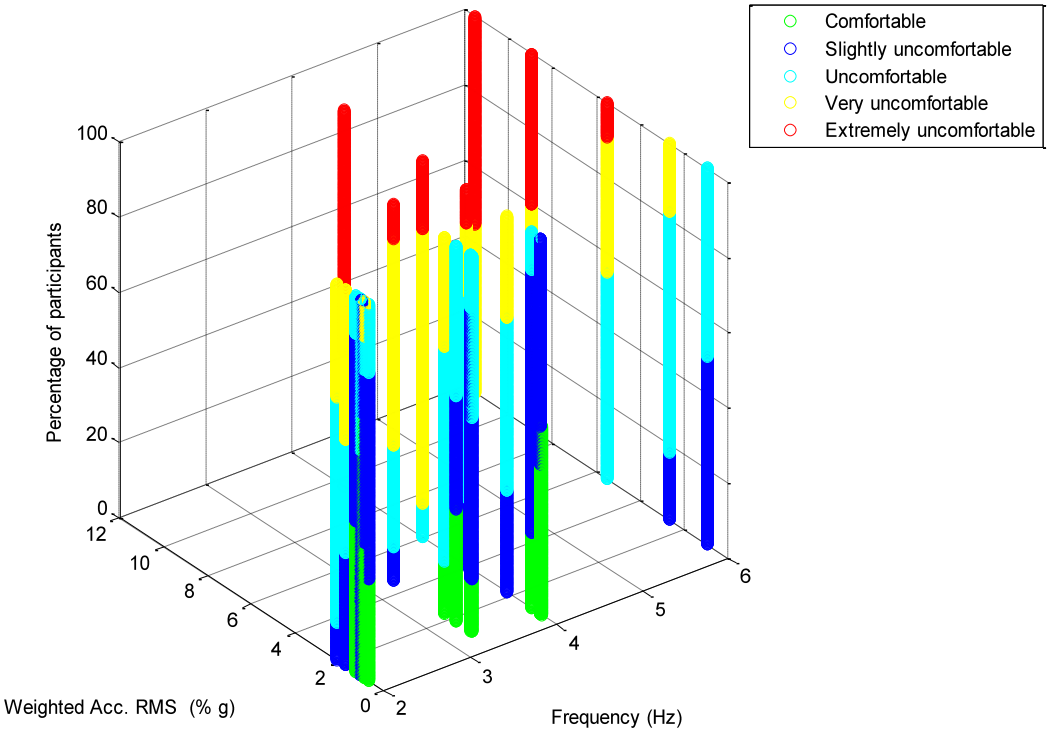

Figure 3.11(b): Sitting vibration comfort data after applying weighting filter of BS6841

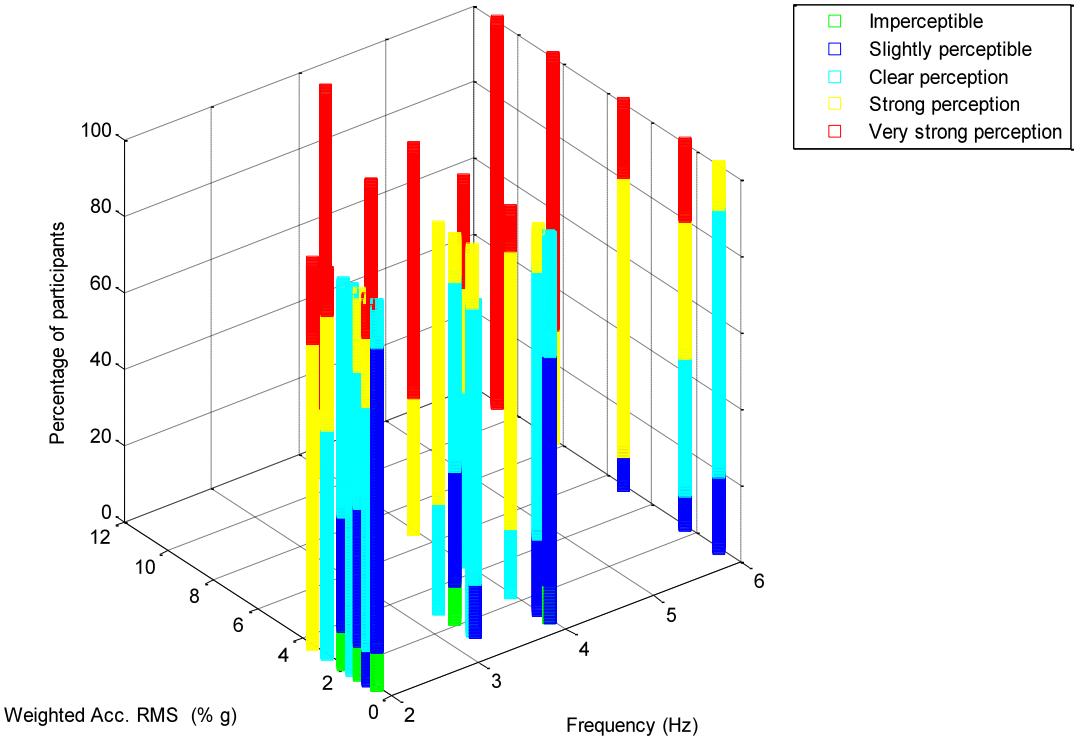

Figure 3.12(a): Sitting vibration perception data after applying weighting filter of BS6472

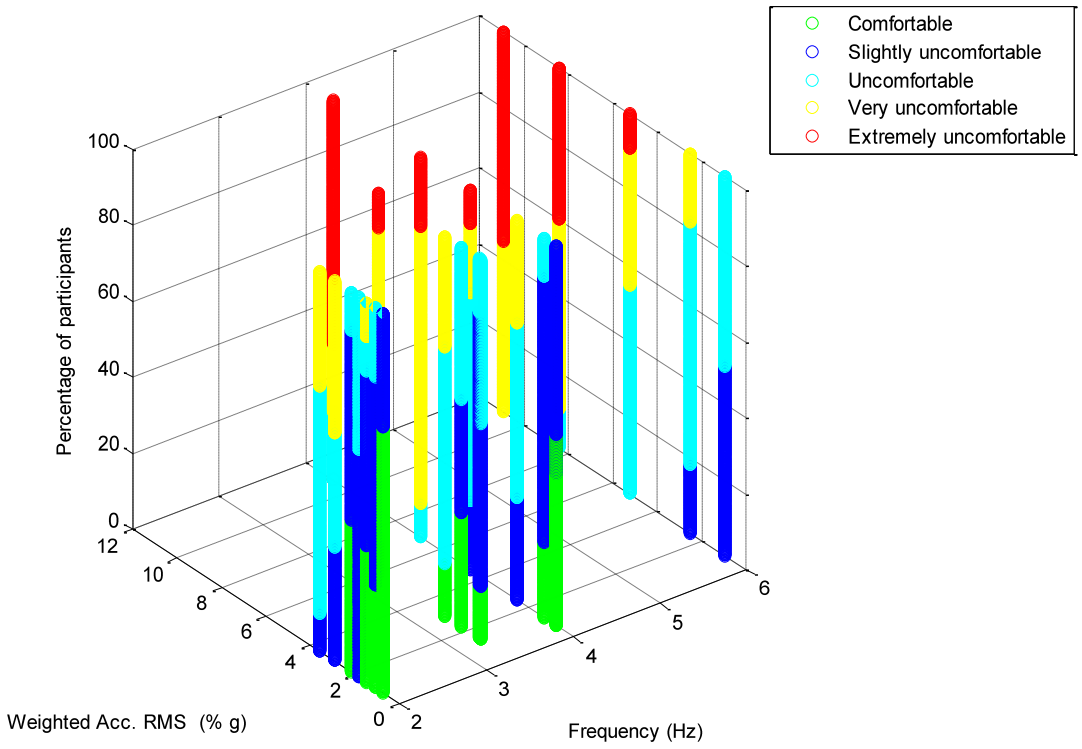

Figure 3.12(b): Sitting vibration comfort data after applying weighting filter of BS6472

When comparing perception and comfort levels, Figures 3.10 to 3.12 show that the perception variable becomes saturated or reaches its extreme level before the comfort variable. This indicates that vibrations are noticed (felt) before they are generally deemed uncomfortable. As the human feeling about the level of comfort on a structure results from the perception of the nature and level of vibrations, the assessment of human perception of vibrations, therefore, is also an important part of establishing safety criteria.

3.3.2. Standing tests data

The standing data was weighted using the same frequency weighting filters shown in Figure 3.9. The results are summarized in Figures 3.13 to 3.15. The results were very similar to the sitting test data with respect to the perception variable reaching its extreme level before the comfort variable. However, the onset of discomfort reported by the majority of the subjects occurred at higher vibration levels than for the sitting data.

The shape of the graph for each of the three different filters used reflects significant differences in the weighting mechanisms (Figure 3.9). For example, at vibration frequencies around 2Hz, the filter from BS6841 suppresses vibration amplitudes more than the other two filters used. The filter from BS6472 provides a moderate suppression, while the filter of ISO2631-2 provides little or no suppression.

By suppressing the vibration amplitudes at frequencies around 2 Hz, the filters from BS6841 and BS6472 account for human tolerance of vibrations around the 2Hz frequency.

(a)

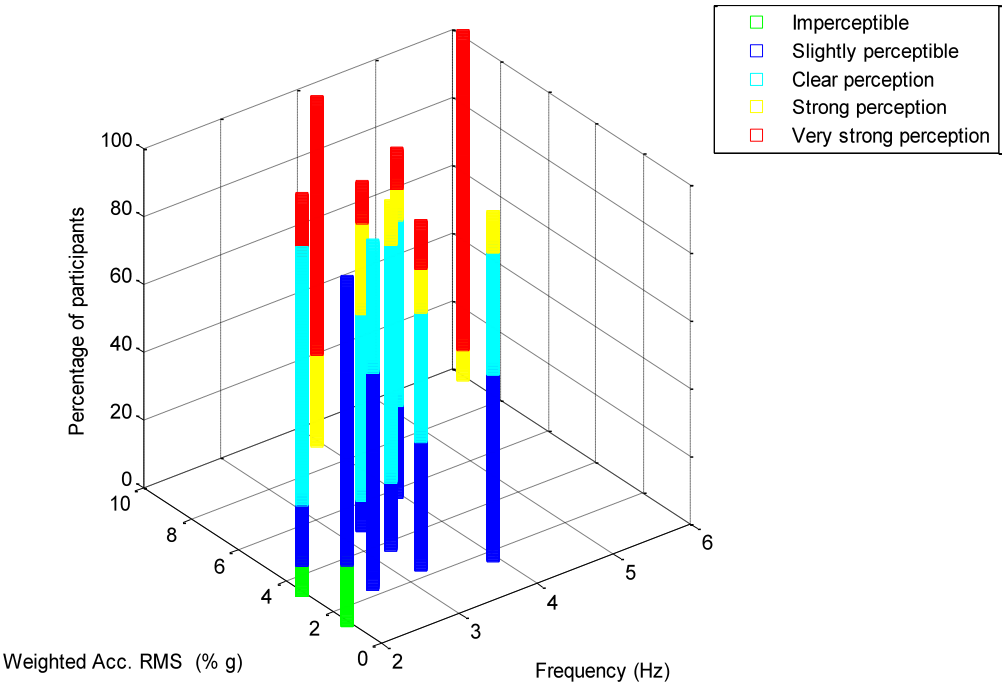

(b)

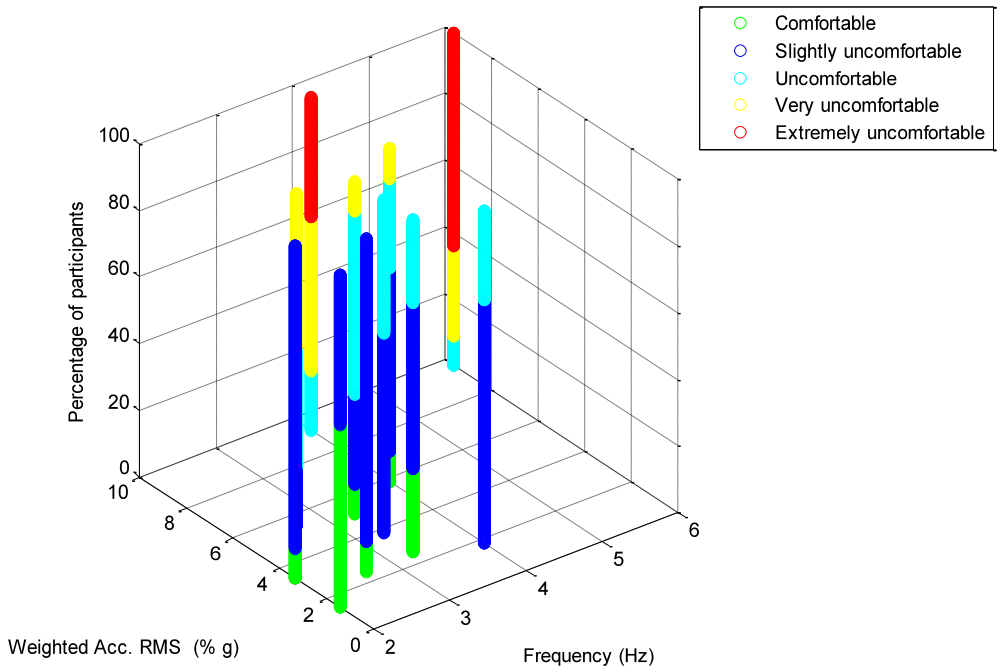

Figure 3.13: Standing data after applying weighting filter of ISO 2631-2: (a) perception (b) comfort

(a)

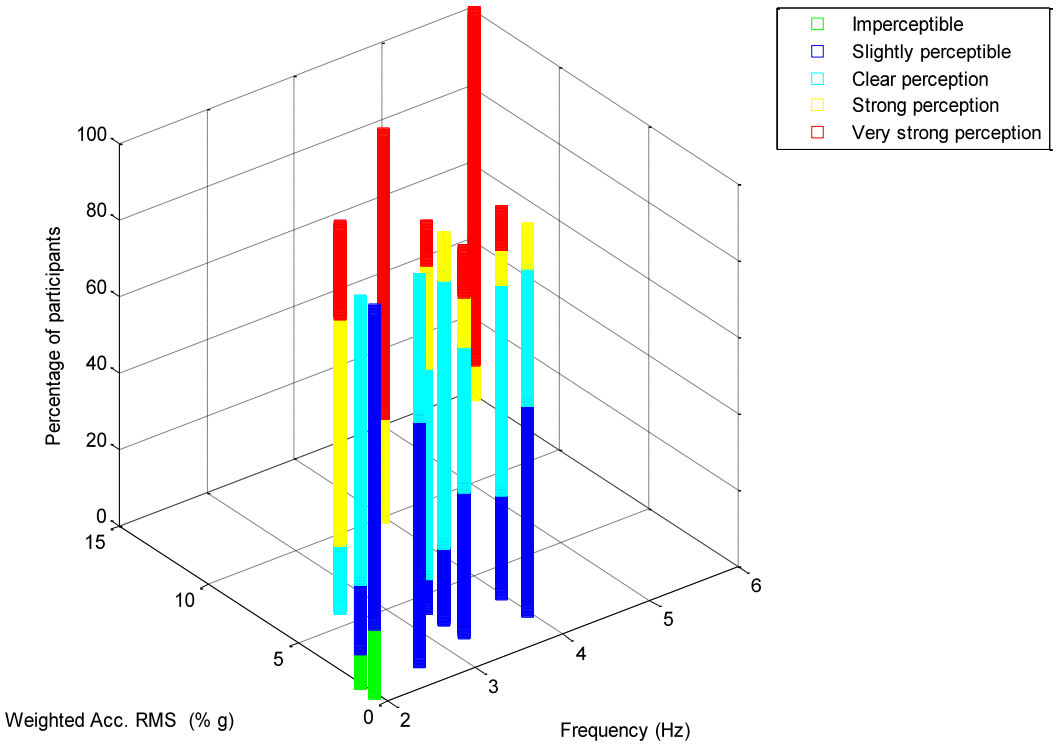

(b)

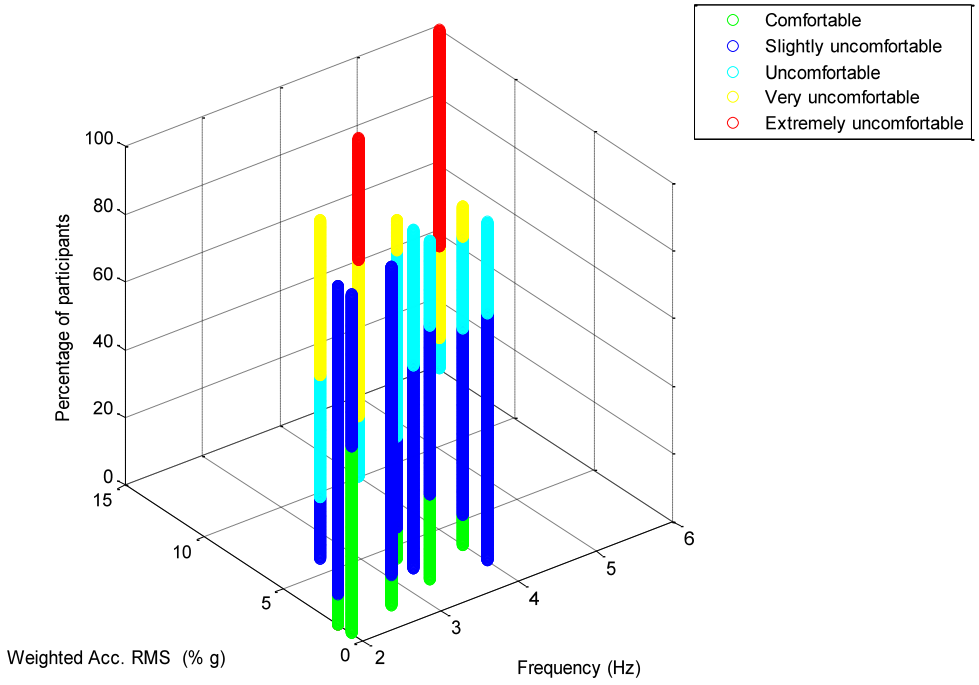

Figure 3.14: Standing data after applying weighting filters of BS 6841/BS7085: (a) perception, (b) comfort data

(a)

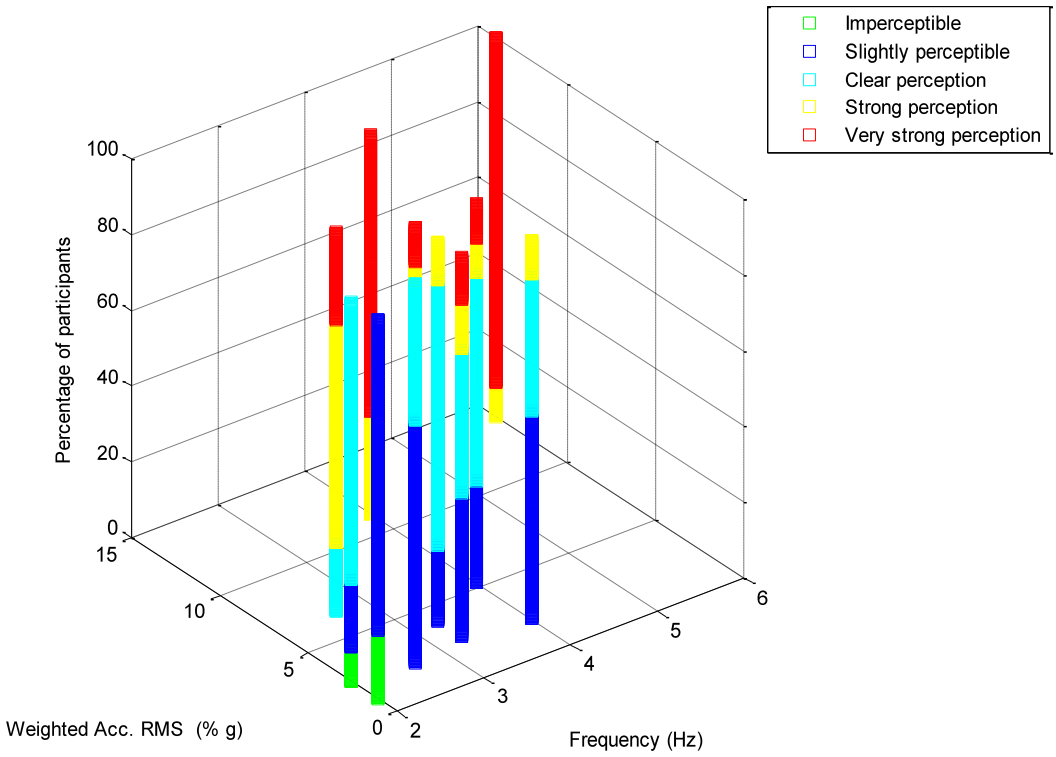

(b)

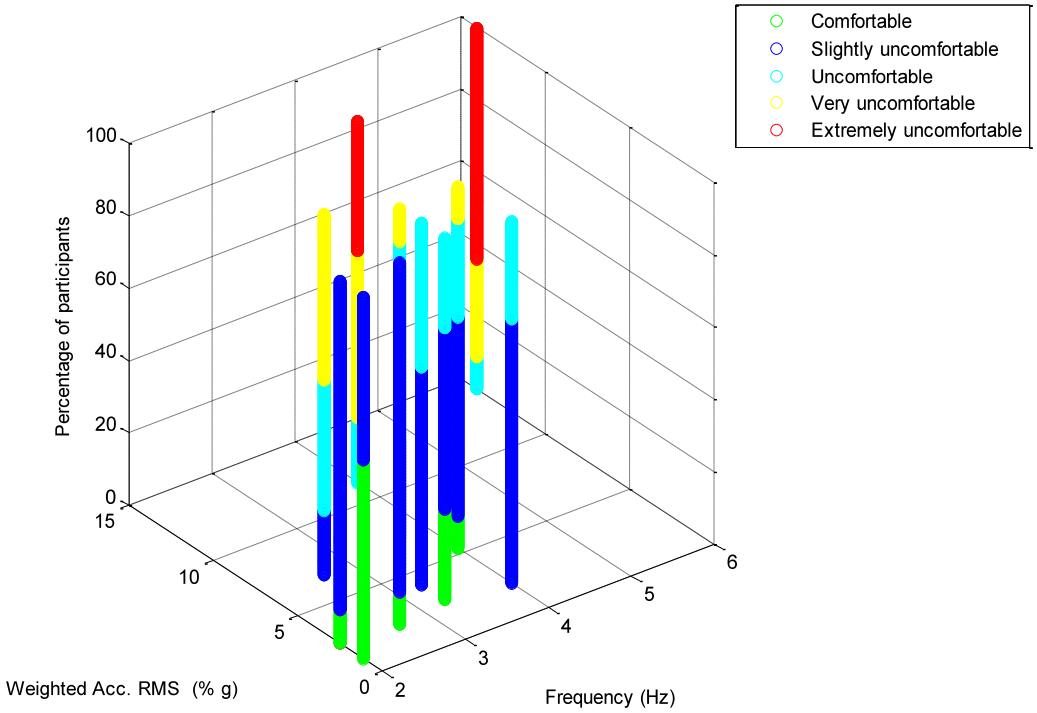

Figure 3.15: Standing data after applying weighting filter of BS 6472: (a) perception, (b) comfort

Conversely, the filter from ISO2631-2 allows for greater sensitivity to vibration motion around 2Hz by little or no suppression of vibration amplitudes. This approach seems more sympathetic to low frequency structures because they are prone to excitation by humans. Thus it may be argued that the filter from ISO2631-2 is more conservative since it does not take into account human tolerance of motion around 2Hz which is likely to lead to uneconomical or expensive structural designs. Finally, at frequencies of structural motion around 6Hz, the performance of BS6841 and BS6472 filters is nearly the same (allowing no suppression), while the ISO2631-2 filter attenuates vibration amplitudes significantly.

3.3.3. Comparisons with other vibration standards and similar research

The sitting and standing comfort levels data were compared with the limits recommended in BS6841 (Figure 3.16).

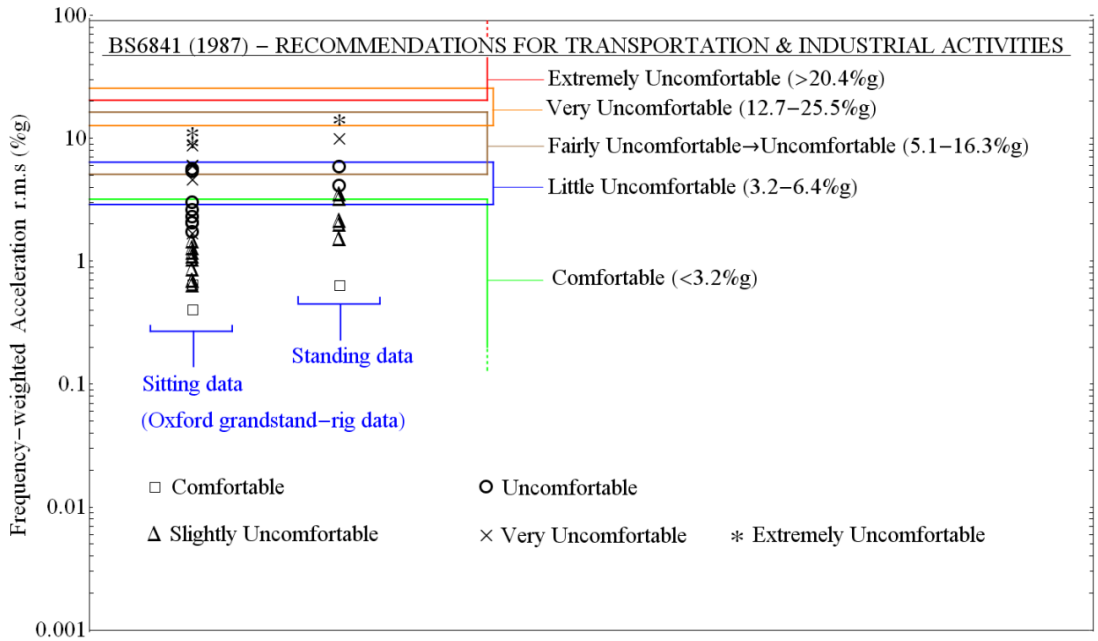

Figure 3.16: Comparison of sitting and standing comfort data with recommendations of BS6841

The provisions of BS6841 are mainly for vibrations encountered in transportation and industrial activities. However, it is useful as a benchmark comparison with the experimental data obtained for the grandstand rig. The standard specifies frequency weighted acceleration limits (in terms of RMS values) at which vibrations become uncomfortable, very uncomfortable, etc. These limits are indicated by solid lines in Figure 3.16.

The sitting and the standing data obtained in the current study show the comfort state reported by the majority of the participants when subjected to a specific vibration level indicated by the markers in Figure 3.16. The data were plotted after frequency-weighting each vibration level as specified in BS6841 and appear below the specified limits. This is not surprising since humans naturally show greater tolerance of vibrations when commuting and the guidance in this standard relates primarily to vibrations encountered in transportation. Comparing the standing and sitting data indicates that the subjects were more tolerant to vibrations when in a standing position than when seated. This difference in subjective responses indicates that each posture leads to a different human-structure interaction mechanism and possibly different natural frequencies for the combined human-structure system. This means that the design criteria for public facilities that accommodate a standing audience should be different to those for a seated audience.

The data for sitting comfort levels were also compared with the design guidelines recommended in BS6472 (Figure 3.17). This standard specifies serviceability acceleration limits (unweighted) for different classes of buildings. However, the standard makes no provisions for grandstand structures. If the mean of the "slightly uncomfortable region" of comfort obtained in this study is used to define the

serviceability limit state for grandstand structures, then the corresponding curve (shown as a broken line) to use as a basis for grandstand design is approximately 25 times the base curve specified in this standard. The acceleration limit at the mean of this region is 2.5 %g (g = 9.81 m/s^2). Alternatively, the acceleration limit of the upper boundary of the same region can also be used to define the serviceability limit equivalent to 5%g which corresponds to 50 times the base curve (Figure 3.17).

These acceleration limits can be compared with limits reported by other investigators. For example, the UK Building Research Establishment has monitored the accelerations due to crowd loading in grandstands at a number of different events (Litter, 2000). Measurements during concerts on seven grandstand tiers gave a maximum acceleration of 8.2%*g* and in other similar measurements the maximum acceleration recorded over a total of six concerts was 3.9%*g*.

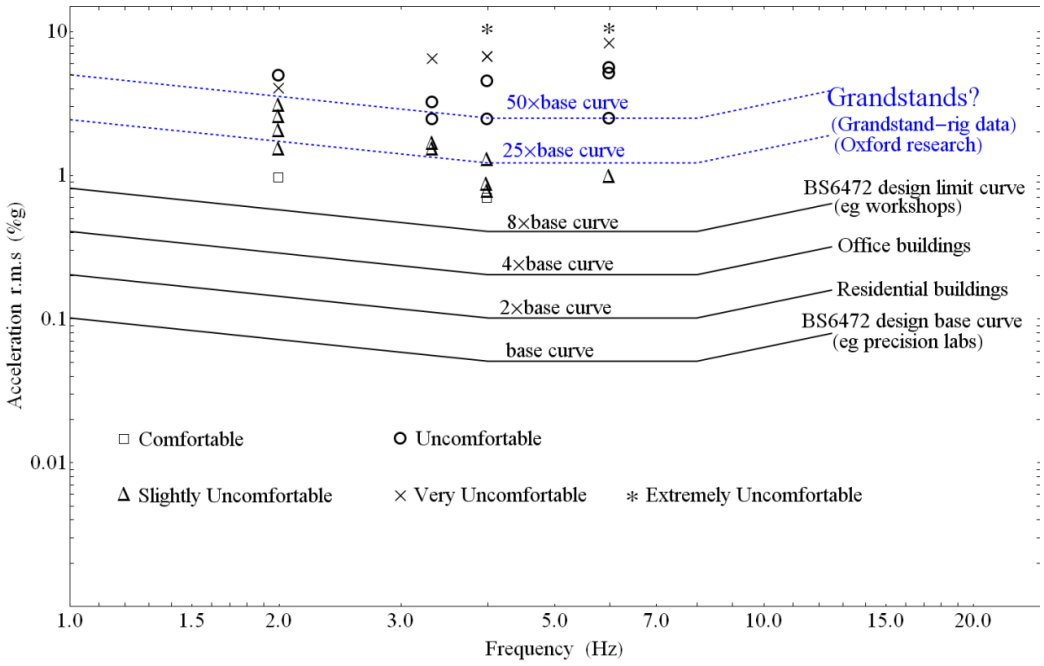

Figure 3.17: Comparison of sitting comfort data with design guidelines of BS6472

Kasperski (2001) obtained higher accelerations at pop-concerts when monitoring two grandstands with natural frequencies of 4.5Hz. The maximum recorded acceleration varied between 6.0%*g* and 19.0%*g* (IStructE, 2001). Earlier, a series of threshold values for human perception of vibrations in grandstands had also been suggested by Kasperski (1996) based on tests carried out on a permanent grandstand. In defining these limits, Kasperski used peak accelerations as a measure of vibration exposure, concluding that vibrations become disturbing at 5%g, unacceptable at 18%g and are likely to induce panic at values exceeding 35%g. However, an evaluation approach based on peak accelerations is not a universal measure of vibration exposure, because, like the RMS measure (see Equation 3.1), it does not take into account the time-varying characteristics of the vibration. The Commentary to the National Building Code of Canada also prescribes acceleration limits of 4%*g*-7%*g* for design for rhythmic activities. IStructE (2008) also recommends values of 3%, 7.5% and 20% g for permanent venues hosting predominantly seated audiences, pop-concerts and extreme events (characterized by jumping), respectively.

Finally, a comparison between Figures 3.16 and 3.17 show that the grandstand data from this study appear below the recommended limits for transportation structures (BS6841) but significantly above the recommended limits for most classes of buildings (BS6472). This suggests that the serviceability limit state for grandstand design lies somewhere between the recommended limits of the two standards.

3.4. Effect of vibration on human-induced forces

Changes in human-induced forces as a result of structural vibration were also observed when selected subjects were bobbing on a static deck compared with those obtained

when the same subjects performed the same movement but on a vibrating deck (Figure 3.18). The vertical axis in Figure 3.18 shows the bobbing force normalized by subject weight. The results show that motion of the supporting surface resulted in the reduction of amplitudes of force impulses (Figure 3.18a), dilation of amplitudes of force impulses (Figure 3.18b), little or no change of force impulses (Figure 3.18c) and secondary lower frequency oscillations (Figure 3.18d). Therefore, in a structural system driven by continuous human loads, the applied forces determine the nature of input forces which causes structural motion. If perceivable, the resulting structural motion in turn has an effect on the input forces applied by the crowd on the structure. This illustrates clearly the interaction or feedback mechanism that exists between human activity on the structure and the resulting motion of the occupied structure. Finally, as in Section 3.3.3 these differences in applied forces can be interpreted as an adjustment of posture or stance leading to different human-structure interaction mechanisms.

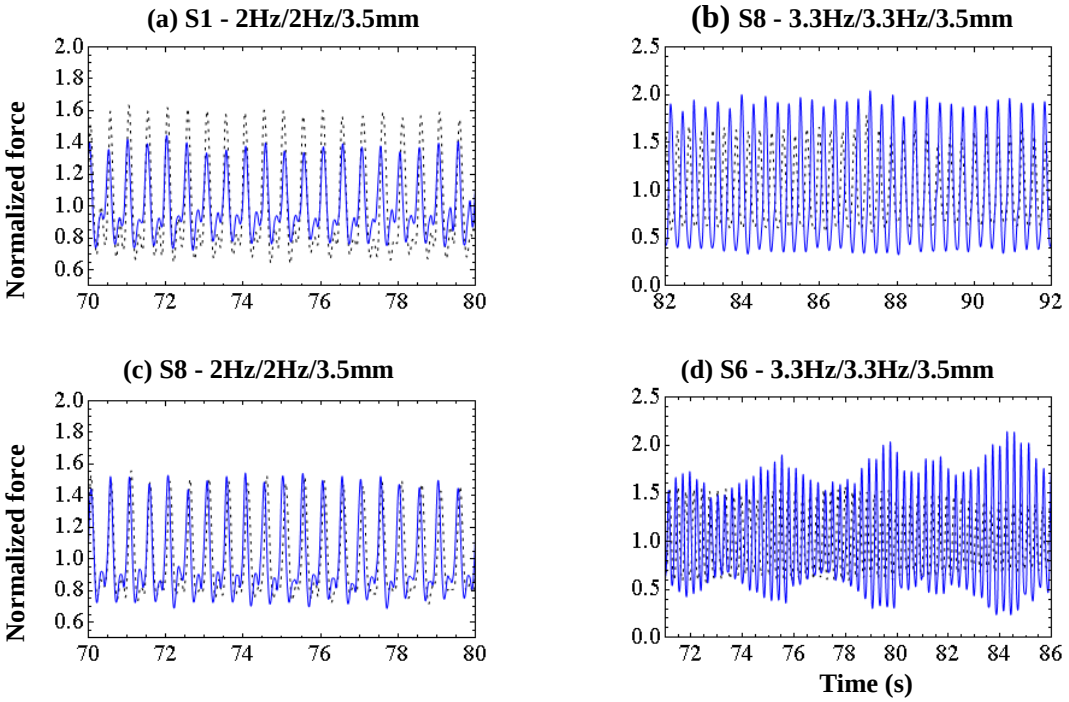

Figure 3.18: Comparison of vertical force wave forms for subjects bobbing on a static deck (broken line) and bobbing at the same frequency but on a moving deck (solid line). Legend above (a) (b) (c) and (d) refer to Subject number - bobbing frequency in Hz/deck motion frequency in Hz/deck motion amplitude in mm

3.5. Conclusions

This chapter has used a controlled laboratory study to investigate changes in the levels of human vibration perception and comfort as a result of a change in the vibration levels of an occupied grandstand rig whose motion could be controlled to simulate a vibrating structure. Graphs presented describe vibration perception and comfort levels of human subjects given a specific movement of the structure and indicated that vibrations are felt long before they are perceived as uncomfortable. This emphasizes the importance of the assessment of human vibration perception and comfort levels in establishing safety criteria. Based on the specifications of BS6472, the acceleration limit at the upper boundary of the "slightly uncomfortable region" was used to identify a design criterion for grandstands as 5 %g RMS. It was also shown that the serviceability data from the current study lies below the recommended limits for transportation structures (BS6841) but significantly above the recommended limits for most classes of buildings (BS6472). This suggested that the serviceability limit state for grandstand design lies somewhere between the recommended limits of the two standards.

The standing data differed from the sitting data indicating that each posture leads to a different human-structure interaction mechanism. Therefore venues which accommodate only a standing audience should be designed differently to venues with a seated audience. Changes in bobbing forces as a result of structural vibration were also observed, namely, dilation of amplitudes of force impulses, constriction of amplitudes of force impulses, little or no change of force impulses and force impulses with lower frequency oscillations. These changes indicate different postures or stance and consequently different human-structure interaction mechanisms.

Chapter 4

4. Horizontal forces and motion generated by swaying and jumping

This chapter reports on tests conducted in the Structural Dynamics Laboratory at the University of Oxford and the Nuffield Orthopaedic Centre Gait Laboratory in Oxford. Many experiments were conducted to measure and characterize horizontal dynamic forces that can be generated by single individuals performing swaying or vertical jumping at various rhythms on a rigid platform in a sitting or standing position. The various analyses of the load measurements are presented in terms of time history wave forms, impulse shapes and frequency spectra. Finally, several experiments were performed to determine the relationship between the side-to-side force and the velocity of the centre of mass of the subject during swaying tests.

4.1. Subjects, experimental procedure and apparatus

Twelve subjects (mean age 27.7 years) were asked to participate in the tests. Basic information about their general state of health was obtained by means of a questionnaire. All subjects were considered to be healthy and with no evidence of disorders of the musculo-skeletal system. Basic information about the mass and gender of the participants is summarized in Table 4.1a.

Table 4.1a: Participant information for horizontal force tests

Subject gender	No. of subjects	Mean mass (kg)	Standard deviation
Male	7	82.07	12.02
Female	5	62.33	15.12

In the first set of tests each individual subject of the 12 total participants was asked to perform side-to-side swaying in a standing position for 60 seconds. This was followed by front-to-back swaying. Later, each subject was asked to adopt a seated position and to repeat the same movements. A metronome set at different rhythms was used to regulate the frequency of the movements. All these tests were performed in the Structural Dynamics Laboratory, Engineering Science Department, University of Oxford (Table B1 Appendix B).

A second set of tests involving 5 subjects from the 12 participants were performed in the Gait Laboratory at the Nuffield Orthopaedic Centre, Oxford (Table B2 Appendix B). In these tests subjects were asked to perform periodic jumping and swaying in either groups of three or two participants (group tests). Furthermore, for these tests, the positions of the centre of mass (back of pelvic region) and the feet during swaying and jumping were also recorded for each subject to in order to evaluate the relationship between the force and the velocity.

One of the main aims of these tests was to capture a wide variety of natural subject movements. As a result the exact manner of swaying side-to-side or back-and-forth was not prescribed. This encouraged each subject to move in a way that was natural to the subject. Two types of equipments were used to collect the two types data (force and position) related to these tests. The equipments are described below.

4.1.1. Force measurement equipment and data acquisition

In all tests conducted, forces were recorded using OR6 (AMTI, USA) tri-axial force plates. The Nuffield Orthopaedic Centre Gait Laboratory in Oxford which was used as a

test venue for the group tests is equipped with three force plates of this type. An additional force plate of the same type was kindly supplied by the Department of Civil Engineering, University of Sheffield and used for tests performed in the Structural Dynamics Laboratory. AMTI force plates are designed to detect forces applied to their top surface. They consist of a top plate connected to a base plate separated by four sensing elements (strain gauges) which produce output signals that are proportional to the forces on the plate.

(a)

Figure 4.1a: Test apparatus: Force plate underneath the feet of a subject at the start of a 'swaying in a standing position' test

Each OR6-AMTI force platform comes with a strain gauge analogue amplifier (MSA-6 Mini-amp) which has a zero facility and additional circuits for converting an analogue output into a digital form. It was designed primarily for use with a computer aided data acquisition system and requires very little user interaction. A typical platform produces six outputs which consist of three orthogonal force components (Fx, Fy and Fz) along the X, Y and Z axes, as well as moments (Mx, My and Mz) about the three axes.

The force plates are calibrated by the manufacturer who provides calibration information. Calibration involves determining the sensitivity of each data channel to all applied load components. The platform's calibration report provided channel sensitivities or calibration matrix in a 6 x 6 matrix. A calibration Matrix *B* is shown below for the platform used (Table 4.1b) for conducting tests in the Structural dynamics laboratory. In this matrix the input load is shown on the left column and the output is represented by the top row, such that an input to channel *i(N,Nm)* is *B(i,j)* times the electrical output *j (micro-volts/volt-of-excitation)*. The main diagonal terms represent the channel sensitivities and the off-diagonal terms are the cross-talk values. It can be seen that the cross-talk terms were negligible and thus channel cross-talk effects did not have any significant effects on the results reported here.

The vertical and horizontal (front-to-back) resonant frequencies of the platform were 1000 Hz and 550 Hz, respectively. These values were well above the frequency range (0-20 Hz) considered in tests. In addition, the platform was capable of measuring forces with very low frequencies (less than 1 Hz) and the amplifier (MSA-6 Mini-Amp) delivered high resolution measurements.

Table 4.1b: Platform calibration matrix B

	VFx	VFy	VFz	VMx	VMy	VMz
Fx	1.4683	-0.0037	0.0100	-0.0047	-0.0064	0.0062
Fy	-0.0112	1.4702	-0.0223	-0.0044	-0.0036	-0.0058
Fz	-0.0009	0.0144	5.7067	-0.0107	0.0001	-0.0002
Mx	-0.0005	0.0007	-0.0079	0.6801	-0.0036	-0.0009
My	0.0008	0.0000	0.0003	0.0040	0.5351	-0.0012
Mz	0.0004	0.0025	0.0006	0.0025	0.0005	0.3158

All force plates were checked for proper calibration by weighing a 10 kg mass at the beginning of each test session. Each force plate had a saturation voltage of 10 V. However, it was possible to manipulate the amplifier gain and excitation voltage such that the saturation voltage is never exceeded in all measurements. In order to obtain good quality data, all force plates used were mounted on a rigid base as prescribed in the guidance provided by the manufacturer. During jumping and swaying in a standing position, the force-plate was mounted on a rigid floor (Figure 4.1a). When multiple force plates were used (i.e. for group tests conducted at the Nuffield Orthopaedic Centre Gait Laboratory) each subject had both feet on a single force plate.

During swaying in a sitting position (Figure 4.1b) the force plate was mounted or sandwiched between an elevated rigid platform and a customized seat designed to resemble a typical grandstand seat (see Figure 4.1c). A foot rest with an adjustable height was provided to accommodate the height of different subjects.

Finally, digital data output from the MSA-6 Mini-amp strain gage amplifier were recorded using data acquisition software (NetForce) from the same manufacture. The software included data processing capabilities and allowed real-time display of time histories and centre of pressure data.

(b)

(c)

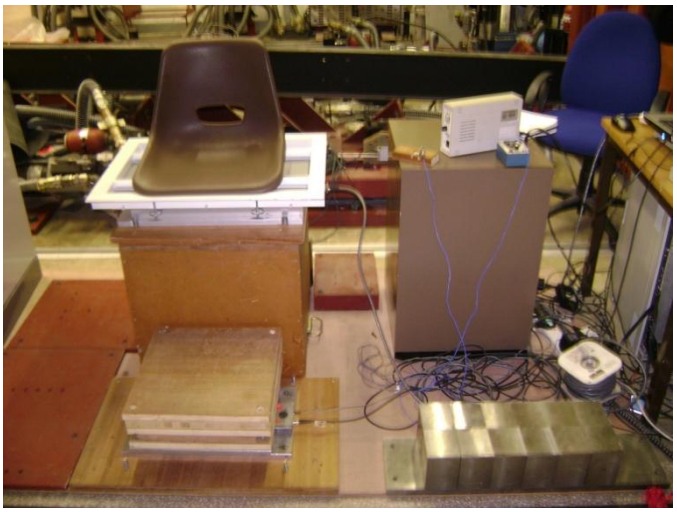

Figure 4.1b&c: Test apparatus (b) Force plate underneath the seat of a subject at start of a 'swaying in a sitting position' test (c) Test seat built to resemble a typical grandstand seat.

4.1.2. Motion measurement equipment and data acquisition

A motion tracker system (Vicon MX, Oxford, UK) operated by the Nuffield Orthopaedic Centre Gait Laboratory in Oxford was used for tests involving position

measurements of selected body parts. The system used was made of twelve high speed, high resolution cameras and reflective markers designed, developed and built specifically for motion tracking (Figure 4.1d). During tracking the markers reflect light that is generated near the cameras lens and the centroid of the marker is estimated as a position within the two dimensional image that is captured.

At the beginning of each test session the system was calibrated by following a procedure which involved placing a calibration frame (a static calibration object used to set the global coordinate system in the capture volume) on a reference position in the lab in the field of view of at least three cameras. The workstation software used to collect data contained configuration entries corresponding to the calibration objects for expressing the position of a tracked object relative to the reference position in the lab. This calibration task was supervised by a senior specialist and clinician who had the necessary technical expertise and extensive experience in operating the system.

(d)

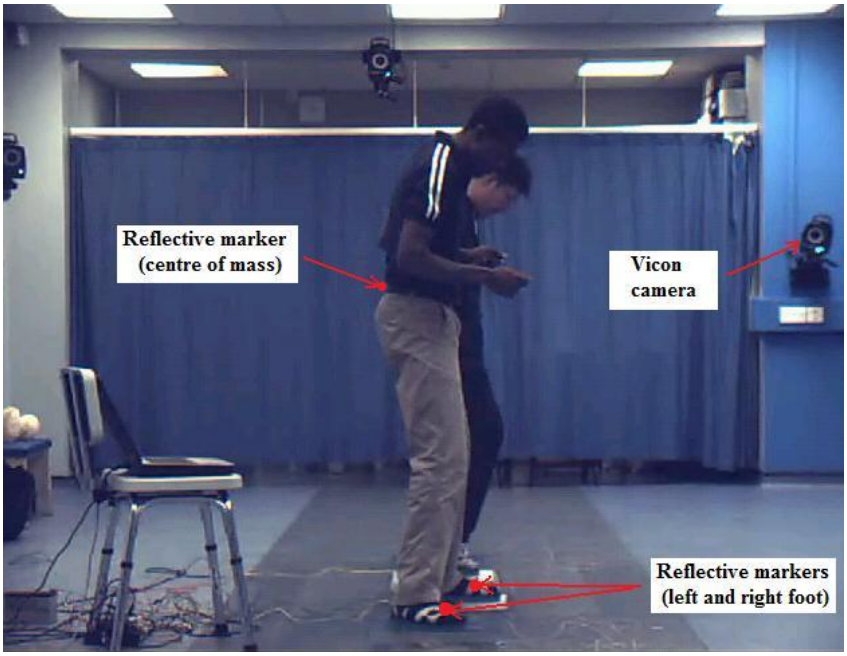

Figure 4.1d: Test apparatus: Motion tracker system

Finally, position data were recorded using software (Vicon Nexus 1.4) produced for motion capture, processing, and analysis by Vicon Systems.

4.1.3. Data handling and analysis

All the data acquisition software used produced output data in CSV (comma separated value) digital format. The data was saved and exported to general processing software packages (Mathematica and Matlab) for further processing and analysis. During processing, the data were digitally filtered to remove recorded time-history forces and motions above 20 Hz in order to focus the analysis on the frequency band of interest (0-10 Hz including higher harmonics). In order to aid data interpretation, various analysis techniques were applied to the filtered data as discussed in the following sections. A notation system of axis was adopted to describe the direction of all horizontal forces as SS or FB for side-to-side and front-to-back forces, respectively. This is shown in Figure 4.1e relative to the x-y basicentric axis system used in BS7085.

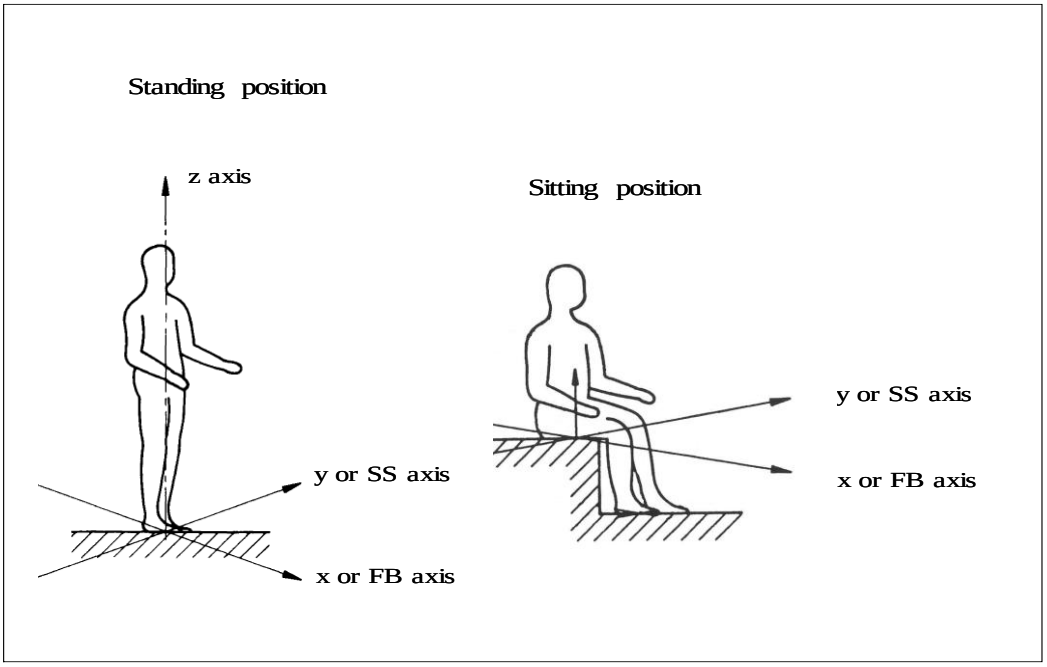

Figure 4.1e: Basicentric axis system used to describe the orientation of forces

4.2. Results: horizontal forces due to swaying and jumping

4.2.1. Time-history wave forms

The force data were plotted to obtain horizontal force time-history graphs which were classified visually and grouped according to dominant and consistent wave form patterns. Each time-history recorded during swaying fell into one of the wave form pattern categories discussed below.

(a) (b)

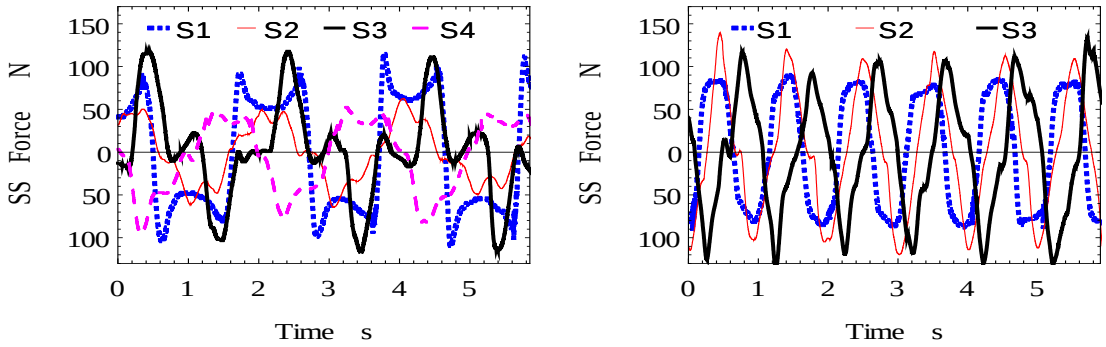

Figure 4.2: Side-to-side swaying at (a) 60 and (b) 120 beats per minute in a standing position.

Figure 4.2a shows types of wave form patterns observed for side-to-side swaying in a standing position for different subjects. Analysis of many individual video clips captured during the tests showed that the shape of each individual's time history profile can be related to each individual's natural preference to wait or adjust his or her movement in response to the next beat. This has been termed the 'subject waiting time preference' (SWTP) or the 'subject waiting time distribution' (SWTD). In Figure 4.2a, for example, it is clear that when swaying at 60 beats per minute, S1 preferred to wait at one turning point of the swaying motion and moved quickly to the other turning point on the call of the next beat and then waited there. S3 did the opposite by always coming back to the vertical or standing still position and waiting there for the next beat to call.

On the other hand, S2 distributed the waiting time throughout the swaying cycle while anticipating the next beat.

The waiting time preference behaviour could have been caused by many factors including how far apart the subject's feet were during swaying. In rare cases the waiting time was a little longer on the same side of motion (S4). All curves, with the exception of S4, are almost symmetrical about the horizontal axis. This means that the dynamic load is very similar regardless of the direction of swaying to the right or to the left. The curves are not smooth (intermediate bumps) due to jerky movements and the wobbling mass of the body at this frequency. However, at high frequencies because each subject now used more muscles to achieve the swaying motion, the rhythm became more natural leading to the smoother curves shown for swaying at 120 b/min. Note that despite the smoothness of the curve, the individual's natural waiting time preference (as shown for swaying at 60 b/min) is still clearly apparent on these curves.

Figure 4.3 shows the wave form patterns obtained for swaying back and forth in a standing position. The same technique as described for side to side swaying can also be used for front to back swaying to explain the differences in the force time-history patterns taking into account the movements the subjects were asked to perform. At low frequencies the dynamic load amplitudes were independent of direction if the SWTD was even throughout each cycle (S1 and S2). Subjects with longer times on the forward or backward tilt led to unsymmetrical peaks (S3). In the majority of cases the dynamic load was larger when the subject moved his or her pelvis forward for two reasons. Firstly, if swaying is achieved by pelvic thrust action with almost straight knees the body becomes stiffer when the pelvis is translated forward and wobbly in the opposite direction. Secondly, if swaying is achieved by bending knees the body can be made

stiffer when the centre of mass moves forward and wobbly in the opposite direction. Force amplitudes were mostly symmetrical for rhythms greater than 120 b/min.

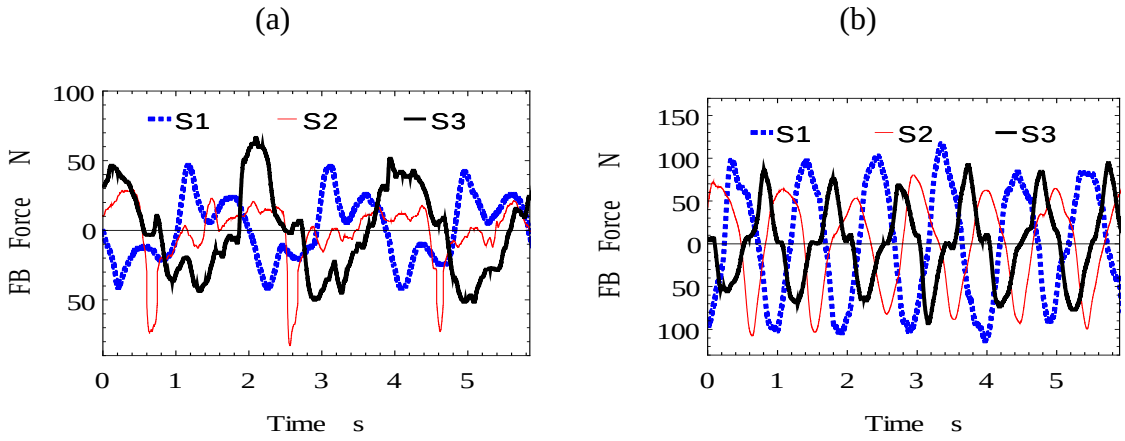

Figure 4.3: Front-to-back swaying at (a) 60 and (b) 120 b/min in a standing position.

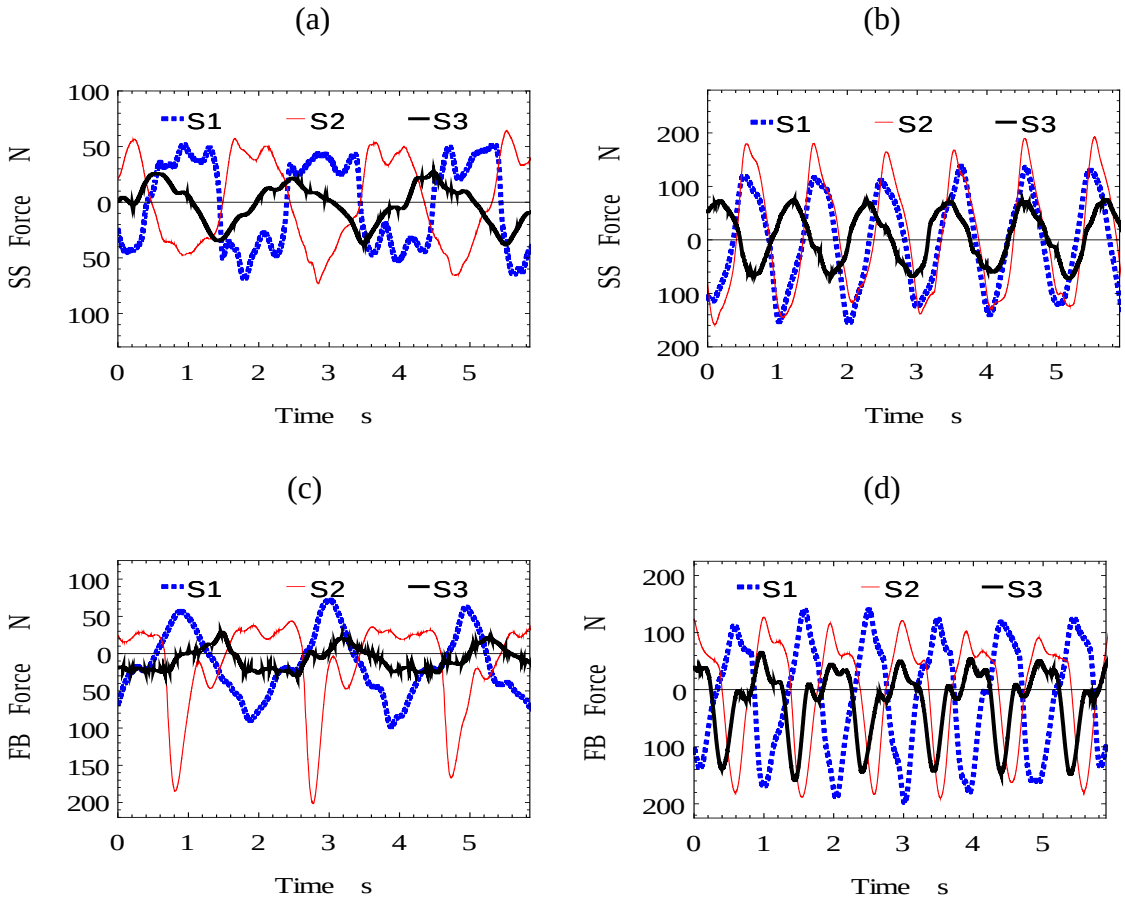

Figure 4.4: Swaying (a, b) side-to-side and (c, d) front-to-back in a sitting position at (a, c) 60 and (b, d) 120 b/min.

Typical force time-histories resulting from side-to-side and front-to-back swaying in a sitting position are shown separately in Figures 4.4a–d. From these graphs it appears

that the shapes of the wave forms were also dependent on the beat frequency and the SWTD. Predictably, force wave forms for side-to-side swaying in a sitting position have the same symmetry characteristics as for side-to-side swaying in a standing position. Similarly, force wave forms for front-to-back swaying in a sitting position have the same symmetry or lack of symmetry characteristics as for front-to-back swaying in a standing position. With the exception of the time-histories for a few of the subjects, the lack of symmetry of the wave forms was characteristic for all frequencies for front-to-back swaying in a standing or sitting position.

Typical horizontal force time-histories for jumping at 2 and 2.5 Hz are shown in Figure 4.5 for the same subject. The shape of the wave forms is significantly different from those of swaying. The waiting time preference for the subject to adjust their motion to the beat is also limited to the contact phase (when both feet of the subject were on the ground) because there is no control of the subject's motion when in the air.

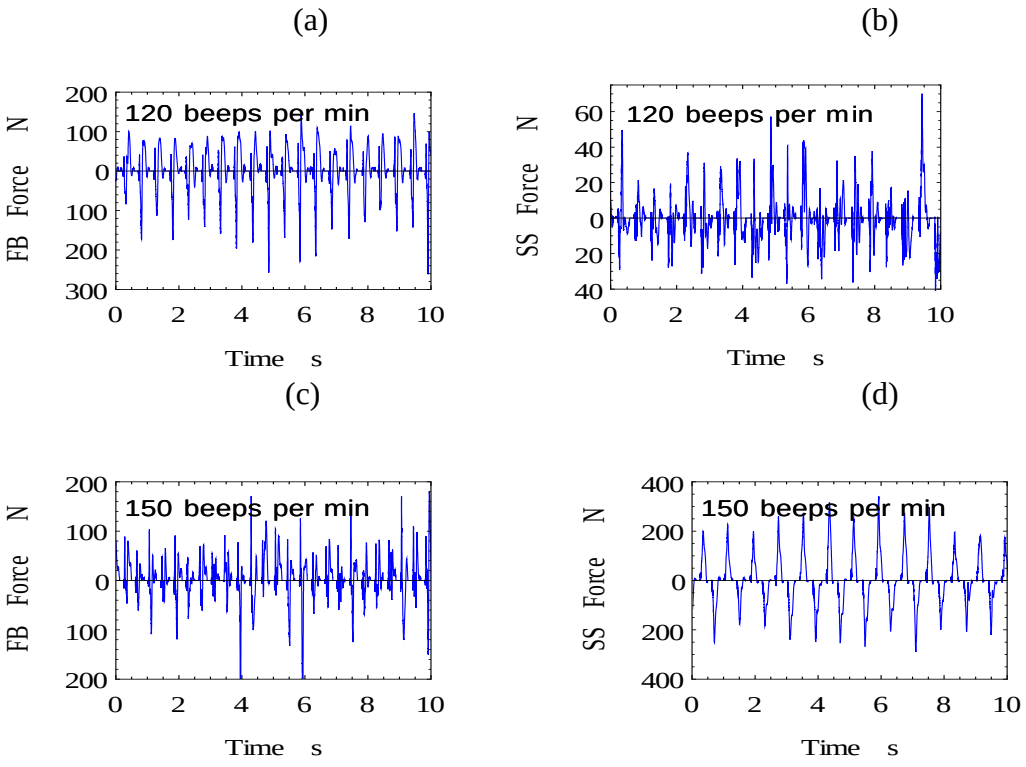

Figure 4.5: Front-to-back (a and c) and side-to-side (b and d) force time-histories due to jumping at 120 and 150 b/min

Wave forms for front-to-back forces due to jumping resembled a train of vertically shifted impulses, some exceeding 400N. Similar wave forms were obtained by Yu (2004). With one exception shown in Figure 4.5d, side-to-side forces were consistently smaller compared to front-to-back forces (Figure 4.5a and c).

4.2.2. Splitting of forces into periodic load impulses

In order to evaluate the dominant shape of the force impulse (Section 4.2.2.1) and the cycle-by-cycle variation of the forcing frequency (Section 4.2.2.2) due to each activity, each force record was separated into individual impulses at periodic intervals as shown in Figure 4.6.

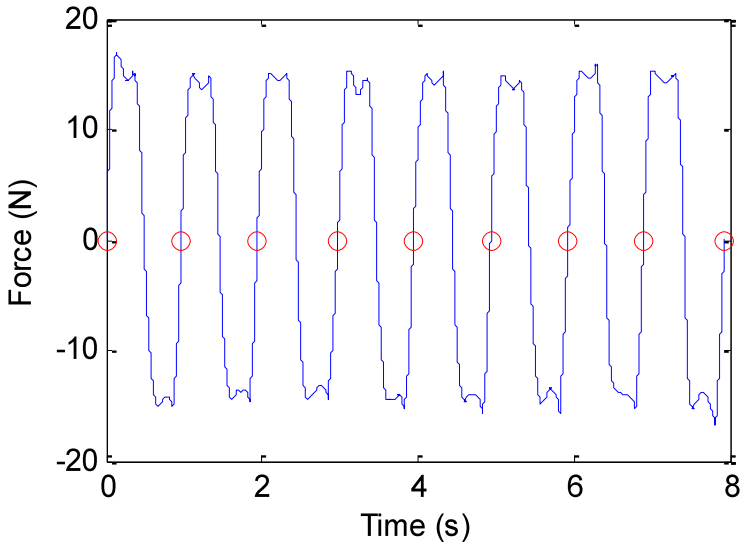

Figure 4.6: Separating individual impulses at periodic intervals

4.2.2.1. Evaluation of mean impulse curves

The separated impulses were plotted in the same window to reveal the dominant shape of the average impulse. The dominant shapes differed depending on the shape of the horizontal force time-history for each individual subject and swaying configuration as

discussed previously. Two types of impulses were observed for side-to-side swaying in a standing position (Figure 4.7).

(a)

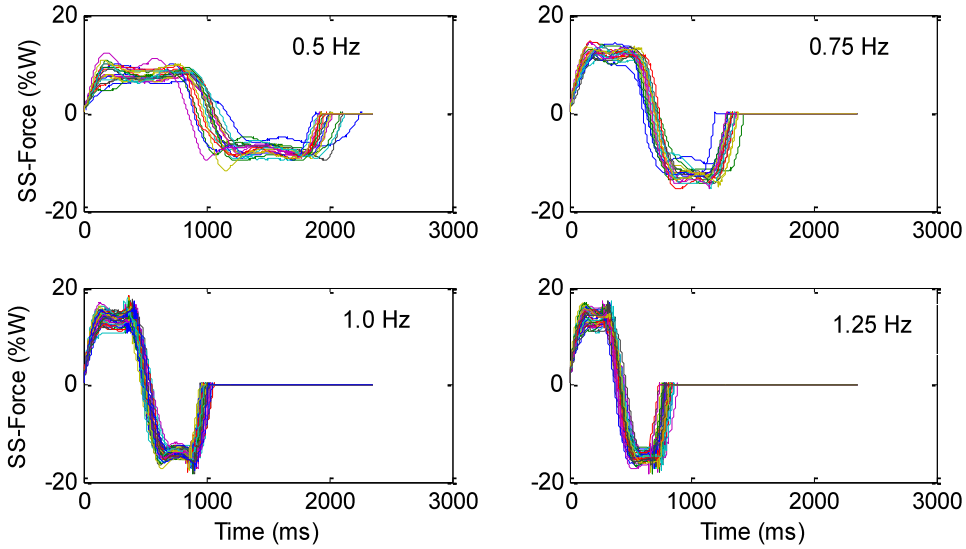

(b)

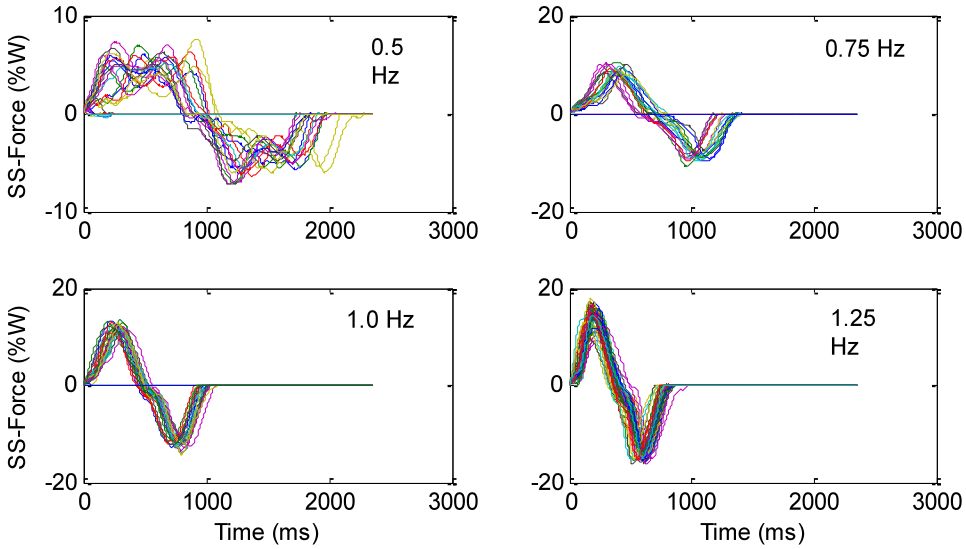

Figure 4.7: (a) Type I and (b) Type II impulses observed for swaying side-to-side in a standing position (0.5-1.25 Hz).

Type II impulses were observed (6 in 12 subjects – see Figure 4.10 in Section 4.2.2.2) when the feet were (visually judged to be) placed closer together while Type I impulses were observed (6 in 12 subjects) when the feet were slightly further apart.

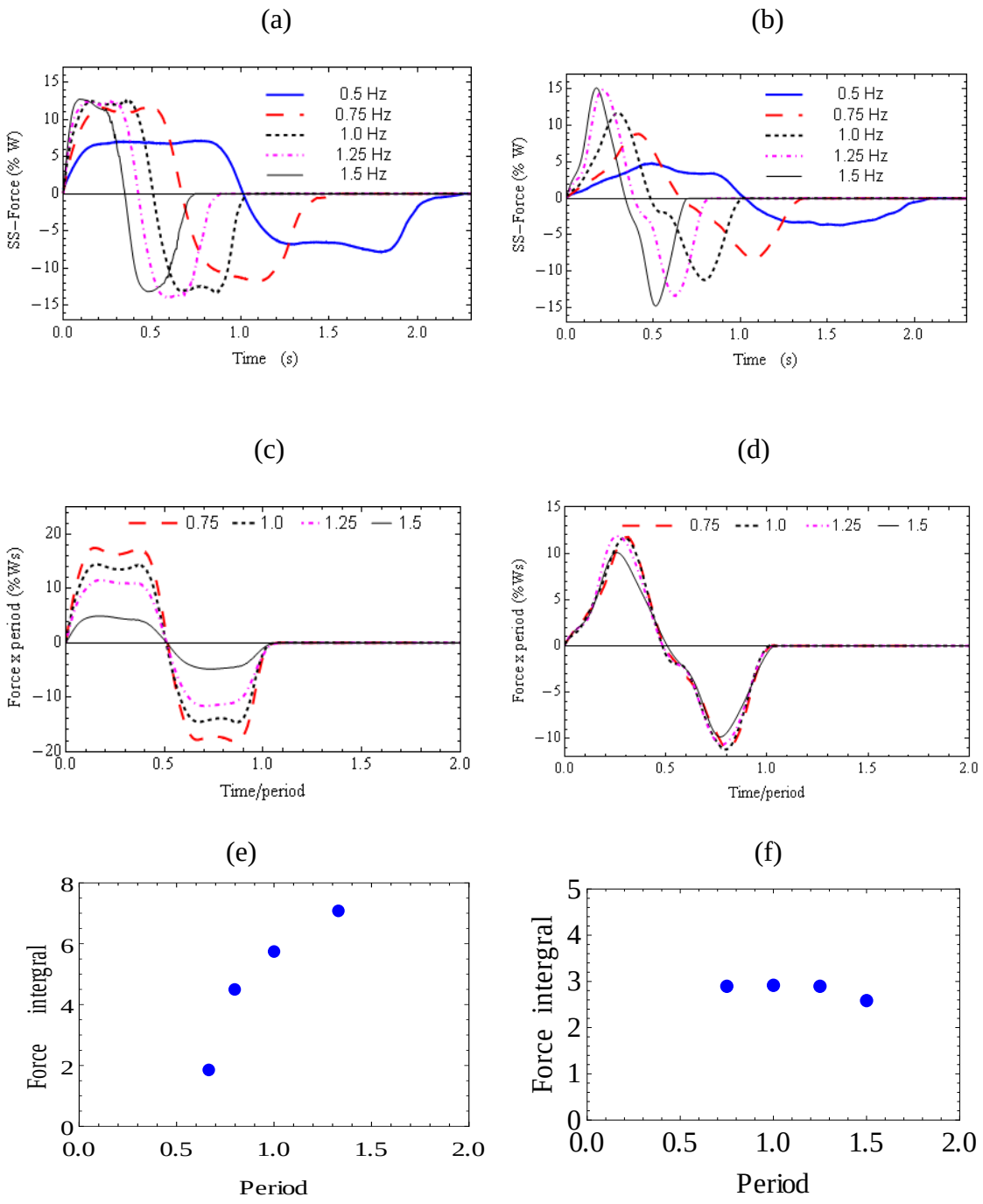

Figure 4.8: (a) Type I and (b) Type II mean curves for horizontal impulses for swaying side-to-side in a standing position, (c, d) parameterized forces and (e, f) integrals of the absolute force value

The separated impulse curves for each subject were added together and divided by the number of cycles to obtain averaged impulse curves at each frequency. Typical results are shown in Figures 4.8a and b for the two types of impulses shown earlier. Note that the results of this evaluation depend on the number of impulse cycles used and that the

mean impulse curve becomes smoother when the number of cycles is increased. Typical mean impulse curves evaluated after the first ten cycles for all 12 subjects can be found in Appendix A, Figure A1. Each curve can be used as a basic shape function for deriving an analytic horizontal load model. For instance it is clear that Type I impulses can be described by a square or rectangular pulse.

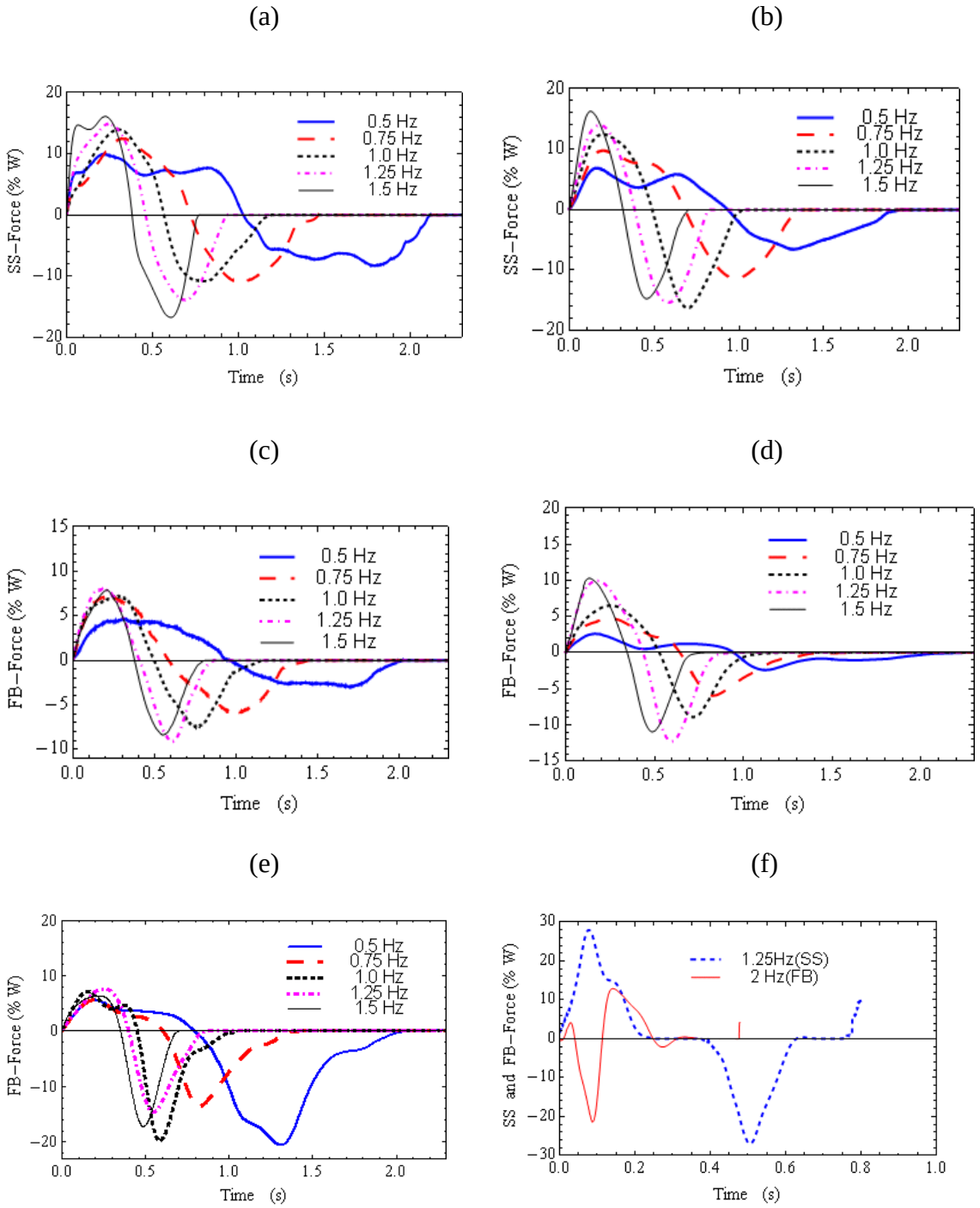

Figure 4.9: Types of horizontal impulses for (a, b) side-to-side sitting, (c, d) front-to-back standing, (e) front-to-back sitting and (f) side-to-side and front-to-back due to jumping at 150 and 120 b/min.

For comparison and to facilitate the evaluation of the impulse response, the mean forces depicted in Figures 4.8a and b were parameterized by scaling the time axis as shown in Figure 4.8c and d (excluding 0.5 Hz). The integrals of the absolute value of the force (defined by the area under the curves) are shown in Figures 4.8e and f.

Similarly, typical mean impulse profiles observed for the other movements are summarized in Figure 4.9. Note that for the particular case shown in Figure 4.9f, jumping at 150 b/min (i.e. 2.5 Hz) produced side-to-side forces at half the beep or jumping frequency. The force time history for this case will be addressed in detail in Section 4.2.5. The whole range of recorded impulses for swaying is shown in Figures A2 to Figure A15 in Appendix A. Typical impulses for jumping at 2 Hz and 2.5 Hz are shown in Figure A16 in Appendix A. Finally, in these analyses periodic zero crossing points (Figure 4.6) were used to isolate the impulses, however, in principle periodic points at any force level can be used.

4.2.2.2. Evaluation of cycle-by-cycle variation of frequency

This analysis dealt with the evaluation of statistical parameters to describe the cycle-by-cycle variation of the frequency of the force time-history. Past experience has shown that it is very important to take into account this effect for the proper evaluation of structural response. Data describing the duration of each force cycle were obtained according to the same analysis procedure involving splitting a force record for each subject as discussed in Section 4.2.2.1. A typical example of force cycles used to evaluate the duration of each cycle is shown below (Figure 4.10) for all 12 male (M) and female (F) subjects.

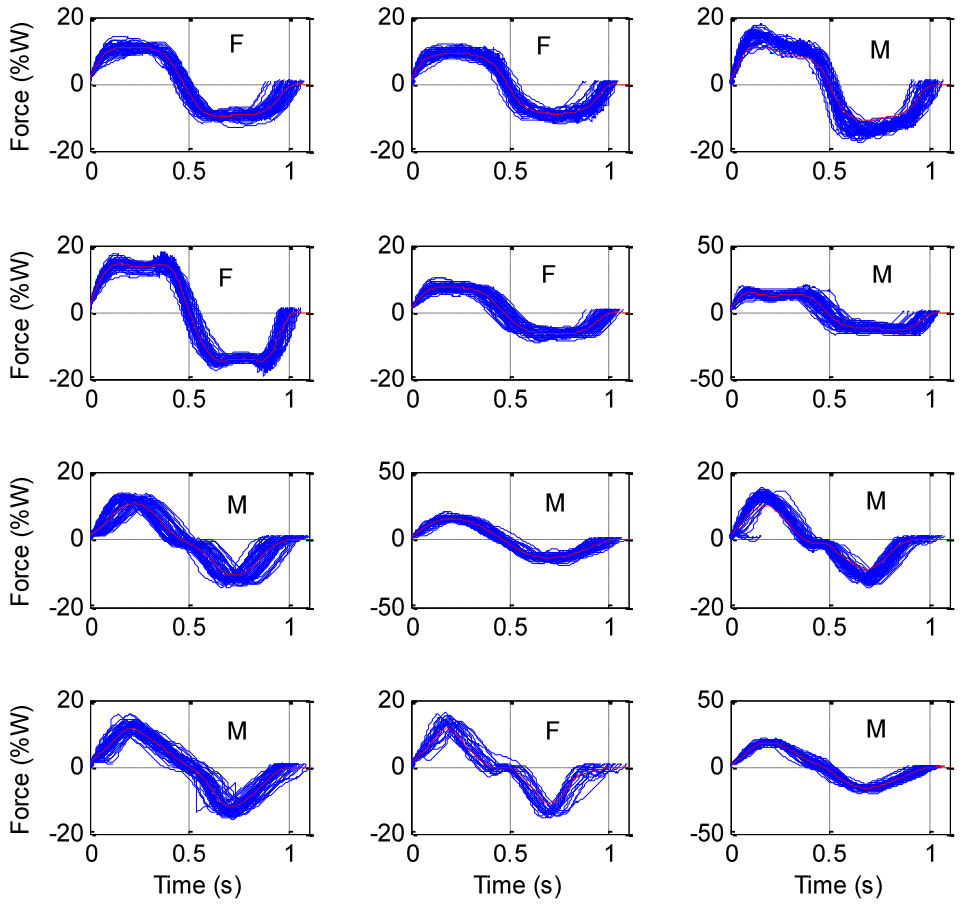

Figure 4.10: Force cycles separated to evaluate cycle durations (side-to-side standing sway)

Each time duration data (T_i for the i^{th} cycle) was inverted to obtain the corresponding frequency using the expression:

$$f_i = 1/T_i \tag{4.1}$$

Normalized histogram curves showing the statistical distribution of the frequency data and the relevant parameters is depicted in Figure 4.11 for the 0.5, 0.75, 1.0, 1.25 and 1.5 Hz swaying frequencies considered. Each curve shown represents measured force frequencies due to swaying at a single beep rhythm after the data has been combined for

all 12 subjects. Figure 4.11 shows that the frequency (f) has a normal distribution with a mean frequency (μ) and a standard deviation (σ). The data for vertical jumping at 2 and 2.5 Hz is summarized in Table 4.2.

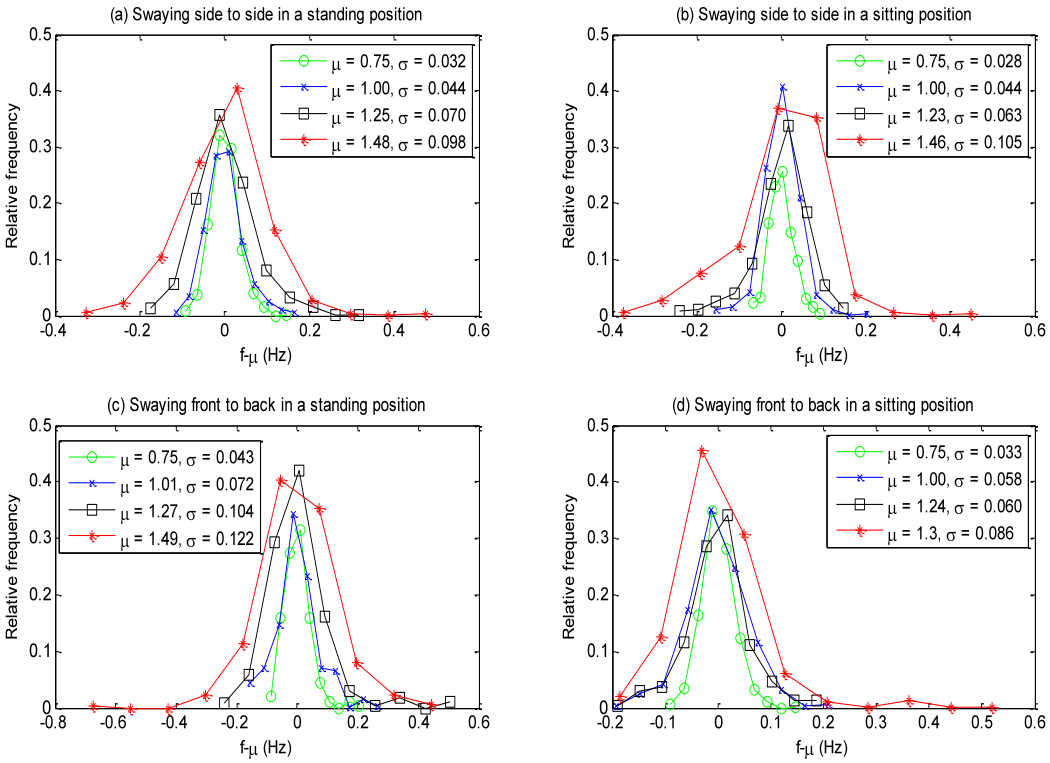

Figure 4.11: Cycle-by-cycle variation of force frequency for swaying at different beep frequencies

Table 4.2: Cycle-by-cycle variation of force frequency for jumping at 2 and 2.5 Hz

Frequency of vertical jumping (Hz)	Mean frequency of FB force (Hz)	Standard deviation (Hz)
2.0	1.990	0.102
Frequency of vertical jumping (Hz)	Mean frequency of SS force (Hz)	Standard deviation (Hz)
2.5	1.254	0.0315

4.2.3. Splitting of load impulses into sub-pulses

These analyses deal with the determination of the mean force component (Section 4.2.3.1) acting in different principal directions (right, left, front or back) during swaying or jumping and the cycle-by-cycle variation of the mean force component (Section 4.2.3.2).

Forces were resolved into principal directions by splitting each force record into sub-pulses where each sub-pulse contained positive or negative forces only. To achieve this, the same zero crossing procedure used previously and illustrated in Figure 4.6 was followed except that instead of splitting the force at periodic intervals, here the force was split further into sub-pulses where each sub-pulse contained positive or negative forces as illustrated in Figure 4.12. Resolving force components this way made the evaluation of the mean force in each direction possible. Note that if the force in a cycle is not separated into positive and negative force components before the evaluation of the mean force, the presence of both negative and positive forces in one cycle would lead to an undesirable situation of a zero mean force (or a mean force that is very close to zero).

Tuan & Saul (1985) also characterized forces in different directions separately. Here a force is defined as positive if it acts to the right (for swaying side-to-side) or front (for swaying front-to-back) and defined as negative for the reverse movements (Figure 4.12). In cases where absolute magnitudes have been used the directions are explicitly specified.

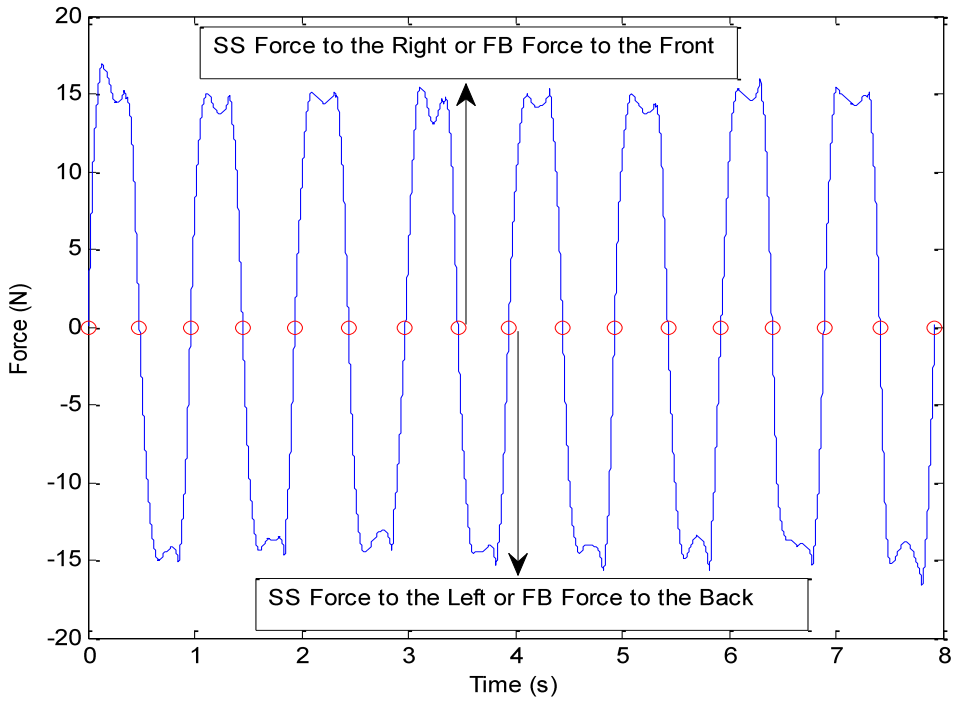

Figure 4.12: Separating forces into sub-pulses to define forces acting in different directions

4.2.3.1. Evaluation of mean force of sub-pulses

Examples of side-to-side forces due to swaying in a standing position that have been separated into sub-pulses containing forces to the right or left, including the evaluation of the mean force in each direction are shown in Figures 4.13a and b, respectively. The sub-pulse mean force for the i^{th} cycle was calculated using the equation:

$$\overline{F_i} = \frac{1}{n}\sum_{k=1}^{n} F_k \qquad (4.2)$$

where n is the total sample size or the number of discrete elements in the sub-pulse force data F.

Thus the total sub-pulse mean force in each direction (represented by each horizontal line in Figures 4.13 a&b) for subject *s* is given by:

$$\overline{\overline{F_s}} = \frac{1}{m}\sum_{i=1}^{m}\overline{F_i} \qquad (4.3)$$

where m is the total number of complete cycles in the recorded time history data and $\overline{F}$ retain the previous meaning (Equation 4.2).

(a)

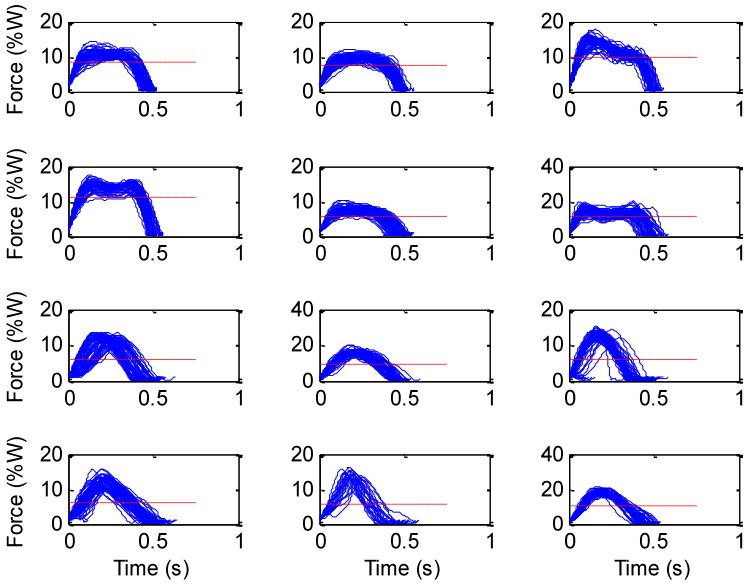

(b)

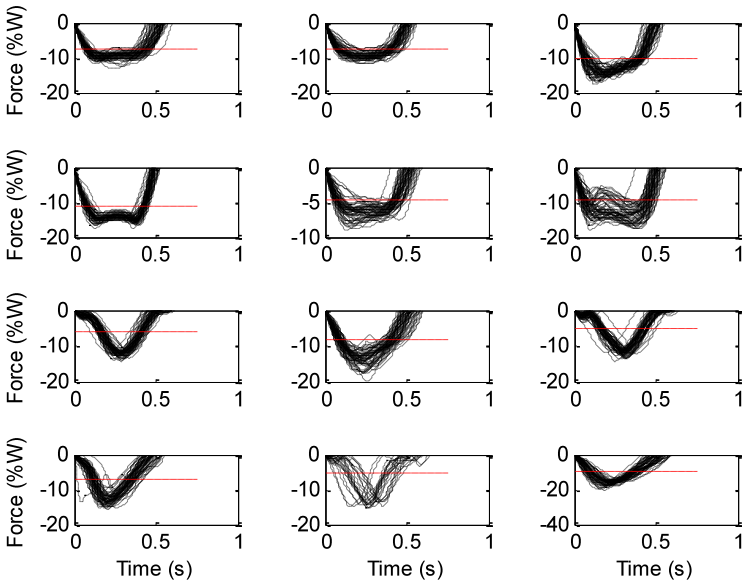

Figure 4.13: Examples of (a) right & (b) left force sub-pulses due to swaying side-to-side (standing)

Further examples are included in Appendix A to illustrate typical separation of front-to-back forces into sub-pulses containing forward and backward forces due to swaying front-to-back in a sitting position (Figures A17 and A18).

The mean forces (as a percentage of body weight) evaluated for each direction of swaying and for each frequency for all twelve subjects are summarized in Figure 4.14. The solid (red) line and broken (blue) line of the upper two graphs represent the mean force to the right and left (respectively) for swaying side-to-side. The solid (red) line and broken (blue) line of the lower two graphs represent the mean force to the front and back (respectively) for swaying front-to-back. It is evident that side-to-side forces were symmetrical while front-to-back forces lacked symmetry, reflecting the lack of symmetry of the musculo-skeletal system of the human body in this direction.

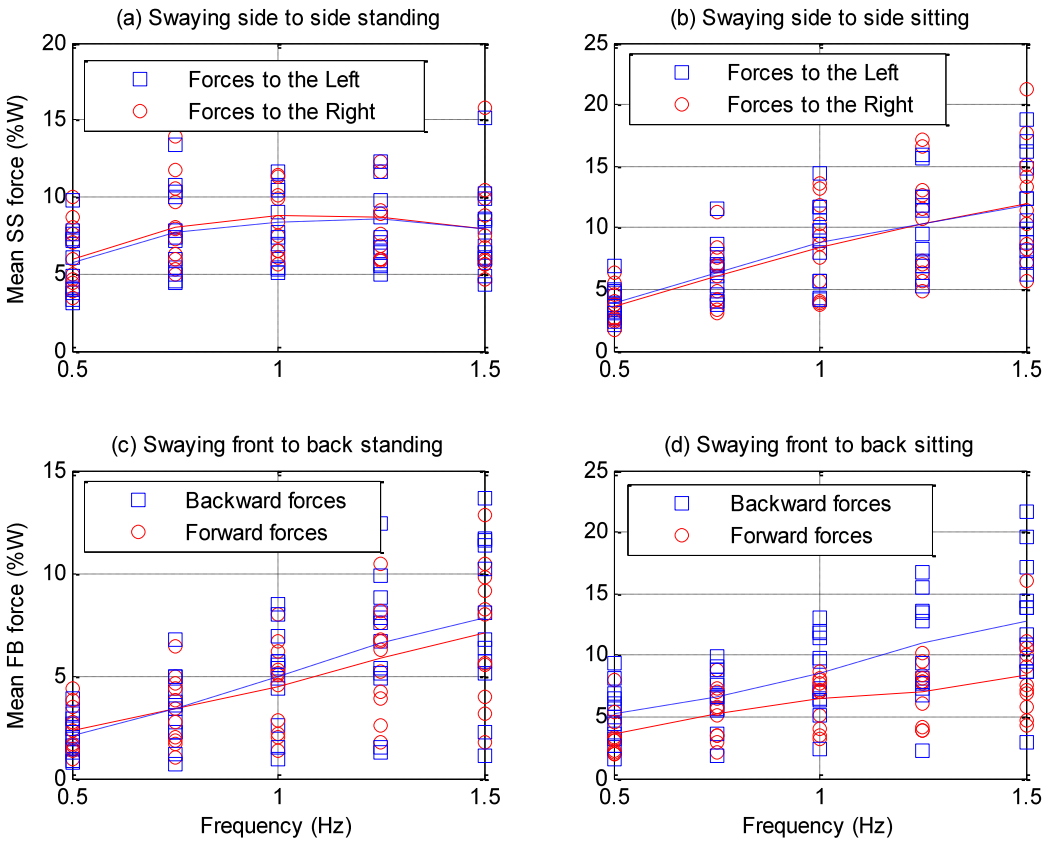

Figure 4.14: Mean sub-pulse forces evaluated for all 12 subjects

4.2.3.2. Evaluation of cycle-by-cycle variation of mean force of sub-pulse

This section presents the evaluation of statistical parameters for describing the cycle-by-cycle variation of the mean force for each sub-pulse. The analysis procedure is similar to that discussed in the previous section (Section 4.2.3.1) except that the focus is on the statistical distributions (and their parameters) of the cycle-by-cycle variation of the sub-pulse mean force. The sub-pulse mean force for a given cycle *i* is given by Equation 4.2.

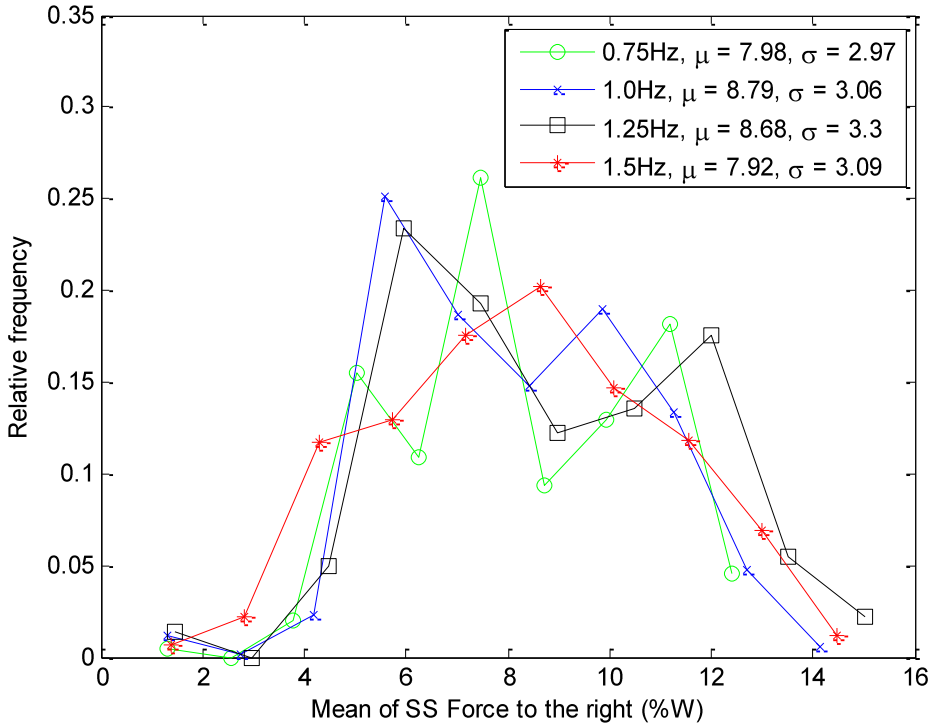

Figure 4.15: Typical cycle-by-cycle variation of right sub-pulse mean force for swaying side-to-side in a standing position at different beep frequencies

Typical normalized histogram curves showing the cycle-by-cycle variation of the sub-pulse mean force to the right due to swaying side-to-side in a standing position at different beep rhythms is depicted in Figure 4.15. Similar data is summarized in Table 4.3 for a typical subject performing vertical jumping at 2 and 2.5 Hz. Each curve in Figure 4.15 represents data (which has been evaluated and combined for all 12 subjects) due to swaying at a single beep rhythm. The curves show that the mean force has a

normal distribution characterized by a mean (μ) and a standard deviation (σ). However, some degree of skewing and multiple peak behaviour are also evident in some curves. The rest of the data for swaying tests are provided in Tables B3-B6 of Appendix B.

Table 4.3: Cycle-by-cycle variation of sub-pulse mean force for jumping at 2 and 2.5 Hz

Frequency of vertical jumping (Hz)	Mean FB force to the front (%W)	Standard deviation (%W)	Mean FB force to the back (%W)	Standard deviation (%W)
2.0	6.905	2.006	7.7075	2.04
Frequency of vertical jumping (Hz)	Mean SS force to the right (%W)	Standard deviation (%W)	Mean SS force to the left (%W)	Standard deviation (%W)
2.5	7.438	2.468	7.340	2.413

4.2.4. Frequency spectra and maximum magnitude trends

The frequency domain spectrum of the horizontal force at each beep frequency was obtained by evaluating the fast Fourier transform of each time-history record using the FFT function in Matlab. This section presents graphs for typical force spectra resulting from this evaluation. An analysis of maximum spectral magnitudes (peaks) at the fundamental and higher harmonics was also conducted to identify trend lines or curves which can be used to interpolate data where measurements were not performed. Separate graphs and tables are presented for this analysis. The maximum spectral magnitudes were extracted from each force spectrum by using a specific algorithm (written in Matlab) which performed a search around the fundamental and higher harmonics of the beep frequency. The width of the search interval could be varied to ensure correct magnitudes and locations were picked by the method.

4.2.4.1. Swaying

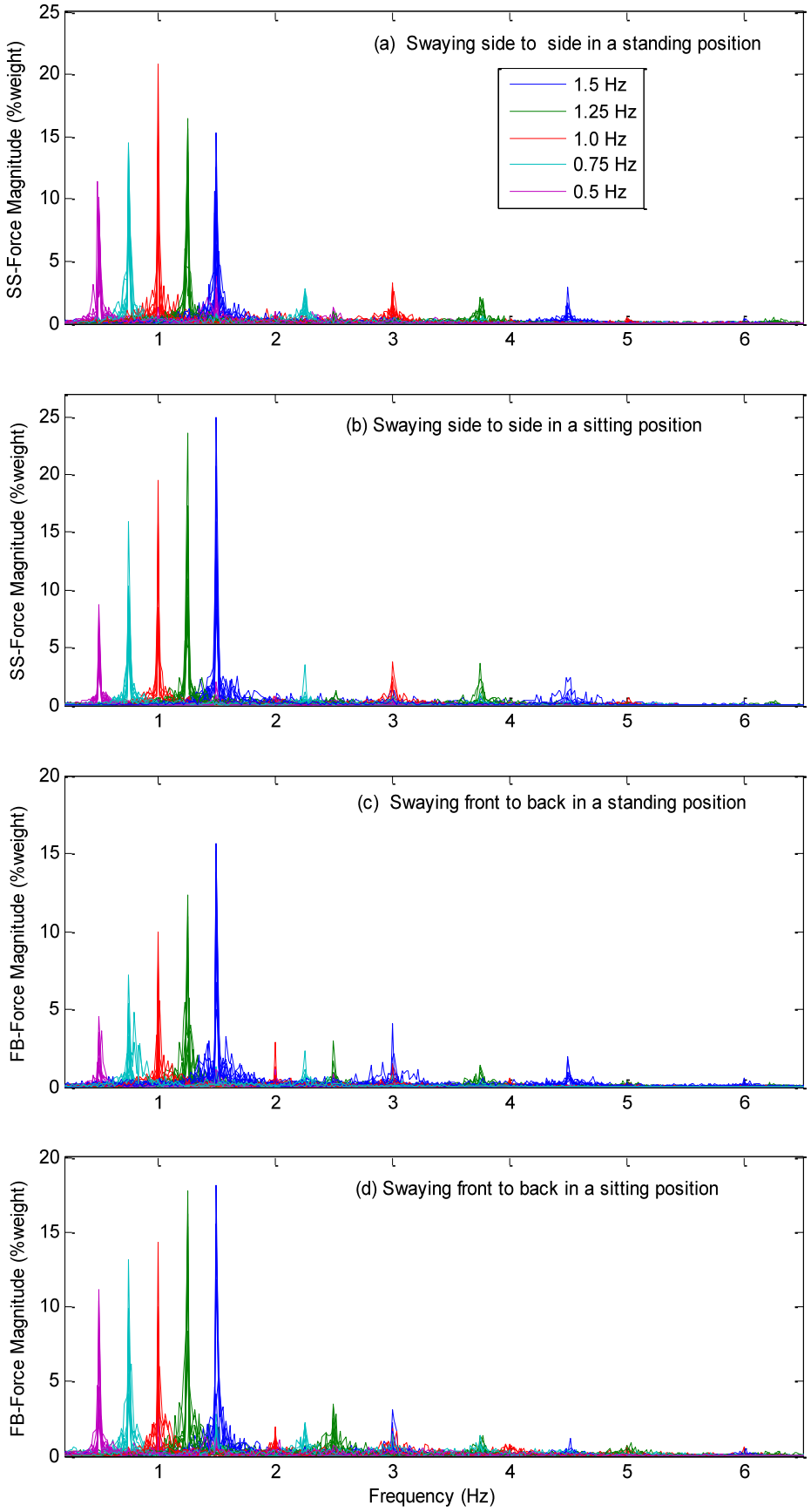

Figure 4.16: Force spectra due to swaying in different positions and directions

Figure 4.16 shows graphs of the swaying force spectra for all subjects. As expected, there is a spread of energy around each harmonic indicating the inability of the subjects to achieve perfectly periodic action.

The maximum spectral magnitudes (peaks) at the fundamental and higher harmonics of the force were extracted using the procedure explained in the introductory section (Section 4.2.4) and plotted separately (Figures 4.17 and 4.18). The statistical parameters associated with the maximum spectral magnitudes at different harmonics are also provided in Tables B7- B10 of Appendix B.

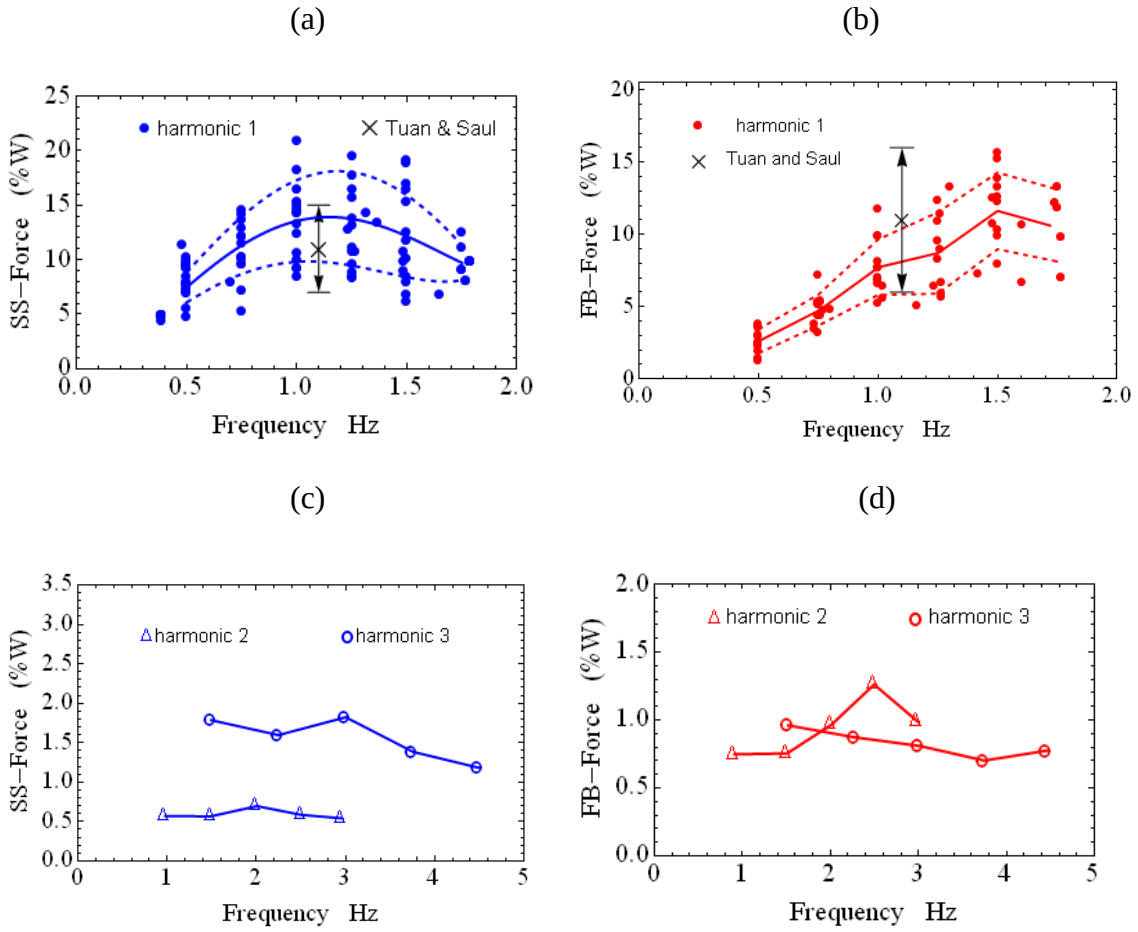

Figure 4.17: Force magnitudes for swaying in a standing position shown at (a)1st, (c) 2nd and 3rd harmonics for side-to-side; and (b) 1st and (d) 2nd and 3rd harmonics for front-to-back

Each point (solid circle) in the upper graphs of Figures 4.17 and 4.18 represents the magnitude of the horizontal forces as a percentage of the subject's body weight at the fundamental swaying frequency (first harmonic). It is clear that the magnitude of the horizontal force varies substantially with frequency as shown by the superimposed trend lines representing the mean with upper and lower standard deviation.

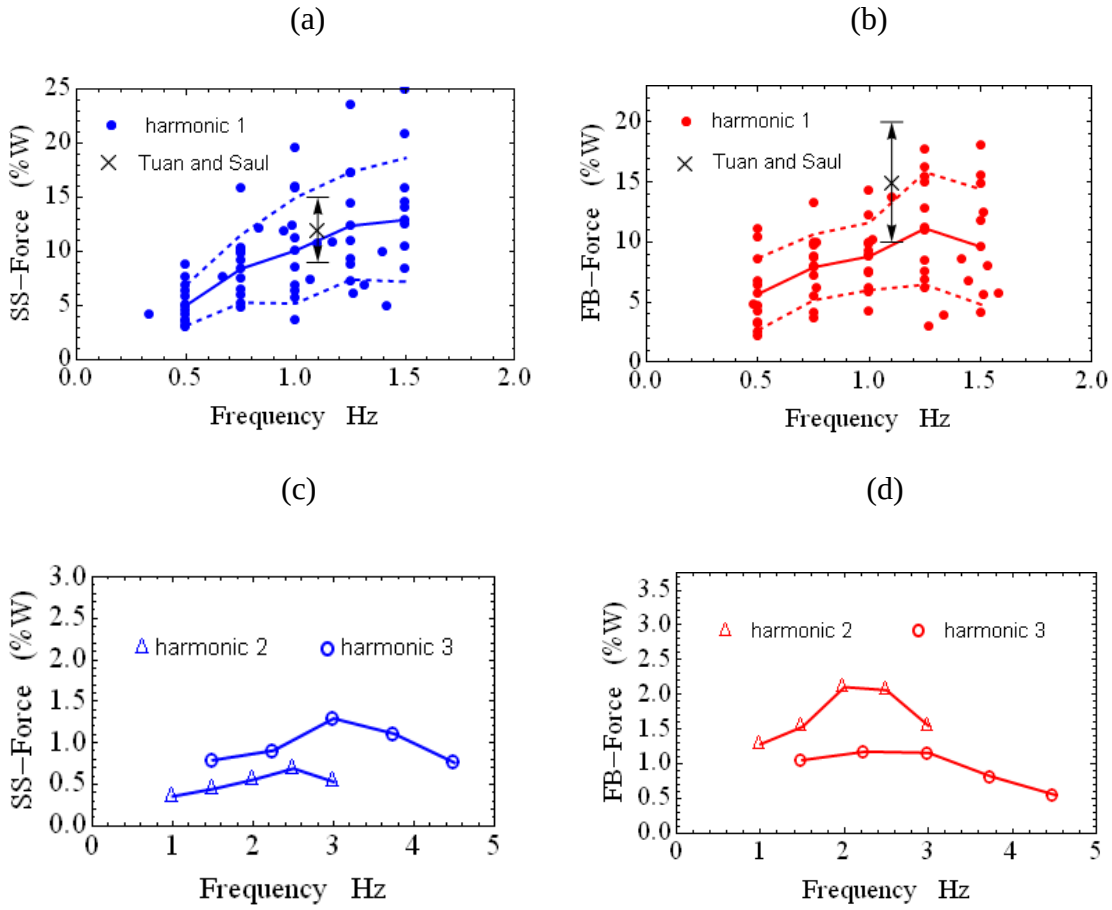

Figure 4.18: Force magnitudes for swaying in a sitting position shown at (a)1st, (c) 2nd and 3rd harmonics for side-to-side; and (b) 1st and (d) 2nd and 3rd harmonics for front-to-back

The measurements by Tuan & Saul (1985) (made at a single frequency) are superimposed on each graph for comparison. For side-to-side forces the mean of their results lie inside the standard deviation of these results (Figure 4.17a and 4.18a) suggesting some agreement. However, the overlap is clearly skewed for front-to-back forces (Figure 4.17b and 4.18b). This may be due to different experimental conditions

and/or the manner of swaying, for example, a gender difference. In this study it was noted that females, particularly, recorded lower forces for front-to-back swaying in a standing position and preferred executing this movement by lowering their knees. Males, on the other hand, achieved the same movement by simply rocking their pelvis back and forth with almost straight knees.

As mentioned previously, Yao *et al*. (2005) and Yu (2004) investigated side-to-side swaying (in a standing position) on a flexible platform and observed a 'force-drop out' whenever the swaying frequency was near the platform frequency (see Section 2.2.1.2). Figure 4.17a shows that no 'force-drop out' effect resulted from performing the same activity on a rigid platform. This indicates that swaying on a rigid platform is different from swaying on a flexible platform. Yu (2004) reported force magnitudes for swaying frequencies up to and beyond 3 Hz. Conversely, Yao *et al*. (2005) presented force magnitudes for swaying frequencies up to 2 Hz as they found swaying at frequencies beyond 2 Hz difficult to perform. For swaying on a rigid platform as addressed here, swaying at frequencies beyond 2 Hz was also found to be very difficult to perform.

It is important to note that the two types of force impulses for swaying side-to-side in a standing position mentioned earlier (see Figure 4.7a&b) had similar frequency spectra (both were dominated by the first and third harmonics). This is despite the significant difference in the shape of their waveforms.

Figures 4.17 & 4.18 both show that there was a significant degree of inter-subject variability in the measured force at each frequency. In the side-to-side direction, there is a clear peak in the force due to swaying in a standing position near 1 Hz (Fig 4.17a). For the same movement in a sitting position a definite peak was not reached although the

graph suggests that it was about to occur at just over 1.5 Hz (Fig 4.18a). Swaying beyond this frequency in a sitting position became uncomfortable. For the front-to-back direction, there are clear peaks near 1.5 and 1.3 Hz (Fig 4.17b & 4.18b) and further peaks (although not so distinct) near 1 and 0.7 Hz for swaying in a standing and sitting position, respectively.

Incidentally, peaks in the front-to-back force due to swaying in a sitting position occur near the resonant modes of the apparent mass responses of a seated human body during exposure to front-to-back whole body vibration. For example, Nawayseh & Griffin (2005) suggested a mode around 1 Hz and another mode between 1 and 3 Hz. The lower graphs (c) and (d) of Figures 4.17 and 4.18 show the magnitude of the force at higher harmonics averaged over all 12 subjects. For all side-to-side forces the magnitude at the third harmonic is larger than the magnitude at the second harmonic. The latter is almost negligible. The force magnitude is larger at the second harmonic than at the third harmonic for most front-to-back forces.

The following fourth order polynomial was proved to be adequate for approximating the mean, the upper and lower standard deviations of the significant harmonics for the data presented in Figures 4.17 and 4.18 and further summarized in Tables B7- B10 of Appendix B.

$$A_n(nf) = a_1 nf + a_2 n^2 f^2 + a_3 n^3 f^3 + a_4 n^4 f^4 \qquad (4.4)$$

where A is the magnitude (%W), f is the frequency ($0.5 < f < 1.5$ Hz), $n = 1$ or 3 for evaluating the magnitude at the 1st harmonic or 3rd harmonic (respectively) for side-to-

side swaying; and $n = 1$ or 2 for evaluating the magnitude at the 1st harmonic or 2rd harmonic (respectively) for front-to-back swaying. The polynomial coefficients a_1 to a_4 have different values for different swaying configurations. The values are listed in Appendix B, Tables B11, B12, B13 and B14. Tables B7- B10 of Appendix B or Equation 4.4 can be used to obtain additional force magnitudes at intermediate frequencies intervals that were not considered in the tests through interpolation.

4.2.4.2. Jumping

Figure 4.19 shows typical horizontal force spectra for a male subject performing vertical jumping at 2 Hz (120 b/min) and 2.5 Hz (150 b/min). The front-to-back force (Figure 4.19a), has the highest magnitude at the second harmonic, not the first. Yu (2004) observed the same behaviour for jumping frequencies at 2 Hz, 2.25 Hz and 2.75 Hz.

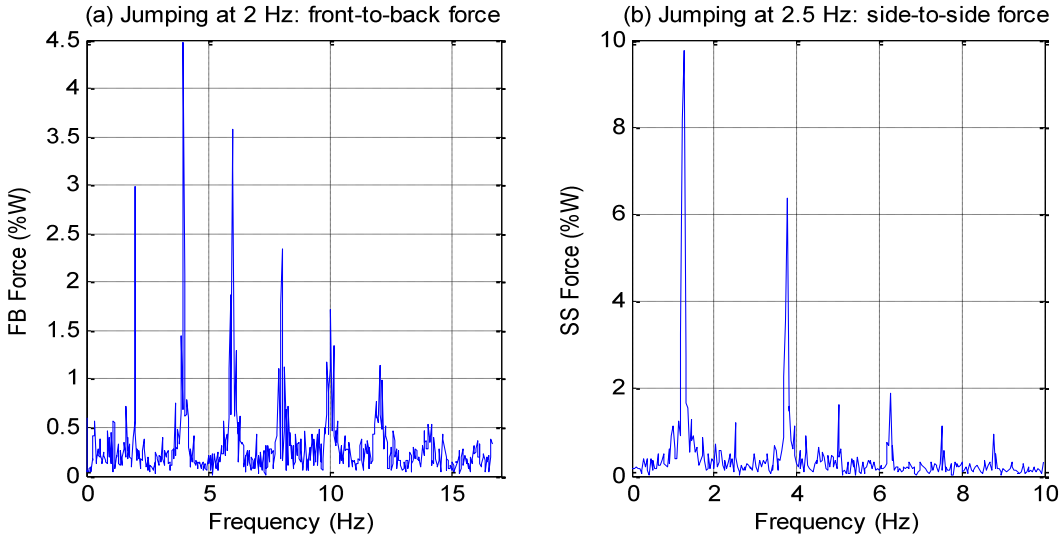

Figure 4.19: Horizontal force spectra due to jumping at 2 and 2.5 Hz

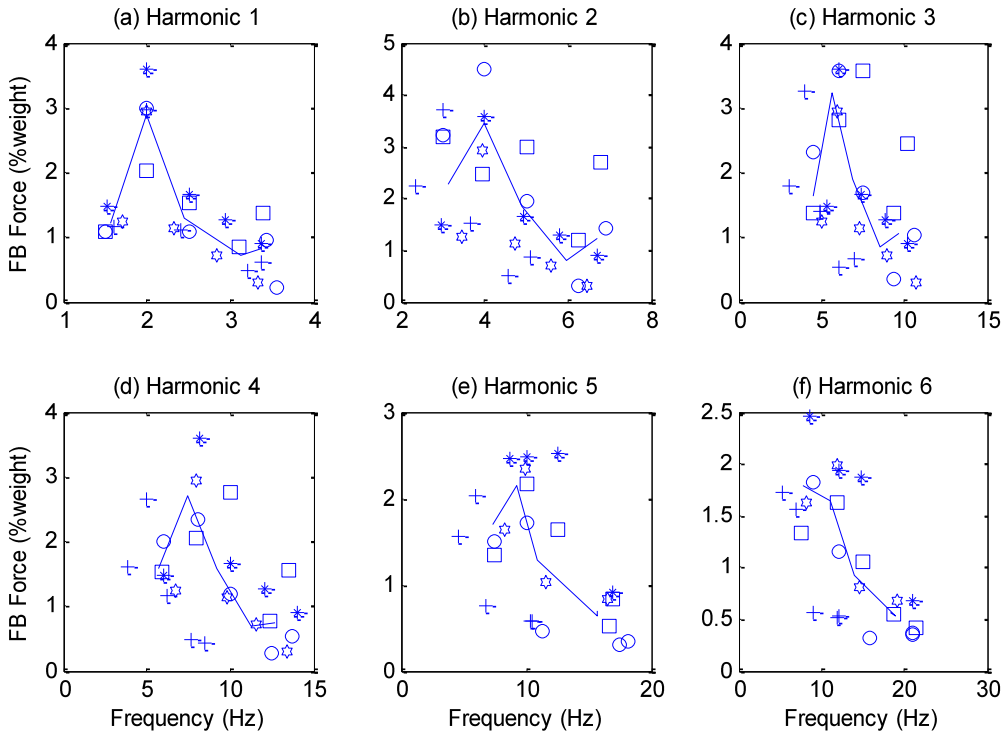

Figure 4.20: (a) Front-to-back force magnitudes measured during jumping

The maximum spectral magnitudes (peaks) for the first 6 harmonics of the side-to-side and front-to-back forces due to vertical jumping were extracted and plotted for each of the 5 subjects who participated in this test series (Figures 4.20a&b). The solid line represents the average magnitude for the 5 subjects. The statistical parameters associated with the maximum spectral magnitudes for the first four harmonics are provided in Table B15 of Appendix B for front-to-back forces. The average magnitudes of the front-to-back forces were nearly equal for the first four harmonics (Figure 4.20a).

The fundamental force occurred at the same value as the jumping frequency. Unlike swaying, the force at higher harmonics was still significant even at the sixth harmonic. Yu (2004) also presented magnitudes of the first 6 harmonics to show the significance of higher harmonics. In fact the spectrum resembles a train of impulses with almost similar magnitudes for the first four harmonics. This is expected because, as pointed out earlier (Figure 4.5a), its time-history contains very sharp impulsive loads resembling a

train of scaled unit impulses. The frequency domain spectrum of the latter also resembles a train of impulses.

Considering side-to-side forces (Figure 4.20b), one subject produced forces that were significantly larger than those of the other subjects when performing vertical jumping at 2.5 Hz (150 b/min). The force spectrum for this case was shown earlier in Figure 4.19b. Furthermore, note that in this case the spectrum has significant peaks at frequencies that are half the jumping frequencies (half-harmonics). This is the reason force magnitudes at half-harmonics (hh force) have been included in Figure 4.20b and Table B15 of Appendix B. Here a half-harmonic (hh) frequency refers to a frequency that is one-half of the jumping frequency.

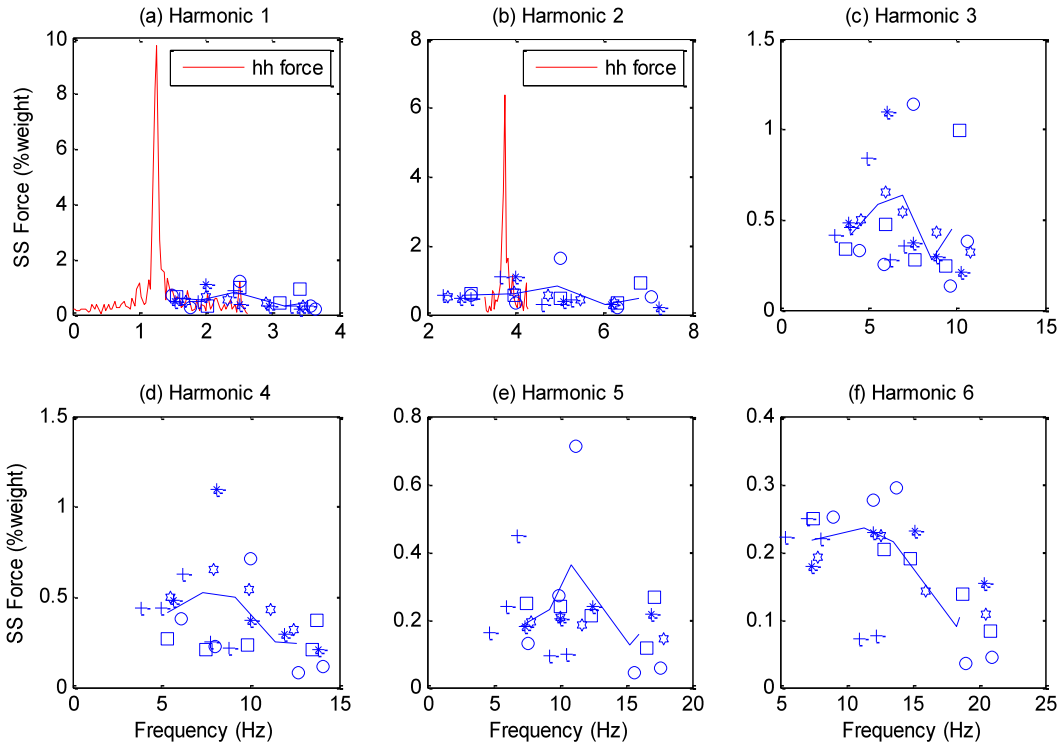

Figure 4.20: (b) Side-to-side force magnitudes measured during jumping

In general, the side-to-side forces occurring at the same frequency of jumping (or higher harmonics) were very small when compared with the front-to-back forces (Figure 4.20b), Therefore, they were excluded from the summary of statistical parameters presented in Table B15 of Appendix B. However, as noted above, one in five subjects produced a substantially large force (about 10% of the body weight) at half the jumping frequency when jumping at 150 b/min. This result is discussed further in Section 4.2.5 to emphasize its significance for a horizontal loading model.

4.2.5. Half-harmonic side-to-side force due to vertical jumping

The force, displacement and velocity time-histories (all side-to-side) corresponding to the special case of a large horizontal force at half the jumping frequency are shown in Figure 4.21a for a subject performing vertical jumping at 150 b/min. It is evident from the displacement time-history (recorded at the subject's centre of mass) in Figure 4.21a that while the subject was jumping vertically he was, at the same time, unconsciously but very consistently, executing a side-to-side, zigzag jump, each time alternating his landing between the right and the left half of the force plate. This type of jump (or the resulting force time history) will now be referred to as the 'zigzag jump' from here onwards in order to distinguish it from other types of jumping.

The frequency spectra for the vertical and the side-to-side force corresponding to the zigzag jump are shown in Figure 4.21b. The spectrum for the side-to-side force has a fundamental peak at 1.25 Hz which was half the jumping frequency for this subject, while the spectrum for the vertical force shows a peak at the jumping frequency (2.5 Hz) as expected. The mechanism for this can be attributed to the inability of humans to

perfectly jump from and land on the same spot and it appears (from the rather limited data set) that, unlike vertical forces, horizontal forces due to jumping do not always occur at the jumping frequency. Thus, a load model similar to the one used for vertical loading is not always appropriate for horizontal loading due to jumping.

(a) (b)

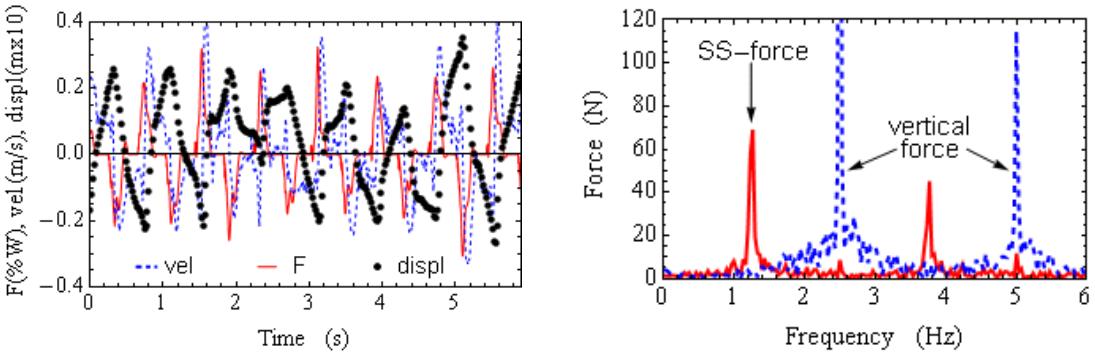

Figure 4.21: (a) Force, displacement and velocity time histories for the zigzag jump at 150 b/min (b) corresponding frequency spectra for vertical and side-to-side forces – all from a single subject

4.3. Results: relationship between the side-to-side force and velocity

As mentioned in Section 4.1, the additional group tests involving motion tracking were conducted to also determine the relationship between the side-to-side force and the velocity of the centre of mass of a typical subject. The analysis focused on this relationship because it leads to recognizable units as demonstrated below (Equation 4.5). The side-to-side velocity data was obtained by numerically evaluating the derivative of the side-to-side position data (measured at the centre of mass of the subject at a sampling rate of 100 Hz) collected using the motion tracker system described in Section 4.1.2. The measured force and velocity amplitudes are shown in Figure 4.22a for 2 subjects swaying side-to-side simultaneously at different rhythms.

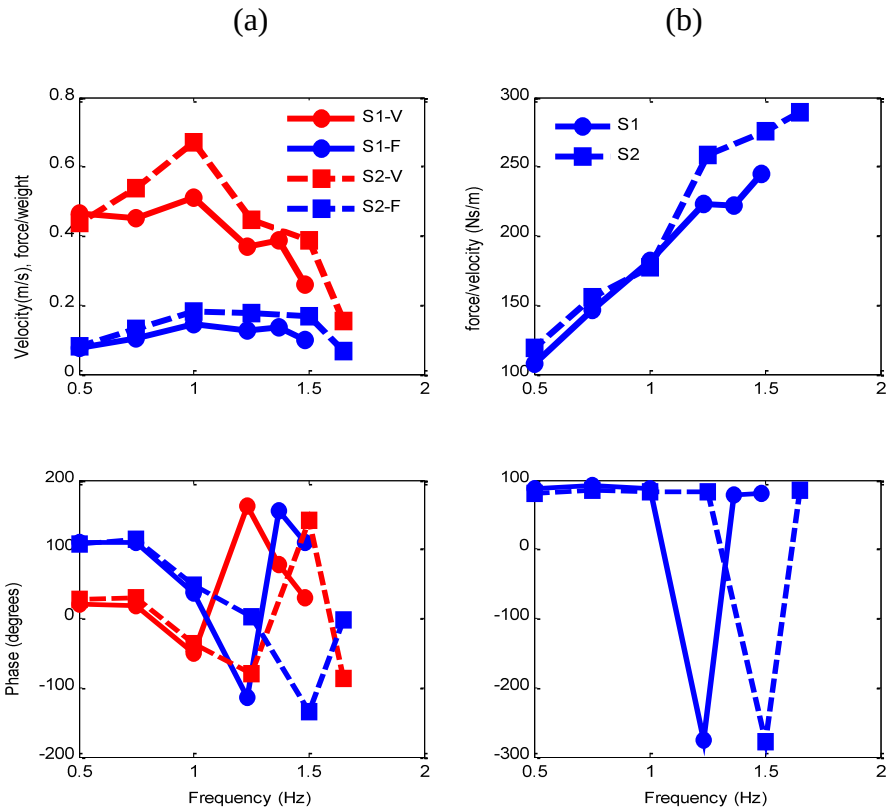

Figure 4.22: (a) Velocity, normalized lateral force and phase during side-to-side swaying (b) Force-velocity ratio and phase

The relationship between the side-to side force and velocity is shown in Figure 4.22b. This relationship was calculated using the equation for mechanical impedance:

$$k_{com}(f) = F_{feet}(f) / v_{com}(f) \qquad \text{[Ns/m]} \qquad (4.5)$$

In Equation 4.5, k_{com} is the complex ratio of the force F_{feet} *(f)* (measured at the interface between the force platform and the feet of the subject) to the velocity v_{com} *(f)* (measured at the subject's centre of mass) at frequency *f*. Note that the resulting units are equivalent to those of the 'negative damping parameter' (discussed in Section 2.2.1.3) which is now used as an important parameter in the assessment of footbridges against side-to-side pedestrian forces (Dallard *et al.* 2001). However, despite similar units, the parameter represented by Equation 4.5 is different from the negative damping parameter

as this equation relates the side-to-side force to the velocity of the centre of mass of the occupant of the structure and not the velocity of the actual structure which is used in the assessment of footbridges.

The lower graphs of Figure 4.22 show that the force and velocity were 90 degrees out of phase (-270 degrees in the case of phase wrapping). As the force is a scalar multiple of the acceleration (F = ma), the 90 degrees phase shift also means that the velocity and the acceleration have a 90 degrees phase lag, confirming that the force is proportional to acceleration as expected. Figure 4.22 also shows that synchronization becomes difficult above 1.25 Hz as the subject started swaying at frequencies that are slightly different from each other and the beep rhythm.

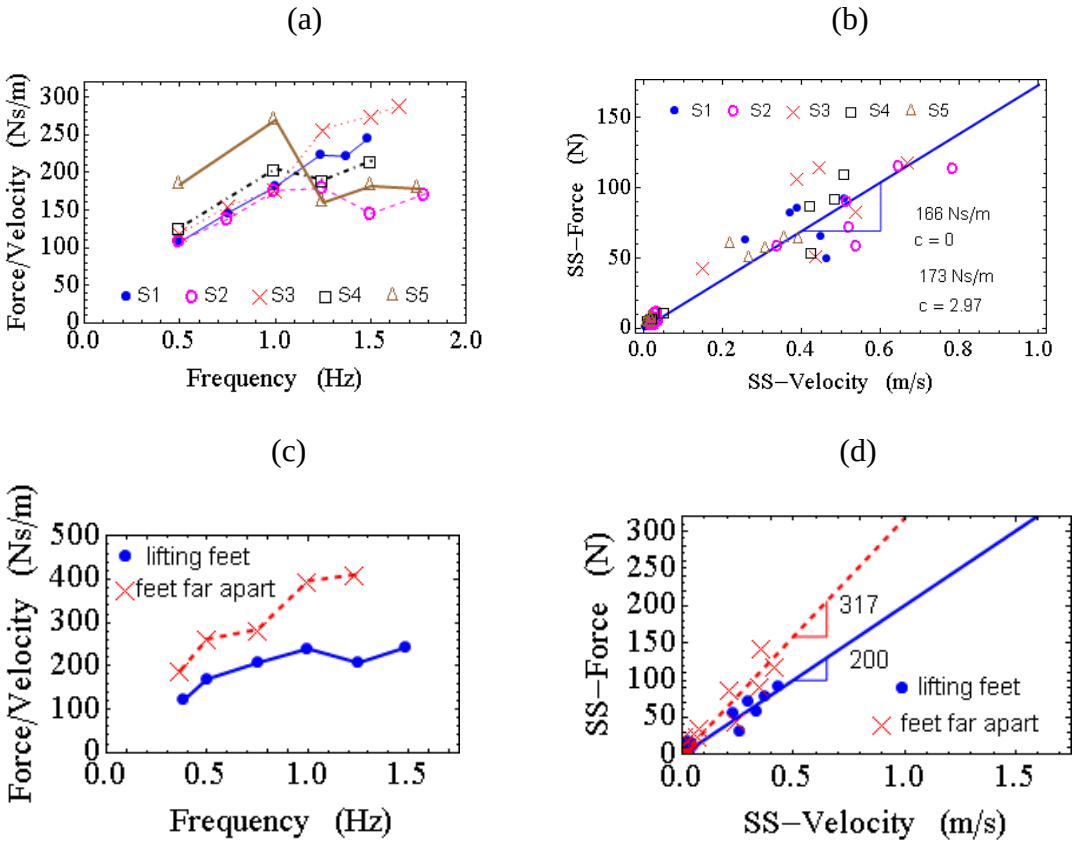

Figure 4.23: Parameter k_{com} evaluated for (a and b) five subjects, (c and d) different swaying conditions.

Figure 4.23a shows a summary of results for the parameter k_{com} evaluated for all five subjects who participated in this category of tests. The dependence of k_{com} on the swaying frequency is evident even though there is inter-subject variability in the result.

The force amplitude was also plotted against the velocity amplitude of the centre of mass for all frequencies considered (Figure 4.23b). There is a clear linearity of the data points which passes through the origin. This indicates that the effective human-induced force measured at the feet of the subject is also proportional to the velocity of the centre of mass of the same subject. The gradient of the fitted straight lines (one with an intercept and another with no intercept) give estimates of the proportionality constant. Obviously this is the same parameter as k_{com} except the dependence on frequency has been ignored by fitting a straight line for all frequencies.

Figures 4.23c and d show that the force-velocity relationship (k_{com}) did not only vary with frequency and subject but also depended on other factors such as how far apart the feet are during swaying. Swaying with feet movements such as that achieved by the alternate lifting of feet also led to a different value for the same subject. Accuracy in locating the centre of mass is another factor although the measurements were only affected if motion track markers were attached on subjects wearing loose clothing that moved significantly during swaying. This was detected very early in the test program and subsequently belts were used to tighten clothing around areas where track markers were attached.

4.4. Discussion and concluding remarks

The measurement and characterization of human-induced horizontal forces in a laboratory setting have been described. The measurements showed that significant horizontal loads can be induced by spectators performing swaying movements (in seated and standing positions) or vertical jumping. Forces were characterized using several properties, such as, (i) the mean impulse curve, (ii) the cycle-by-cycle variation of frequency due to the inability of humans to execute repetitive movements precisely, (iii) the cycle-by-cycle variation of the sub-pulse mean force and (iv) the frequency spectrum.

The fundamental horizontal force due to swaying occurred at the swaying frequency. The fundamental horizontal force due to vertical jumping occurred at the jumping frequency for most subjects. However, contrary to expectation, one in five subjects produced a fundamental side-to-side force at half the jumping frequency. This means that a load model similar to the one used for vertical loading due to jumping is not always appropriate for horizontal loading due to jumping. The measurements were also used to establish the relationship between the side-to-side force and the velocity of the subject's centre of mass. The data showed that the lateral force is proportional to the velocity of the centre of mass of the subject.

Finally, the results presented in this chapter will be used to form an analytic load model that can be used for horizontal dynamic loading of assembly structures during design (Chapter 6).

Chapter 5

5. Footswitch development and foot-timing measurements

Horizontal forces of subjects performing either as single individuals or groups of up to three subjects were presented in Chapter 4. In actuality, forces must be determined for crowds. Therefore, it is essential to monitor the synchronization or lack of synchronization of the applied forces for a realistic design model. In order to measure synchronization a force-plate is required for every member of the group or crowd and the costs involved would make it prohibitive to monitor the synchronization of applied human forces in this way.

The first section of this chapter describes briefly the background to footswitch systems and the development of a customized footswitch system which was used as a proxy tool for monitoring synchronization without using expensive force-plate instruments. In order to establish the capabilities and limitations of the proposed system for civil engineering applications, validation tests involving groups of participants were conducted (Section 5.2) and the footswitch output was compared with that of force-plate instruments and motion tracking technology (Section 5.3). In these sections, results are presented to show that the method is capable of measuring synchronization of crowd forces accurately. Following this simple validation, the footfall timing data collected was analysed to gather together essential parameters that would be needed to form an analytic lateral loading model due to side-to-side swaying movements for both an individual (Section 5.4.1) and a group (Section 5.4.2).

5.1. Background on footswitch systems and proposed footswitch

Footswitch based measurement techniques are a well established and proven concept in the field of biomechanics. For decades, footswitch systems, including instrumented insoles and instrumented mats have been used successfully by gait laboratory clinicians and biomechanics researchers to obtain footfall timing measurements (Crouse *et al*. 1987; Gardner & Murray 1975; Alexander *et al*. 1990; Hausdorff *et al*. 1995; Minns 1982; Lagginns & Bowker 1991; Gabel *et al*. 1979). Footswitch systems can precisely measure footfall timing and so makes them suitable proxy instruments for monitoring the synchronization of subject forces during dynamic testing of public structures using human subjects. Currently, there are hundreds of footswitch and instrumented insole products that are commercially available, each differing with respect to the degree of sophistication and cost (Alexander *et al*. 1990), many of which can be adapted and used for the topic addressed here. The footswitch described in this research is a simple, custom-made, inexpensive system based on the use of an aluminum foil sheet which is easily obtainable from a supermarket for less than £0.30 per metre. Other components of the system such as the probe leads are reusable and were available in the laboratory.

The circuit used for the footswitch system is shown in Figure 5.1. The circuit diagram is for a single subject and was replicated in the case of multiple subjects. The probe leads L (left) and R (right) were fixed to a subject standing on an aluminium mat. The leads were clipped to an aluminium foil sheet wrapped around the subject's shoes. The circuit is suitable for a subject moving in a restricted area which would mimic a spectator in a stadium. It can also be adapted for a subject walking on a footbridge if a portable data acquisition system such as a notebook or laptop is carried by the subject. Alternatively, wireless telemetry technology can be utilized.

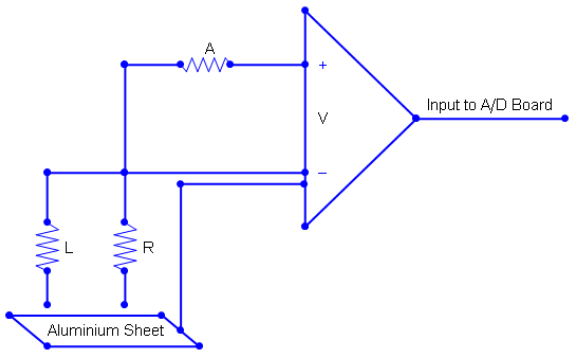

Figure 5.1: Circuit used for footswitch system.

Large forces are created by movement of the feet in spectator activity and normally are treated as a worse case design scenario. In order to validate the footswitch system, the foot movements which generated the largest forces were selected such as side-to-side swaying/dancing movements that involve alternate lifting of each foot. The cycle for this activity can be divided into three phases distinguished by foot events with descriptive terms similar to a gait cycle during normal walking. Figure 5.2 depicts these phases in terms of horizontal forces. The phases can be described as follows; the double limb support (DLS) phase corresponds to the time period when both feet are on the ground), the right single limb support (RSLS) phase - when only the right foot is in contact with the ground and similarly for the left single limb support (LSLS) phase. Each of the last two phases is also called the swing phases of the other foot which would be in the air during this phase. It is important to distinguish which foot is being referred to in each of these phases. Therefore, the parameters of the circuit indicated with symbols in Figure 5.1 were chosen such that the circuit gave distinct outputs for each leg during each of these events, i.e. during the right foot single limb support (RSLS) phase the output is *RSLS volts*. Similarly, the output for the left foot single limb support phase is *LSLP volts* and finally, the output for the double limb support phase is *DLS volts*.

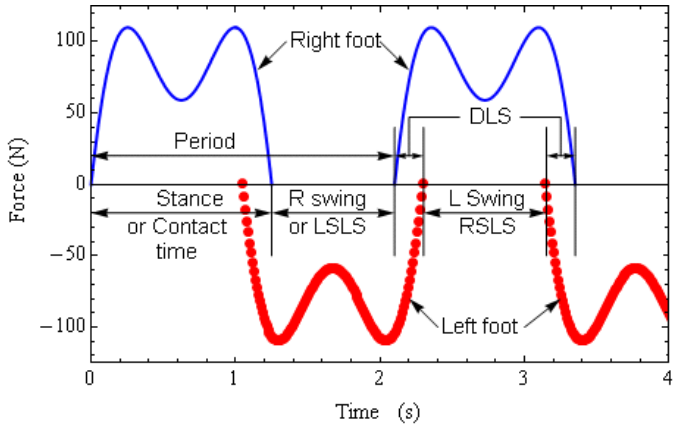

Figure 5.2: Swaying phases in terms of lateral forces

Further additional parameters and events can be derived or evaluated from these three measured events and used to form a lateral loading model due to human subjects swaying from side-to-side. These include: (1) the phase difference between the right and left foot forces on landing; (2) the swaying cycle period that is, the time period starting when the right or left foot lands on the ground and ending when the same foot lands on the ground again; (3) the contact time or stance phase (the time period starting when the right or left foot lands on the ground and ending when the same foot leaves the ground); (4) the contact ratio (the ratio of the stance phase duration to the swaying period) can be evaluated from the previous two parameters; (5) the swing phase and the double support phase are measured directly and are also significant to the load cycle.

Note that by rearranging the same circuit shown in Figure 5.1 a total of three circuit configurations can be achieved with different objectives, namely, measurement of left or right foot placement time history, combined measurement of left and right foot placement time history and measurement of the double limb support phase time history only. To obtain non-intrusive measurements, it is important for the instrumentation to be implemented on the structure rather than on the subject. Finally, if the monitored

movement does not involve foot movement a pressure switch should be incorporated in the circuit shown in Figure 5.1.

5.2. Description of validation and group synchronization tests

Groups of 2, 3 and 5 subjects volunteered to perform movements to replicate behaviour typical of standing spectators responding to rhythmic music in a stadium. All subjects were healthy and showed no signs of obvious limb abnormalities. Gender and age group of each subject is shown in Table 5.1.

Table 5.1: Participant information for footswitch tests

Group Number	Subject	Sex	Age group
G1	S1	M	31-35
	S2	M	41-45
G2	S1	M	25-30
	S2	M	25-30
G3	S1	M	21-25
	S2	M	21-25
	S3	M	25-30
G4	S1	F	21-25
	S2	M	26-30
	S3	M	21-25
G5	S1	F	21-25
	S2	F	26-30
	S3	M	26-30
G6	S1	M	26-30
	S2	M	21-25
	S3	F	40-45
	S4	F	40-45
	S5	M	36-40

Each member of a group was required to assume a standing position and to perform side-to-side swaying/dancing movements that involved alternately lifting each foot during a period of 60 seconds. A metronome set to provide six beep rhythms (45, 60, 90,

120, 150 and 180 beats per minute) was used as a musical stimulus. All tests were conducted at the Nuffield Orthopaedic Centre Gait Laboratory in Oxford.

Figure 5.3: Group of five subjects

Footfall timing measurements for all subjects' feet were recorded in three ways: (1) using the footswitch described in Section 5.1; (2) using a 12 camera motion capture system (Vicon MX, Oxford, UK) which tracked markers on the feet of subjects (as described in Section 4.1.2) and (3) using force-plate instruments (OR6, AMTI, USA) embedded on the floor of the laboratory (as described in Section 4.1.1). Two force-plates were available which enabled measurements of horizontal forces for the left and right foot (separately) of only one of the subjects in a group and this data was used to compare footfall timings for all three methods. All signals were collected simultaneously. Footswitch and force-plate data was sampled at 1000 Hz and tracking data was sampled at 100 Hz.

5.3. Validation

The swaying gait time history outputs obtained from the same foot of a single subject (swaying at 60 beat/min) when measured by the three different methods is shown in Figure 5.4. The force-plate output refers to the side-to-side force applied by the foot, the footswitch output refers to whether the foot is on or off the aluminium sheet which was spread on the force-plate and the tracker output refers to the vertical displacement of the foot with respect to the floor. The periodic intervals for all three signals coincide indicating that the three methods give similar results. The intervals were evaluated by shifting the base of each signal slightly below zero to determine the zero crossing point.

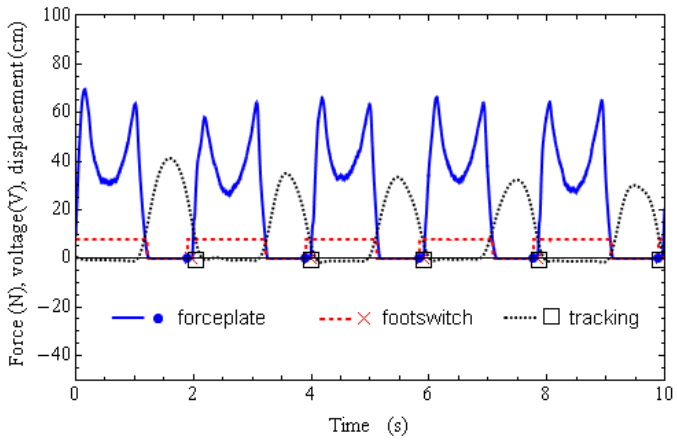

Figure 5.4: Side-to-side swaying gait time histories

When the mean period and the standard deviation evaluated from the 60 second time histories (Figure 5.4) are compared as shown in Figure 5.5 and Table 5.2, the random pattern of the variation of the swaying period from cycle to cycle demonstrated a very close correspondence between all three methods. In particular, the standard deviation of the footswitch data was almost equivalent to that of the force-plate data.

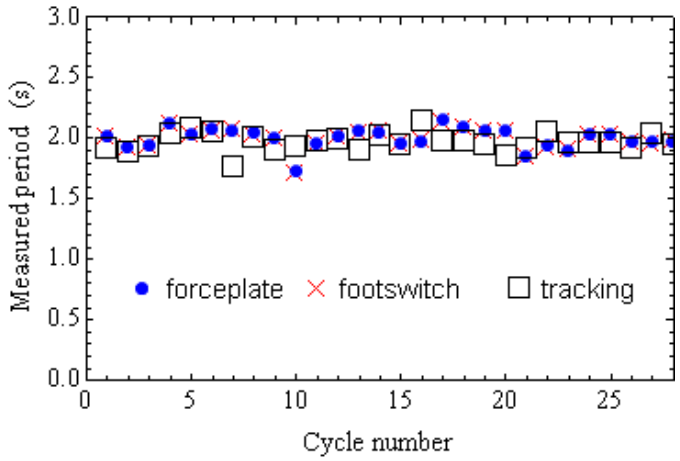

Figure 5.5: Variation of period for swaying at the same beep.

Table 5.2: Comparison of estimated mean period

Method	Mean period (s)	Standard deviation
Force-plate	1.996	0.085
Footswitch	1.997	0.084
Tracking	1.997	0.076

5.4. Side-to-side swaying load model parameters

This section introduces the use of the validated footswitch system as a proxy tool for the measurement and evaluation of essential parameters required for the development of a human loading model due to swaying from side-to-side either during walking (for footbridges) or dancing on the spot (for entertainment venues). Currently such a model does not exist and its development will be useful for lateral dynamic assessment of public structures due to lateral human loading. Initially, all three methods were used to determine the parameters when a single individual is involved (Section 5.4.1). This is followed by the measurement of parameters for a group which involved monitoring of group synchronization. Statistical parameters are introduced and finally, several

observations on the usefulness and interpretation of this data are discussed (Section 5.4.2).

5.4.1. Swaying of a single individual

A desirable force model for an individual swaying from side-to-side on the spot or walking requires experimental measurement of the phase difference between the right and left foot forces, the cycle period or frequency, the stance or contact phase, the swing or flight phase and the contact ratio (see earlier definitions). In addition, the double support phase duration was also measured to show its significance on the loading cycle.

The mean phase differences between the right and left foot forces or landing recorded when one of the subjects was swaying at different beep frequencies are shown in Figure 5.6. As expected, all values recorded are close to 180 degrees. The values are slightly more or slightly less than 180 degrees because of the small overlapping region between the left foot landing and right foot take off during the double support phase (see Figure 5.2).

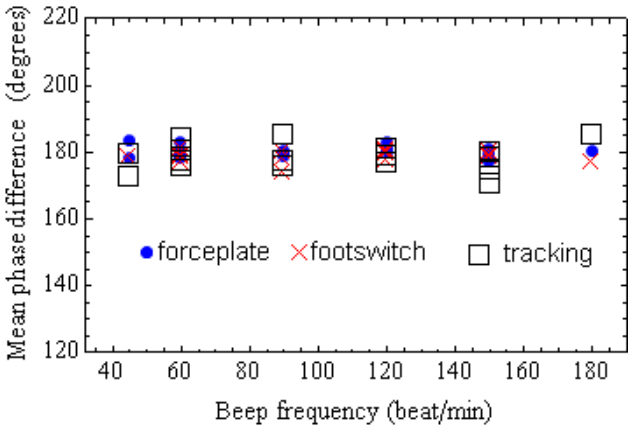

Figure 5.6: Mean phase difference between left and right foot.

Figure 5.7 shows mean values for the swaying period, the stance or contact phase and the swing or flight phase recorded during the same tests described above. Again all

three methods of measurement show very good agreement. Curves were fitted to each relevant data set to obtain analytic expressions for the period, stance and swing durations as a function of the beep frequency (f). These simple expressions are included in Figure 5.7 and can be used to interpolate values at the intermediate points where measurements were not made. It would be prudent to avoid extrapolation when using these curves.

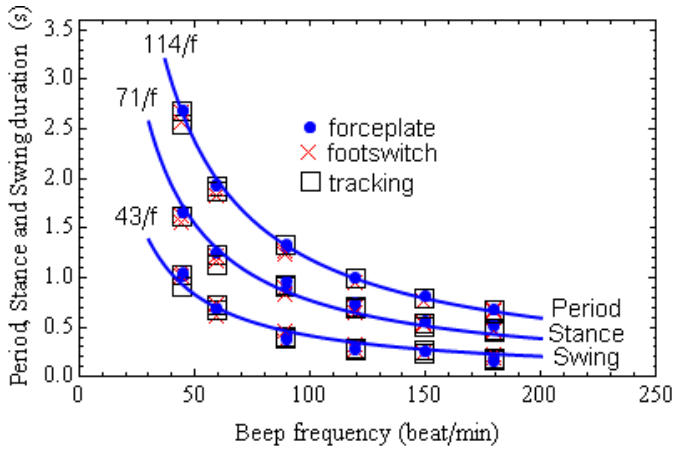

Figure 5.7: Period, Stance and Swing durations.

Similarly, the measurements for the contact ratios for swaying at different beep frequencies are shown in Figure 5.8.

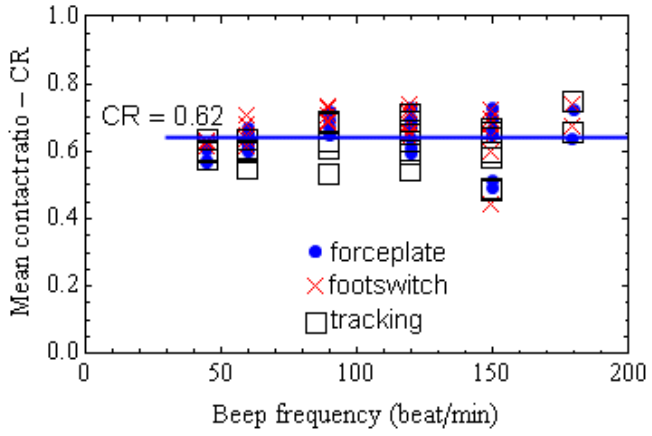

Figure 5.8: Mean contact ratios.

The data from all three methods indicate that the contact ratio is constant across different frequencies with a mean value of approximately 0.62. Note that evaluating the contact ratio from its definition by dividing the expression for the stance curve by the expression for the period curve in Figure 5.7 also yields a horizontal straight line with a 0.62 intercept which is in agreement with Figure 5.8. Figure 5.8 also shows that the footswitch is better at determining the contact ratio than tracking.

Figure 5.9 shows typical values for double support phase duration as a function of beep frequency. Even though there is some scatter in the measured results, all three methods of measurement are consistent. However, the footswitch and the tracking methods have a tendency to overestimate slightly the double support phase duration as both methods do not measure force to define contact initiation. Figure 5.9 shows a decreasing pattern in the duration of the double limb support phase as the beep frequency increases. For walking movement, this is analogous to increasing walking speed.

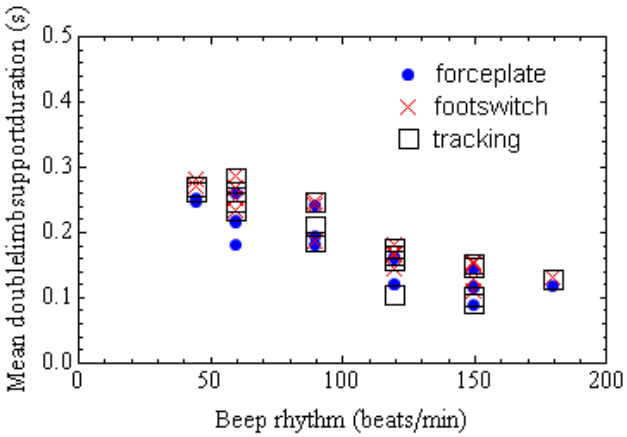

Figure 5.9: Double limb support phase duration.

The duration of the double limb support phase can also be represented as a proportion of the gait cycle by dividing the values of Figure 5.9 by the period data shown earlier in Figure 5.7. Performing this operation leads to the results shown in Figure 5.10. The

graph indicates that there was an overall increase of the double support phase as the beep frequency increases, indicating its significance on the loading cycle.

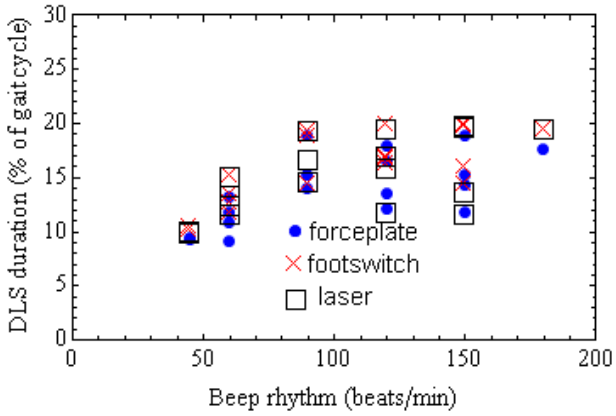

Figure 5.10: Double limb support as a proportion of gait cycle

5.4.2. Swaying of groups

When the groups of 2, 3 and 5 subjects were asked to perform side-to-side swaying at various beep frequencies as described earlier, footfall timings or gait event signals were recorded simultaneously for all subjects. Figure 5.11 shows examples of signals recorded for Groups 1, 2 and 4. The signals correspond to swaying at a beep rhythm of 60 beat/min. The events that were monitored for each subject are: the right single limb support (RSLS) phase, the left single limb support (LSLS) phase and the double limb support (DLS) phase. The specific voltage output used to identify each event is displayed on each graph.

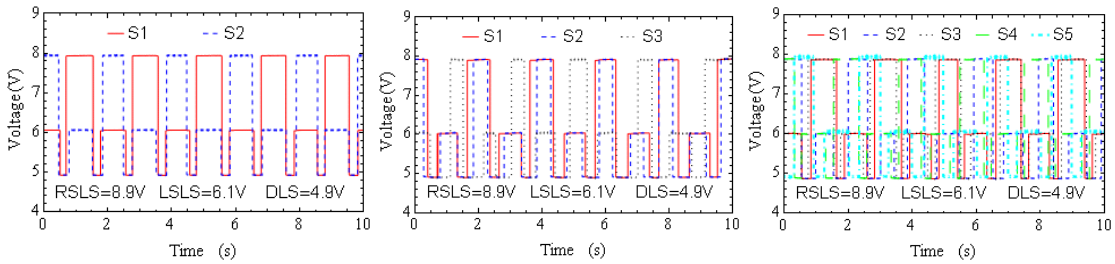

Figure 5.11: Gait event signals for different groups. The voltage output values 9.9V, 6.1V and 4.9V were measured during the Right single limb support (RSLS), Left single limb support (LSLS) and Double limb support (DLS) phases, respectively

These time history graphs were used to visualize the degree of subject synchronization. For example in the first graph of Figure 5.11 the signals are almost 180 degrees out of phase indicating that the subjects were moving out of phase. The data was also used to evaluate statistical swaying characteristics of each individual in a group including his or her deviation from the group mean. The key parameters evaluated and the techniques used are discussed below.

5.4.2.1. Statistical parameters for group swaying

Recent and improved statistical parameters necessary to form a group loading model have been contributed by Sim (2006), Parkhouse & Ewins (2006) and Ellis & Ji (2004) for describing jumping loads. Both Sim (2006) and Parkhouse & Ewins (2006) used a beep signal to segment individual time history data in order to form group loads. The parameters they used were adopted in this research with slight modifications to reflect a preferred strategy for segmenting data (instead of using the beep signal) as explained below.

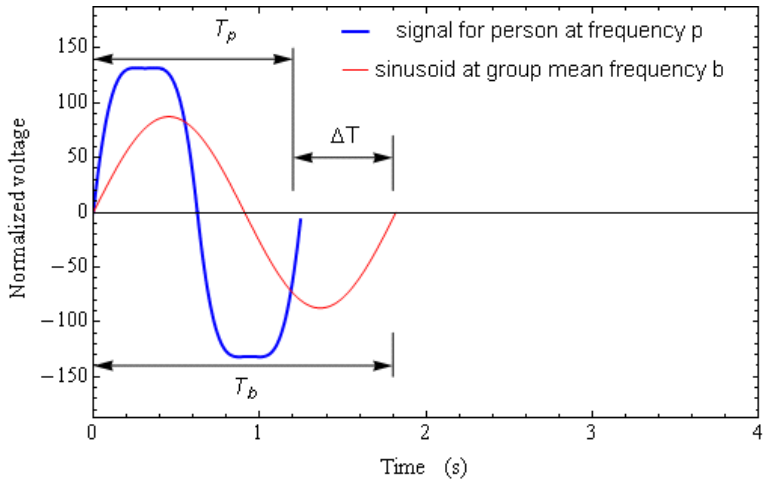

Figure 5.12: Idealized local time delay for each swaying cycle

Parameters for describing cycle-by-cycle variation of each subject's swaying behaviour at frequency *p* relative to the group mean were determined by fitting a sinusoid with unit amplitude and a frequency *b* equivalent to the group mean frequency (which may or may not correspond to the beep) and started at the beginning of each data capture (Figure 5.12).

Referring to Figure 5.12 the local time delay, $t_{dL,k}$ or period deviation for the *k*th cycle, is defined as the time lag of each swaying cycle relative to the group cycle at any periodic zero crossing point.

$$t_{dL,k} = \Delta T_k = T_{p,k} - T_{b,k} \tag{5.1}$$

The positions at which T_p and T_b occur in the data are evaluated directly by determining zero crossing points. The frequency for each cycle is related to the period by:

$$f_{p,k} = 1/T_{p,k} \tag{5.2}$$

Considering a test record made of *m* cycles, the accumulated total time lag at any intermediate cycle *k* is obtained by summing all previous local time delays according to the equation shown below.

$$t_{dT,k} = \sum_{n=i}^{k} t_{dL}(n) = t_{dL}(i) + t_{dL}(i+1) + t_{dL}(i+2) \ldots\ldots + t_{dL}(k) \tag{5.3}$$

The mean time delay, $\bar{t}_{dT,m}$, is the average of the total time delay at the end of a full test record made of *m* cycles.

$$\bar{t}_{dT,m} = \frac{1}{m} t_{dT}(m) \tag{5.4}$$

The time deviation after *k* complete cycles is defined as the difference between the time delay and the mean time delay (Equation 5.5). The mean time delay removes the DC offset and thus the time deviation has a mean of zero.

$$t'_{dT}(k) = t_{dT}(k) - \bar{t}_{dT} \qquad (5.5)$$

It is useful to express the time parameters defined earlier in terms of the group period, T_b, giving the local phase delay, $\theta_{dL,k}$, mean phase delay, $\bar{\theta}_{dT,m}$, and phase deviation, $\theta'_{dT,k}$:

$$\theta_{dL,k} = 360° \times t_{dL,k} / T_b \qquad (5.6)$$

$$\bar{\theta}_{dT,m} = 360° \times \bar{t}_{dT,m} / T_b \qquad (5.7)$$

$$\theta'_{dT,k} = 360° \times t'_{dT,k} / T_b \qquad (5.8)$$

Below the cycle by cycle variation of the swaying activity of the subjects is presented in four ways through the parameters presented above (i) as the variation of the period duration in seconds (Figure 5.13), (ii) as the variation of frequency (Figure 5.14), (iii) as the variation of the local or period deviation (Figure 5.15) and (iv) as the phase deviation (Figure 5.16). Figure 5.14 shows that the variability of the swaying frequency increased as the beep frequency increased. This expected behaviour simply indicates that it was more difficult for the subjects to match the frequency of a faster beep than a slower beep.

All graphs suggest that each set of data can reasonably be represented by a normal distribution using the statistical parameters corresponding to each graph shown. Note that the statistical parameters of these distributions are also related to each other by the transformation or equations discussed above. For example, each standard deviation shown in Figure 5.15 is related to the corresponding standard deviation shown in Figure 5.13 by Equation 5.6. Similarly, given frequency data (Figure 5.14), the statistical distribution parameters for the period data can be obtained by firstly performing an

inverse operation on the frequency data and vice versa. Similarly, the mean phase delays for each individual record were evaluated using Equation 5.4. In the absence of evidence that mean phase delays are frequency dependent, the results for all frequencies were combined to form a large data set whose histogram distribution is shown in Figure 5.17. The histogram shows a peak around the mean indicating that there is a tendency for subjects to synchronize.

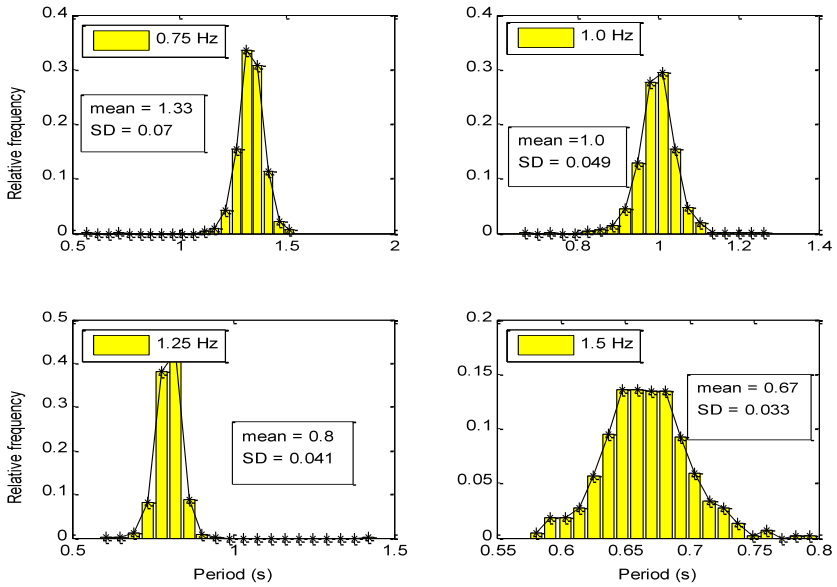

Figure 5.13: Histograms for period variation for group-swaying at different beep frequencies

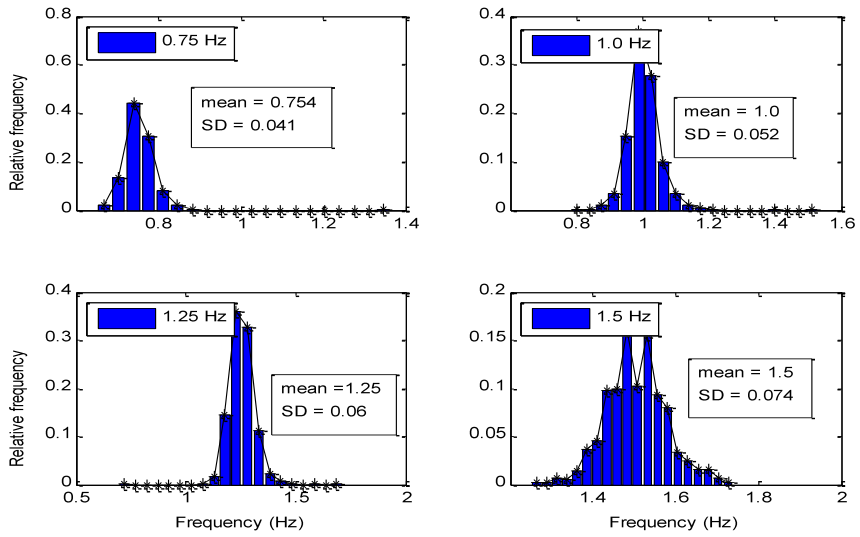

Figure 5.14: Histograms for frequency variation for group-swaying at different beep frequencies

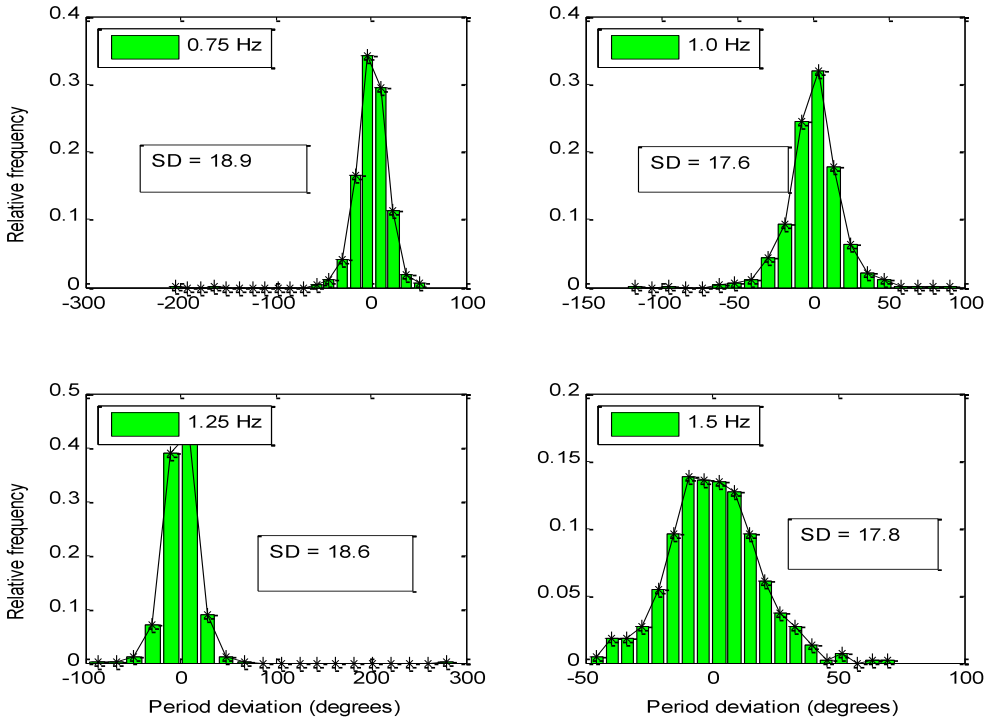

Figure 5.15: Histograms for period deviation for group-swaying at different beep frequencies

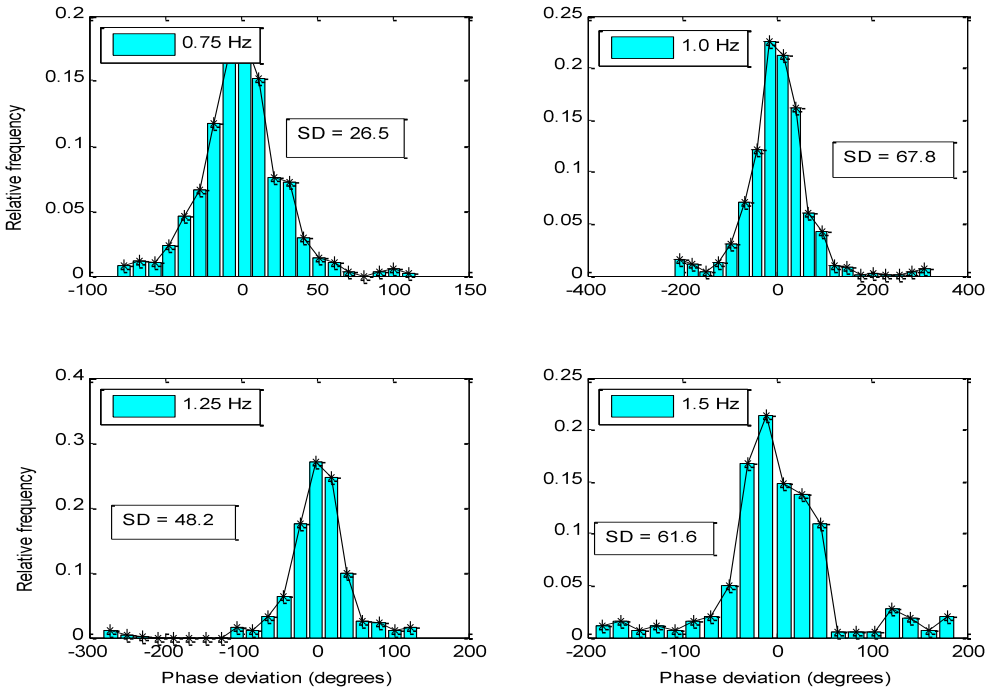

Figure 5.16: Histograms for phase deviation for group-swaying at different beep frequencies

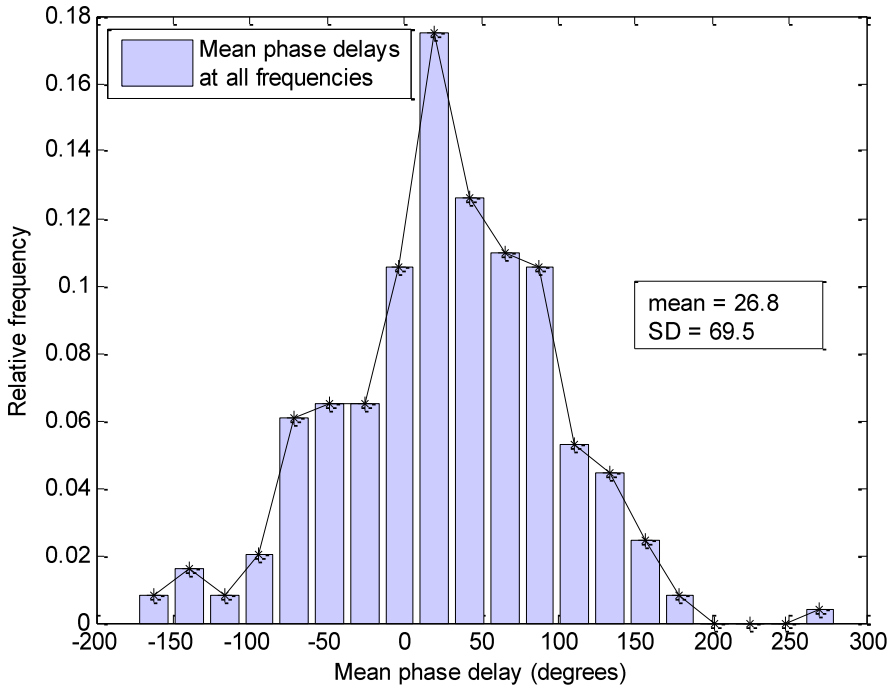

Figure 5.17: Histogram for mean phase delays for group-swaying - all frequencies

Since the parameters of Figures 5.13 to 5.16 are related, it is necessary to focus on modeling the statistical distributions of key parameters. The main parameters chosen, which will be used in Chapters 6 and 7 of this thesis, are the period, or cycle-by-cycle variation of frequency, or period deviation (local phase delay) and group mean phase delays (Figure 5.17). The remaining parameters can be evaluated from these key parameters by the transformations and equations presented earlier. For example Figure 5.18 shows how the phase deviation data, $\theta'_{dT,k}$, can be generated or synthesized from only knowing the data of local time delays, $t_{dL,k}$ or its statistical distribution parameters through Equations 5.3, 5.4, 5.5 and 5.8. The solid line in the graph represent a complete set of measured data, $t_{dL,k}$, used to evaluate the phase deviation $\theta'_{dT,k}$. The other lines represent the phase deviation evaluated if it was assumed that only the first ½ or first ¾ of the sample were recorded. As expected, the simulated values get closer to those of the complete sample when more data from the complete sample are used.

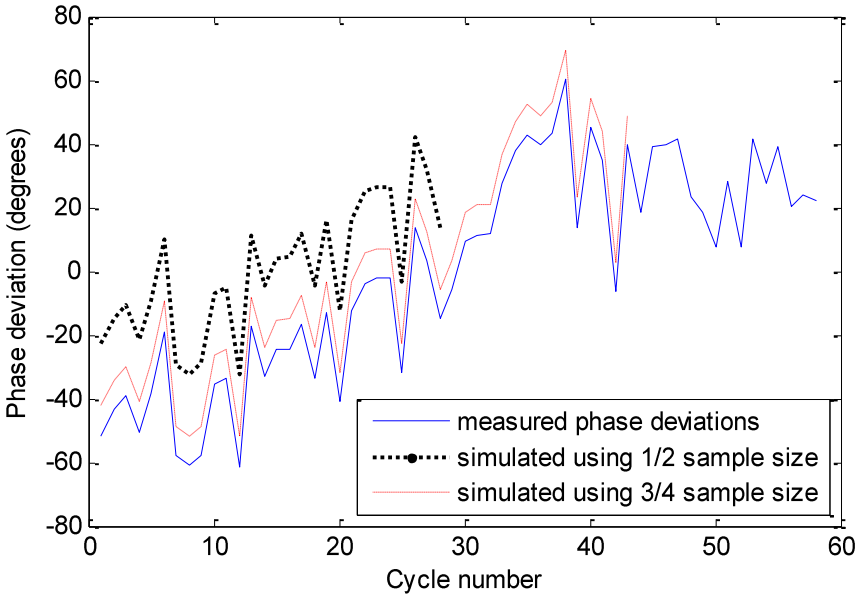

Figure 5.18: Phase deviation data simulated using different sample sizes

5.5. Conclusions

Footswitch based measurement techniques are a well- established and proven concept in the field of biomechanics. This section has described the development and validation of a customized footswitch system used for collecting the foot-timing statistics of human induced forces. The validated footswitch was used successfully for measuring essential parameters required for the development of the lateral human loading model for single individuals and groups of subjects swaying from side-to-side. Foot-timing data for individuals and groups of subjects were presented. The main parameters which were shown to be important for group loads are the time varying frequencies and the mean phase delays. Finally, it is important to emphasize that the swaying movement which involved alternate lifting of each foot was a proxy movement intended to extract statistical parameters for timing of foot placement among subjects.

Chapter 6

6. Analytical modelling of human-induced horizontal forces

This chapter presents a procedure for describing horizontal forces analytically in a manner that is suitable for structural design. The traditional approach makes a distinction between a model that represents the effect of a single individual and a model for a group or crowd. Here, the model for an individual has been derived first (Section 6.1). The individual model was then used as a basis for the crowd model (Section 6.2).

6.1. Individual model

The most widely used procedure for formulating forcing functions for human loading involves three steps, (i) choosing a basic shape function or pulse wave form that best describes the mean of the measured force data, (ii) constraining the parameters of the shape function using the measured data in the time domain and (iii) representing the shape function by a Fourier series and checking if the chosen function reproduces the same frequency spectrum as the measured force. For the models presented here, the steps were slightly modified. It was decided to perform the steps in reverse order starting from the frequency domain in order to prioritize the prediction of the correct frequency spectrum of the force rather than prioritizing the description of its wave form in the time domain. The following steps were executed:

i. Evaluating Fourier coefficients of the force record to form model constraint parameters
ii. Splitting the force time-histories into two records where each record contains a time history of horizontal force pulses to the right (H_{pR}) or to the left (H_{pL}) for

swaying side-to-side (H_{pF} or H_{pB} for swaying front-to-back) and evaluating the mean separately

iii. Approximating each pulse by a rectangular pulse as generating or basic shape function and using a Fourier series to represent each pulse

iv. Applying the Fourier coefficients from the first step as constraint parameters for the respective pulses

v. Summing the expressions for the rectangular pulses representing positive and negative forces and optimising until the measured wave forms and Fourier coefficients are reasonably predicted

Steps (i) and (ii) have been discussed in Sections 4.2.4 and 4.2.3 of Chapter 4, respectively. This section deals with steps (iii)-(v) and demonstrates the application of the results from Sections 4.2.4 and 4.2.3.

For the description of a rectangular pulse (Figure 6.1) the following basic theory on Fourier analysis was used.

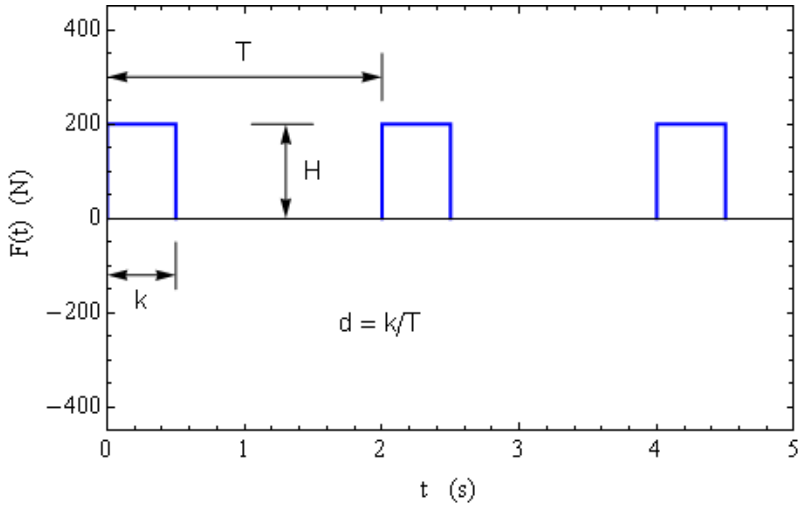

Figure 6.1: Time domain wave form for a rectangular pulse

The Fourier coefficients (a_n) and the mean (a_0) for a rectangular pulse (Figure 6.1) are given by the expressions (Smith, 1997):

$$a_n = \frac{2H\sin(\pi nd)}{\pi n} \qquad (6.1a)$$

$$a_0 = Hd \qquad (6.1b)$$

When using a rectangular pulse to represent the measured forces, Equation 6.1a led to a set of simultaneous equations that solved directly for the duty cycle d (or k/T) provided at least two Fourier coefficients (a_n) were known constraint parameters evaluated from the measured data. Although the value of the parameter H was also obtained from solving Equation 6.1a, solving for H using Equation 6.1b by substituting the mean of the split measured data (a_0) and the calculated value of d gave results that were more consistent with measurements.

Figure 6.1 relates to a rectangular pulse in one direction. However, for swaying, there is a pulse in each direction of swaying. Therefore, each right (H_{pR}) or left (H_{pL}) pulse of the split horizontal forces due to swaying side-to-side (H_{pF} or H_{pB} for swaying front-to-back) can be represented schematically in the same time history as follows:

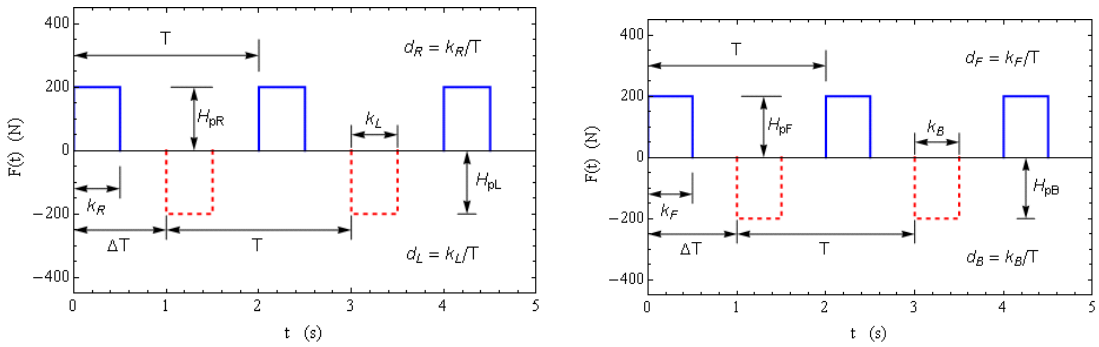

Figure 6.2: Idealized (a) right and left rectangular force pulses for swaying side-to-side (b) Front and back rectangular force pulses for swaying front-to-back

6.1.1. Side-to-side swaying force model

Referring to Figure 6.2a, for side-to-side swaying (standing or seated), the model parameters that needed to be optimized to match the measured forces are: ΔT , d_R (or k_R), d_L (or k_L), H_{pR} and H_{pL}. Due to the symmetry of forces for swaying from side-to-side (as indicated by the data shown previously in Figures 4.14a&b) the force model shown in Figure 6.2a was reduced as shown in Figure 6.3, leaving only two unknown parameters to be determined using the measured data as a constraint.

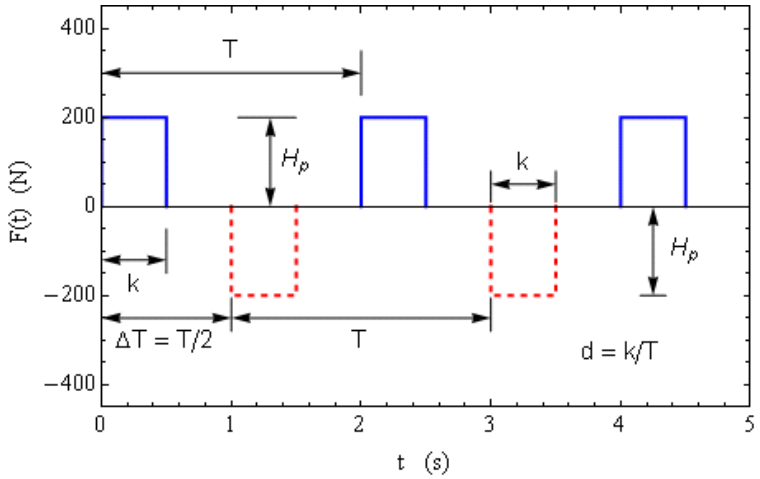

Figure 6.3: Simplified side-to-side model

The parameters H_p and d (or k/T) were determined using the first and third harmonic (the 2nd harmonic was less than 1%W and was ignored for side-to-side swaying) of the measured data at each frequency by solving the Equations 6.2a which follows directly from Equation 6.1a:

$$MFH_1 = \frac{2H_P \sin(1\times \pi d)}{1\times \pi};\ MFH_3 = \frac{2H_P \sin(3\times \pi d)}{3\times \pi};\ MFH_1 > MFH_3 \qquad (6.2a)$$

where MFH_1 and MFH_3 are the force magnitudes at the first and third harmonics which were obtained by performing a Fast Fourier transform on the measured data.

In Table 6.1 the parameter *d* for side-to-side swaying in a standing position has been evaluated by solving Equations 6.2a using the mean (and the corresponding standard deviation) of the measured spectral data which was discussed in Section 4.2.4 of Chapter 4. In the latter chapter the spectral data was presented in two ways, firstly through Table B7 of Appendix B and secondly, through Equation 4.1 which was used to approximate spectral magnitude data by a forth order polynomial. Table 6.1 shows that mean values for the parameter *d* lie between 0.27 and 0.3 for swaying side-to-side in a standing. The minimum and maximum values represent values calculated at upper and lower standard deviations. Values are not provided where standard deviation values were not available and/or solutions to Equations 6.2a were not obtainable.

Table 6.1: Values for parameters *d* and H_p evaluated for swaying side-to-side in a standing position

Frequency (Hz)	Maximum *d*	Mean *d*	Minimum *d*
0.5	0.342	0.278	0.242
0.75	0.389	0.295	0.250
1.0	0.389	0.299	0.255
1.25	0.408	0.306	0.260
1.5	(-)	0.308	0.250
Frequency (Hz)	Minimum H_p	Mean H_p	Maximum H_p
0.5	10.963	21.487	33.924
0.75	12.930	27.087	43.754
1.0	14.714	29.378	46.423
1.25	13.184	28.355	46.124
1.5	(-)	25.710	44.046

Values for H_p were also obtained from solving Equations 6.2a. This is possible because performing the substitutions described in the previous two paragraphs leads to a set of simultaneous equations that solve for both *d* and H_p. However, as the measured pulses do not have regular or constant amplitudes (due to imperfect human swaying or jumping), the values for H_p, determined using Equations 6.2a, gave slight over-

estimates of the amplitude compared to the data. Consequently, an improved estimate of the parameter H_p which reflected the time varying amplitude of the force was obtained directly from the measured data (or the associated statistical parameters) using the expression for the mean or constant term of a rectangular pulse. The following expression which is an equivalent statement of Equation 6.1b was used:

$$H_{pi} = \frac{\frac{1}{n}\sum_{k=1}^{n} F_k}{d} = \frac{\overline{F_i}}{d} \qquad (6.2b)$$

where H_{pi} is the H_p parameter for the i^{th} cycle of the force and d is obtained from Table 6.1 and is assumed constant throughout the time history. Note that the numerator term of Equation 6.2b is the sub-pulse mean force and its statistical parameters were discussed in Section 4.2.3 of Chapter 4 and presented in Figure 4.15 for swaying side-to-side in a standing position. Values for H_p evaluated this way are also shown in Table 6.1.

Finally, after evaluating H_p and d, the following truncated Fourier series was used to describe (cycle-by-cycle) the significant magnitudes of the measured force which were the first and third harmonics.

$$F_{ss}(t) = \frac{2H_p \sin(1\times\pi d)}{1\times\pi}\sin(1\times 2\pi f t) \pm \frac{2H_p \sin(3\times\pi d)}{3\times\pi}\sin(3\times 2\pi f t) \qquad (6.3)$$

Using the $\pm$ sign in Equation 6.3 interchangeably led to two different wave profiles (Type I and Type II) that were also observed in the recorded data. To implement the procedure presented above a program was written in Matlab to predict side-to-side

forces due to swaying in a standing position for each of the twelve subjects. The main steps of the program are listed below:

i. At each swaying rhythm generate a column vector (f) of stochastic frequencies characterized by a mean and standard deviation as presented in Figure 4.11(a)

ii. Assume a symmetrical pulse (with equal right and left force amplitudes) and generate a column vector $\overline{F}$ of sub-pulse mean forces characterized by a mean and standard deviation as presented in Figure 4.15

iii. Convert each frequency (f_i) generated in Step (i) into a cycle duration (T_i) using $T_i = 1/f_i$

iv. Subdivide each cycle duration (T_i) into small time intervals (here 1/1000 sec was used) at which to evaluate the force

v. Assume d to be a constant for the frequency vector generated in Step (i) and choose a mean value for d from Table 6.1

vi. For each sub-pulse mean force $\overline{F}_i$ calculate H_{pi} using Equation 6.2b

vii. Generate a force pulse for each cycle using Equation 6.3

viii. Rearrange the force pulse cycles generated in Step (vii) with their order preserved into a single force vector to form a single force time history. If measured time history data is available for comparison of synthetic and measured forces proceed to the next final two steps.

ix. Optimise by adjusting the value for d in Step (v) within the suggested range of values given in Table 6.1 until the frequency spectrum of the simulated force matches the measured force spectrum.

x. If necessary repeat the entire procedure.

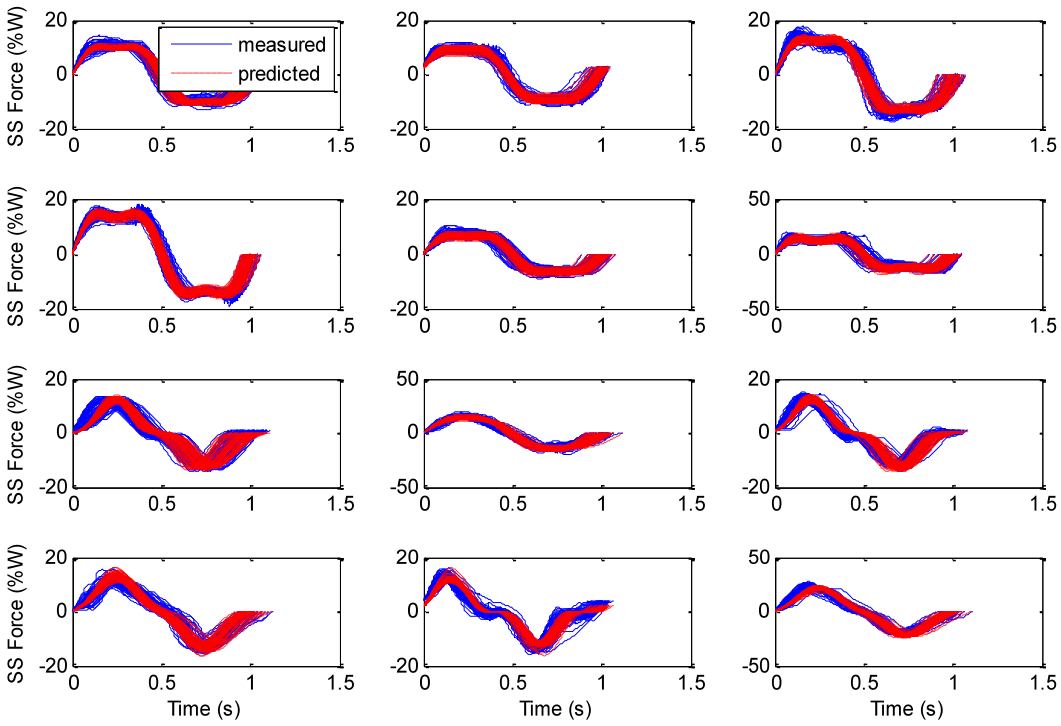

Figure 6.4: Typical measured and predicated side-to-side force comparison in the time domain (standing sway at 1.0 Hz)

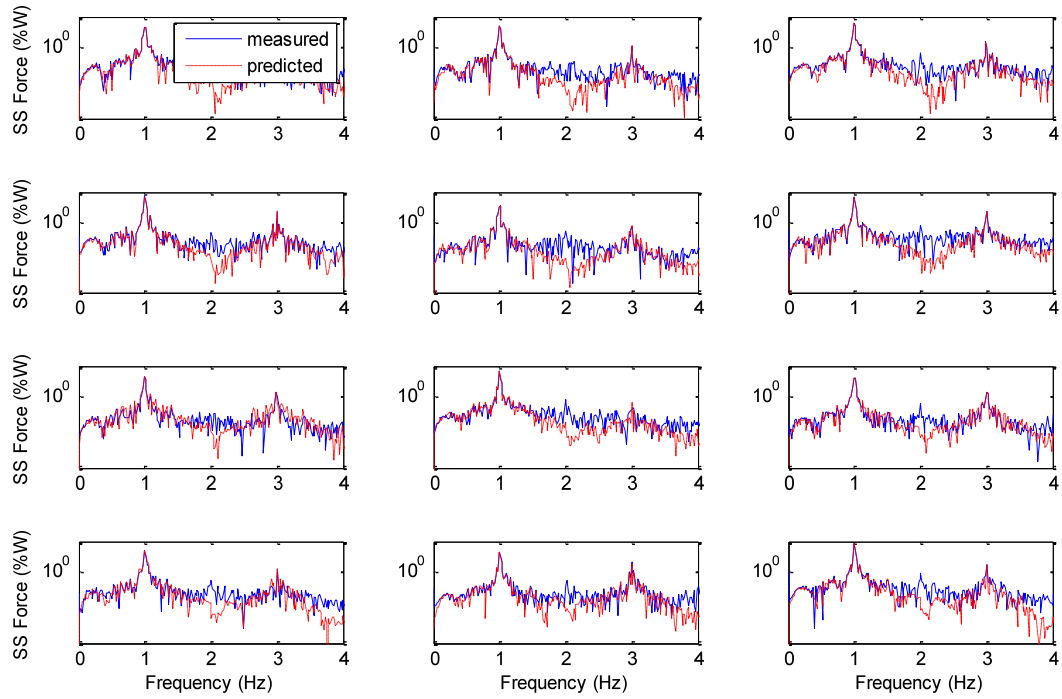

Figure 6.5: Typical measured and predicated side-to-side force comparison in the frequency domain (standing sway at 1.0 Hz)

A typical comparison of measured and predicted time history wave forms simulated for all 12 subjects using the above procedure is shown in Figure 6.4. A comparison of the measured and predicted frequency spectra is also shown (Figure 6.5).

The same procedure was followed for side-to-side swaying in a sitting position except that Figure 4.11b and Table B4 (Appendix B) were used to generate the frequency and the sub-pulse mean force column vectors, respectively. The d and H_p values obtained are summarized in Table B16 of Appendix B.

6.1.2. Front-to-back force model

The model illustrated in Figure 6.2 (b) was used for front-to-back swaying. Unlike the model for side-to-side forces, the model for front-to-back swaying is not simplified further due to lack of symmetry in the measured forces which was more significant for swaying in a seated position. The truncated Fourier series expressions used to describe the split time histories and the combined time history are given below up to the third harmonic.

$$F_F(t) = 2H_{pF}\left(\sum_{n=1}^{3}\frac{\sin(n\times\pi d_F)}{n\times\pi}\sin(n\times 2\pi ft + n\times\phi_F)\right) \tag{6.4}$$

$$F_B(t) = -2H_{pB}\left(\sum_{n=1}^{3}\frac{\sin(n\times\pi d_B)}{n\times\pi}\sin(n\times 2\pi ft + n\times\phi_B)\right) \tag{6.5}$$

$$F_{FB}(t) = F_F(t) + F_B(t) \tag{6.6}$$

$$\Delta T = 360°(\phi_B - \phi_F)/T \tag{6.7}$$

Furthermore the second harmonic was more dominant than the third harmonic in the measured data. Thus data corresponding to the first and second harmonics were used when solving Equation 6.1a for the parameter *d* leading to the following equations:

$$MFH_1 = \frac{2H_P \sin(1\times \pi d)}{1\times \pi};\ MFH_2 = \frac{2H_P \sin(2\times \pi d)}{2\times \pi};\ MFH_1 > MFH_2 \qquad (6.8a)$$

Note that Equation 6.8a results from the simplifications $d \approx d_F \approx d_B$ and $H_{pF} \approx H_{pB}$. The latter simplification only affected the estimation of *d* since the actual values for the parameters H_{pF} and H_{pB} were obtained from the sub-pulse mean data and the already estimated value of *d* using the following equations:

$$H_{pFi} = \frac{\frac{1}{n}\sum_{k=1}^{n} F_{Fk}}{d} = \frac{\overline{F_{Fi}}}{d} \qquad (6.8b)$$

$$H_{pBi} = \frac{\frac{1}{n}\sum_{k=1}^{n} F_{Bk}}{d} = \frac{\overline{F_{Bi}}}{d} \qquad (6.8c)$$

where F_F and F_B represent the sub-pulse force data to the front and back (respectively) for each cycle of the force. The remaining parameters retain their previous meaning.

Numerical values for the parameter *d*, obtained by substituting into Equation 6.8a appropriate data presented in Tables B9 and B10 of Appendix B is shown in Tables B17 and B18 for swaying front-to-back in a standing and sitting position, respectively. The corresponding values for H_{pF} and H_{pB} evaluated by substituting relevant data presented in Table B5 and B6 of Appendix B into Equations 6.8b&c are also presented. The same step-by-step numerical procedure presented for the side-to-side model was applied to the front-to-back model with obvious modifications such as the generation of asymmetrical sub-pulse mean forces in step (ii) using relevant data presented in Tables B5 or B6 of Appendix B and invoking tables and equations relevant to the evaluation of

front-to-back forces in steps (v, vi and vii). Finally, Section 6.1.4 will demonstrate that the model can be used to generate synthetic front-to-back forces by showing that it can predict the mean impulse curve of the measured front-to-back force due to swaying front-to-back in a sitting position.

6.1.3. Side-to-side and front-to-back force models due to vertical jumping

Equation 6.3 was also found to be adequate for simulating a side-to-side force caused by a zigzag jump demonstrated earlier to be the worst case scenario for side-to-side forces during vertical jumping. Table B19 of Appendix B show typical values for *d* evaluated for vertical jumping at 2.5 Hz by substituting magnitudes of the 1st and 3rd harmonics presented in Figure 4.19b of Chapter 4 into Equation 6.2a. The corresponding values for H_p evaluated by substituting appropriate data presented in Table 4.3 of Chapter 4 into Equations 6.2b are also shown. In Section 6.1.6, these parameters will be used to demonstrate that the side-to-side model is capable of representing side-to-side forces resulting from the zigzag jump by focusing on the 2 significant harmonics.

The same procedure outlined for the front-to-back force model for swaying was followed for the front-to-back force due to jumping. However, Equations 6.1a had no solutions when the magnitudes of any two harmonics used in the evaluation of *d* using Equations 6.1a were equal or when the magnitude at the higher harmonic was larger than the magnitude at the smaller harmonic. This was often the situation with the first three harmonics for front-to-back forces due to vertical jumping. Fortunately, since the magnitudes will eventually drop at higher harmonics it was always possible to find two successive harmonics where the magnitudes are unequal and the magnitude at the higher harmonic is smaller than the magnitude at the lower harmonic. This made the

application of the procedure more general and robust. Thus, any suitable equation among the following (Equations 6.9a-e) was used to evaluate *d* after comparing the magnitudes of successive harmonics.

$$MFH_1 = \frac{2H_P \sin(1\times \pi d)}{1\times \pi};\ MFH_2 = \frac{2H_P \sin(2\times \pi d)}{2\times \pi};\ MFH_1 > MFH_2 \quad (6.9a)$$

$$MFH_2 = \frac{2H_P \sin(2\times \pi d)}{2\times \pi};\ MFH_3 = \frac{2H_P \sin(3\times \pi d)}{3\times \pi};\ MFH_2 > MFH_3 \quad (6.9b)$$

$$MFH_3 = \frac{2H_P \sin(3\times \pi d)}{3\times \pi};\ MFH_4 = \frac{2H_P \sin(4\times \pi d)}{4\times \pi};\ MFH_3 > MFH_4 \quad (6.9c)$$

$$MFH_4 = \frac{2H_P \sin(4\times \pi d)}{4\times \pi};\ MFH_5 = \frac{2H_P \sin(5\times \pi d)}{5\times \pi};\ MFH_4 > MFH_5 \quad (6.9d)$$

$$MFH_5 = \frac{2H_P \sin(5\times \pi d)}{5\times \pi};\ MFH_6 = \frac{2H_P \sin(6\times \pi d)}{6\times \pi};\ MFH_5 > MFH_6 \quad (6.9e)$$

Values for H_{pF} and H_{pB} were evaluated from the sub-pulse mean data as discussed previously (see Equations 6.8a&b). For front-to-back forces due to jumping it is important to consider a number of harmonics as Figure 4.20a showed that the force magnitude can still be significant even at the sixth harmonic. Table B19 of Appendix B shows a typical value for *d* evaluated for vertical jumping at 2 Hz by substituting magnitudes of the 2nd and 3rd harmonics presented in Figure 4.19b of Chapter 4 into Equation 6.9b. The corresponding values for H_{pF} and H_{pB} evaluated by substituting appropriate data presented in Table 4.3 of Chapter 4 into Equations 6.8a&b are also shown. In Section 6.1.6, these parameters will be used to demonstrate that the front-to-back model is capable of representing front-to-back forces resulting from jumping by focusing on the first four harmonics.

6.1.4. Application of models to regular mean force pulse of individual subjects

This section presents various comparisons of simulated and measured forces based on the theoretical framework and the step-by-step numerical procedure for implementing the proposed models discussed in Section 6.1. The objective is to demonstrate a variety of prediction capabilities for the models.

The discussion below will demonstrate the capabilities of the side-to-side and front-to-back models to predict the mean impulse curve corresponding to following time histories: (i) side-to-side forces consisting of Type I pulses (Figure 6.6) recorded during standing sway; (ii) side-to-side forces consisting of Type II pulses (Figure 6.7) recorded during standing sway (iii) and front-to-back forces recorded during seated swaying (Figure 6.8). Section 6.1.5 will demonstrate the capabilities of the models in predicting the random variability (cycle-by-cycle variations) of the force amplitude and frequency observed in the measured force data leading to the generation of a stochastic time history from the models. Section 6.1.6 will show that the models can be applied to horizontal forces due to vertical jumping.

The mean impulse curve of the recorded data was determined by separating each recorded time-history into individual pulse cycles and aligning them by a zero crossing point for each cycle (Figures 6.6-6.8). Aligning impulse cycles this way minimized the distortion of the mean impulse curve because the zero crossing point chosen was approximately the point of symmetry or anti-symmetry.

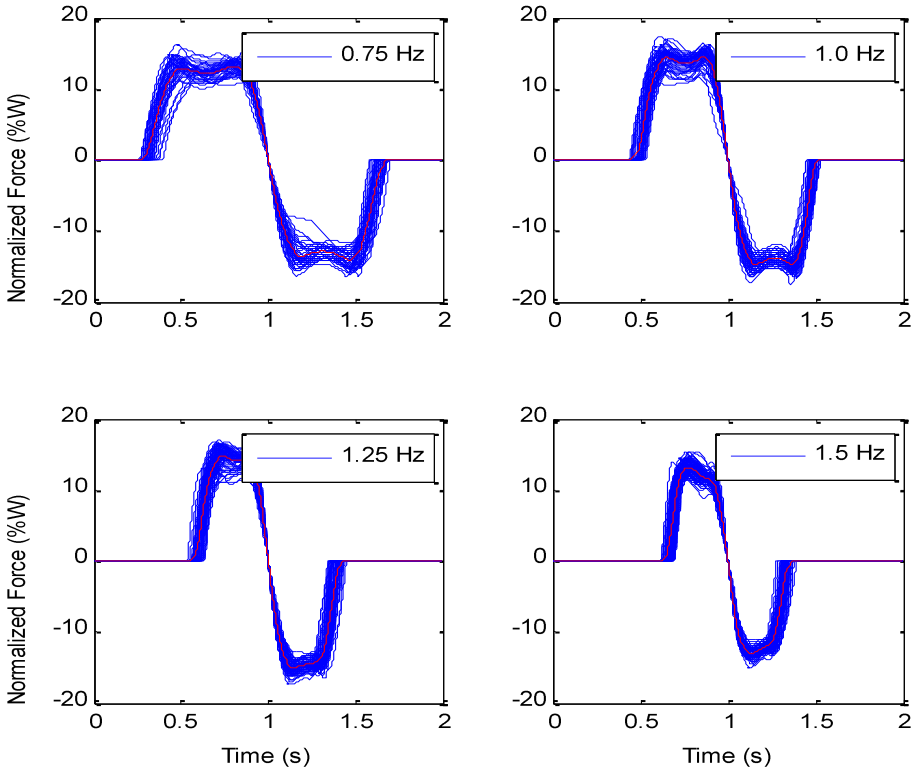

Figure 6.6: Type I impulses for swaying side-to-side in a standing position

Comparisons of analytic models and the mean impulse curves for side-to-side forces due to swaying in a standing position are shown in Figures 6.9 and 6.10. Type I pulses for side-to-side swaying were predicted when a positive sign was used in Equation 6.3, while a negative sign led to Type II pulses. For assessing the goodness of the fit, the root-mean-squared-error (RMSE) for each impulse curve can be calculated using Equation 6.10. However, this subject will be addressed in detail in Section 7.1.1 where different methodologies for aligning individual impulse cycles before averaging will be presented to show their influence on the calculated RMSE.

$$RMSE = \sqrt{\frac{\sum (F_m - F_a)^2}{N_p}} \qquad (6.10)$$

where F_m is the force of the mean pulse evaluated from the measured force time-history data , F_a, is the fitted analytic function and N_p is the number of fitted points.

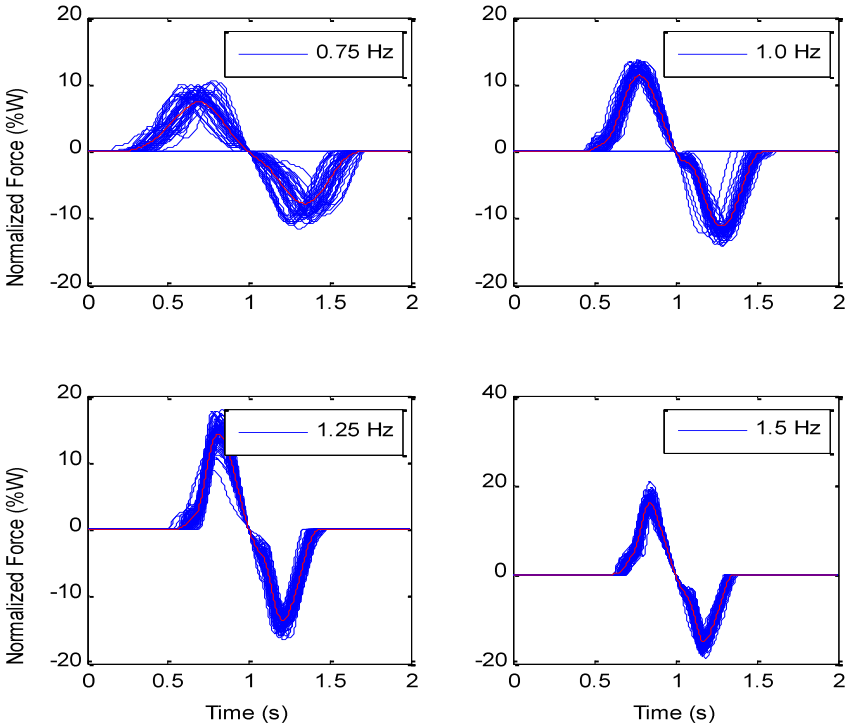

Figure 6.7: Type II impulses for swaying side-to-side in a standing position

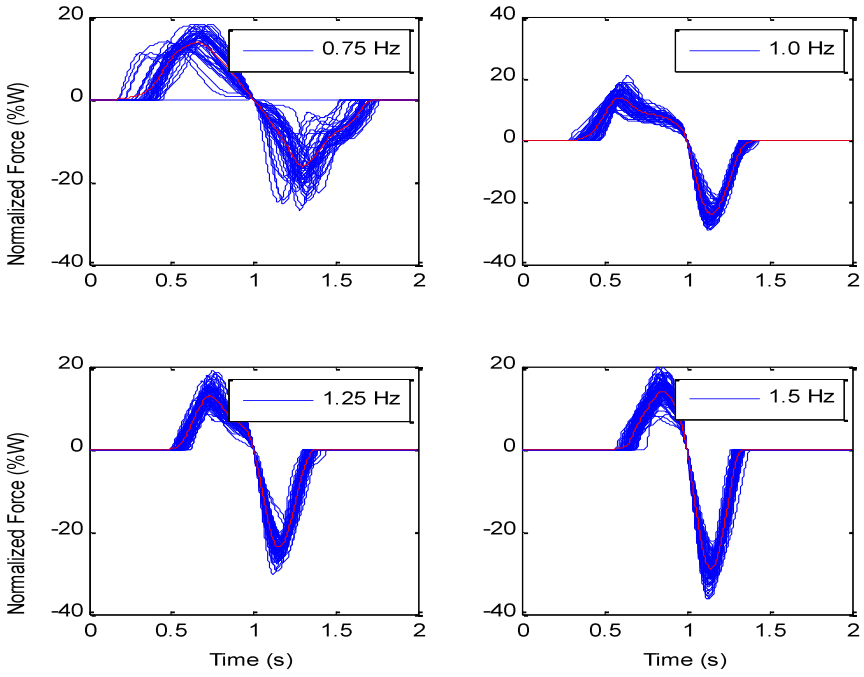

Figure 6.8: Impulses for swaying front-to-back in a sitting position

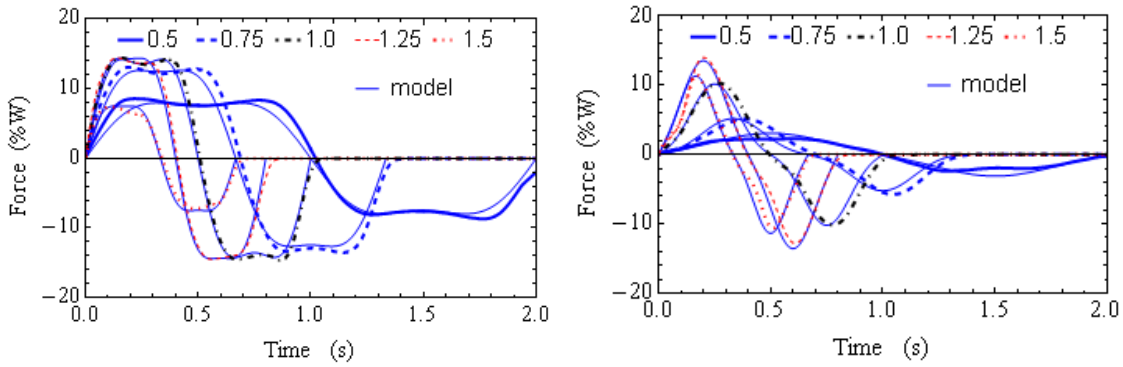

Figure 6.9: Comparison of typical analytic and measured mean force for Type I and Type II impulses

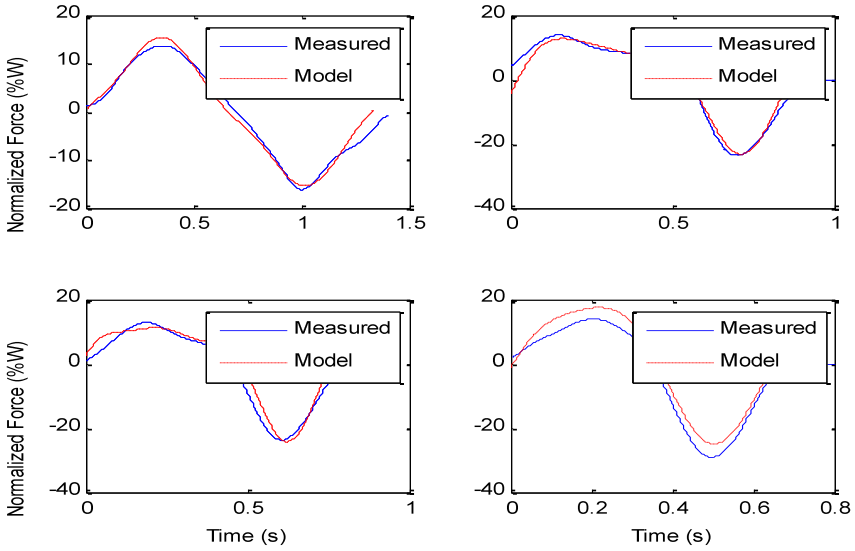

Figure 6.10: Comparison of typical analytic and measured mean forces for swaying (seated) front-to-back pulses

6.1.5. Fitting of models to stochastic swaying force of individual subjects

In addition to describing the measured force by the mean regular pulse of the applied force, it can be represented more realistically by simulating the swaying of an imperfect subject whose swaying frequency might vary by small random deviations leading to a stochastic force-time history. To model this, firstly, the recorded time history was separated into individual cycles which were aligned by the first point of separation as shown in Figure 6.11. Following this, Equation 6.3 was used to predict each cycle using

the steps presented in Section 6.1.1. Finally the simulated cycles were joined together to form a single vector with their order preserved. The comparisons shown in Figure 6.12 indicate that both the waveform and frequency content of two types of measured swaying forces were adequately predicted

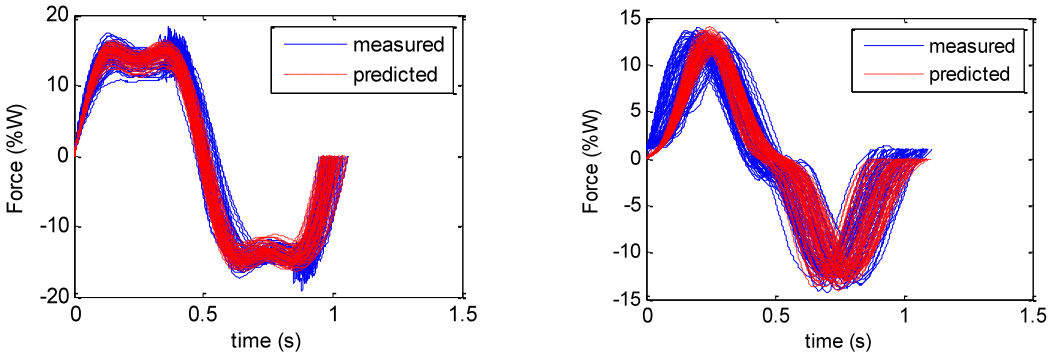

Figure 6.11: Fitting of analytic model to stochastic force impulses made of Type I and II forces

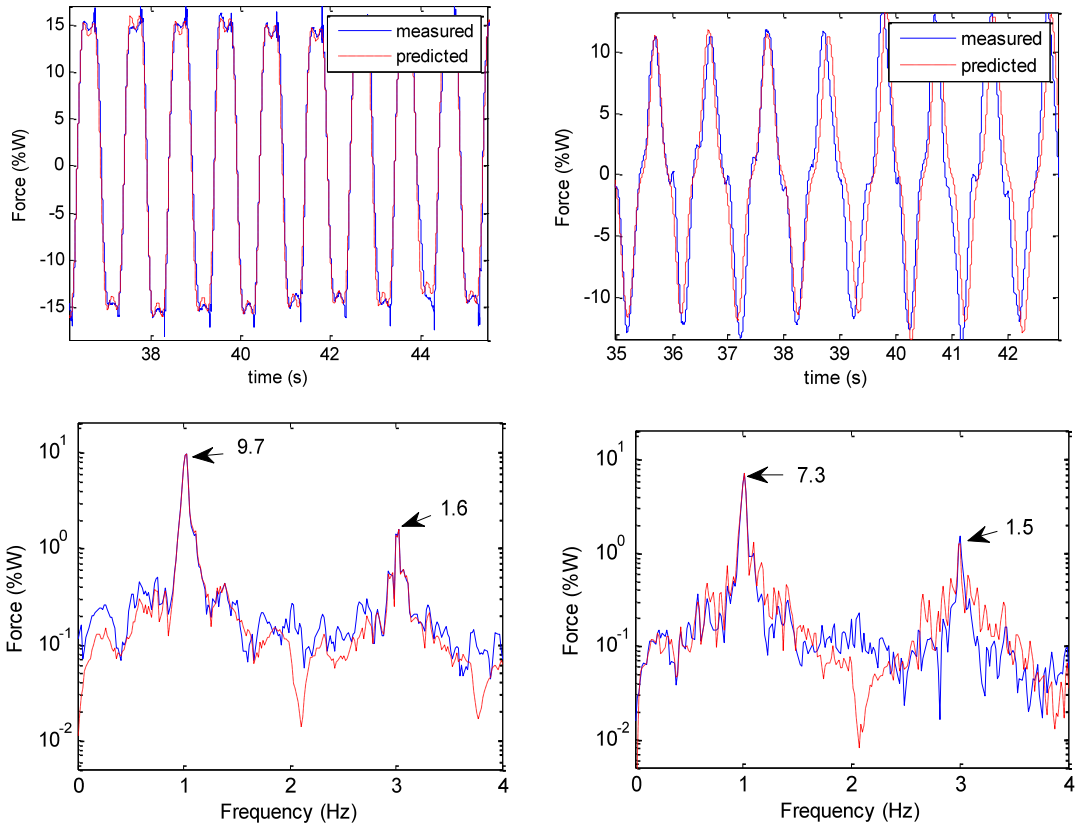

Figure 6.12: Comparison of simulated and measured force in the time and frequency domain

6.1.6. Fitting of models to horizontal forces due to vertical jumping

The models presented previously (Sections 6.1.1 and 6.1.2) were also applied to time-histories recorded during vertical jumping. The front-to-back force model for swaying was used for simulating the front to-back force cycle-by-cycle due to vertical jumping at 120 b/min (Figure 6.13a) by focusing on the first four harmonics. Similarly, the side-to-side force model used for swaying was used to predict the side-to-side force cycle-by-cycle for the zigzag jump at 150 b/min (Figure 6.13b) by considering the 2 significant harmonics at 1.25 and 3.75 Hz while ignoring negligible harmonics (with peaks <1%W) in measured data. The comparisons shown in Figure 6.13 indicate that waveforms and the frequency spectra were reasonably matched.

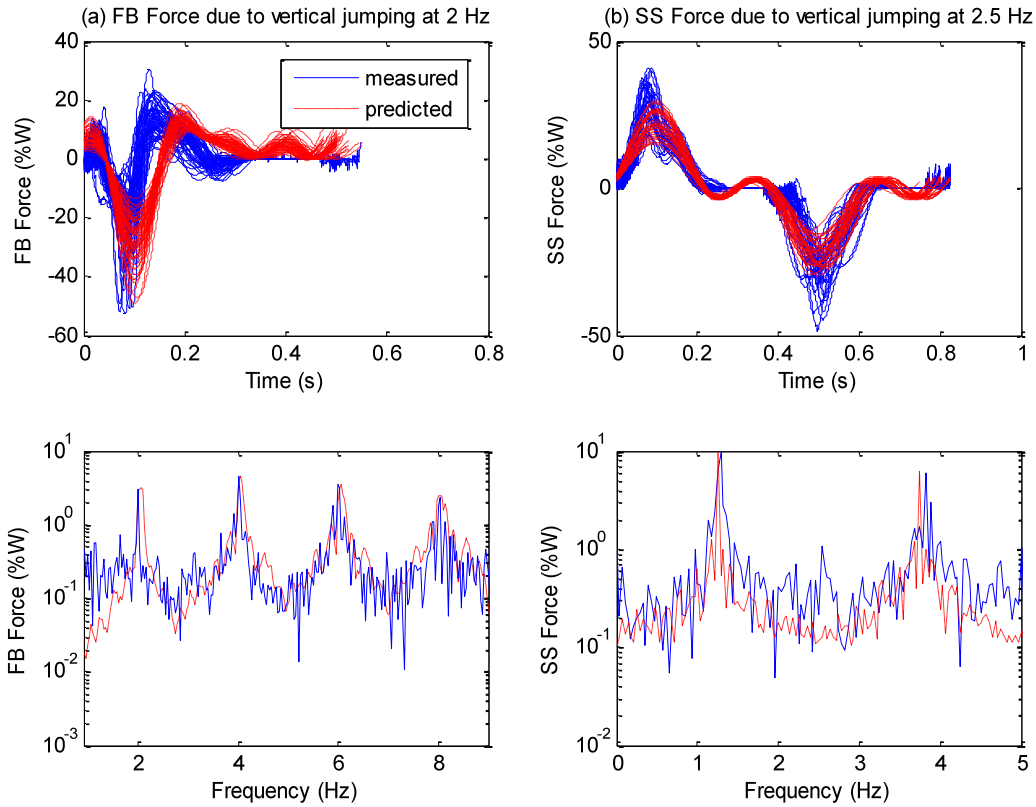

Figure 6.13: Simulated and measured side-to-side and front-to-back forces due to jumping

6.2. Crowd model for side-to-side swaying

Forces due to swaying side-to-side in a standing position were larger than forces due to swaying front-to-back in the same position, thus individual time-histories recorded during side-to-side swaying were treated as a severe load case. The measured forces for each individual were simulated (using the computer program described in Section 6.1.1) and added together to form group loads of 12, 24, 36 and 60 subjects. To generate group loads for more than 12 subjects the data gathered from 12 subjects was used more than once. Before summation, the individual time histories were offset by random phase lags taking into account the statistics of mean phase delays presented in Figure 5.17 of Chapter 5 for groups of subjects performing side-to-side swaying at the same time.

For each group and each swaying frequency, the amplitude of the simulated dynamic force per person was evaluated and compared with that of a single individual for 10 randomly simulated cases (Figures 6.14-6.17).

The simulations shown in Figures 6.14-6.17 indicate that as the crowd size increases above 12 subjects, the mean force at the first harmonic becomes asymptotic to 5% of subject weight. The force at the third harmonic also became smaller compared to that of a single individual. This means that a model that ignores the lack of synchronization among crowd members would be over conservative. Vertical forces due to jumping are also known to exhibit asymptotic behaviour (Ebrahimpour & Sack 1989; Parkhouse & Ewins 2006).

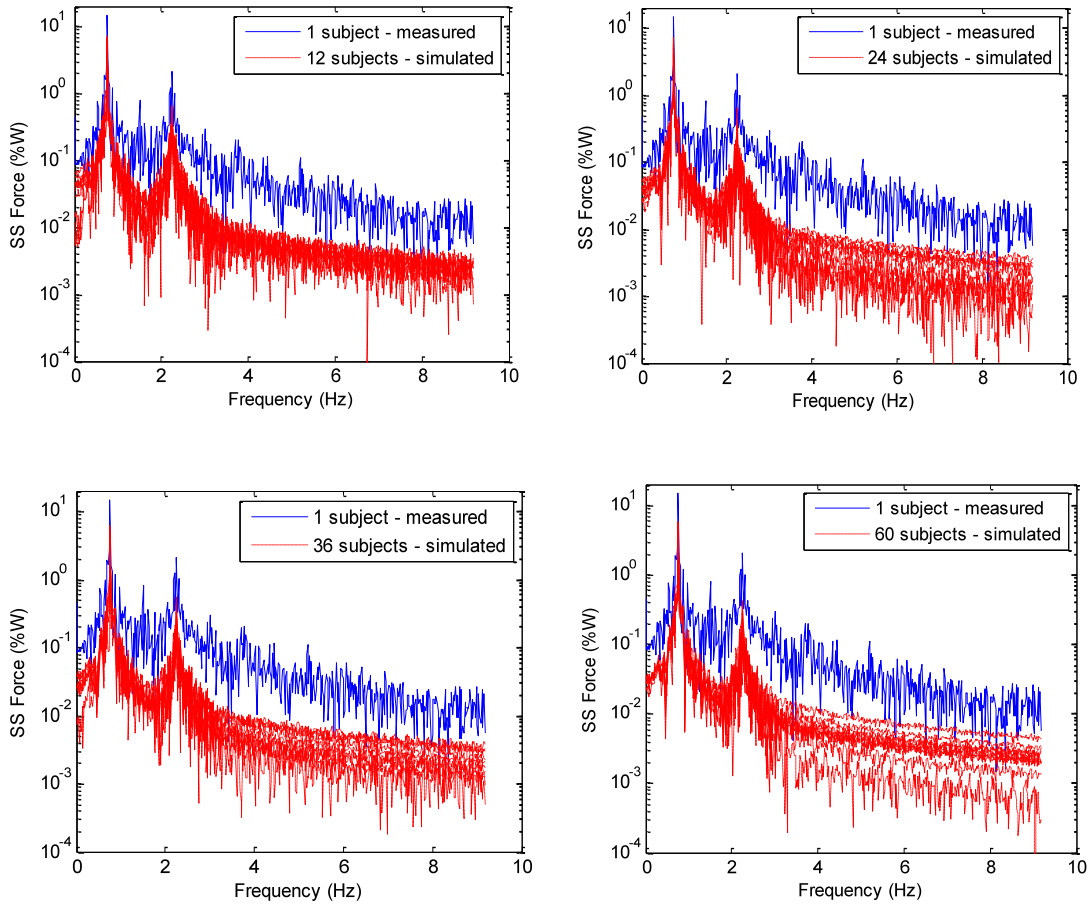

Figure 6.14: Spectral magnitudes/person for swaying side-to-side at 0.75 Hz for different groups

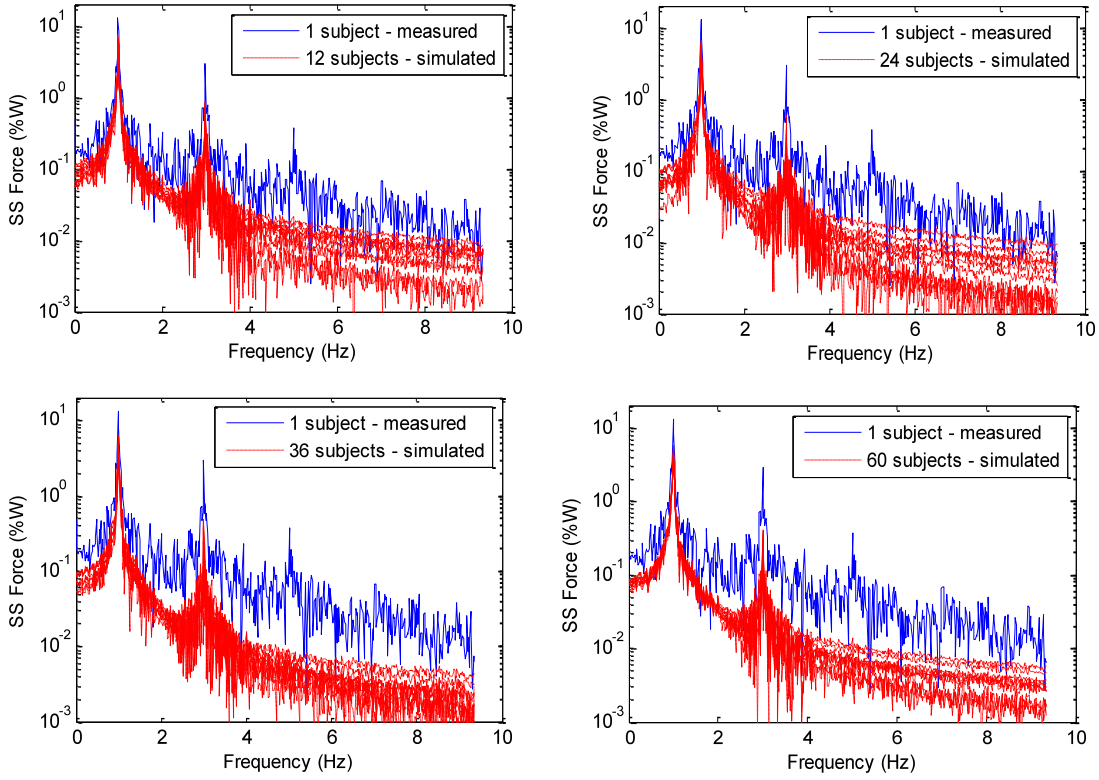

Figure 6.15: Spectral magnitudes/person for swaying side-to-side at 1.0 Hz for different groups

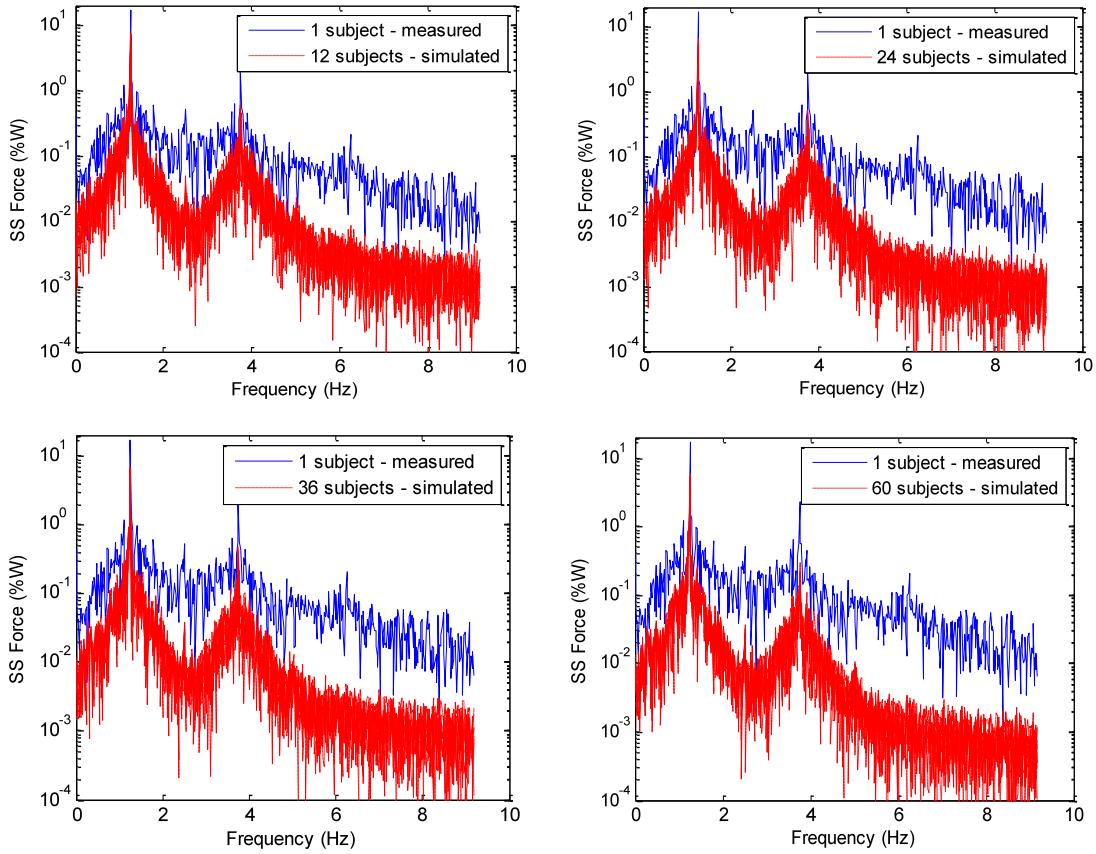

Figure 6.16: Spectral magnitudes/person for swaying side-to-side at 1.25 Hz for different groups

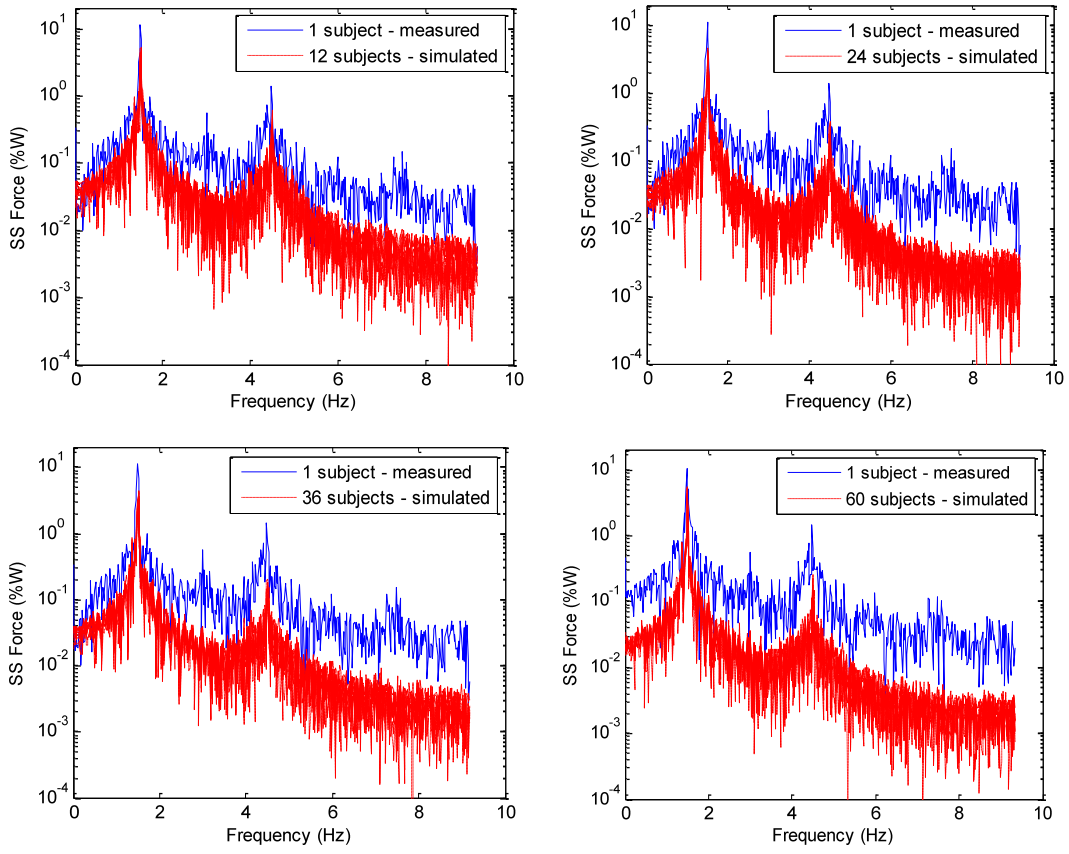

Figure 6.17: Spectral magnitudes/person for swaying side-to-side at 1.5 Hz for different groups

6.3. Concluding remarks

This chapter presented a procedure for describing horizontal forces analytically. Positive and negative parts of the force pulse were each modelled using a Fourier series of a rectangular pulse (Equation 6.1) which were shifted and added together to form a total pulse. The Fourier series was reduced to a simple formula to predict side-to-side forces (Equation 6.3).

Side-to-side forces due to swaying in a standing position simulated using the side-to-side model (Equation 6.3) compared well with the corresponding laboratory-measured data when the first and third harmonics were considered. The main parameters (d and H_p) of the model relevant for the prediction of side-to-side forces due to swaying side-to-side in a standing position are summarized in Table 6.1. In addition, the model can be applied to the prediction of side-to-side forces due to swaying in a sitting position (using the parameter presented in Table B16 of Appendix B). It was also demonstrated that the same model can be used to predict side-to-side forces due to the zigzag jump at 2.5 Hz (which produced the largest side-to-side forces for vertical jumping) from the parameters presented in Table B19 of Appendix B.

For front-to-back forces, positive and negative parts of the force pulse were modelled separately and the resulting Fourier series was not reduced further to account for the lack of symmetry observed in the measured data. Front-to-back forces due to swaying in a sitting position simulated using the front-to-back model (Equations 6.4-6.7) compared well with the corresponding laboratory-measured data when the first and second harmonics were considered. The main parameters (d, H_{pF} and H_{pB}) of the model

applicable to the prediction of front-to-back forces due to swaying front-to-back in a standing position and sitting position are summarized in Tables B17 and B18 of Appendix B, respectively. It was also shown that the model can be applied to the prediction of front-to-back forces due to vertical jumping by focusing on the parameters presented in Table B19 of Appendix B for jumping at 2 Hz.

Finally, a group model for swaying was formed by summation of simulated individual forces due to side-to-side swaying as an enveloping load case scenario for all swaying forces. Before summation the simulated individual time histories were shifted by normally distributed phase lags which were presented in Figure 5.17 of Chapter 5. As the crowd size increased beyond 12 subjects, the mean force at the first harmonic became asymptotic to 5% of subject weight.

Chapter 7

7. Numerical parametric studies and finite element simulations

This chapter discusses the excitation of a single-degree-of-freedom oscillator, representing a typical structure, by a side-to-side or front-to-back force of a single person swaying or jumping (Section 7.1). In Section 7.2 this analysis is extended to a specific finite element model of a demountable grandstand structure which is characterized by some nonlinear behaviour.

7.1. Numerical parametric studies

The response of the oscillator was assessed as a function of the damping and natural frequency of the oscillator and the horizontal force of the person. The horizontal response due to swaying was examined by considering the force generated by swaying side-to-side at 120 b/min as the worst case and most probable scenario. As spectators are free to face any direction on a grandstand, the side-to-side force was used to determine both the side-to-side and front-to-back responses. The horizontal response due to jumping was obtained by considering the front-to-back force due to jumping at 120 b/min and the side-to-side force due to the zigzag jump at 150 b/min. For these analyses it was assumed that the forcing function for the jumping subject can be described by a perfectly periodic function represented by the mean impulse force curve. For swaying side-to-side, the mean impulse curve was first determined from the average of many individual cycles and then approximated by the analytic model presented in Section 6.1.1. The procedure for determining the mean impulse force curve and its analytical approximation is discussed below.

7.1.1. Determination of mean impulse from force data

In order to determine the mean impulse curve from the average of many individual cycles it is necessary to split and align individual cycles before evaluating the average. This evaluation has already been performed in Sections 4.2.2 and 6.1.4 without any acknowledgement that different strategies for splitting and aligning impulses exist and each will lead to different results. The method used by Sim (2006) for vertical jumping forces was based on aligning individual cycles by the centroid of each impulse. The centroid for each impulse was calculated by using Equation 2.7b. Parkhouse & Ewins (2006) used the beep to align individual cycles. Whilst both methods work for vertical forces they could not be used in this research because the impulse contains symmetric positive and negative values which makes the denominator term of Equation 2.7b to be zero.

After many trials, three methods which produced similar results were selected (see Figures 7.1-7.3). Method 1 was based on simply aligning individual cycles by the first point of each split impulse as reported in Section 4.2.2. In the second method, the cycles were aligned by a zero crossing point for each cycle as discussed in Section 6.1.4. For the third method, each cycle was first aligned according to Method 2 assuming its period is exactly equal to the period of the beep. If the cycle exceeded the beep period it was shifted slightly to the left by half the amount it exceeded the peep period and vice versa. After fitting the analytic model for side-to-side forces (using the procedure explained in Chapter 6.1.4) to each of the evaluated mean curves, the root mean square error was evaluated using Equation 6.8. The results are shown in Table B20 in Appendix B. The lowest error is obtained with Method 2; however, the RMSE values are nearly similar. This indicates that any of the methods could be used.

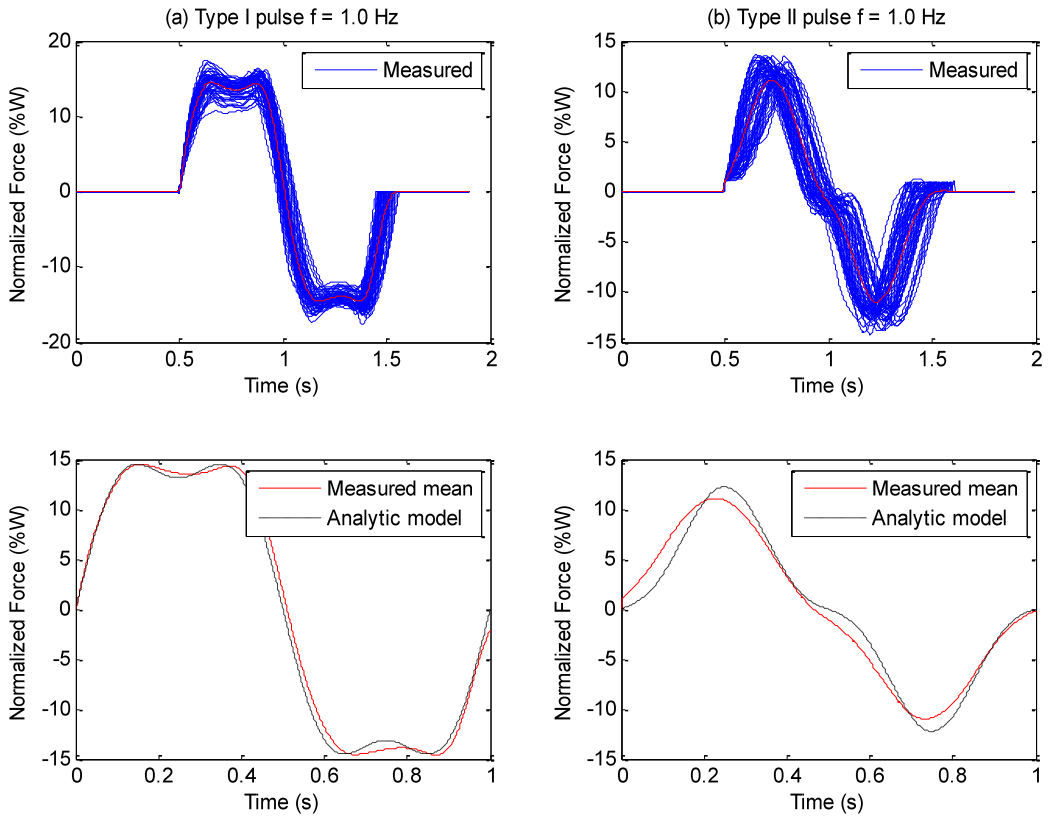

Figure 7.1: Evaluating mean impulse curve using Method 1

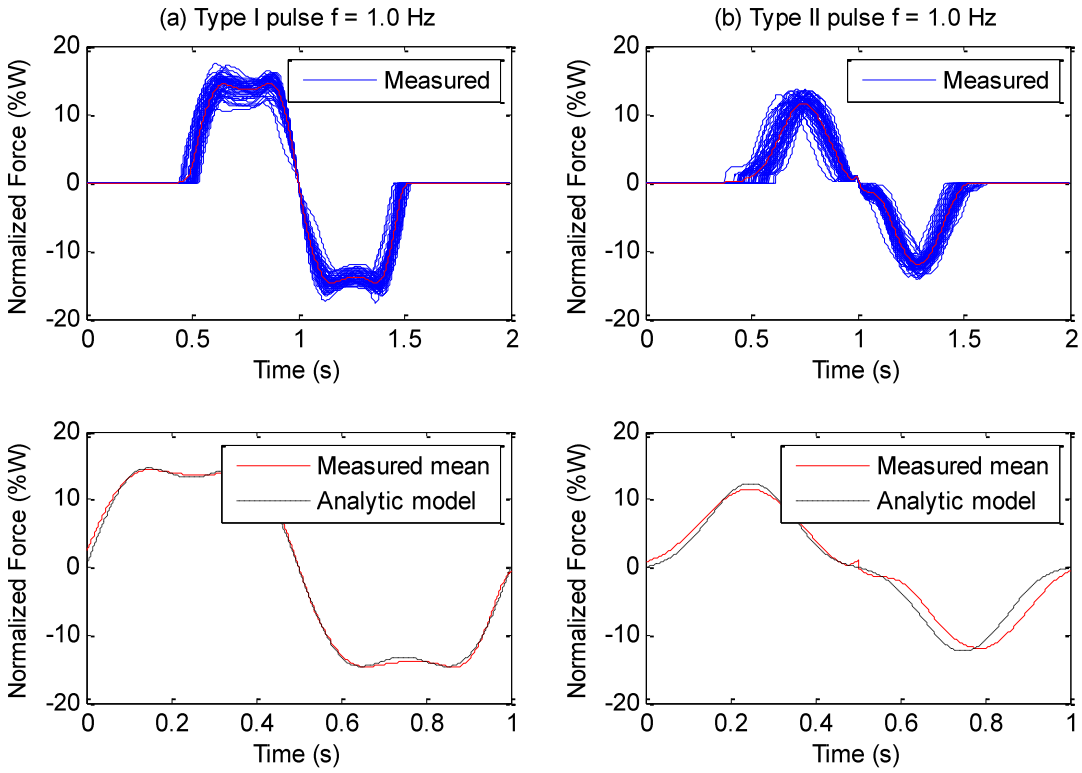

Figure 7.2: Evaluating mean impulse curve using Method 2

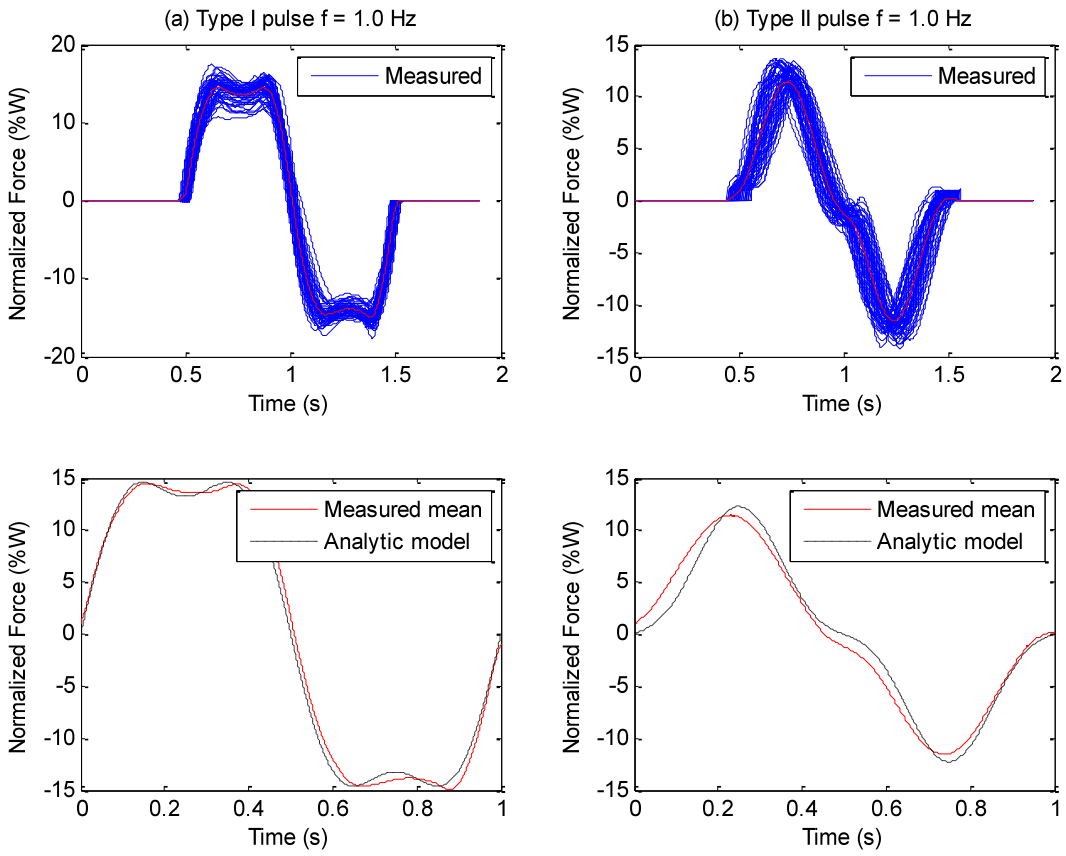

Figure 7.3: Evaluating mean impulse curve using Method 3

7.1.2. Time-history analysis: Single-degree-of-freedom systems

Assuming no significant human-structure interaction effects, the motion of a single-degree-of-freedom system with a mass, m_s, a circular natural frequency, ω , and a damping ratio, ζ , due to a horizontal force *f(t)* is governed by the equation:

$$\ddot{x}(t) + 2\zeta\omega\dot{x}(t) + \omega^2 x(t) = f(t)/m_s \qquad (7.1)$$

$$f(t) = \alpha m_H g U(t)$$

where

x(t) = displacement response

f(t) = exciting horizontal force as a proportion of the weight of human subject(s)

$U(t)$ = time varying force amplitude of $f(t)$ normalized to have unit positive peaks

m_H = mass of human subject(s)

g = gravity constant

α = proportionality constant between the horizontal force and subject weight

The response $x(t)$ to an arbitrary force $f(t)$ can be determined by a variety of numerical methods. One such method involves the use of the Duhamel integral which can be evaluated numerically for linear systems (Chopra 1995). An alternative is to use one of the many well-known time stepping techniques in which the state of the system is determined at small increments, each state being calculated from its immediate predecessor. The latter approach can be used for all types of systems including non-linear systems and was adopted here. The time-stepping technique called the constant average acceleration method or Newmark $\beta = 1/4$ method has been used in this research for solving Equation 7.1. The method can be found in well-known references (Chopra 1995; Hart & Wong 2000) and it was chosen because it is unconditionally stable. To check for inaccuracies associated with the size of the numerical integration time step, the time step used for each simulation was reduced until identical results were obtained.

7.1.2.1 Forcing functions

The following force time-histories were used as input parameters to Equation 7.1: (i) a pure sinusoidal force with a unit amplitude and a frequency of 1 Hz (note that 1 Hz is equivalent to 120 b/min for swaying) (ii) synchronous Type I forces due to swaying side-to-side at 120 b/min (Figure 7.4a), (iii) synchronous Type II forces due to swaying side-to-side at 120 b/min (Figure 7.4b), (iv) synchronous side-to-side forces due to

vertical jumping (zigzag jump) at 150 b/min (Figure 6.16a), (v) synchronous front-to-back forces due to vertical jumping at 120 b/min (Figure 6.16b) and (vi) unsynchronized crowd forces due to swaying side-to-side at 120 b/min simulated for 60 subjects (Figure 6.19). In order to compare the frequency spectra of different solutions to Equation 7.1, all forces were normalized further such that each time history had unit amplitudes for all positive peaks (see Figures 7.5, 7.6 and 7.7). This was achieved by dividing all time histories by the following normalization factor:

$$NF = (max-min)/2 \qquad (7.2)$$

where *max* and *min* are the maximum and minimum values of the force, respectively.

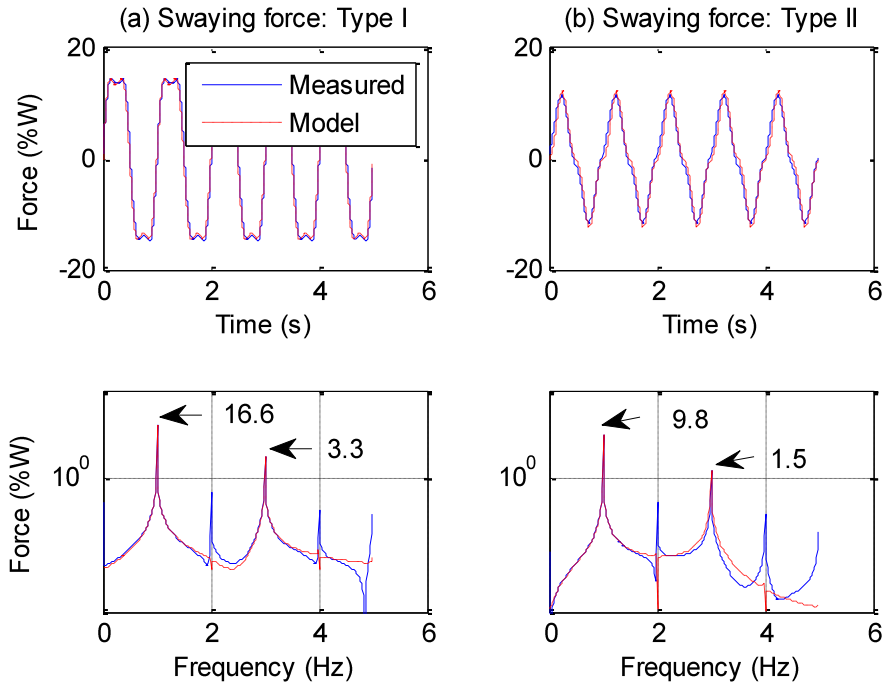

Figure 7.4: Side-to-side swaying forces

Finally, the right hand side of Equation 7.1 was scaled by the following scale factor:

$$s.f = m_s / \alpha m_H g \qquad (7.3)$$

This is equivalent to assuming that the maximum force and the mass parameter m_s have unit positive magnitudes such that a solution of any other amplitude can be evaluated by multiplying the unit solution by the inverse of the scale factor (Equation 7.3).

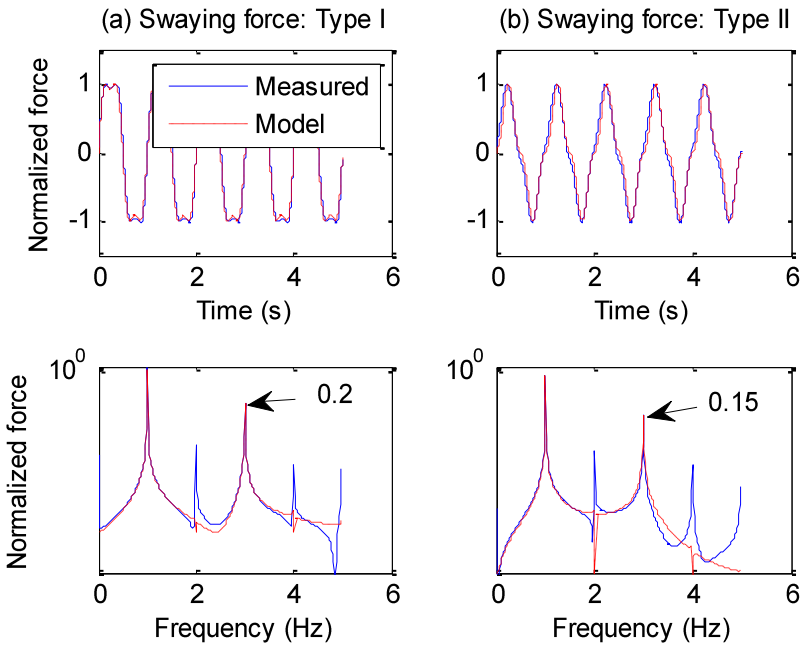

Figure 7.5: Normalized swaying forces used as input

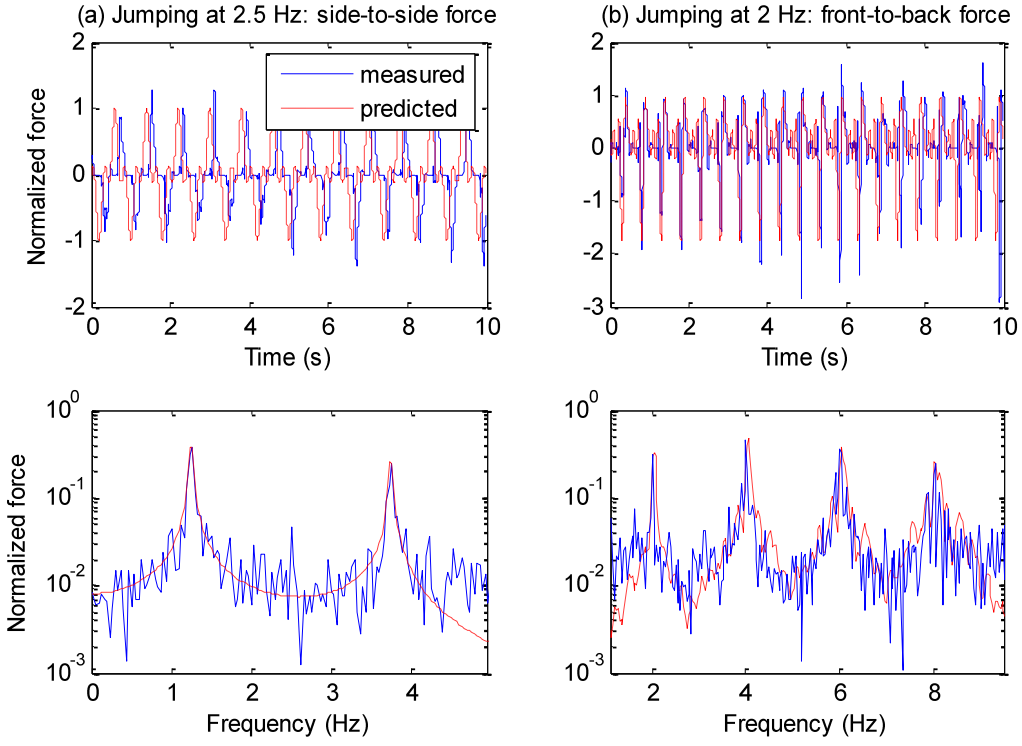

Figure 7.6: Normalized jumping forces used as input

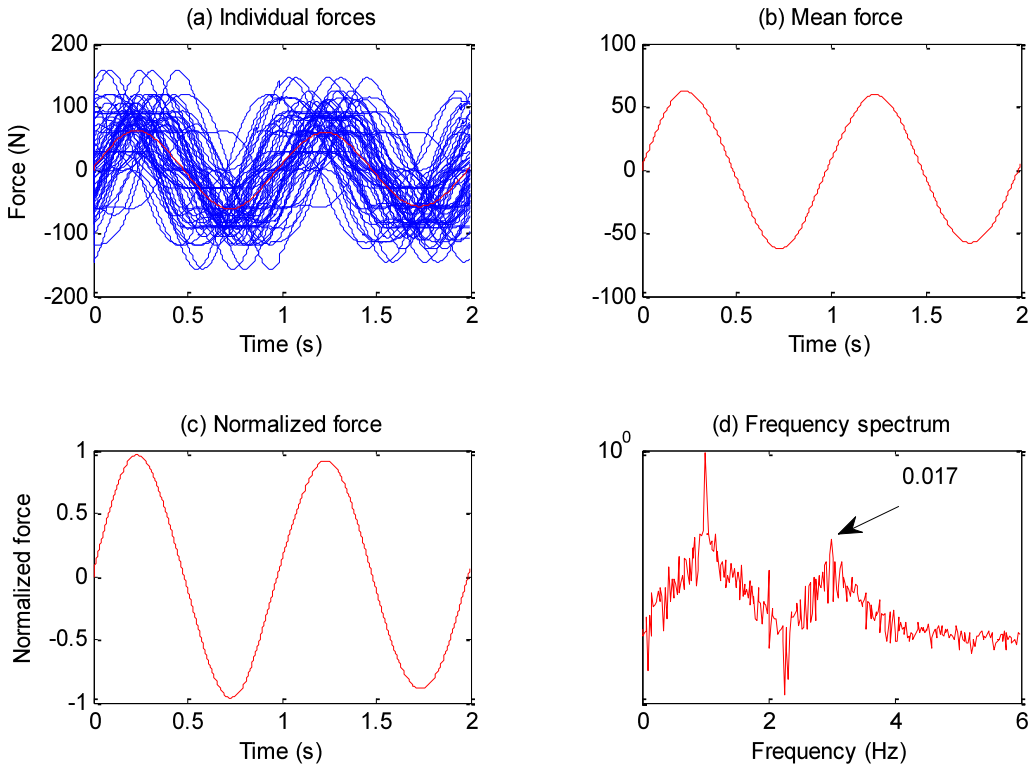

Figure 7.7: Simulated crowd swaying forces (60 subjects) used as input

7.1.2.2 Oscillator responses

Equation 7.1 was evaluated by varying both the damping ratio and the frequency ratio between the structures damped natural frequency (*fd*) and the music beat or force frequency (*fb*). The values for the peak displacement, peak acceleration and the dynamic magnification factor (DMF) were plotted against *fd/fb* ratios for the five cases shown in Figures 7.8 to 7.13. Each graph shows clear peaks when the natural frequency of the structure coincide with the harmonics of the force. As damping increases all the peaks become less sharp. With the exception of the jumping case, the contribution of the higher harmonics to the peak displacement is negligible. Conversely, the higher harmonics have clear contribution to the dynamic magnification factor (DMF) and peak acceleration. This is more significant for jumping. Peak values of the DMF are

important in limit state design, while peak values of acceleration have also been used as important criteria for serviceability conditions (Kasperski 1996).

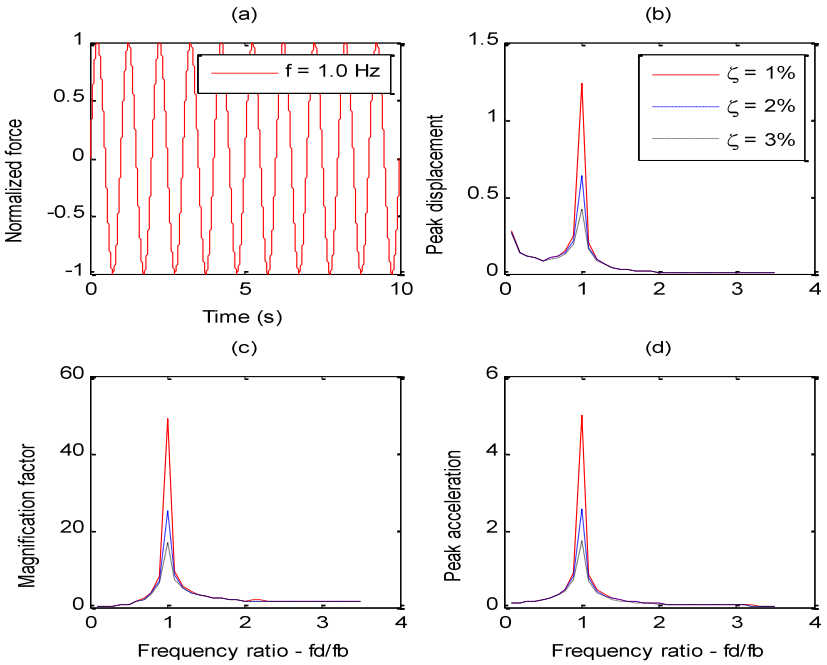

Figure 7.8: (a) Unit sinusoidal force (b) peak displacement (c) dynamic magnification factor and (d) peak acceleration

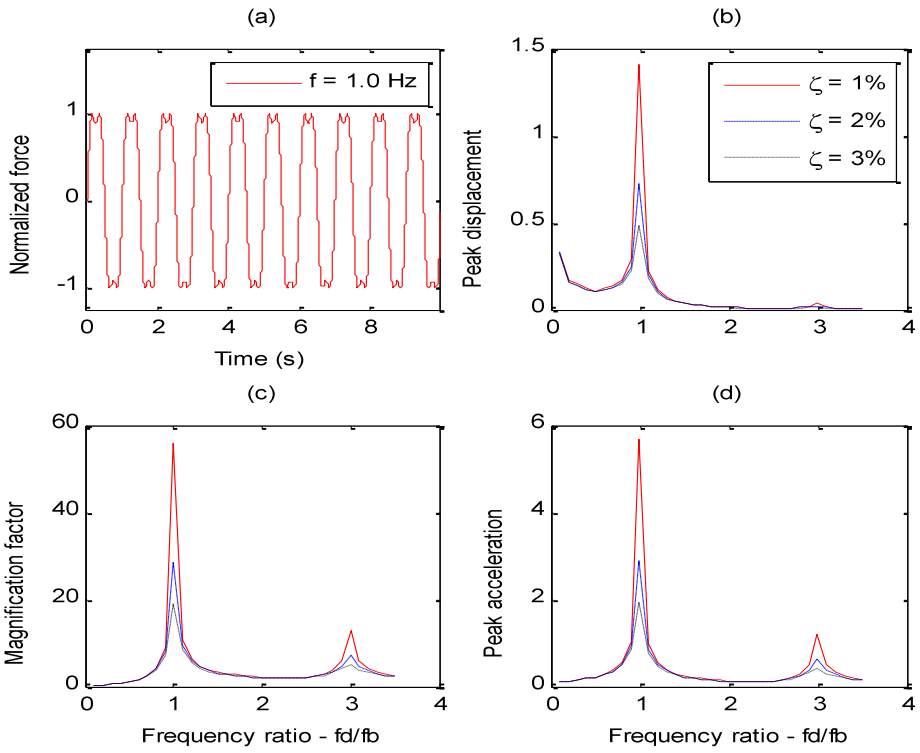

Figure 7.9: (a) Normalized swaying force –Type I (b) peak displacement (c) dynamic magnification factor and (d) peak acceleration

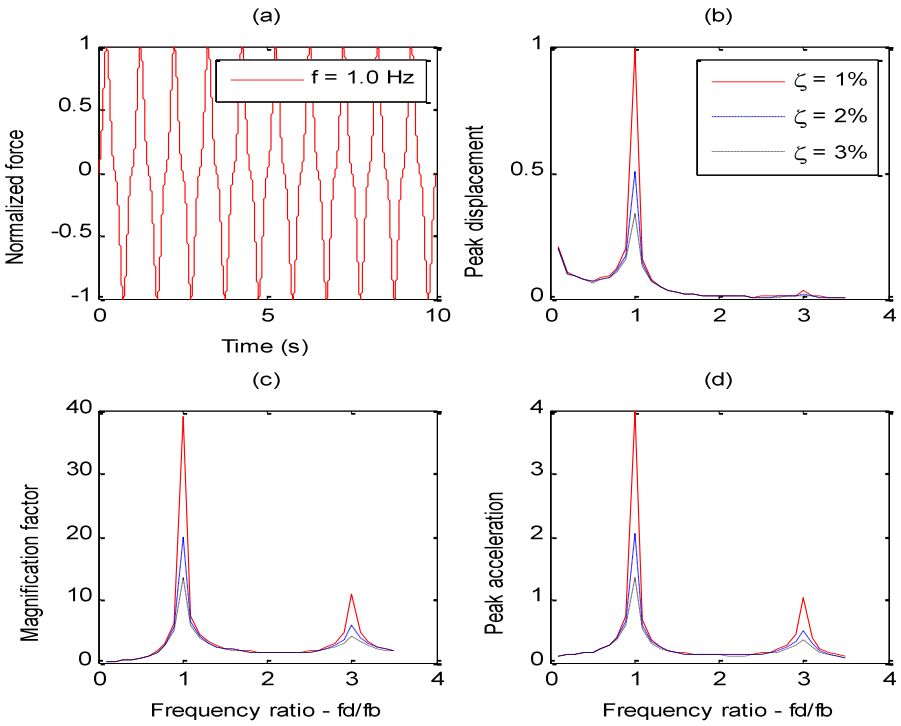

Figure 7.10: (a) Normalized swaying force –Type II (b) peak displacement (c) dynamic magnification factor and (d) peak acceleration

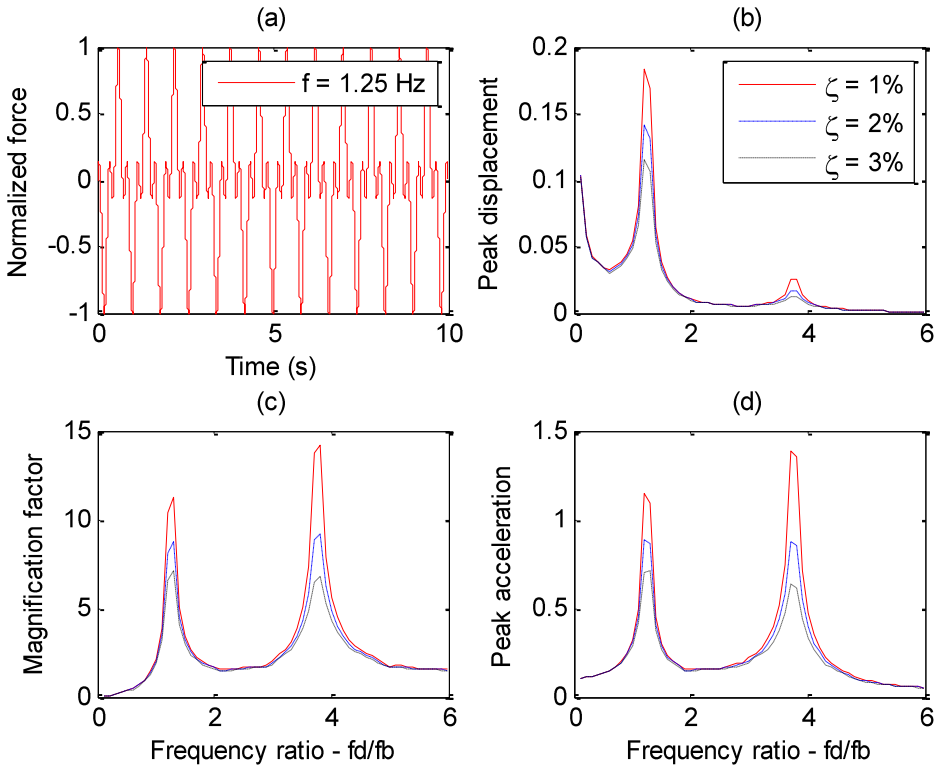

Figure 7.11: (a) Normalized side-to-side jumping force (b) peak displacement (c) dynamic magnification factor and (d) peak acceleration

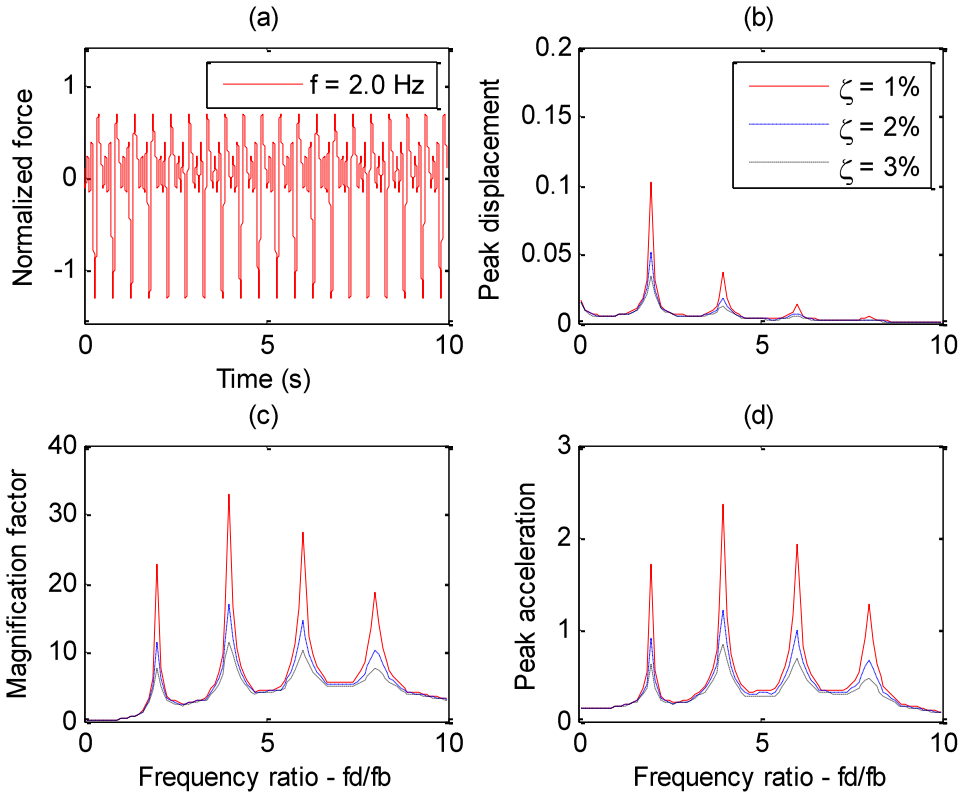

Figure 7.12: (a) Normalized front-to-back jumping force (b) peak displacement (c) dynamic magnification factor and (d) peak acceleration

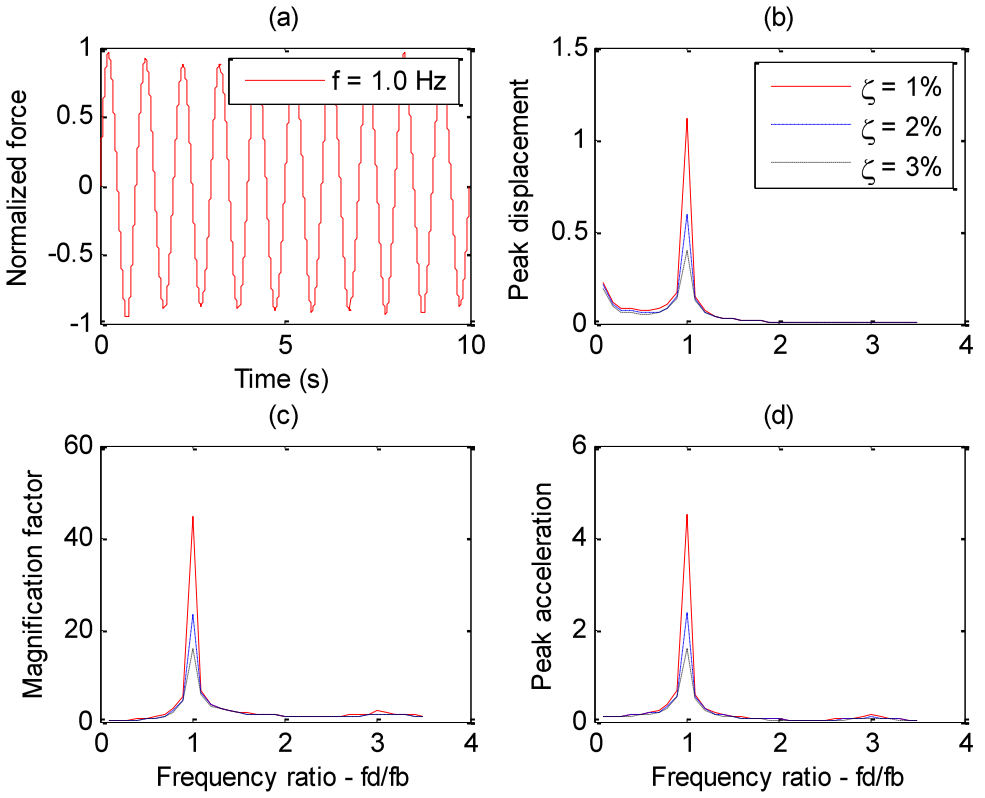

Figure 7.13: (a) Normalized group swaying force for 60 subjects (b) peak displacement (c) dynamic magnification factor and (d) peak acceleration

7.2. Grandstand tests and finite element simulations

Dynamic tests were undertaken in order investigate structural properties of a typical demountable grandstand structure and to compile and calibrate a finite element model of the structure. Subsequently, the model was used to examine the significance of horizontal forces on the response of the structure. The demountable grandstand investigated is called the ClearView™ system and is currently being developed by Arena Seating (commercial supplier of spectator facilities and seating structures to stadia, UK) as a prototype product. The deck assembly for this structural system is characterized by variable-height seat-mounts which allow the adjustment of seat rows to optimize viewing or sight lines.

A demountable grandstand structure was chosen for this analysis because demountable structures are known to have a low horizontal stiffness. They also exhibit some degree of nonlinear behaviour. Therefore horizontal excitation is the controlling influence in their design, including consideration for nonlinear behaviour.

7.2.1. In-situ dynamic tests

In order to calibrate the finite element model both the static and dynamic behaviour were examined by conducting in-situ tests on a prototype structure for which bracing patterns were varied. The dynamic tests and the bracing patterns will be discussed in Section 7.2.1.1 Static tests were carried out by pulling the frame side-to-side and front-to-back. In contrast to the dynamic tests, these tests were carried out by Arena Seating and were only performed on one bracing pattern. Arena Seating kindly provided this data for the purpose of calibrating the finite element model. These tests will not be

discussed in detail in this research but the data that was provided will be shown in Section 7.2.3 for comparison with the finite element model.

7.2.1.1. Description of grandstand system and bracing patterns

The full-scale prototype module for the grandstand system consisted of two sub systems, a deck assembly (made from aluminum, timber and steel components) and a variable-height scaffold assembly made from steel. Figure 7.14 shows the grandstand module which can be propagated sideways, backwards and upwards to accommodate a variety of audience capacities and sight lines. The stand has a total capacity of 60 seats.

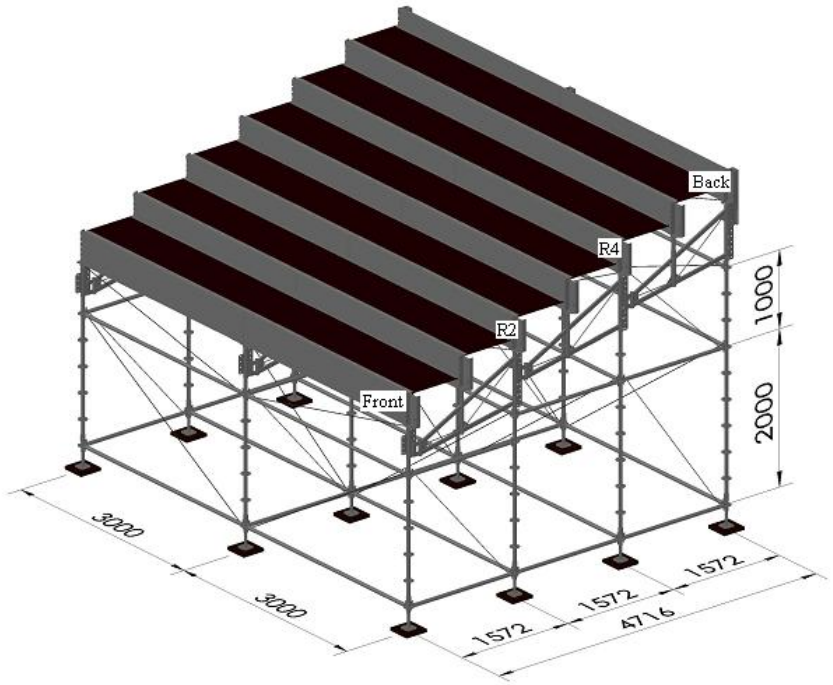

Figure 7.14: ClearView™ grandstand system

It was desirable to characterize the horizontal dynamic behaviour (lateral or front-to-back, longitudinal or side-to-side and torsion) of the grandstand unit for as wide a range of bracing patterns as possible. A number of possibilities were considered giving rise to a total of 15 bracing patterns and permutations. The choice of each bracing pattern was based on a trial and error process guided by previous experience, prevailing industry

practice and recommendations in the literature (Ji 2003; Lian *et al.* 2000; Ji *et al.* 1997). Figure 7.15 shows one of the tested bracing patterns referred to as Pattern 1. This particular bracing pattern was also used for the finite element model discussed in Section 7.2.3.

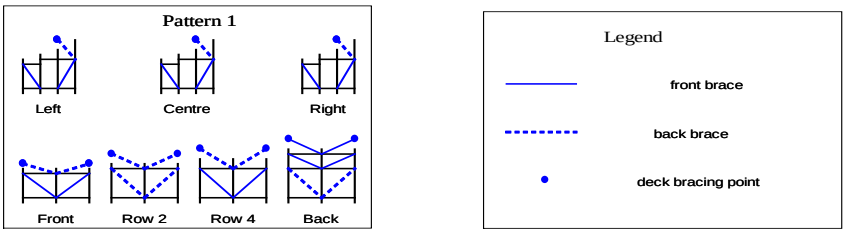

Figure 7.15: Bracing pattern 1 used for the finite element model

The top row frames depicted in Figure 7.15 span side-to-side while the bottom row is for front-to-back. Row 2 refers to a frame under seat row 2 on the deck in Figure 7.14. All braces have some eccentricity (4.5-7.5 mm) at the connections. In Figure 7.15, the solid line represents positive (in front of the frame) and the broken line represents negative (behind the frame) eccentricity when each frame is viewed from the front or from the right. Eccentricity refers to the perpendicular distance between the longitudinal axis of the brace member and the neutral or mid plane of the frame on which the brace member lies. The top nodes provide connection points to the deck truss which is a separate system. The remaining bracing patterns are illustrated in Figure A19 of Appendix A. In order to increase the lateral stiffness, patterns 8-11 had an intermediate extra layer of horizontal members midway along the scaffold height.

7.2.1.2. Dynamic testing apparatus and methodology

(a) Eccentric mass exciter and mounting assembly

The eccentric mass shaker (100 Kg) used and its mounting assembly (30 Kg) are shown in Figure 7.16. All the components shown were transported to the test site, assembled

and attached to the test structure. The shaker is owned by the Department of Civil Engineering, University of Oxford and has been used in previous projects. However, the mounting assembly was designed specifically for this project. It comprised a rigid base attached to both the test structure and a rotatable base (for changing the orientation of the exciter to load the structure front-to-back or side-to-side) which in turn was welded to an upper frame assembly. In order to monitor the applied forces a force plate was bolted directly to the upper frame assembly before the eccentric mass exciter was attached to it (Figure 7.16a).

(a)

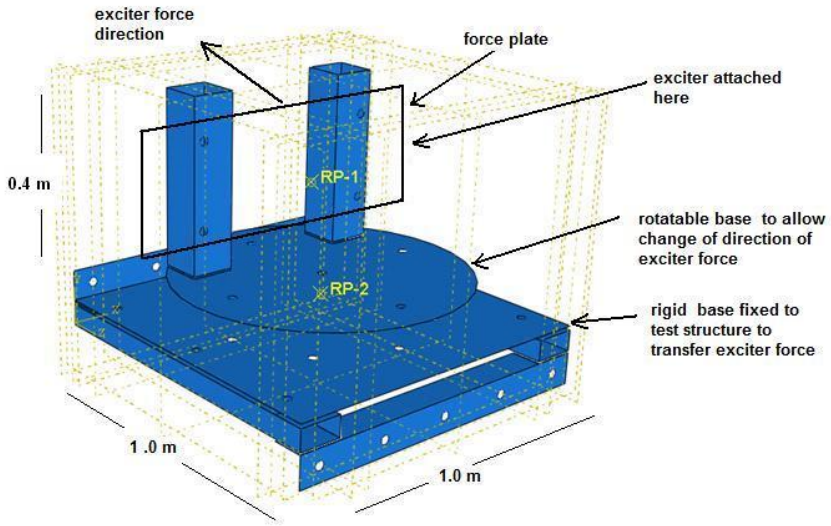

(b)

Figure 7.16: (a) Exciter mounting assembly (b) Attaching the eccentric mass shaker to the test structure

The eccentric mass shaker consisted of a drive motor, an adjustable frequency drive control system and an eccentric mass assembly that rotated about a shaft to produce a rotating force vector in a horizontal plane. The shaker's eccentricity was kept fixed while the rotating mass could be adjusted.

(b) Accelerometers and data acquisition

Piezoelectric uni-axial accelerometers (PCB 357A06, PCB Piezotronics, Inc) were used for vibration monitoring. A typical piezoelectric accelerometer consists of a small mass (seismic mass) attached to a piezoelectric element. When the instrument is shaken or attached to a vibrating object, the small mass loads the piezoelectric element which in turn generates a voltage proportional to the acceleration of the mass. The PCB accelerometer used is a shear type device and generates a voltage proportional to its shear deformation when shaken. The operating limits and calibration of the accelerometers were checked and verified to ensure good quality performance in the frequency band of interest (2-8 Hz). Finally, the accelerometers were connected to charge amplifiers (to modify signal amplitude to desired level) before connection to a data acquisition board (DT9804, Data Translation, Inc) which used a data acquisition software package (quickDAQ) from the same manufacturer.

(c) Test procedure, sample positions data handling and pre-processing

During testing, the exciter was located at the back right corner of the structure in order to excite all critical horizontal vibration modes, including torsion. In a typical test the structure was driven by a sinusoidal force (at a discrete frequency and force amplitude) to a steady state response followed by data collection. This procedure was repeated until

the frequency band of interest (2-8 Hz) had been reasonably sampled to achieve 1/10 Hz frequency increments or resolution. Some tests were conducted with an upward sweep followed by a downward sweep, while in others only an upward sweep was performed. In the frequency band of interest the exciter had the load spectrum shown in Figure 7.17a for two loading cases (L1 and L2) that were investigated. In this figure, the exciter force amplitude in L2 is twice that in L1. Eventually, only loading case L1 was used as L2 produced very large structural vibrations. The load spectrum varied generally with the square of the excitation frequency as expected; however slight peaks were observed at resonant frequencies of the structure as evident in Figure 7.17a. This was likely caused by high vibration levels which induced additional inertial or feedback forces on the structure-exciter interface.

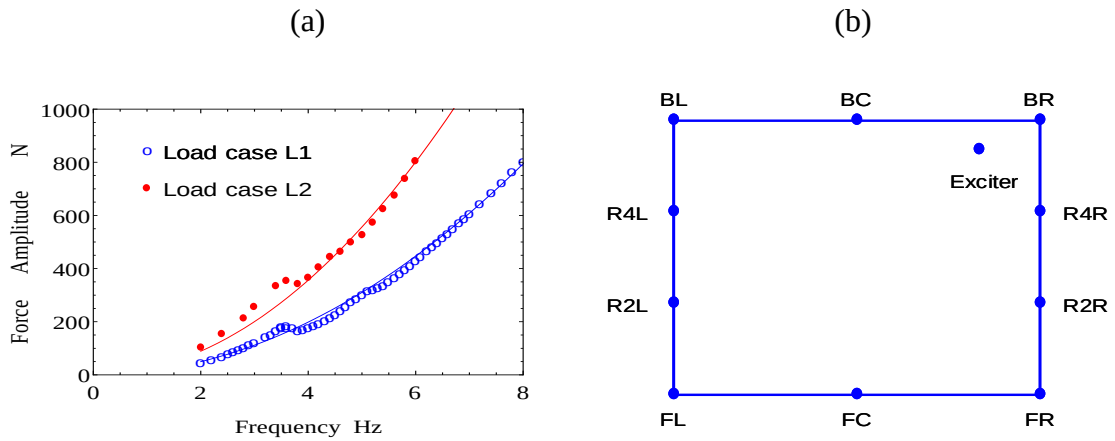

Figure 7.17: (a) Exciter load spectrum (b) exciter and accelerometer positions

Accelerometers were attached to the deck locations as shown in Figure 7.17b and connected to a data acquisition system used to collect vibration time history data. Monitoring the coupling between side-to-side and front-to-back vibration allowed torsional modes to be identified. All tests undertaken are listed in Table B5 in Appendix B. Most tests involved testing a unique bracing pattern, but on a few occasions the same

bracing pattern was tested more than once. In addition, some tests were conducted with an additional payload of 25 or 50 Kg of ballast (sand) per seating area for a total of 60 seats.

The data acquisition software produced output data in CSV (comma separated value) digital format. The data was saved and exported to a general processing software package (Matlab) for further processing and analysis. During processing, the data were digitally filtered to remove recorded time-history motions above 20 Hz in order to focus the analysis on the frequency band of interest.

7.2.1.3. Dynamic test results and discussion

The filtered data were processed further by evaluating the fast Fourier transform (FFT) to produce frequency response functions (FRFs). Typical FRF data points have been plotted using circular markers in Figure 7.18. To extract modal parameters such as stiffness, damping and mode shapes, analytical FRFs defined by stiffness, frequency and damping were fitted to the measured FRF data points. These are represented by continuous curves in Figure 7.18. The fitting procedure was implemented using a program written in Matlab and was based on the use of a standard function in Matlab called ‘lsqnonlin’. The function solves nonlinear least-squares problems, including non-linear data-fitting problems. A comparison of FRFs generated from the measured data and the fitted analytical FRFs is shown in Figure 7.18 for one of the test series. The analytic FRFs shown were fitted in more than one way to the measured points by adjusting parameters (stiffness, frequency and damping) until general agreement with the measured data was obtained. However general agreement was not always observed

due to the presence of nonlinear structural behaviour in the measured response. The "^" superscript indicates an orientation orthogonal to the rest.

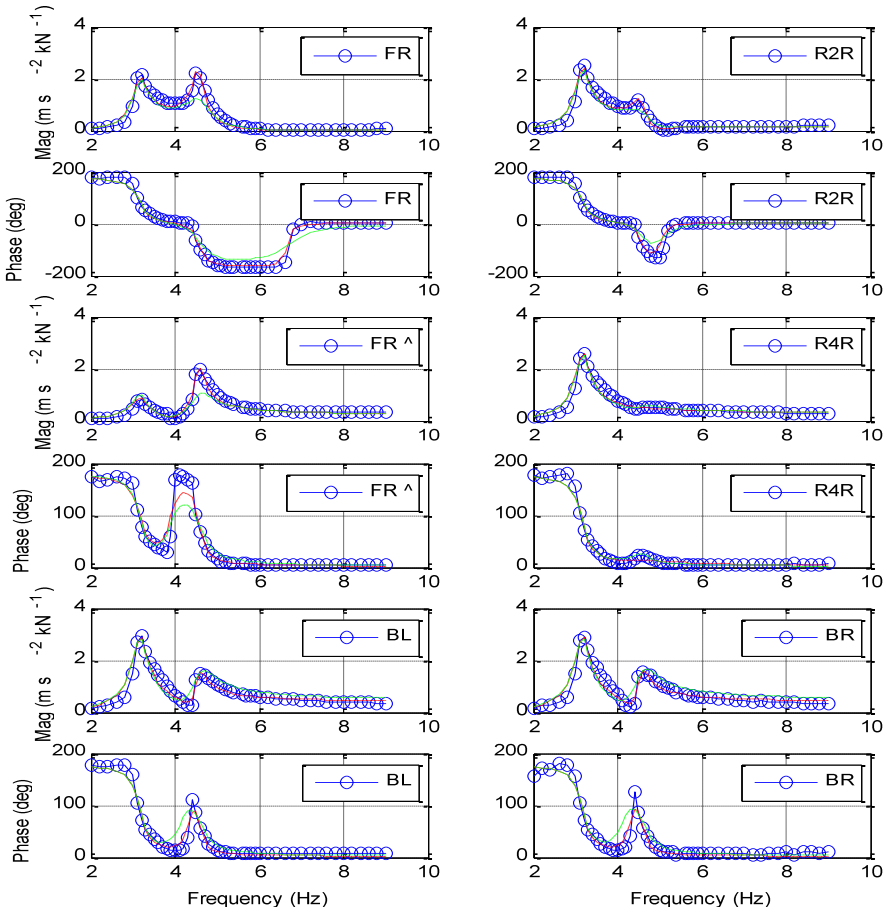

Figure 7.18: Examples of frequency response functions obtained from processed data

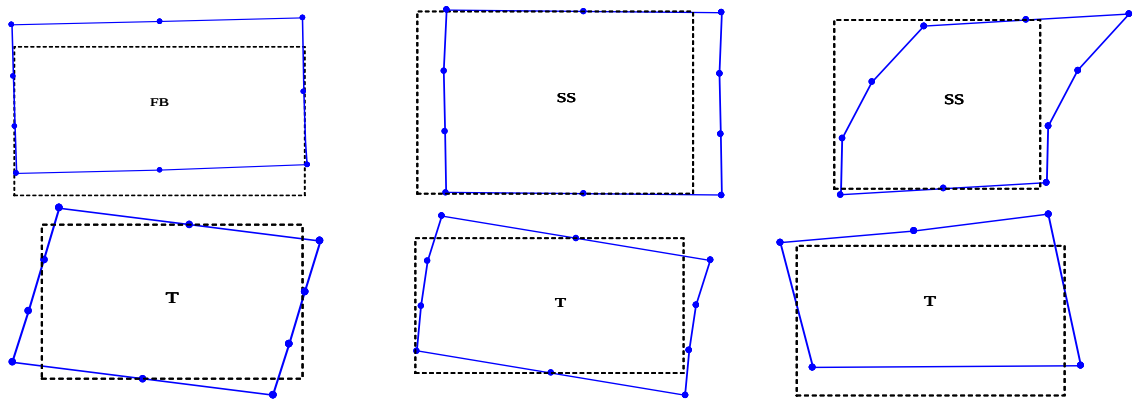

Figure 7.19: Examples of horizontal mode shapes

Examples representing vibration modes observed throughout the test program are shown in Figure 7.19. In this figure, the symbols FB, SS and T represent front-to-back, side-to-side and torsional vibration modes, respectively.

A summary of the test results is shown in Figure 7.20 where important dynamic characteristics are plotted for each bracing pattern investigated. Figure 7.20a shows a comparison of frequencies observed for the two lowest frequency modes in each bracing pattern. The frequency limit of 4 Hz (dashed line) which is the recommended requirement for an empty temporary grandstand is also shown. The empty stand has an approximate total mass of 2300 Kg; however, the exact values vary very slightly with each bracing pattern.

Some tests were performed with an additional payload and the effect of this on the natural frequencies was taken into account when generating Figure 7.20a. The results show that the majority of the tested configurations exceeded the 4Hz requirement significantly, the exact amount depending on the bracing pattern. In some tests there was a significant (and beneficial) increase in the effective stiffness when the stand was loaded with additional mass compared to when it was empty, indicating nonlinear behaviour.

Figure 7.20b shows how structural damping varied depending on the bracing pattern and additional mass on the stand. Damping values for the empty stand were consistently high and averaged 8 % of critical damping; however, for the loaded configurations damping values reduced significantly, averaging 5 % of critical damping. Figure 7.20c shows that there was a slight decrease in frequencies when the excitation force amplitude was doubled, indicating another aspect of nonlinear behaviour.

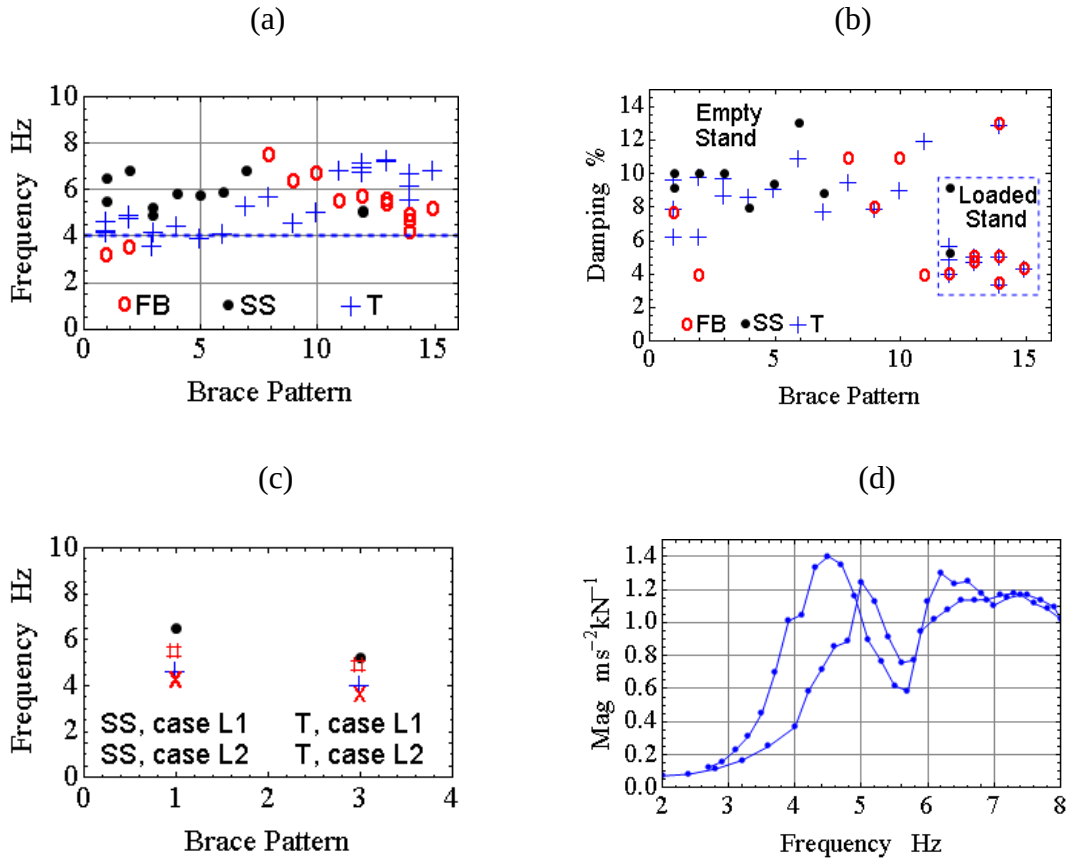

Figure 7.20: (a) Frequencies and (b) damping values observed for each brace pattern. (c) changes in frequencies with a change in excitation level. (d) FRF showing nonlinear behaviour

Several aspects of nonlinear structural behaviour of the stand were evident in the measurements and confirmed by visual observations. Firstly, occasional lifting-off of certain base joints during large resonant deflections was observed for tests involving the empty stand. This possibly explains the increase in effective stiffness observed in tests conducted when the stand was loaded since greater forces would be required to lift the joints. Secondly, a slip-sliding movement of brace ends at connections during structural vibrations was also common. In extreme cases some braces became loose and had to be knocked back in place. When this occurred the upward sweep curve of the response spectrum did not coincide with the downward sweep curve. This led to problems in data fitting and interpretation as shown in Figure 7.20d where according to the upward

sweep, the lowest mode observed in this test is 5 Hz, but 4.5 Hz for the downward sweep.

Finally, it is important to highlight that a number of torsional modes were observed because the tests were conducted on an elevated grandstand module which represented a more extreme case. The global lateral dimensions are many times larger than the height and depth of the stand for typical applications. Under these conditions torsional modes are likely to occur at significantly higher frequencies.

7.2.2. Summary of findings from dynamic tests

The results showed that the majority of the tested configurations exceeded the 4 Hz requirement by significant margins, the exact amount depending on the bracing pattern. A number of observations indicated the presence of nonlinear behaviour. It was clear from the results that the bracing pattern has a primary effect on the dynamic characteristics of the stand however, the effect of nonlinear structural behaviour on the dynamic response was also significant; firstly due to the observed dependence of frequencies on the excitation levels (Figure 7.20c) and secondly due the dependence of slip-sliding movement of joints on vibration levels leading to occasional lifting of some base joints and/or loosening of some braces (Figure 7.20d) . Recommendations for further testing and analysis are given below.

The results presented here indicate that similar grandstand configurations might be expected to meet the 4 Hz requirement; however, it is important to conduct further investigations to characterize the performance of grandstand structures that are occupied by crowds. Due the significance of nonlinear behaviour on the dynamic response, it was

important to adopt a nonlinear analysis approach when constructing a finite element model to predict the observed behaviour. Complying with the frequency based design approach which is intended strictly for linear structural behaviour was also less justifiable, making a nonlinear analysis approach necessary. Finally, in future tests, torsional behaviour could be investigated by the use of more than one exciter to provide torsional forcing directly.

7.2.3. Description of finite element model and validation

Model drawings of the stand braced according to bracing pattern P1 (Figure 7.15) were kindly supplied by Arena Seating and used to compile a finite element model in Abaqus Version 6.8-4. Due to copyright constraints, dimensions were estimated for some parts of the system such as the deck assembly. Thus, the results reported here do not necessarily reflect the performance of the copyrighted prototype product. However, the model is an adequate representation of the type of static and dynamic behaviour expected for demountable grandstand structures.

The necessity to model different types of connectors present throughout the structure and the potential for nonlinear structural behaviour on the dynamic response, led to the adoption of a nonlinear analysis approach. Abaqus/Standard provides ‘key options’ for describing linear or nonlinear behaviour for connector elements (Abaqus Version 6.8-4). These are switches used to turn various element options on or off. Key options include linear or nonlinear stiffness behaviour choices, printout controls, element coordinate system choices and user input parameters, etc. Two main types of connector elements were used in the model, namely UJOINT and GAP elements. UJOINT has biaxial (in-plane and out-of-plane) bending capabilities about any suitably defined local axis orientation system as shown in Figure 7.21.

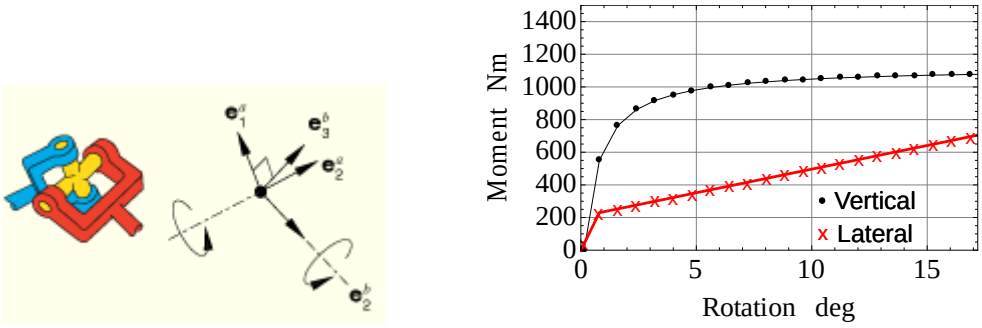

Figure 7.21: An example of a connector element and moment rotation data

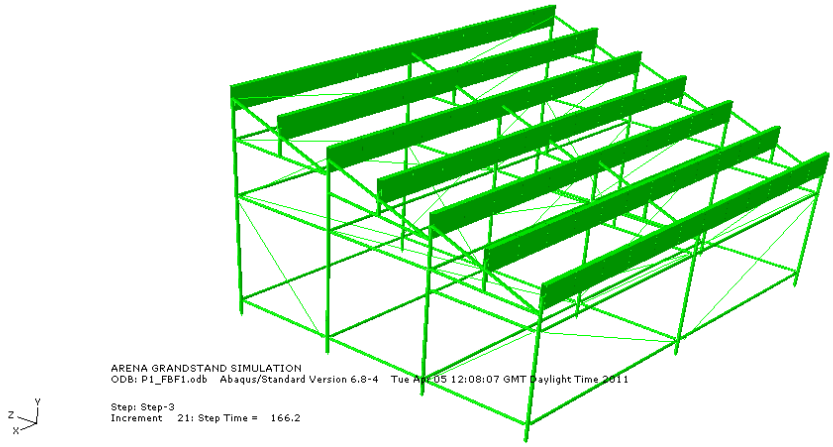

Figure 7.22: Finite element model

The moment-rotation data used as input for connecting the horizontal members to the vertical members in the model using the UJOINT connector is also shown in Figure 7.21. The data was obtained from the manufacturer of the scaffold structure. Gap elements were used to model the lack of fit in diagonal members (braces) including the lifting of the stand from some of its supports. The data from static tests suggested that the latter occurred when a horizontal load beyond a certain threshold caused an overturning effect when applied at the top of the stand. All structural members were modelled using beam elements with an average mesh length of 0.3 m as shown in Figure 7.22.

Figure 7.23 shows a comparison of measured and simulated static behaviour of the stand for this bracing pattern. The static tests involved pulling the deck of the stand by applying a horizontal force (side-to-side or front-to-back using a spreader beam to distribute the horizontal force) and measuring the resulting deflection at key locations on the deck. It is clear that the there was significant nonlinearity in the behaviour of the structure for large deflection amplitude. In particular, the lifting of some support led to a reduction in stiffness. Both the linear and post linear static behaviour was used as a basis for calibrating the finite element model and checked against frequencies measured from the dynamic tests.

(a) Front-to-back

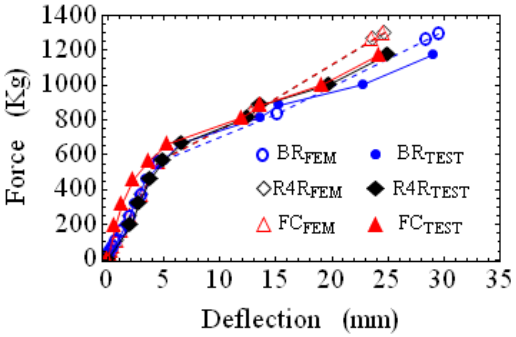

(b) Side-to-side

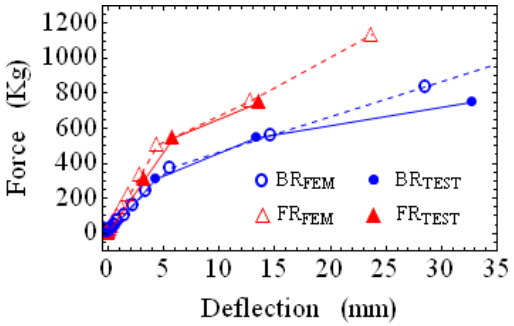

(b) Simulated lifting support

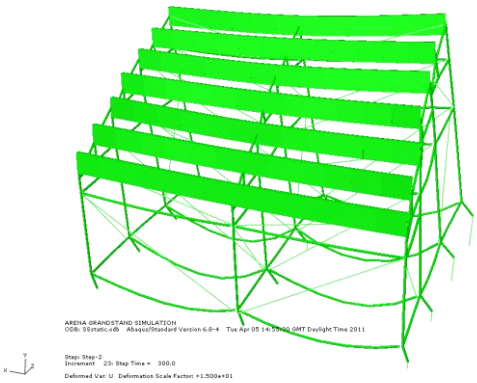

(d) Lifting support reactions

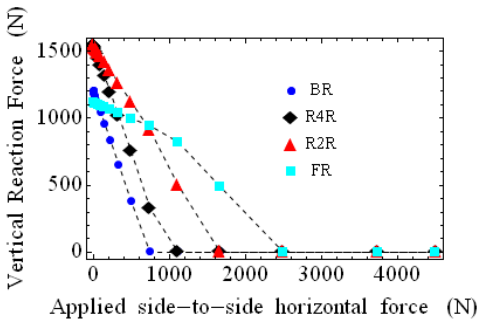

Figure 7.23: Static behaviour of stand and calibrated model

The initial stiffness in the FEM model corresponds to two horizontal frequencies of 3.1 (front-to-back) and 4.2 Hz (side-to-side or torsional). The values are slightly lower than those obtained from dynamic testing of the empty stand which were 3.2 and 4.3 Hz, respectively. This is due to the estimated mass of seats which was distributed to the deck beams by altering material density to give a total mass of 2467.6 kg for the FEM model. The mass for the prototype calculated by accurate weighing of all components was 2300 Kg. Finally, material properties that gave a minimum damping value of 3% critical for the first frequency (first linear region of Figure 7.23a) were specified in the model used for all horizontal excitation simulations which are discussed in Section 7.2.4.

7.2.4. Horizontal excitation simulations

A number of simulations were conducted to examine the behaviour of the structural model when excited by the force time-histories due to swaying side-to-side as presented in Section 7.1.2.1. In the first set of investigations three analyses were performed using the Type I force time-history at 1.0 Hz presented earlier in Figure 7.5a. The force time-history was scaled to have amplitudes of 20, 40, and 65 N per person for a total capacity of 60 people. To simulate the worst case scenario and to examine the effect of large levels of excitation on the response of the structure the forces were assumed to be perfectly periodic and synchronous. Both the front-to-back and side-to-side behaviour were examined using the same input of forces. The second set of analyses involved a more realistic case in which imperfect and non-synchronous crowd forces for swaying side-to-side were used as input. The procedure used for generating group forces was presented previously in Section 6.2. Since forces are not deterministic for crowds the

response evaluated due to crowd swaying loads at 1.0 Hz was repeated up to ten simulations.

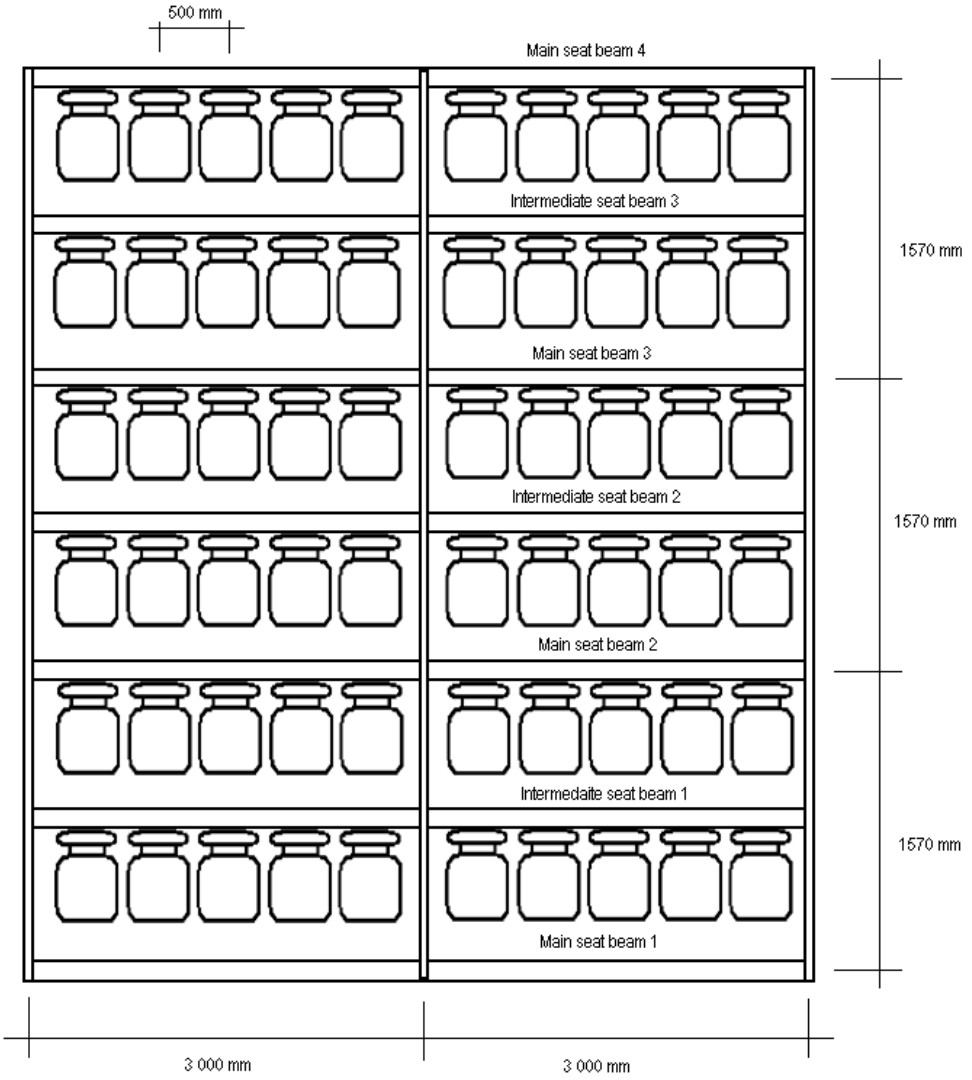

Figure 7.24: Plan view of grandstand

All forces were applied as point loads on seat beams making up the deck assembly. The first main seat beam was omitted because it does not accommodate seats in the prototype structure (Figure 7.24). Ten force time-histories per beam were applied on ten evenly spaced nodes to give a total of 60 force time-histories, each lasting 60 seconds. Each occupant weight (75 Kg) was applied in a static step before the dynamic analysis step.

The frequency spectra of displacement and acceleration responses at selected points on the structure were evaluated from the output of the FEM computation for all analyses (Figures 7.25-7.32). There are clear peaks at the fundamental and the third harmonic of the exciting force. For both the 20N and unsynchronized loading cases there is a significant response at 3 Hz which is the first structural frequency for the model. This shows the role of higher harmonics in exciting resonance.

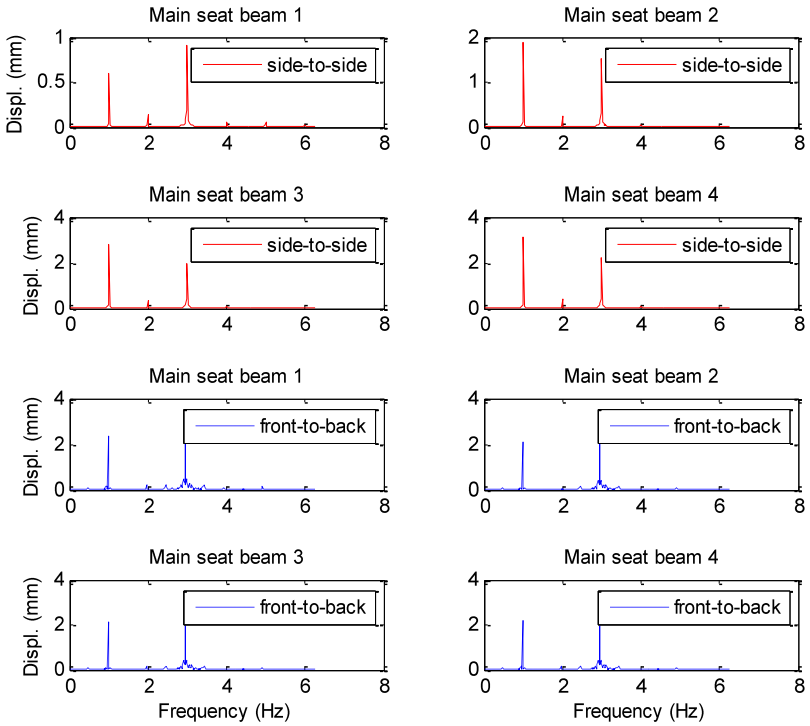

Figure 7.25: Displacement responses due to 20N amplitude of synchronized Type I forces at 1.0 Hz

Interestingly, the 40 and 65 N load cases shifted the second peak to 2.7 (Figure 7.30) and 2.5 Hz (Figure 7.31), respectively. This indicated a reduction in the stiffness or the onset of nonlinear behaviour at higher excitation levels which should be expected from the force-displacement curves shown earlier in Figure 7.23.

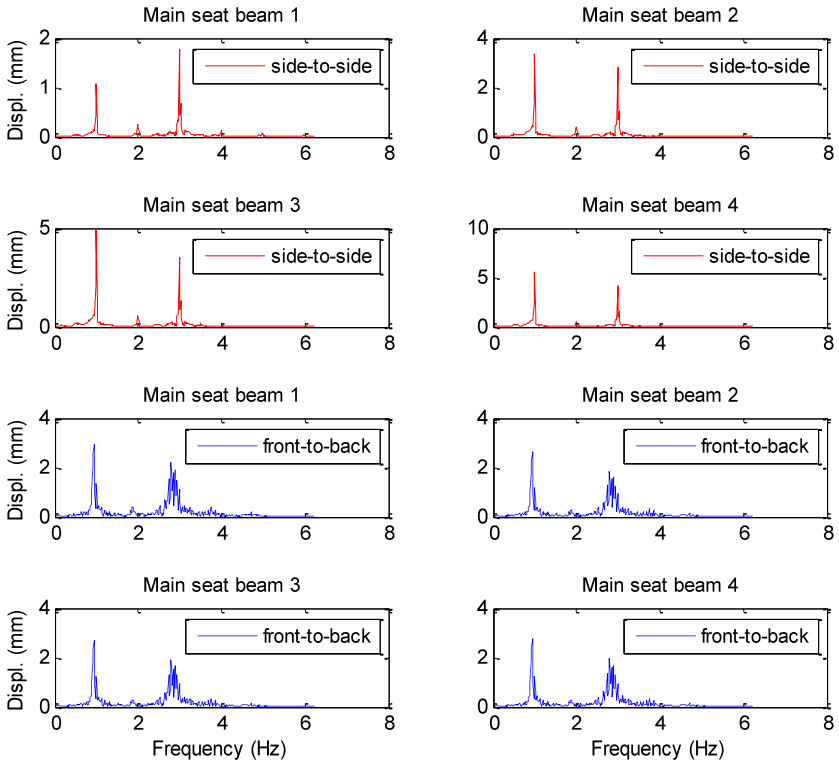

Figure 7.26: Displacement responses due to 40N amplitude of synchronized Type I forces at 1.0 Hz

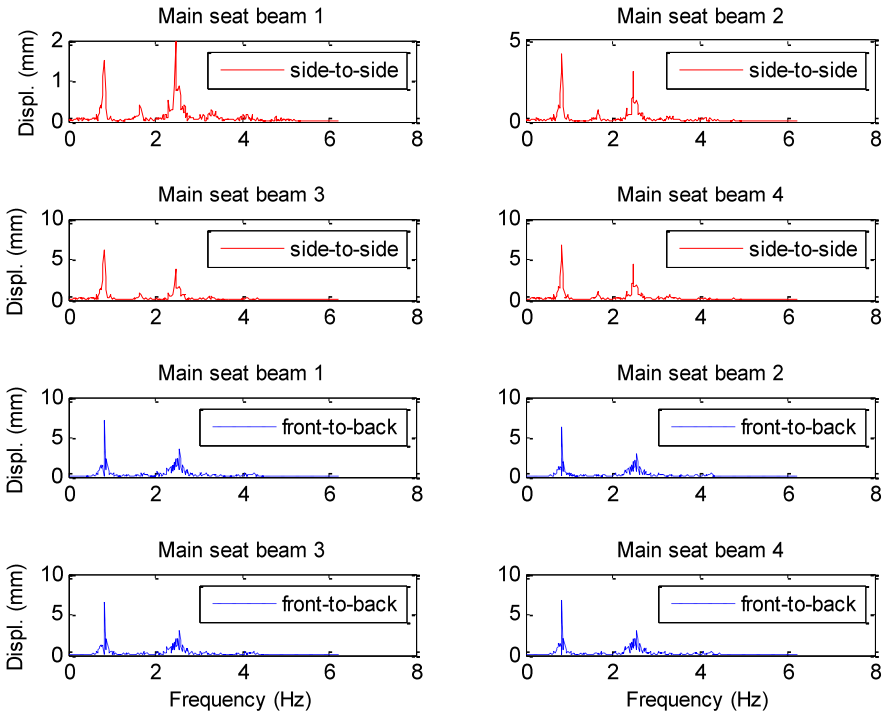

Figure 7.27: Displacement responses due to 65N amplitude of synchronized Type I forces at 1.0 Hz

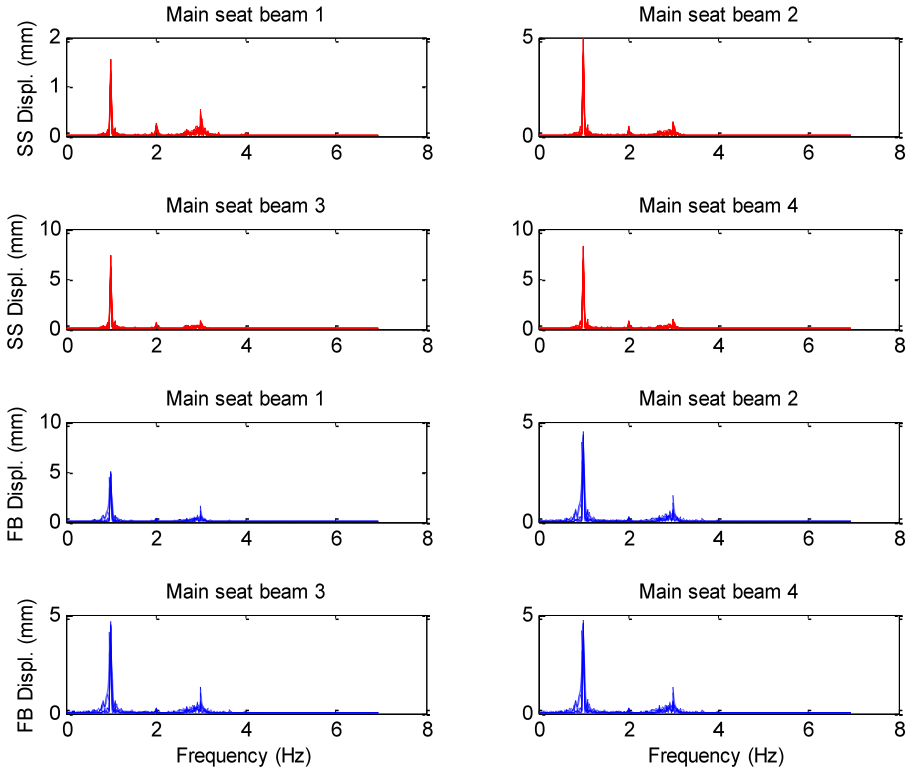

Figure 7.28: Displacement responses due to unsynchronized crowd swaying loads at 1.0 Hz

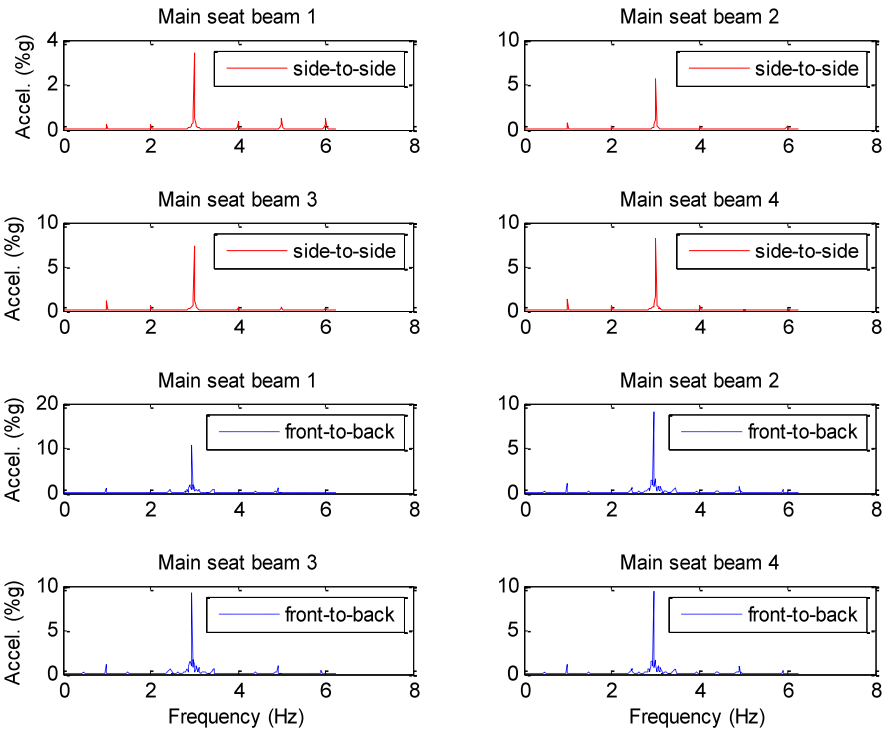

Figure 7.29: Acceleration responses due to 20N amplitude of synchronized Type I forces at 1.0 Hz

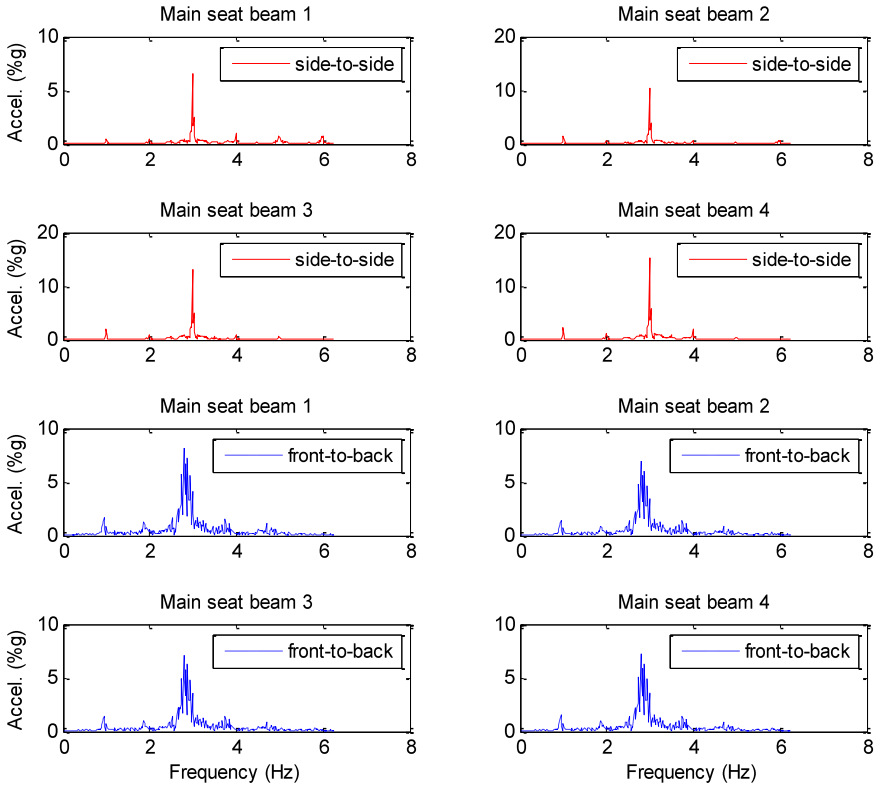

Figure 7.30: Acceleration responses due to 40N amplitude of synchronized Type I forces at 1.0 Hz

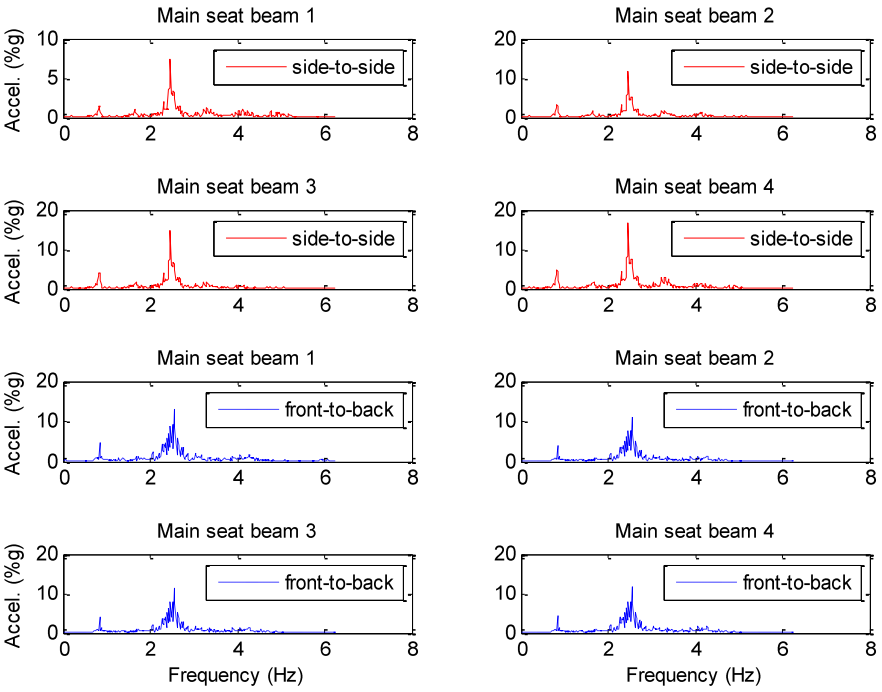

Figure 7.31: Acceleration responses due to 65N amplitude of synchronized Type I forces at 1.0 Hz

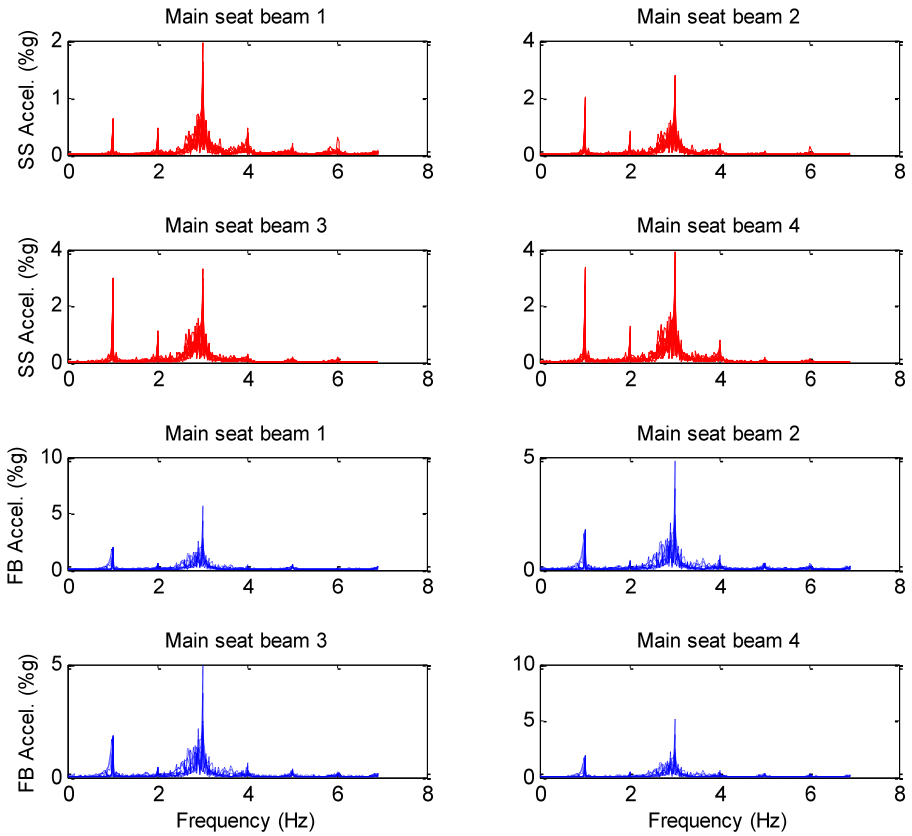

Figure 7.32: Acceleration responses due to unsynchronized crowd swaying loads at 1.0 Hz

The displacement and acceleration time-history responses and the corresponding peak and RSM values are presented below for the same analyses (Figures 7.33-7.36). The displacement amplitude time histories at the locations shown were evaluated by removing the mean of the FEM output while the acceleration was obtained directly from this output.

The results show that extreme motion occurred on the back seat beam for side-to-side excitation and on the front seat beam for front-to-back excitation. This was not unexpected since the back of the stand is higher due to the raking. Extreme motion occurred on the front seat beam for front-to-back excitation because this beam had no additional vertical constraining forces as it was left empty since no seats are attached to

it in the prototype. However, in reality, vertical loads will also be distributed to this beam by the supporting floor board which span across the seat beams.

As expected the 65 N synchronized load case (Figure 7.35) gave a significantly higher RMS value (approximately 20%g) compared to the unsynchronized group loading case (approximately 5%g) even though the force amplitudes per person were comparable. This indicates that ignoring lack of synchronization will lead to a conservative and expensive design.

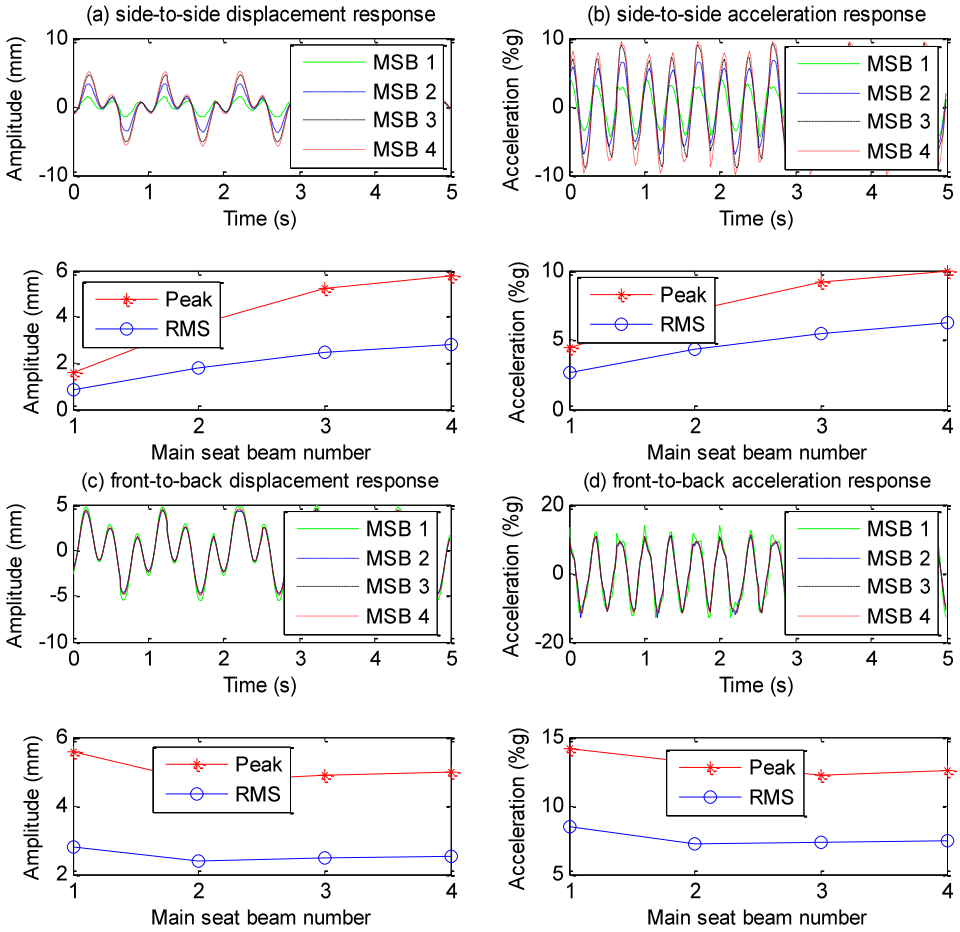

Figure 7.33: Peak and RMS responses due to 20N amplitude of synchronized Type I forces at 1 Hz

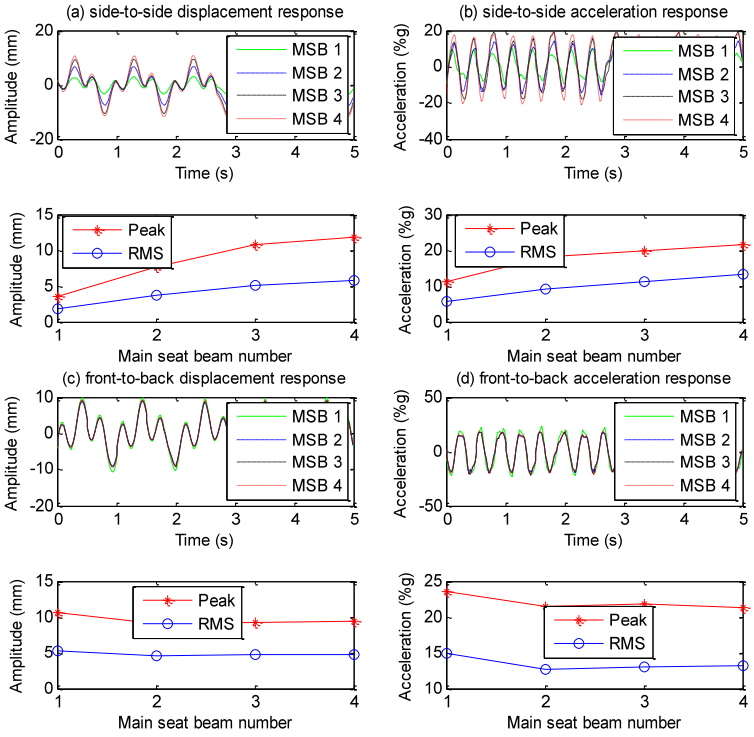

Figure 7.34: Peak and RMS responses due to 40N amplitude of synchronized Type I forces at 1 Hz

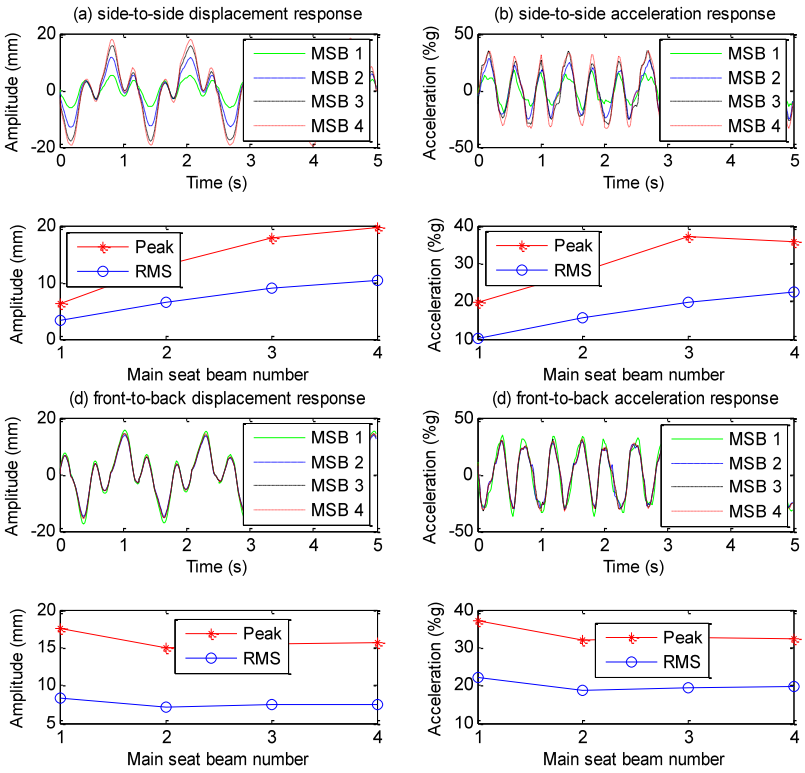

Figure 7.35: Peak and RMS response due to 65N amplitude of synchronized Type I forces at 1.0 Hz

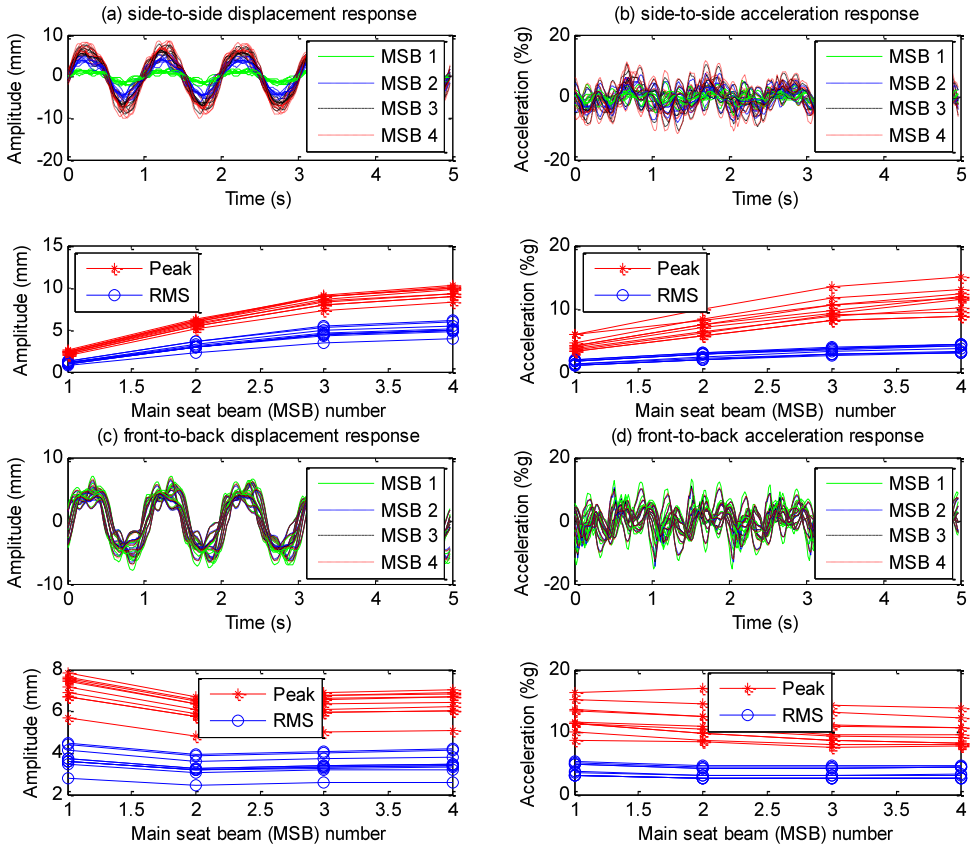

Figure 7.36: Peak and RMS responses due to unsynchronized crowd swaying loads at 1. 0 Hz

Although swaying at 1.0 Hz is a comfortable movement and a more likely scenario to lead to maximum forces, analyses for non-synchronous crowd forces applied at 0.75, 1.25 and 1.5 Hz were also under taken for comparison with the 1.0 Hz load case. The frequency spectra of the displacement and the acceleration response are shown in Figures A20 and A21 in Appendix A, respectively for comparison. Figures A22-A24 in Appendix A show the RMS and peak values of the displacement and the acceleration response obtained for multiple simulations conducted for each frequency of the crowd swaying motion.

To put the RMS values of Figure 7.33 to 7.36 into perspective, IStructE (2008) recommends values of 3%, 7.5% and 20% g for permanent venues hosting predominantly seated audiences, pop-concerts and extreme events (characterized by jumping and bobbing), respectively. However, these values are recommended for vertical vibration and strictly apply to permanent venues. In this context, the comparison given involving a temporary structure and horizontal vibrations is only presented in the absence of a similar provision for dealing with demountable structures and horizontal vibrations.

7.3. Concluding summary

Section 7.1 presented a brief description of the analytical theory for the study of single-degree-of-freedom systems. In section 7.2, dynamic and static tests performed in order to compile and calibrate a finite element model of a typical demountable grandstand structure were described. These tests showed that the structure is characterized by nonlinear behaviour which was incorporated in the finite element model. The finite element model of the grandstand was used to examine the effect of side-to-side forces on the response of the structure. The frequency spectra of the displacement and acceleration responses showed peaks at the fundamental and third harmonic of the exciting force. This demonstrated the capability of higher harmonics to excite resonance. The resonant frequency of the structural model decreased at higher excitation levels due to the onset of nonlinear behaviour. Finally, load cases assuming synchronized and perfectly periodic group forces led to higher responses compared to unsynchronized and imperfect group loads.

Chapter 8

8. Conclusions and recommendations for future work

Modern public structures are prone to excessive vibration levels induced by crowds. Whilst significant progress has been made in understanding the nature of this problem in the recent past, a review of literature highlighted a number of specific areas that required further research. The research presented in this thesis has focused on the following five areas.

1) Human tolerance of vertical vibration motion when occupying a grandstand structure
2) Measurement of human-induced horizontal forces generated by swaying and vertical jumping
3) Footswitch based measurements of group synchronization during swaying
4) Analytical modelling of human-induced horizontal forces
5) Modelling the horizontal response of a demountable structure characterized by nonlinear behaviour

The main conclusions drawn from each area of research are summarized below.

8.1. Human tolerance of vertical vibration motion

Tests were performed on an experimental grandstand rig in order to determine the threshold of perceptible and comfortable vibration levels for grandstand structures (Chapter 3). The test rig was moved at a known frequency and displacement. The test subjects were asked to score their perception and comfort state for each level of

vibration. The acceleration limit at the onset of discomfort was found to be 5%g RMS. It was discovered that test subjects perceived the levels of vibration to be relatively high before they deemed it to be uncomfortable. In addition, it was found that the levels of vibration that were required to cause discomfort were higher than those suggested for most buildings, but were lower than those that are acceptable in transport. Finally, when the test subjects were bobbing, it was found that the human-induced forces were affected by the motion of the deck, leading to dilation, constriction and little or no change of force amplitudes depending on the subject's bobbing movement and the deck motion. These changes indicate different postures or stance and consequently different human-structure interaction mechanisms.

8.2. Measurement of horizontal forces due to swaying and jumping

This part of research involved measurement and characterization of human-induced horizontal forces for different individuals performing movements in a laboratory setting (Chapter 4). Swaying and vertical jumping movements were chosen to maximise horizontal forces. Two types of impulse shapes (Type I and Type II) were observed for swaying side-to-side in a standing position. In general, horizontal forces due to swaying were characterized using several parameters, such as the average impulse curve, the mean of the split sub-pulse (including its cycle-by-cycle variation), the fundamental or swaying frequency (including its cycle-by-cycle variation) as well as the force magnitude at fundamental and higher harmonics. The fundamental force due to swaying occurred at the activity frequency. The fundamental horizontal force due to vertical jumping did not always occur at the activity frequency. The implication of this for design is that a load model similar to the one used for vertical loading due to jumping is not always appropriate. The tests conducted for swaying were also used to establish the

relationship between the side-to-side force and the velocity of the subject's centre of mass. The data showed that the lateral force is proportional to the velocity of the centre of mass of the subject.

8.3. Measurement of group synchronization

A customized footswitch system was developed and validated for the measurement of crowd synchronization by gathering foot-timing data during crowd activity (Chapter 5). The validated footswitch was used successfully to obtain data for groups of subjects performing side-to-side swaying movements involving movement of the feet. The data presented in graphical form described essential statistical parameters required for the development of the lateral human loading model and their distributions. The main parameters which were shown to be important for group loads are the time varying frequencies and the mean phase delays.

8.4. Analytical modelling of horizontal forces

Dynamic horizontal loads due to swaying and vertical jumping were described analytically using data from individuals performing predefined manoeuvres in a laboratory setting (Chapter 6). The measured force time-history data was split into negative and positive pulses corresponding to each direction of swaying. Positive and negative parts of the force pulse were each modelled using a Fourier series of a rectangular pulse. The resulting pulses were then shifted and added together to form a total pulse for swaying and jumping forces. The Fourier series was reduced to a simple formula for modelling individual side-to-side forces which were also shown to correspond to a worse case design scenario for swaying.

A group model for swaying was formed by summing up simulated individual forces which were shifted by normally distributed phase lags. The mean force at the first harmonic became asymptotic to 5% of subject weight when the crowd size increased beyond 12 subjects.

8.5. Modelling of structural response due to swaying

A brief presentation of the analytical theory for the study of single-degree-of-freedom systems in Chapter 7 provided the basis for finite element analyses undertaken to examine the significance of horizontal forces in the evaluation of structural response. Dynamic and static tests performed in order to compile and calibrate a finite element model of a typical demountable grandstand structure were also described. These tests showed that the structure is characterized by nonlinear behaviour which was incorporated in the finite element model. This model was used to examine the effect of side-to-side forces on the response of the structure.

The frequency spectra of displacement and acceleration responses showed clear peaks at the fundamental and the third harmonic of the exciting force, demonstrating the capability of the third harmonic to excite resonance. Furthermore, the resonant frequency decreased at higher levels of excitation, indicating a reduction in the stiffness or the onset of nonlinear behaviour. Finally, load cases assuming synchronized and perfectly periodic group forces gave a significantly higher response compared to unsynchronized and imperfect group loads.

8.6. Limitations and recommendations for future work

The serviceability data presented in Chapter 3 focused on vertical vibration. Future studies should consider the importance of both the front-to-back and the side-to-side directions.

In Chapter 4, swaying force data obtained from individuals performing on a rigid platform was presented and later used to evaluate the response of a low frequency structure. Previous research has shown that it is important to collect data on a platform whose stiffness properties reflect those of the intended application such as a grandstand. Thus, models were derived to describe horizontal forces for individuals and crowds based on the measured data presented in Chapters 4 and 5 and the results were summarized in Chapter 6. The functional forms derived are not more important than the measured data and this work shows that it is especially more appropriate, in view of ever more stringent safety regulations, to use well-constrained analytical models which are based on measured data.

In the structural model presented in Chapter 7, human-structure interaction effects were ignored. It is recommended that future work should include these effects. Inclusion of these effects can be accomplished by the characterization of the lateral dynamic properties of spectator subjects for representation in the structural model as an additional degree of freedom.

Finally, a finite element model of a two bay demountable structure was used to represent the typical dynamic behaviour of temporary grandstands and to conduct a parametric study. In reality, typical grandstands have very large planar dimensions.

Consequently, their dynamic behaviour might be slightly different from this model. For example, if the planar dimensions are large, the torsional vibration modes will occur at significantly higher frequencies than those of the two bay model reported here. Therefore, it is recommended that the measurement of the side-to-side and front-to-back responses of typical grandstands during entertainment events should be prioritised to further the results obtained from this research.

REFERENCES

1. Abaqus Standard® Analysis User's Manual, (Abaqus Version 6.8-4), *Hibbitt, Karlsson & Sorensen, INC.*
2. Abaqus® Theory Manual, (Abaqus Version 6.8-4), *Hibbitt, Karlsson & Sorensen, INC.*
3. Alexander, I., Chao, E. Y., and Johnson, A. K. (1990). "The assessment of dynamic foot-to-ground contact forces and plantar pressure distribution: a review of the evolution of current techniques and clinical applications." *Foot Ankle, 11*, pp. 152-167.
4. Allen, D. E., Rainer, J. H., and Pernica, G. (1985). "Vibration criteria for assembly occupancies." *Canadian Journal of Civil Engineering*, 12, pp. 617-623.
5. Allen, D. E., and Rainer, J. H. (1976). "Vibration criteria for long-span floors." *Canadian Journal of Civil Engineering*, 3(2), 165-173.
6. Almeida, P. A. O., and Rodrigues, J. F. S. (1998). "Investigation of the vibrations induced by people in soccer stadiums." *1998 SEM Spring Conference and Exhibition*, Houston, Texas, 271-274.
7. Bachmann, H., and Ammann, W. (1987). "Vibrations in structures: induced by man and machines". *IABSE, Structural Engineering Document (SED) 3.* Zurich, Switzerland.
8. Bachmann, H. (1992). "Case studies of structures with man-induced vibrations." *ASCE, Journal of Structural Engineering*, 118 (3), pp. 631-647.
9. Bachmann, H. (2002). "Lively footbridges – a real challenge." In: *Proceedings of the International Conference on the Design and Dynamic Behaviour of Footbridges*, pp. 18-30. Paris, France, November 20-22.

10. Batista, R. C., and Magluta, C. (1993). "Spectator-induced vibration of Maracaña Stadium." *EURODYN '93,* Trondheim, Norway, 985-992.
11. BBC News (24 November 2010).
    Accessed 10/11/2011: http://www.bbc.co.uk/news/world-asia-pacific-11827313
12. Blakeborough, A., and Williams, M.S. (2005). "Human-structure interaction in cantilever grandstands." *Department of Engineering Science, University of Oxford.*
    Accessed 15/06/2008: http://www-civil.eng.ox.ac.uk/research/grandstands.pdf
13. Browning, G. G., Darby, A. P., and Ian Walker, I. (2008). "Human Perception of vibrations due to synchronized crowd loading in Grandstands." In: *7th European Conference on Structural Dynamics*, 7-9 July 2008, Southampton.
14. Brownjohn, J.M.W. (2004). "Vibration serviceability of footbridges." In: *Progress in Structural Engineering and Computation*, pp. 419-422., July 4-7, Cape Town, South Africa.
15. Brownjohn, J.M.W., Pavic, A., and Omenzetter, P. (2004). "A spectral density approach for modelling continuous vertical forces on pedestrian structures due to walking." *Canadian Journal of Civil Engineering*, 31, pp. 65-77.
16. Brownjohn, J. M. W., Fok, P., Roche, M., and Omenzetter, P. (2004). "Long span steel pedestrian bridge at Singapore Airport-part 2: crowd loading tests and vibration mitigation measures." *The Structural Engineer, 82,* pp. 28-34.
17. BS6399, (1996). "Loading for buildings. Part 1: Code of practice for dead and imposed loads." *British Standards Institution*, London, UK.
18. BS 6472 (1992). "Guide to evaluation of human exposure to vibration in buildings (1Hz to 80Hz)." *British Standards Institution*, London, UK.

19. BS 6841 (1987). "Guide to measurement and evaluation of human exposure to whole body mechanical vibration and repeated shock." *British Standards Institution*, London, UK.
20. BS 7085 (1987). "Medical contra-indications to participation in experiments involving whole-body mechanical vibration." *British Standards Institution*, London , UK.
21. Caetano, E., Cunha, A. Magalhães, F., and Moutinho, C. (2010). "Studies for controlling human-induced vibrations of the Pedro and Inês footbridge, Portugal. Part 1: Assessment of dynamic behaviour", *Engineering Structures*, pp. 1069–10814.
22. NBC (2005). "Canadian Commission on Building and Fire Codes: User's Guide Structural Commentaries (Part 4 of Division B) Commentary D." *National Research Council Canada*, 2005.
23. Chopra, A.K. (1995). *Dynamics of structures: Theory and applications to earthquake engineering*. Upper Saddle River, New Jersey, USA: Prentice-Hall.
24. Comer, A., Blakeborough, A., and Williams, M. (2007). "Human-structure interaction in cantilever grandstands - design of a section of a full scale raked grandstand." *25th International Modal Analysis Conference*.
25. Crouse, J., Wall, J. C., and Marble, A. E. (1987). "Measurement of the temporal and spatial parameters of gait using a microcomputer based system.", *J. Biomed. Eng., 9*, pp. 64-68.
26. Crowe, A., Schiereck, P., de Boer, R. W., and Keeson, W. (1995). "Characterization of human gait by means of body center of mass oscillations derived from ground reaction forces." *IEEE Trans. Biomed. Eng*, 42, pp. 293–303

27. Dallard, P. Fitzpatrick, T., Flint, A., Low, A., Smith, R., Willford, M., and Roche, M. (2001). "London millennium bridge: Pedestrian-induced lateral vibration." *ASCE, Journal of Bridge Engineering*, 6 (6) pp. 412-417.
28. Dallard, P., Fitzpatrick, A. J., Flint, A., Le Bourva, S., Low, A., Smith, R. M., and Willford, M. (2001). "The London Millenium Footbridge." *The Structural Engineer*, 79, pp. 17-33.
29. Dougill, J. W., Wright, J. R., Parkhouse, J. G., and Harrison, R. E. (2006). "Human structure-interaction during rhythmic bobbing." *The structural Engineer*, 84:32–39.
30. Dougill, J. W. (2005). "Recommendations for design of grandstands subject to dynamic crowd excitation." *Proceedings of EURODYN*, pp. 467-472. September 4-7, Paris, France.
31. Ebrahimpour, A. (1986). "Measuring dynamic occupant loads by a micro-computer." In: *Proceedings of the ASCE 9th Conference on Electronic Computation*, pp. 11, February 23-26, Birmingham, Ala.
32. Ebrahimpour, A., and Sack, R.L. (1989). "Modeling dynamic occupant loads." *ASCE, Journal of Structural Engineering*, 115 (6) pp. 1476-1496.
33. Ebrahimpour, A. and Sack, R.L. (1992). "Design live loads for coherent crowd harmonic movements." *ASCE, Journal of Structural Engineering*, 118 (4) pp. 1121-1136.
34. Ellis, B.R., and Ji, T. (1997). "Human-structure Interaction." *Proceedings of the Institute of Civil Engineers, Structures and Buildings*, 122(1), pp 1-9.
35. Ellis, B.R., and Littler, J.D. (2004). "Response of Cantilever Grandstands to Crowd Loads. Part 1: Serviceability Estimation." *Proceedings of the Institution of Civil Engineers, Structures and Buildings*, 157 Issue SB4, p235-241.

36. Ellis, B.R., and Ji, T. (2004). "Loads generated by jumping crowds: numerical modelling." *The Structural Engineer*, 17, pp 35-40.
37. Football Spectators Act (1989). *HMSO*, London.
38. Fujino, Y., Pacheo, B. M., Nakamura, S., and Warnitchai, P. (1993). "Synchronization of human walking observed during later vibration of a congested pedestrian bridge." *Earthquake Engineering and Structural Dynamics*, 22, 741-758.
39. Gabel, R. H., Johnston, R. C., and Crowninshield, R. D. (1979). "A gait analyser/trainer instrumentation system." *J. Biomech., 12*, pp. 543.
40. Gardner G. M., and Murray, M. P. (1975). "A method of measuring the duration of foot-floor contact during walking." *Phys. Ther., 11*, pp. 751-756.
41. Glackin, K. (2000). "Stadia design rethink prompted by Cardiff fiasco." *Building*.
42. Greimann, L. F., and Klaiber, F. W. (1978). "Dynamic forces induced by spectators." *ASCE, Journal of Structural Engineering* 104 (2) pp. 348-351.
43. Griffin, M. J. (1990). *Handbook of human vibration*. London, UK: Academic Press.
44. Guilford, J. P (1954). *Psychometric methods*, McGraw-Hill, New York.
45. Harper, F.C., Warlow, W.J., and Clarke, B. L. (1961). "The forces applied to the floor by the foot in walking: Walking on a level surface." *National building studies*, Research paper 32. London.
46. Harrison, R. E. (2008). *Human-structure dynamic interaction in stadia grandstand design*. Ph.D. Thesis, University of Manchester.
47. Harrison, R. E., and Wright, J. R. (2004). "Combined active and passive human loading on a flexible platform." *23rd International Modal Analysis Conference (IMAC XXIII),* Orlando, Florida, USA.
48. Hart, G. C., and Wong, K. (2000). *Structural dynamics for structural engineers*. John Wiley & Sons, Inc, New York.

49. Hausdorff, J. M., Ladin, Z., and Wei, J. Y. (1995). "Footswitch system for measurement of the temporal parameters of gait." *J. Biomechanics,* 28, 4, pp. 347-351.

50. HMSO (1997). "Guide to safety at sports grounds (Green Guide – 4th edition)." *Department of National Heritage, Scottish Office: The Stationary Office*.

51. Helbing, L., Buzna, T., Werner, D.O.I. (2003). "Self-Organized Pedestrian Crowd Dynamics and Design Solutions." *Traffic Forum*, 2003-12. Accessed 10/06/2008: http://vwisb7.vkw.tu-dresden.de/TrafficForum/forumArticles/pedopus.pdf

52. Hoath, R. (2009). *Application of image processing methods to study the correlations between people jumping on a grandstand*. Ph.D. Thesis, University of Oxford.

53. Hoath, R., Blakeborough, A., and Williams, M. (2007). "Using video tracking to estimate the loads applied to grandstands by large crowds." In: *25th International Modal Analysis Conference.*

54. ICE (2002). "Design and practice guides, Dynamics: An introduction for civil and structural engineers." *The Institution of Civil Engineers*.

55. ISO 10137 (2007), "Basis for the design of structures - Serviceability of buildings against vibration." *International Organization for Standardization (ISO),* Geneva.

56. ISO 2631 (1997-2003), "Mechanical Vibration and Shock – Evaluation of Human Exposure to Whole-body Vibration. Part 1: General Requirement, 1997 and Part 2: Vibration in Buildings (1Hz to 80Hz), 2003." *International Organization for Standardization (ISO),* Geneva.

57. ISO 8041 (2005), "Human response to vibration – Measuring instrumentation." *International Organization for Standardization (ISO),* Geneva.

58. IStructE (2008). "Dynamic performance requirements for permanent grandstands subjected to crowd action, Recommendations for management, design and assessment." *The Institution of Structural Engineers*, London, UK.
59. IStructE (2007). "Temporary demountable structures, Guidance on procurement, design and use." *The Institution of Structural Engineers*, London, UK.
60. IStructE (2001). "Dynamic performance requirements for permanent grandstands subjected to crowd action, Interim guidance on assessment and design." *The Institution of Structural Engineers*, London, UK.
61. Ji, T. (2003). "Concepts for designing stiffer structures." *The Structural Engineer* 81(42): 36-42.
62. Ji, T., and Ellis, B. R. (1997). Effective bracing systems for temporary grandstands. *The Structural Engineer*, 75(6): 95-100.
63. Ji, T., Ellis, B. R., and Bell, A. J. (2003). "Horizontal movements of frame structures induced by vertical loads." *Proceedings of the Institution of Civil Engineers, Structures and Buildings, 156,* pp. 141-150.
64. Ji, T., and Ellis, B. (1994). "Floor vibrations induced by dance type loads: Theory." *The Structural Engineer*, 72 (3). pp. 37-44.
65. Ji, T., and Ellis, B. (1994). "Floor vibrations induced by dance type loads: Verification." *The Structural Engineer*, 72 (3), pp. 45-50.
66. Kasperski, M., and Agu, E. (2005). "Prediction of crowd-induced vibrations via simulation." *XXIII International Modal Analysis Conference*, Florida.
67. Kasperski, M. (2001). "Safety assessment of stadia in regard to human induced vibrations." *One Day Institution of Civil Engineers' Conference: Safer Solutions in Sport and Leisure*, Manchester, England, 5 April 2001.

68. Kasperski, M. (1996). "Actual problems with grandstand structures due to spectator-induced vibrations." *Proceedings of the Third European Conference on Structural Dynamics: EURODYN '96*, Florence, Italy, 5-8 June 1996, pp. 455-461

69. Keller, T.S., Weisberger, A.M., Ray, J.L., Hasan, S.S., Shiavi, R.G., and Spengler, D.M. (1996). "Relationship between vertical ground reaction force and speed during walking, slow jogging, and running." *Clinical Biomechanics*, 11, 253–259.

70. KljajiC, M., and Krajnik, J. (1987). "The use of ground reaction measuring shoes in gait evaluation." *Clinical Physics and Physiological Measurement*; 8, pp. 133-142

71. Lagginns, A. B., and Bowker, P. (1991). "A simple low cost footswitch." *J. Biomed. Eng., 13*, pp. 87-88.

72. Lenzen, K. H. (1996). "Vibration of steel joist-concrete slab floors." *American Institute of Steel Construction (AISC) Engineering Journal*, 3(July), 133-136.

73. Lian, Q, Xie, Y. and Steven, G. (2000). "Optimal topology design of bracing systems for multi storey steel frames." *ASCE Journal of Structural Engineering*, 126(7): 823-829.

74. Littler, J. D. (2000). "Permanent cantilever grandstands: dynamic response." *Building Research Establishment,* Information Paper 5/00, Watford, UK.

75. Littler, J. D. (2000). "Retractable grandstand: Dynamic response." *Building Research Establishment*, Information Paper 4/00, Watford, UK.

76. Littler, J. D. (1999). "The dynamic response of a three tier cantilever grandstand." *3rd European Conference on Structural Dynamics – EURODYN '99*, 623-628.

77. Littler, J. D. (1998). "Full-scale testing of large cantilever grandstands to determine their dynamic response: Stadia, arenas and grandstands." Thompson, P.D., Tollocako, J.J.A., Clarke, J.N. eds. E and FN Spon, London, 123-134.

78. Macdonald, J. H. G (2008). "Pedestrian-induced vibrations of the Clifton Suspension Bridge, UK." *Proceedings of the institution of the Institution of Civil Engineers. Bridge Engineering* 161, BE2, pp. 60-77.
79. Matsumoto, Y., and Griffin, M. J. (2003). "Mathematical models for the apparent masses of standing subjects exposed to vertical whole-body vibration." *Journal of Sound and Vibration*, 2003, 260(3), 431-451.
80. Minns, R. J. (1982). "A conductive rubber footswitch design for gait analysis." *J. Biomed. Eng., 4*, pp. 328-330.
81. Moreland, R. (1905). "The weight of a crowd." letter to the editor, *London Engineering, LXXIX*, p. 551.
82. Murray, T. M. (1979). "Acceptability criterion for occupant-induced floor vibrations." *Sound Vib.* 67(4), 24-30.
83. NRCC (1995). *Users guide National Building Code of Canada (NBC) 1995. Commentary A: Serviceability criteria for deflections and vibrations,* Ottawa, Canada: NRCC.
84. Nawayseh, N., and Griffin, M. J. (2005). "Non-linear dual-axis biodynamic response to fore-and-aft whole-body vibration", *Journal of Sound and Vibration*, 282, pp. 831–62.
85. Nhleko, S. P., Blakeborough, A., Williams, M. S., and Whittle J. (2010). "Dynamic testing of bracing patterns of a demountable grandstand." *4th International Conference on Structural Engineering, Mechanics and Computation,* Cape Town.
86. Nhleko, S. P., Williams, M. S., and Blakeborough, A. (2009). "Vibration perception and comfort levels for an audience occupying a grandstand with perceivable motion." *In 27th International Modal Analysis Conference*, Florida.

87. Nhleko, S. P., Blakeborough, A., and Williams, M. S. (2009). "Ground reaction forces on vibrating structures." In: *27th International Modal Analysis Conference*, Florida.

88. Nhleko, S. P., Zingoni, A., and Moyo, P. (2008). "A variable mass model for describing forces due to periodic jumping." *Journal of Engineering Structures*, 30 (6), pp. 1760–1769.

89. Nhleko, S. P. (2006). *Modelling of human-induced vibrations in stadium structures.* M.Sc. thesis. University of Cape Town.

90. Parkhouse, J. G., and Ewins D. J. (2006). "Crowd-induced rhythmic loading." *Proceedings of the Institute of Civil Engineers, Structures and Buildings*, 159(5), pp 247-259.

91. Pavic, A., Reynolds, P., and Stana, Z. (2004). "Dynamic testing and analysis of a footbridge under walking-induced excitation in Podgorica, Montenegro." In: *Progress in Structural Engineering and Computation*, pp. 413-418. Cape Town, South Africa, July 4-7.

92. Pavic, A., Yu, C. H., Brownjohn J. M. W., and Reynolds, P. (2002). "Verification of the existence of human-induced horizontal forces due to vertical jumping." In: *The XX International Modal Analysis Conference*, Los Angeles, February, pp 120-126.

93. Pavic, A., Pimentel, R.L., and Waldron, P. (2001). "Evaluation of design Requirements for footbridges excited by vertical forces from walking." *University of Sheffield*, published on the NRC Research Press Web site on August 16. 2001, University of Sheffield.

94. Pernica, G. (1990). "Dynamic load factors for pedestrian movements and rhythmic exercises." *Canadian Acoustics*, 18(2), 3-18.

95. Petersen, C. (1972). *Theory of random vibrations with applications* (in German) referenced by Sachse, 2002.
96. Pimentel, R.L. (1997). *Vibration performance of pedestrian bridges due to human-induced loads*. Thesis (PhD). University of Sheffield, Sheffield, UK.
97. Poon, M. K.Y. (2007). *Human-structure Interaction in Cantilever Grandstands*. M.Sc. Thesis, University of Oxford.
98. Preuss, R., and Fung, J. (2004). "A simple method to estimate force plate inertial components in a moving surface." *Journal of Biomechanics,* 37, pp. 1177–1180.
99. Racic, V., and Pavic, A. (2010). "Stochastic approach to modelling near-periodic jumping force signals." *Mechanical Systems and Signal Processing,* 24, 3037-3059.
100. Racic, V., Brownjohn, and J.M.W., Pavic, A. (2010). "Reproduction and application of human bouncing and jumping forces from visual marker data." *Journal of Sound and Vibration,* 329, 3397-3416.
101. Racic, V., Pavic, A, and Brownjohn, J.M.W. (2009). "Experimental identification and analytical modelling of human walking forces: literature review." *Journal of Sound and Vibration,* 326, pp. 1–49.
102. Rainer, J. H., Pernica, G., and Allen, D. E. (1986). "Dynamic loading and response of footbridges." *Canadian Journal of Civil Engineering*, 15(1), 66-71.
103. Rainer, J. H., and Pernica, G. (1981). "Damping of a floor sample." *The Second Speciality Conference on Dynamic Response of Structures: Experimentation, Observation, Prediction and Control,* Atlanta, USA, G. Hart ed., 859-873.
104. Reid, W.M., Dickie, J. F., and Wright, J. (1997). "Stadium structures: are they excited?" *The structural engineer,* 75 (22) pp. 383-388.
105. Reid, W.M., Dickie, J. F., and Wright, J. (1994). "Design of stadia structures – A safety-first approach." *IABSE Symposium*, Birmingham.

106. Reynolds, P., Pavic, A., and Ibrahim, Z. (2004). "Changes of modal properties of a stadium structure occupied by a crowd." *Proceedings of IMAC-XXII*, January 26-29, Dearborn, Michigan.

107. Reynolds, P., and Pavic, A. (2005). "The dynamic performance of sports stadia under crowd dynamic loading at concert events." *Proceedings of EURODYN*, pp. 473-478. Paris, France, September 4-7.

108. Ries, L. L. (1928). "Removable steel stadium for University of Chicago." *Engineering news*, July, pp. 13-15.

109. Rimell, A. N., and Mansfield, N. J. (2007). "Design of digital filters for frequency weighting required for risk assessment of workers exposed to vibration." *Industrial Health*, 45 pp. 512-19.

110. Rogers, D. (2000). "Two more 'wobbly' stands." *Construction News*, 17 August.

111. Rogers, D., and Thompson, R. (2000). "Liverpool stand gets a red card." *Construction News*, 10 August 2000.

112. Sachse, R., Pavic, A., and Reynolds, P. (2004). "Parametric study of modal properties of damped two-degree-of-freedom crowd-structure dynamic systems."*Journal of Sound and Vibration*, 274 (3-5) pp. 461-480.

113. Sachse, R. (2002). *The influence of Human Occupants on the Dynamic properties of Slender Structures.* Ph.D. Thesis, University of Sheffield, 2002.

114. SCOSS (2001). "Structural Safety 2000-01: 13th Report of SCOSS (The Standing Committee on Structural Safety)." *The Institution of Structural Engineers*, London, UK.

115. Serby, M. W. (1930). *The stadium*, AISC Inc.

116. Sim, J., Blakeborough, A., Williams, M.S., and Parkhouse, G. (2008). "Statistical model of crowd jumping loads." *ASCE, Journal of Structural Engineering,* 134 (12) pp. 1852-1861.

117. Sim, J. (2006). *Human-structure Interaction in Cantilever Grandstands*. Ph.D. Thesis, University of Oxford.

118. Sim, J., Blakeborough, A., and Williams, M.S. (2005). "Dynamic loads due to rhythmic human jumping and bobbing." *Proceedings of EURODYN*, pp. 467-472. Paris, France, September 4-7.

119. Staalduinen, V. P., and Courage, W. (1994). "Dynamic loading of Feyenoord stadium during pop concerts." *Symposium: Places of Assembly and Long-Span Building Structures,* Birmingham, UK, Report 71, 283-288, IABSE, Zürich, Switzerland.

120. Taun, C.Y., and Saul, W.E. (1985). "Loads due to spectator movements." *ASCE, Journal of Structural Engineering,* 111 (2) pp. 418-434.

121. Taun, C.Y., and Saul, W.E. (1986). "Review of live loads due to human movements." *Journal of Structural Engineering*, Vol 112 (5) pp. 995-1004.

122. Tilden, C. J. (1913). "Kinetic effects of crowds." *Proceedings of the American Association of Civil Engineers,* 34 (3), pp. 325-340.

123. The Scottish Office and Dept. of National Heritage (1997). *Guide to safety at sports grounds*. Stationary Office.

124. Thorburn, S. (1999). "Safety at sports grounds in the UK." *Structural Engineering International (IABSE),* 9 (3), pp. 156-188.

125. Timoshenko, S. (1937). *Vibration Problems in Engineering. Second edition*. London Constable & Company, Ltd, Orange Street, Leicester Square.

126. Tylor R. (1989, 1990). "The Hillsborough Stadium Disaster, Interim/Final Report." *HMSO*, London.

127. Waldau, N., Schreckenberg, M., and Gattermann, P. (2003). "Design Criteria Related to Orientation in Buildings during High Stress." In: *Proceedings of the 2nd International Conference on Pedestrian and Evacuation Dynamics*, pp. 307-318, Greenwhich, UK, August 20-22.

128. Wei, L., and Griffin, M. J. (1998). "Mathematical models for the apparent mass of the seated human body exposed to vertical vibration." *Journal of Sound and Vibration*, 212(5), 855-874.

129. Willford, M. (2001). "An investigation into crowd-induced vertical dynamic loads using available measurements." *The Structural Engineer*, 79(12), 21-25.

130. Wheeler, J. E. (1982). "Prediction and control of pedestrian-induced vibration in footbridges." *Proceedings of the ASCE: Journal of the Structural Division*, 108 (ST9), 2045-2065.

131. Yao, S., Wright, J.R., Pavic, A., and Reynolds, P. (2006). "Experimental study of human-induced dynamic forces due to jumping on a perceptibly moving structure." *Journal of Sound and Vibration,* 296, pp. 150–165.

132. Yao, S., Wright, J.R., Yu, C. H., Pavic, A., and Reynolds, P. (2005). "Human-induced swaying forces on flexible structures." *Proceedings of the institution of the Institution of Civil Engineers. Structures and Buildings* 158(2), pp. 109-117.

133. Yao, S., Wright, J.R., Pavic, A., Reynolds, P., and Sachse, R. (2003). "Experimental study of human-induced dynamic forces due to jumping on a perceptibly moving structure." *Proc., IMAC XXI Conference,* Florida.

134. Yu, C. H. (2004). *The Identification and Modelling of Human-Induced Dynamic Forces on Perceptibly Moving Structures.* Ph.D. Thesis, University of Sheffield.

APPENDIX A

This appendix contains additional figures.

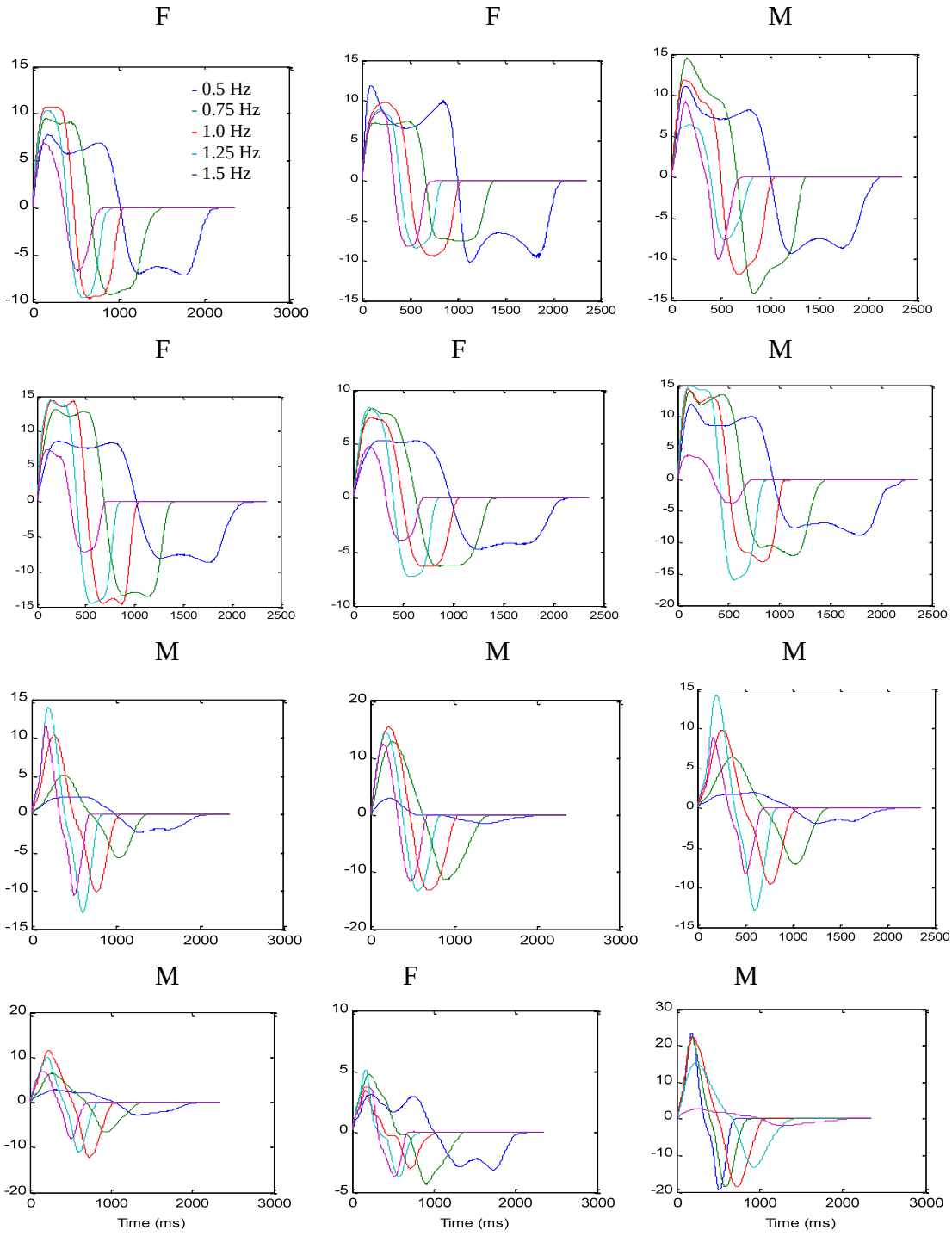

Figure A1: Typical average impulse curves (10 cycles) due to swaying side-to-side in a standing position - all subjects (the vertical axis shows the SS force as a percentage of body weight, F= female, M = male)

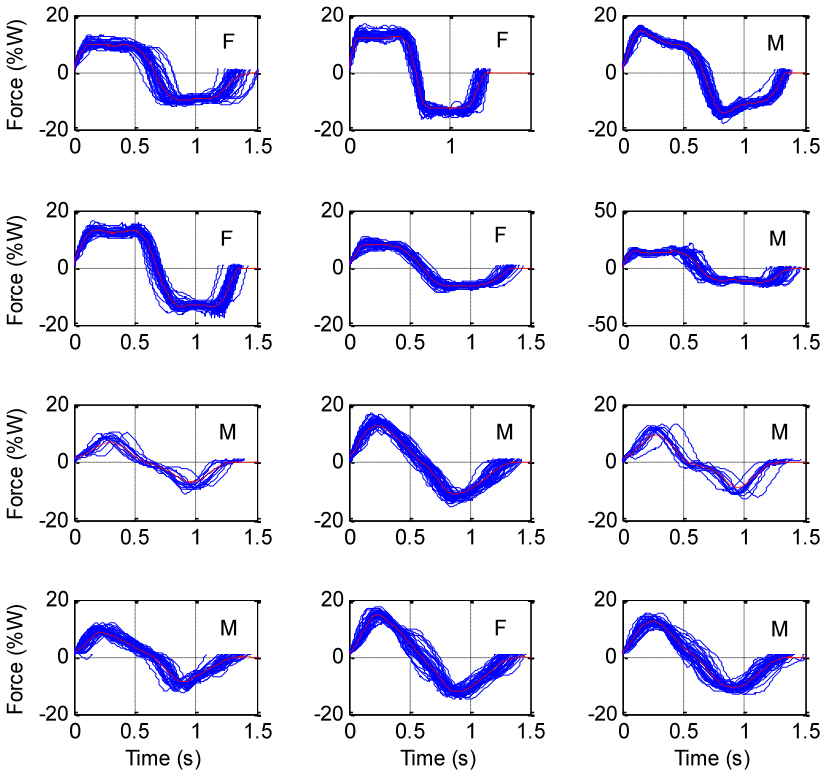

Figure A2: SS Force impulses for 12 subjects swaying side-to-side at 0.75 Hz in a standing position

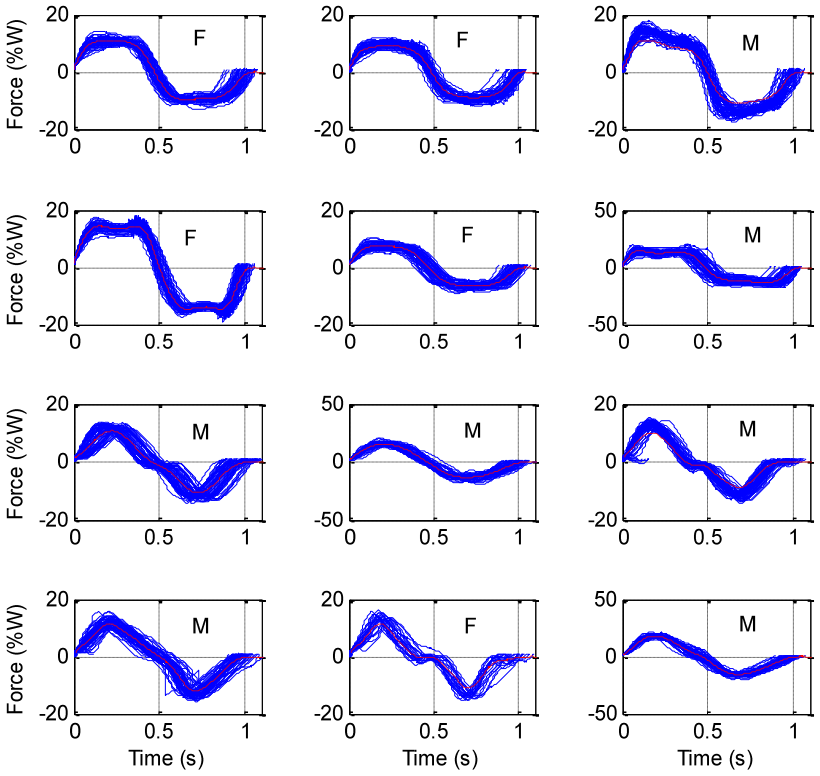

Figure A3: SS Force impulses for 12 subjects swaying side-to-side at 1.0 Hz in a standing position

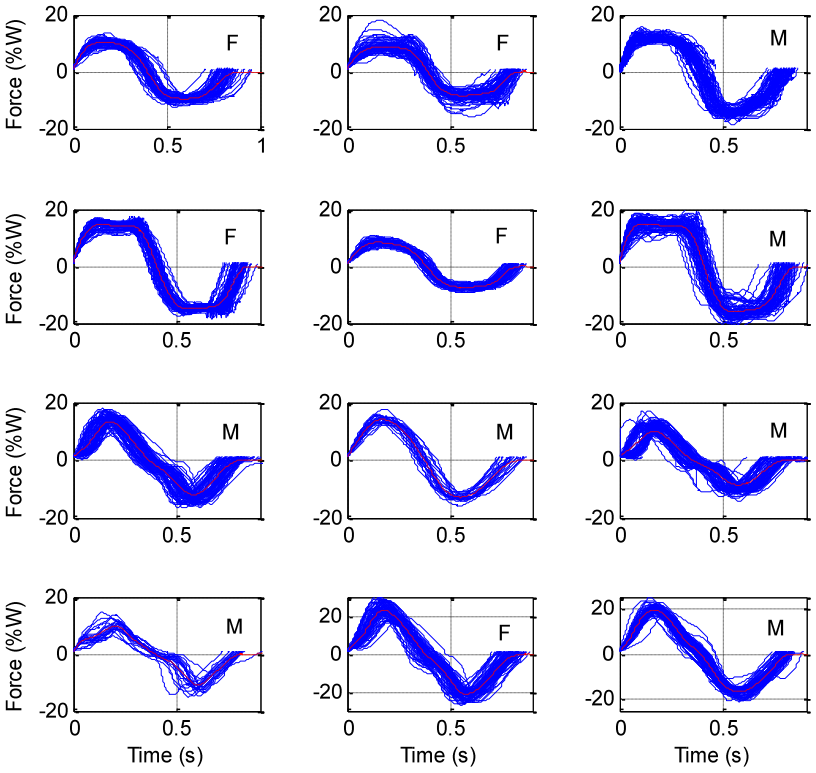

Figure A4: SS Force impulses for 12 subjects swaying side-to-side at 1.25 Hz in a standing position

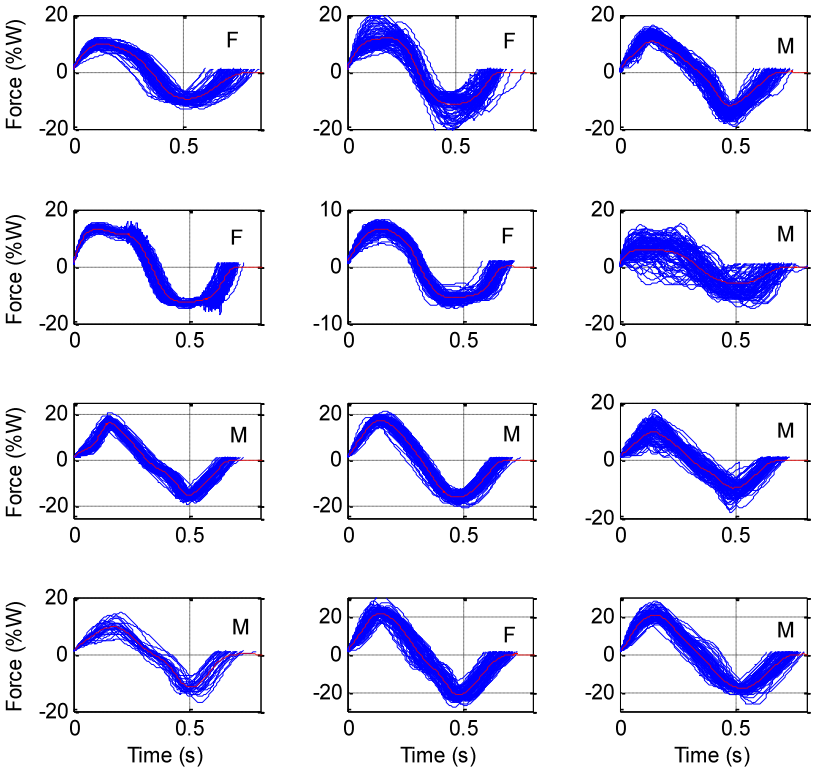

Figure A5: SS Force impulses for 12 subjects swaying side-to-side at 1.5 Hz in a standing position

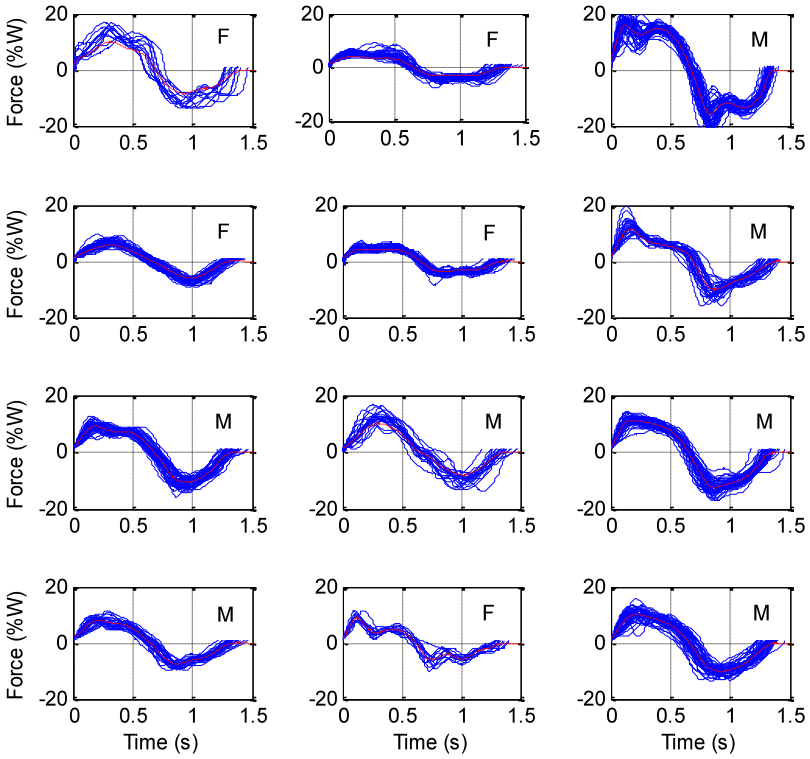

Figure A6: SS Force impulses for 12 subjects swaying side-to-side at 0.75 Hz in a sitting position

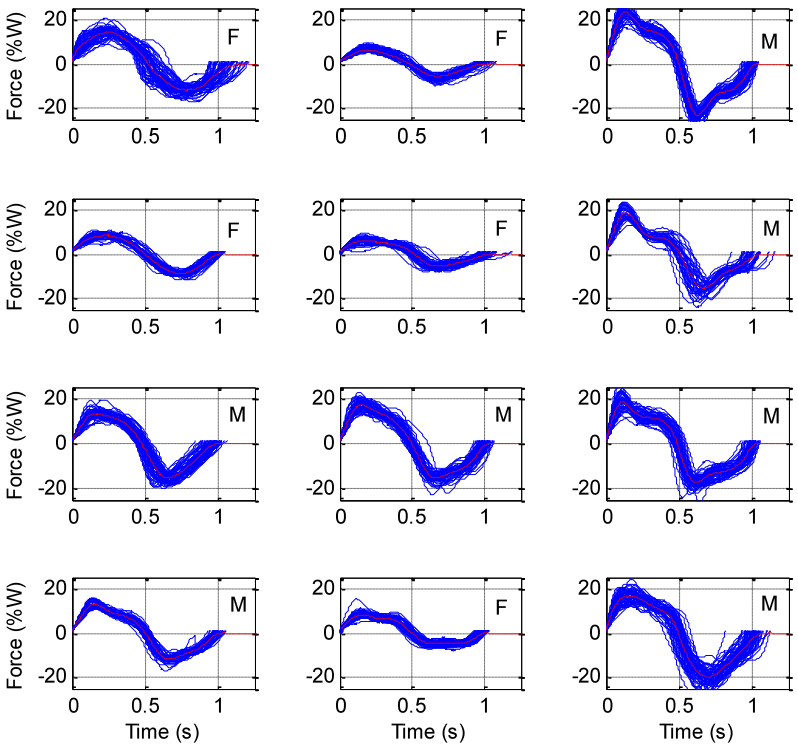

Figure A7: SS Force impulses for 12 subjects swaying side-to-side at 1.0 Hz in a sitting position

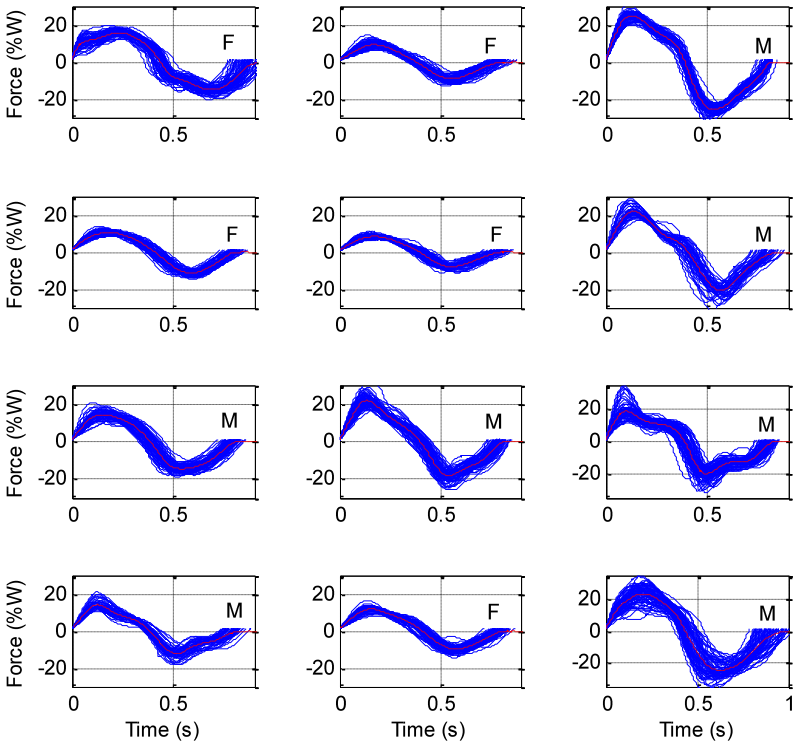

Figure A8: SS Force impulses for 12 subjects swaying side-to-side at 1.25 Hz in a sitting position

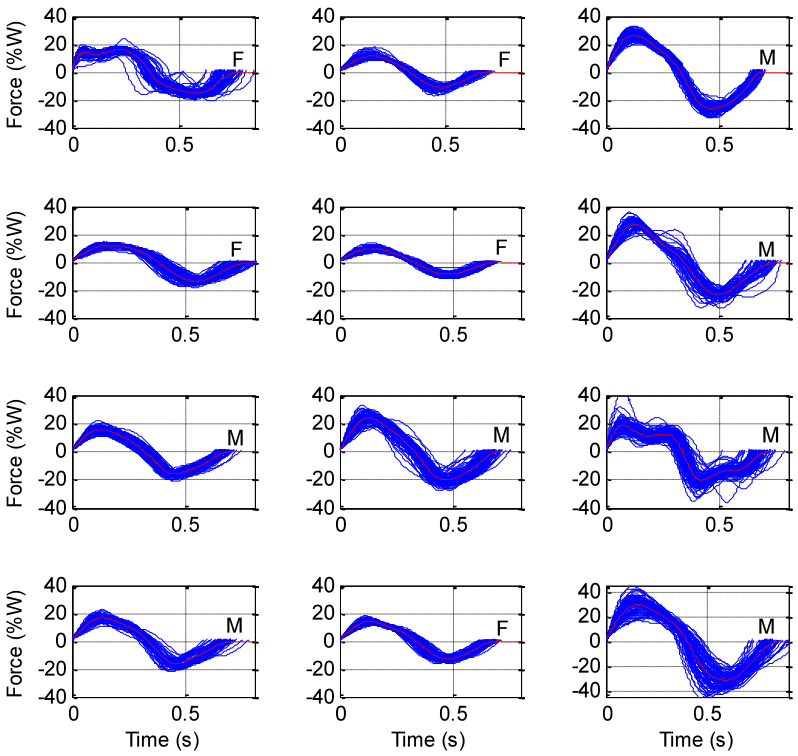

Figure A9: SS Force impulses for 12 subjects swaying side-to-side at 1.5 Hz in a sitting position

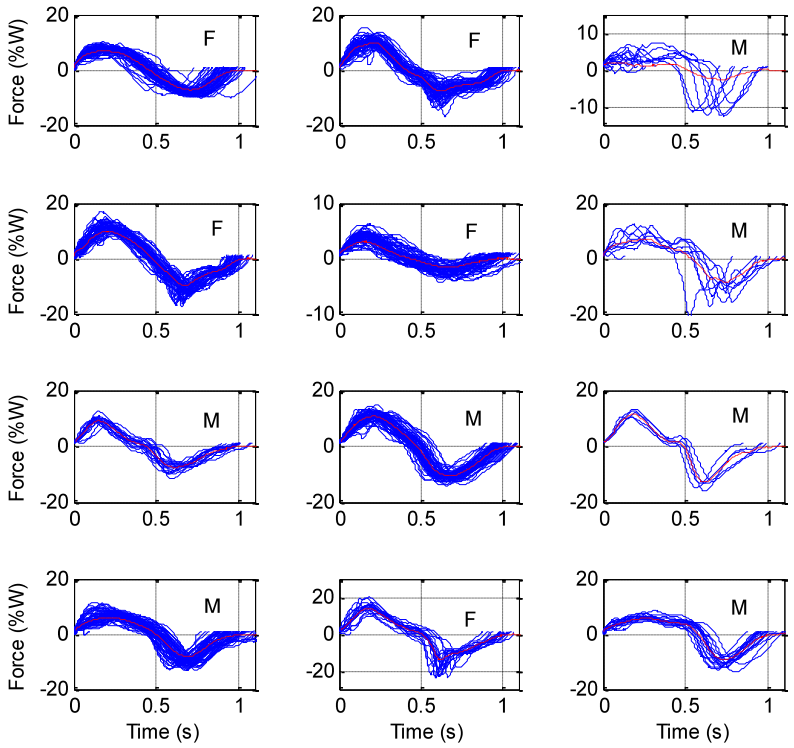

Figure A10: FB Force impulses for 12 subjects swaying front-to-back at 1.0 Hz in a standing position

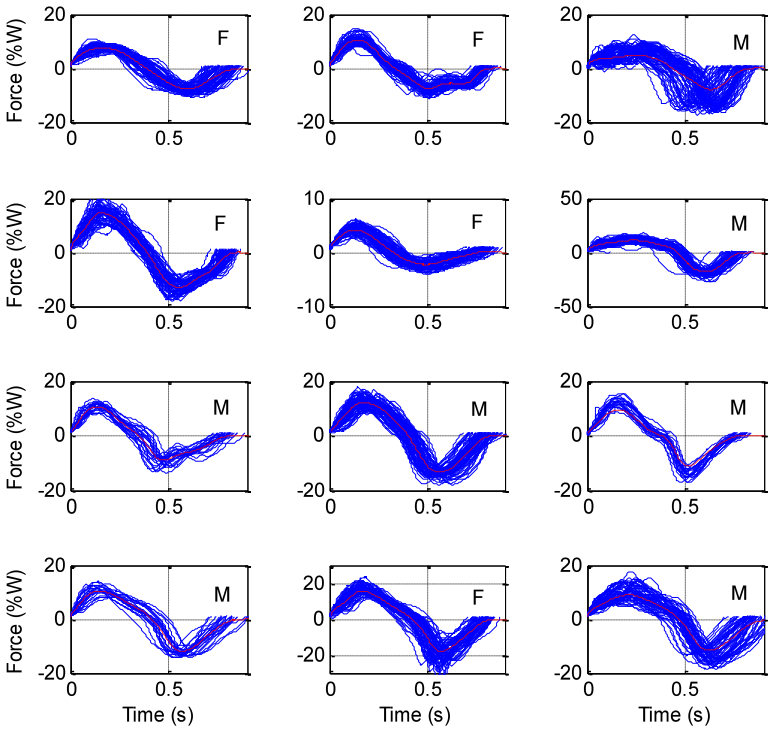

Figure A11: FB Force impulses for 12 subjects swaying front-to-back at 1.25Hz in a standing position

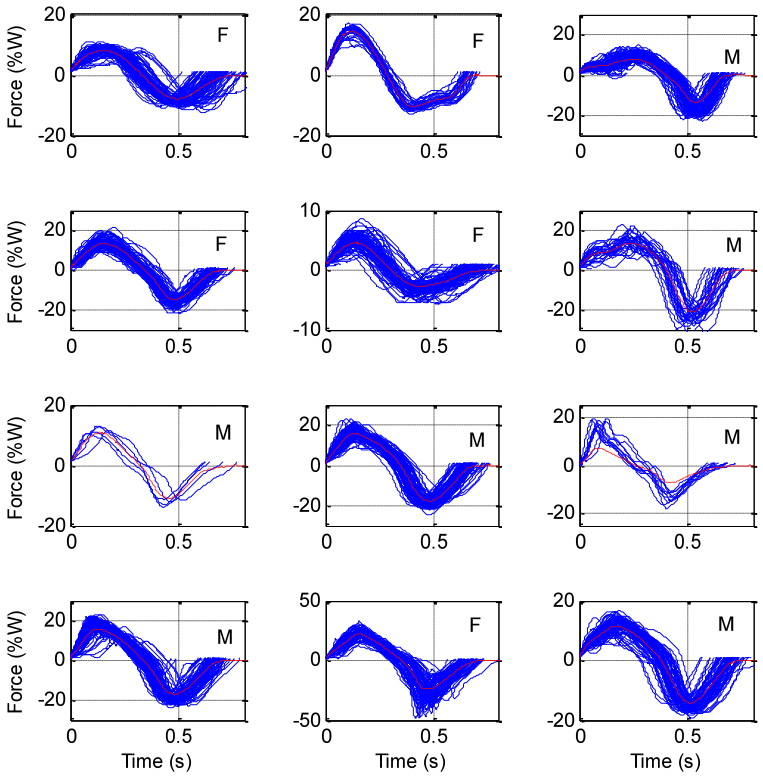

Figure A12: FB Force impulses for 12 subjects swaying front-to-back at 1.5 Hz in a standing position

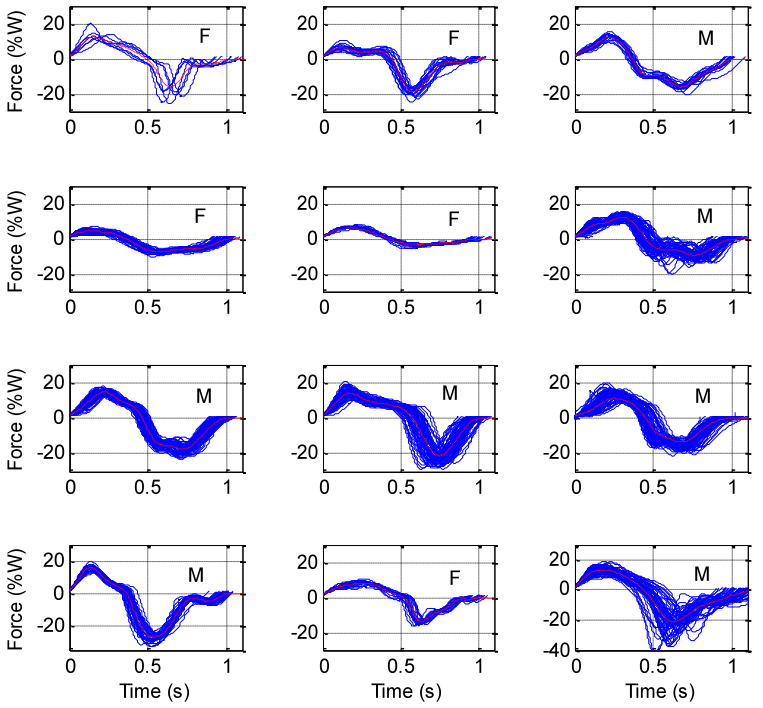

Figure A13: FB Force impulses for 12 subjects swaying front-to-back at 1.0 Hz in a sitting position

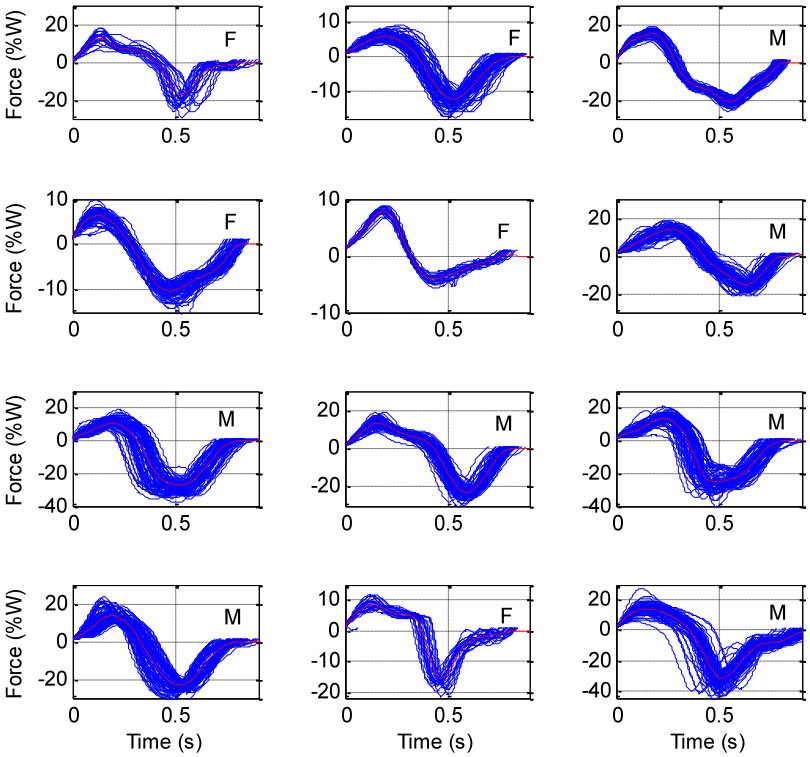

Figure A14: FB Force impulses for 12 subjects swaying front-to-back at 1.25 Hz in a sitting position

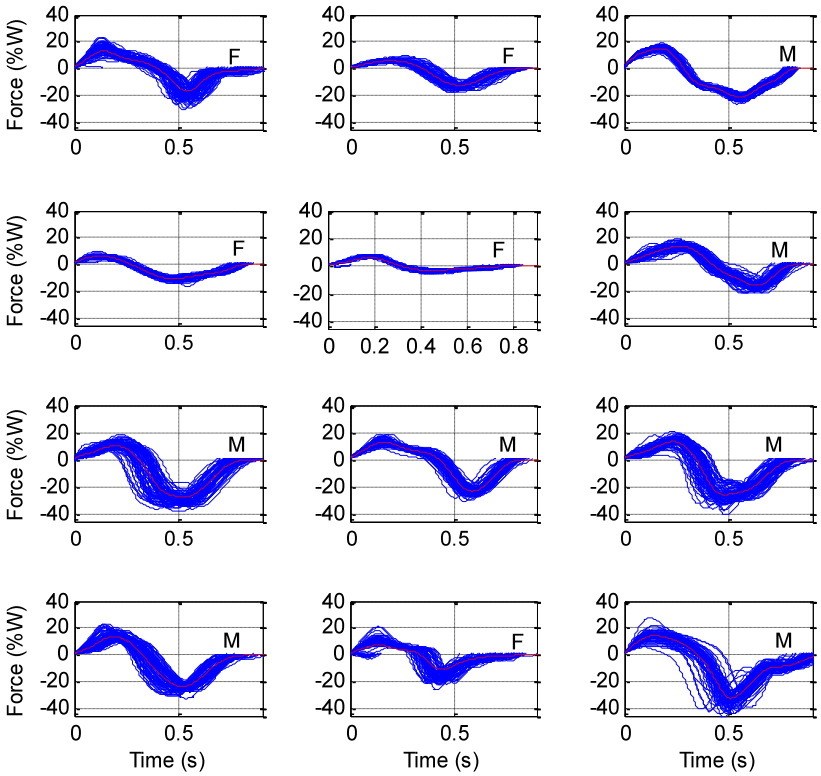

Figure A15: FB Force impulses for 12 subjects swaying front-to-back at 1.5 Hz in a sitting position

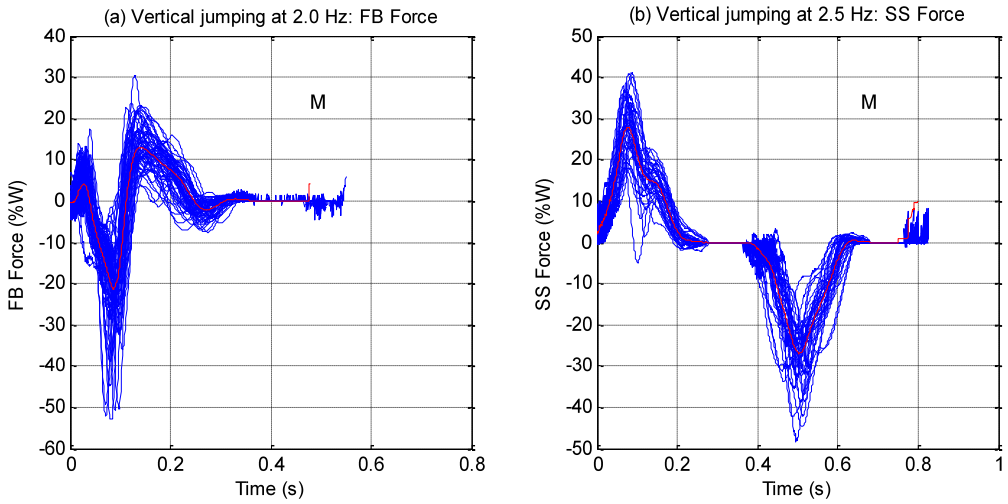

Figure A16: (a) FB and (b) SS Force impulses for a subjects jumping at 2 and 2.5 Hz

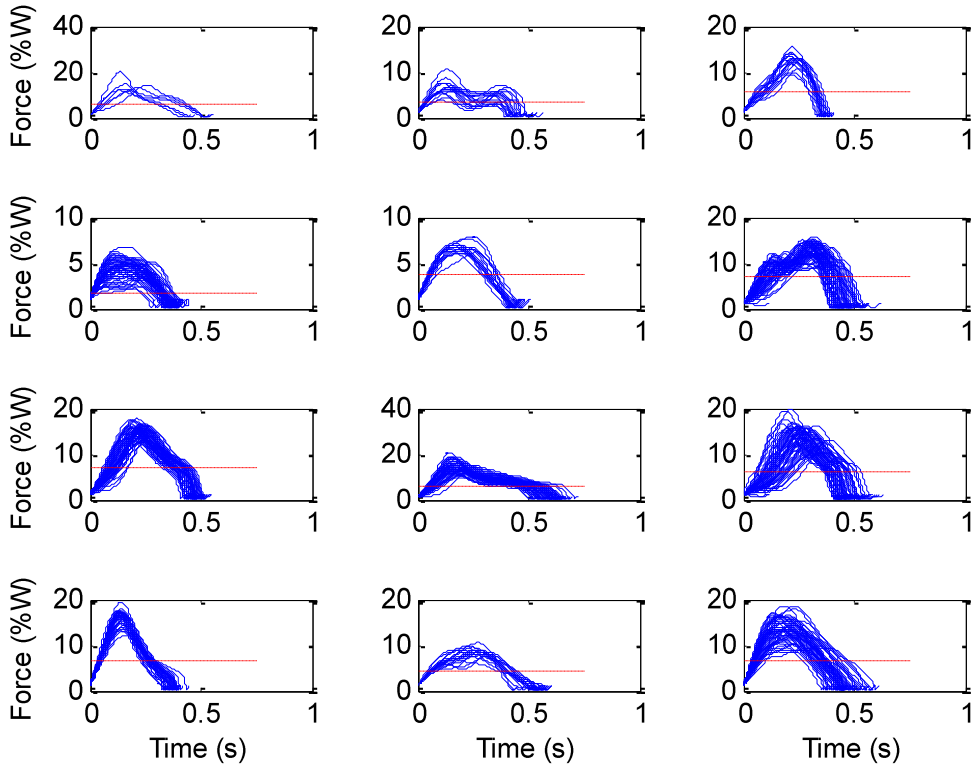

Figure A17: FB sub-pulses showing forward forces due to swaying front-to-back at 1.0 Hz in a sitting position

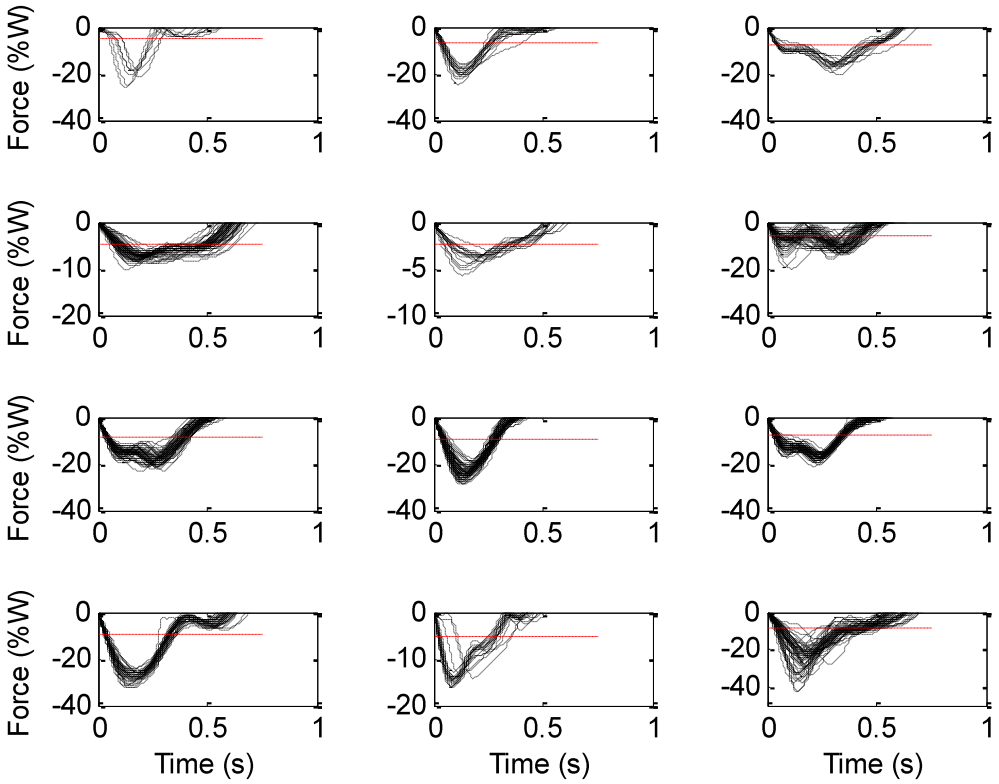

Figure A18: FB sub-pulses showing backward forces due to swaying front-to-back at 1.0 Hz in a sitting position

Figure A19: Bracing patterns tested for the 2-bay demountable grandstand system

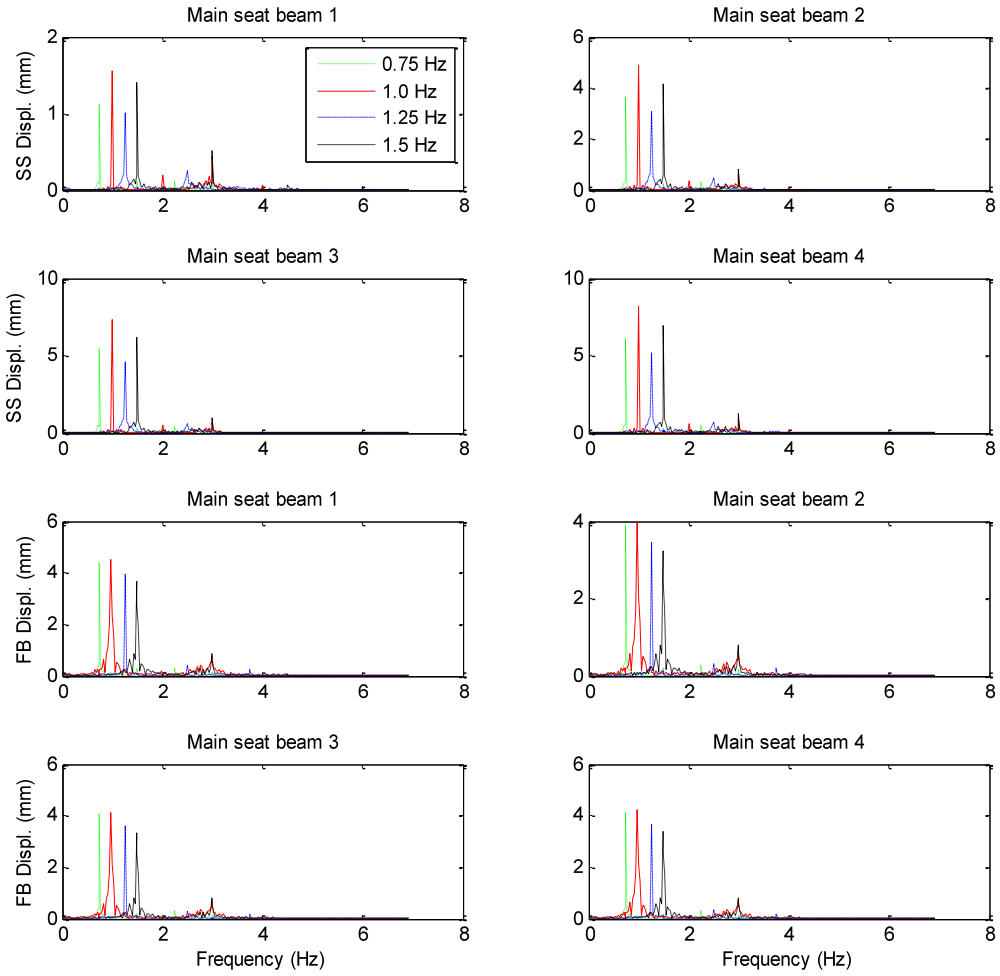

Figure A20: Displacement responses due to crowd swaying loads at 0.75, 1.0, 1.25 and 1.5 Hz

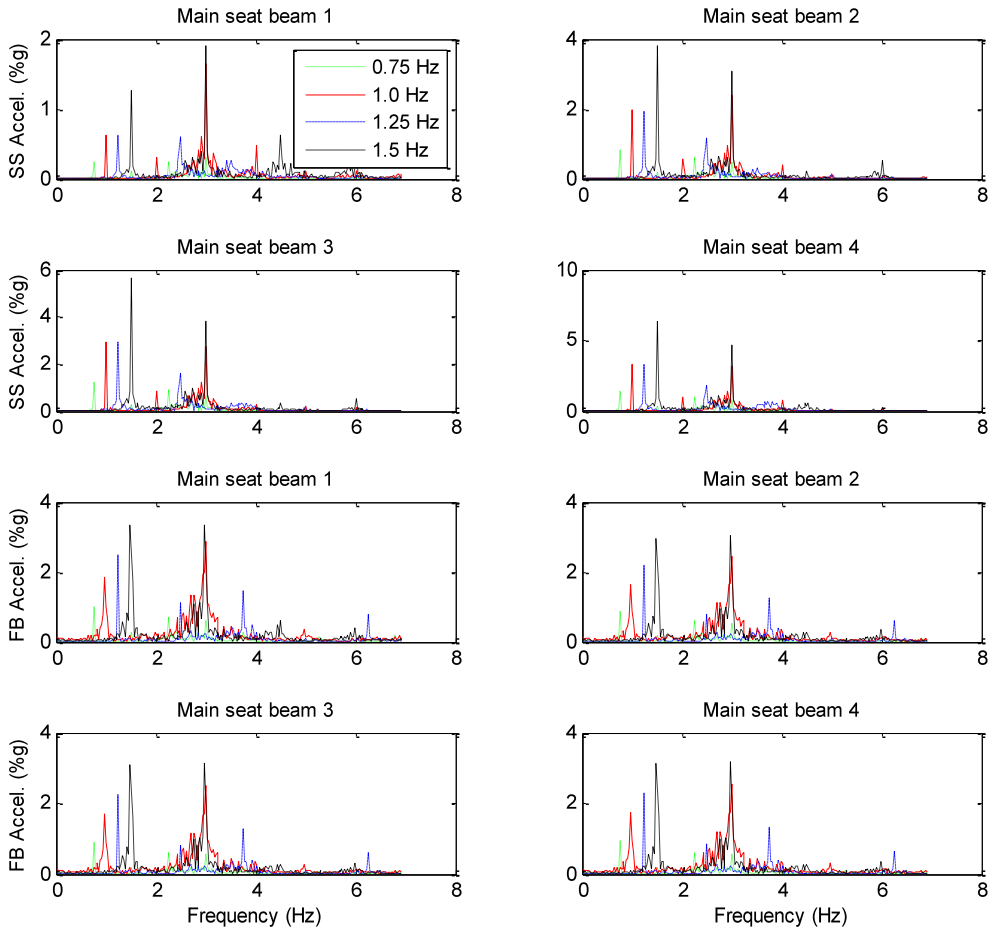

Figure A21: Acceleration responses due to crowd swaying loads at 0.75, 1.0, 1.25 and 1.5 Hz

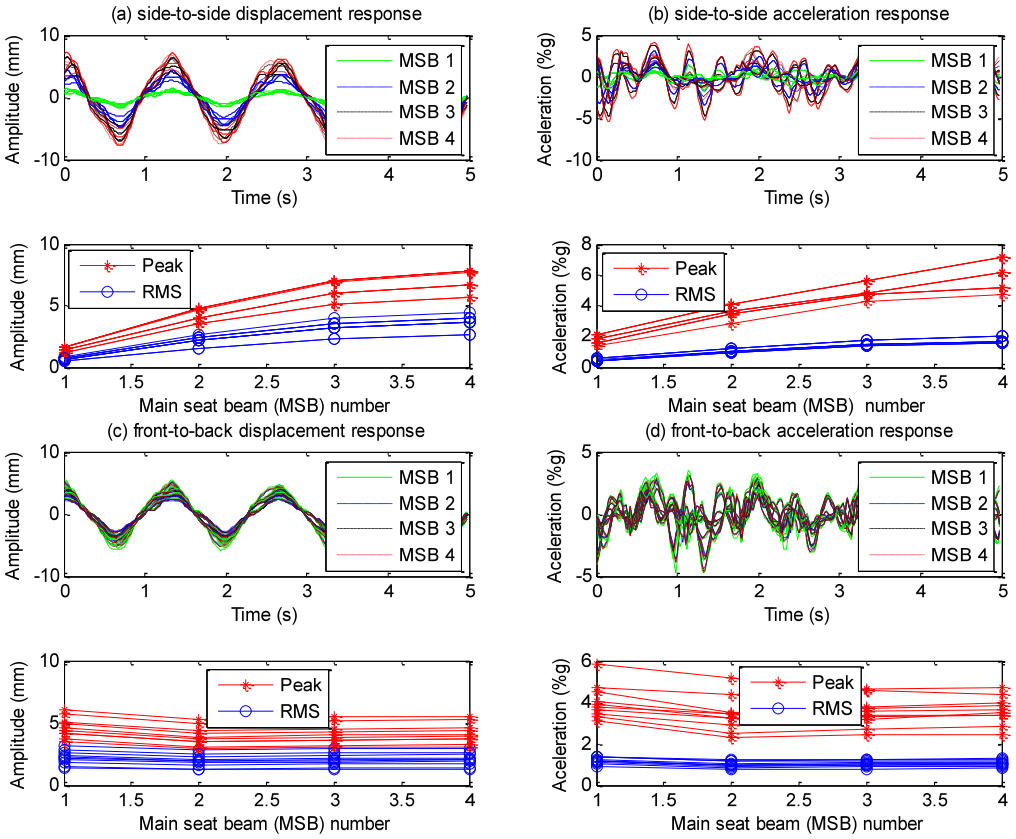

Figure A22: Peak and RMS responses due to crowd swaying loads at 0.75 Hz

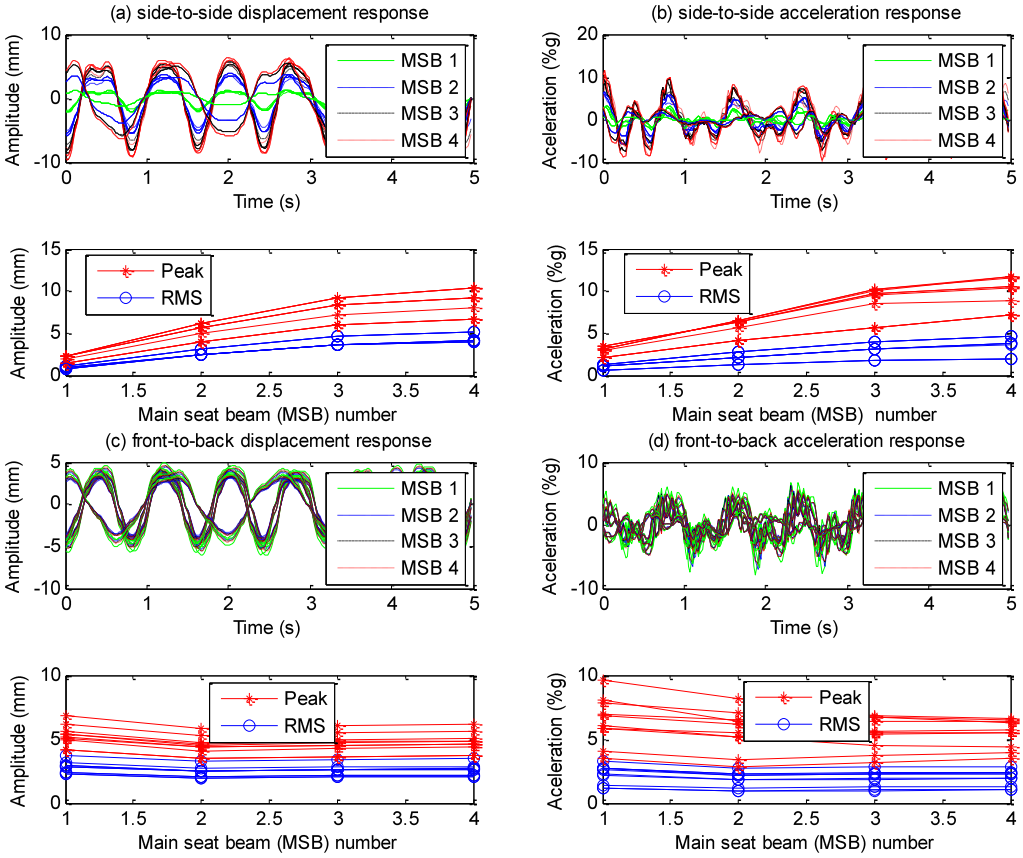

Figure A23: Peak and RMS responses due to crowd swaying loads at 1.25 Hz

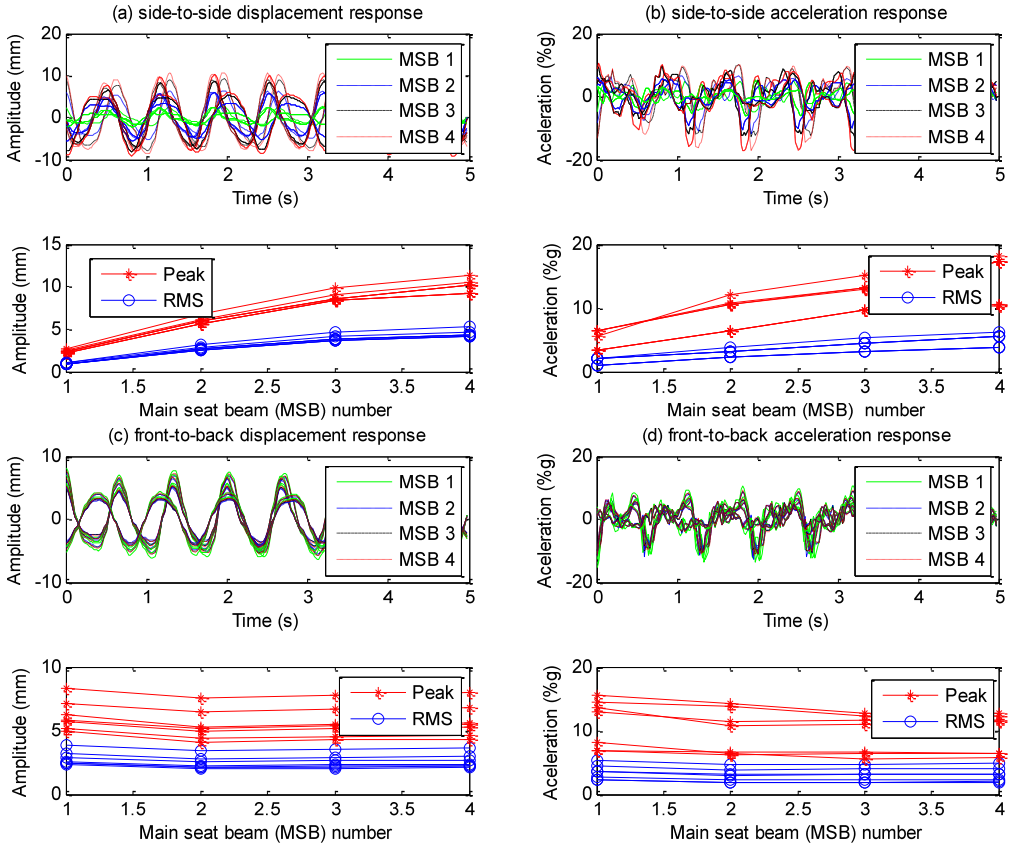

Figure A24: Peak and RMS responses due to crowd swaying loads at 1.5 Hz

APPENDIX B

This appendix contains additional tables.

Table B1: List of tests performed in the Structural dynamics laboratory (force measurements only)

Test session and subject gender	Swaying direction and posture	Metronome rhythms [beeps/min]	Test date
S1-F	SS-standing, SS-Sitting, FB-Standing, FB-Sitting	60, 90,120,150, 180	08-11-10
S2-F	SS-standing, SS-Sitting, FB-Standing, FB-Sitting	60, 90,120,150, 80	08-11-10
S3-M	SS-standing, SS-Sitting, FB-Standing, FB-Sitting	60, 90,120,150, 180, 210	09-11-10
S4-F	SS-standing, SS-Sitting, FB-Standing, FB-Sitting	60, 90,120,150, 180	09-11-10
S5-F	SS-standing, SS-Sitting, FB-Standing, FB-Sitting	60, 90,120,150, 180	10-11-10
S6-M	SS-standing, SS-Sitting, FB-Standing, FB-Sitting	60, 90,120,150, 180, 210	10-11-10
S7-M	SS-standing, SS-Sitting, FB-Standing, FB-Sitting	60, 90,120,150, 180,210	11-11-10
S8-M	SS-standing, SS-Sitting, FB-Standing, FB-Sitting	60,90,120, 150,180, 210	11-11-10
S9-M	SS-standing, SS-Sitting, FB-Standing, FB-Sitting	60, 90,120,150, 180, 210	12-11-10
S10-M	SS-standing, SS-Sitting, FB-Standing, FB-Sitting	60, 90,120,150, 180	12-11-10
S11-F	SS-standing, SS-Sitting, FB-Standing, FB-Sitting	60, 90,120,150, 180	15-11-10
S12-M	SS-standing, SS-Sitting, FB-Standing, FB-Sitting	60, 90,120,150, 180	16-11-10

Table B2: Group tests performed in the gait laboratory (force measurements and motion tracking)

Test session and number of subjects (all males)	Activities	Metronome rhythms [beeps/min]	Test date
T1-3	SS and FB swaying in a standing position, and vertical jumping	60, 90,120,150, 180 (sway) 90,120,150, 180, 210 (jump)	03-12-10
T2-2	SS and FB swaying in a standing position, and vertical jumping	60, 90,120,150, 180 (sway) 90,120,150, 180, 210 (jump)	03-12-10

Table B3: Sub-pulse mean force for swaying side-to-side in a standing position

Beep rhythm [beep/min]	Mean frequency [Hz]	Mean SS force to the Right [%W]	Standard Deviation [%W]	Mean SS force to the Left [%W]	Standard Deviation [%W]
60	0.50	5.98	2.24	5.74	2.16
90	0.75	7.98	2.97	7.69	2.88
120	1.00	8.79	3.06	8.39	3.11
150	1.25	8.68	3.30	8.53	3.42
180	1.49	7.92	3.09	7.90	2.94

Table B4: Sub-pulse mean force for swaying side-to-side in a sitting position

Beep rhythm [beep/min]	Mean frequency [Hz]	Mean SS force to the Right [%W]	Standard Deviation [%W]	Mean SS force to the Left [%W]	Standard Deviation [%W]
60	0.49	3.92	1.38	3.62	1.35
90	0.73	6.38	2.28	6.12	2.38
120	0.98	8.76	3.26	8.45	3.54
150	1.20	10.25	3.62	10.26	4.13
180	1.42	11.84	4.10	11.91	4.58

Table B5: Sub-pulse mean force for swaying front-to-back in a standing position

Beep rhythm [beep/min]	Mean frequency [Hz]	Mean FB force to the Front [%W]	Standard Deviation [%W]	Mean FB force to the Back [%W]	Standard Deviation [%W]
60	0.50	2.33	1.08	2.08	0.95
90	0.76	3.36	1.59	3.40	1.71
120	1.00	4.48	2.03	4.99	2.36
150	1.25	5.84	2.45	6.61	3.22
180	1.50	7.13	3.25	7.82	3.96

Table B6: Sub-pulse mean force for swaying front-to-back in a sitting position

Beep rhythm [beep/min]	Mean frequency [Hz]	Mean FB force to the Front [%W]	Standard Deviation [%W]	Mean FB force to the Back [%W]	Standard Deviation [%W]
60	0.50	3.58	1.74	5.27	2.30
90	0.75	5.27	1.99	6.67	2.31
120	1.00	6.50	2.00	8.52	3.24
150	1.24	7.08	2.10	11.05	4.91
180	1.49	8.37	3.25	12.76	5.18

Table B7: Spectral magnitudes for swaying side-to-side in a standing position

Beep rhythm [beep/min]	Harmonic number	Mean frequency at harmonic [Hz]	Mean magnitude at harmonic [%W]	Standard Deviation [%W]
60	1	0.50	8.31	1.97
	2	0.98	0.57	0.27
	3	1.49	1.78	1.08
90	1	0.75	10.74	2.96
	2	1.49	0.57	0.21
	3	2.25	1.60	0.58
120	1	1.00	13.99	3.66
	2	2.01	0.69	0.45
	3	3.00	1.82	0.86
150	1	1.25	13.39	3.59
	2	2.50	0.58	0.22
	3	3.76	1.38	0.63
180	1	1.49	12.35	4.41
	2	2.95	0.54	0.19
	3	4.49	1.18	0.76

Table B8: Spectral magnitudes for swaying side-to-side in a sitting position

Beep rhythm [beep/min]	Harmonic number	Mean frequency at harmonic [Hz]	Mean magnitude at harmonic [%W]	Standard Deviation [%W]
60	1	0.49	5.04	1.88
	2	0.96	0.36	0.16
	3	1.47	0.79	0.50
90	1	0.73	8.41	3.14
	2	1.44	0.44	0.20
	3	2.20	0.91	0.87
120	1	0.98	10.10	4.89
	2	1.94	0.56	0.22
	3	2.91	1.29	1.10
150	1	1.20	12.38	4.97
	2	2.42	0.69	0.31
	3	3.62	1.11	1.03
180	1	1.42	12.93	5.70
	2	2.90	0.53	0.32
	3	4.32	0.76	0.66

Table B9: Spectral magnitudes for swaying front-to-back in a standing position

Beep rhythm [beep/min]	Harmonic number	Mean frequency at harmonic [Hz]	Mean magnitude at harmonic [%W]	Standard Deviation [%W]
60	1	0.50	2.61	0.83
	2	0.91	0.75	0.54
	3	1.52	0.96	0.46
90	1	0.76	4.77	1.07
	2	1.51	0.75	0.34
	3	2.27	0.87	0.58
120	1	1.00	7.73	1.92
	2	2.01	0.97	0.45
	3	3.01	0.81	0.35
150	1	1.25	8.72	2.82
	2	2.50	1.26	0.80
	3	3.75	0.70	0.29
180	1	1.50	11.63	2.65
	2	2.99	0.99	0.46
	3	4.46	0.77	0.48

Table B10: Spectral magnitudes for swaying front-to-back in a sitting position

Beep rhythm [beep/min]	Harmonic number	Mean frequency at harmonic [Hz]	Mean magnitude at harmonic [%W]	Standard Deviation [%W]
60	1	0.50	5.67	3.00
	2	1.00	1.28	0.92
	3	1.49	1.05	0.59
90	1	0.75	7.90	2.74
	2	1.50	1.53	0.70
	3	2.26	1.18	0.79
120	1	1.00	8.80	2.81
	2	2.00	2.11	1.29
	3	3.00	1.16	0.62
150	1	1.24	11.13	4.68
	2	2.49	2.06	0.90
	3	3.73	0.82	0.48
180	1	1.49	9.60	4.80
	2	2.98	1.55	0.87
	3	4.48	0.56	0.30

Table B11: Harmonic magnitude coefficients: Swaying side-to-side standing

Harmonic	a_1	a_2	a_3	a_4
H_{1M}	6.727	29.562	-30.024	7.285
H_{3M}	2.567	-1.327	0.292	-0.025
H_{1U}	6.614	36.892	-32.988	6.777
H_{1L}	6.840	22.232	-27.061	7.793
H_{3U}	5.092	-3.231	0.813	-0.072
H_{3L}	0.212	0.420	-0.183	0.019

Table B12: Harmonic magnitude coefficients: Swaying side-to-side sitting

Harmonic	a_1	a_2	a_3	a_4
H_{1M}	6.863	11.172	-9.322	1.777
H_{3M}	0.756	-0.276	0.091	-0.013
H_{1U}	3.011	35.382	-31.195	7.860
H_{1L}	10.716	-13.038	12.552	-4.306
H_{3U}	0.619	0.221	-0.047	-0.004
H_{3L}	0.894	-0.772	0.228	-0.022

Table B13: Harmonic magnitude coefficients: Swaying front-to-back standing

Harmonic	a_1	a_2	a_3	a_4
H_{1M}	6.727	29.562	-30.024	7.285
H_{2M}	2.801	-3.537	1.761	-0.286
H_{1U}	6.614	36.892	-32.988	6.777
H_{1L}	6.840	22.232	-27.061	7.793
H_{2U}	6.296	-8.582	4.264	-0.683
H_{2L}	-0.613	1.422	-0.712	0.109

Table B14: Harmonic magnitude coefficients: Swaying front-to-back sitting

Harmonic	a_1	a_2	a_3	a_4
H_{1M}	24.797	-44.504	44.144	-15.088
H_{2M}	2.269	-1.751	0.896	-0.169
H_{1U}	51.53	-112.52	107.44	-34.024
H_{1L}	-1.936	23.506	-19.15	3.848
H_{2U}	4.066	-3.218	1.491	-0.261
H_{2L}	0.473	-0.285	0.301	-0.078

Table B15: Spectral magnitudes for jumping

Frequency of jumping (Hz)	Harmonic number	Mean frequency at harmonic (Hz)	Mean FB magnitude at harmonic (%W)	Standard deviation (%W)
1.5	1	1.558	1.858	0.519
	2	3.109	3.665	2.121
	3	4.825	2.512	1.104
	4	6.159	2.653	0.527
2.0	1	2.000	4.383	1.460
	2	3.984	5.214	2.058
	3	5.992	4.969	1.489
	4	8.026	4.637	1.155
2.5	1	2.459	2.093	0.767
	2	4.917	3.075	1.619
	3	7.417	3.217	2.063
	4	9.934	2.869	1.283
3.0	1	3.109	1.185	0.793
	2	5.988	1.367	0.851
	3	9.117	1.456	0.930
	4	12.134	1.289	0.699
3.5	1	3.384	1.446	0.842
	2	6.717	2.201	1.800
	3	10.417	1.936	1.602
	4	13.676	1.401	0.916
Frequency of jumping (Hz)	Harmonic number	Mean frequency at harmonic (Hz)	Mean SS magnitude at harmonic (%W)	Standard deviation (%W)
2.5	1	1.254	9.9	-
	3	5.016	6.5	-

Table B16: Values for parameters *d* and H_p evaluated for swaying side-to-side in a sitting position

Frequency (Hz)	Mean *d*	Minimum *d*
0.5	0.293	0.237
0.75	0.305	0.246
1.0	0.300	0.231
1.25	0.310	0.246
1.5	0.318	0.247
Frequency (Hz)	Mean H_p (%W)	Maximum H_p (%W)
0.5	13.396	22.307
0.75	20.929	35.200
1.0	29.222	52.043
1.25	33.108	56.392
1.5	37.302	64.611

Table B17: Values for parameters *d*, H_{pF} and H_{pB} for swaying front-to-back: standing position

Frequency (Hz)	Maximum *d*	Mean *d*	Minimum *d*
0.5	0.514	0.408	0.349
0.75	0.527	0.449	0.399
1.0	0.552	0.460	0.403
1.25	0.585	0.454	0.385
1.5	0.559	0.473	0.418
Frequency (Hz)	Minimum H_{pF} (%W)	Mean H_{pF} (%W)	Maximum H_{pF} (%W)
0.5	2.416	5.705	9.778
0.75	3.361	7.479	12.413
1.0	4.437	9.746	16.158
1.25	5.794	12.869	21.536
1.5	6.941	15.077	24.830
Frequency (Hz)	Minimum H_{pB} (%W)	Mean H_{pB} (%W)	Maximum H_{pB} (%W)
0.5	2.199	5.112	8.712
0.75	3.194	7.558	12.812
1.0	4.769	10.853	18.229
1.25	5.795	14.565	25.531
1.5	6.907	16.542	28.191

Table B18: Values for parameters *d*, H_{pF} and H_{pB} for swaying front-to-back: sitting position

Frequency (Hz)	Maximum *d*	Mean *d*	Minimum *d*
0.5	0.724	0.427	0.335
0.75	0.575	0.575	0.368
1.0	0.538	0.423	0.361
1.25	0.633	0.441	0.360
1.5	0.737	0.448	0.355
Frequency (Hz)	Minimum H_{pF} (%W)	Mean H_{pF} (%W)	Maximum H_{pF} (%W)
0.5	2.541	8.368	15.840
0.75	5.696	9.161	19.719
1.0	8.374	15.356	23.536
1.25	7.861	16.070	25.533
1.5	6.948	18.668	32.773
Frequency (Hz)	Minimum H_{pB} (%W)	Mean H_{pB} (%W)	Maximum H_{pB} (%W)
0.5	4.104	12.325	22.553
0.75	7.584	11.596	24.378
1.0	9.821	20.135	32.587
1.25	9.691	25.063	44.346
1.5	10.281	28.446	50.573

Table B19: Values for parameter *d*, H_{pF}, H_{pB} and H_p evaluated for jumping

Frequency of jumping (Hz)	*d*	Range of H_{pF} values (%W)	Range of H_{pB} values (%W)
2.0	0.12	40.83-74.26	47.23-81.22
Frequency of jumping (Hz)	d	Range of H_p values (%W)	
2.5	0.17	28.95-57.74	

Table B20: Residuals for aligning impulses using different methods

Method	Type I pulse RMSE	Type II pulse RMSE	Mean RMSE
Method 1	0.863	1.268	1.065
Method 2	0.537	1.40	0.969
Method 3	0.836	1.195	1.016

Table B21: List of grandstand dynamic tests

Test series name	Excitation level (Number of rotating masses)	Brace pattern	Shaker and accelerometer arrangement	Imposed load per seating area (Kg)	Test date
A	2	1	Front-to-back	Empty	27-08-09
B	1	1	Side-to-side	Empty	27-08-09
C	2	1	Side-to-side	Empty	27-08-09
D	1	2	Front-to-back	Empty	27-08-09
E	1	2	Side-to-side	Empty	27-08-09
F	1	3	Side-to-side	Empty	02-09-09
G	2	3	Side-to-side	Empty	02-09-09
H	1	4	Side-to-side	Empty	02-09-09
J	1	5	Side-to-side	Empty	02-09-09
K	1	6	Side-to-side	Empty	02-09-09
L	1	7	Side-to-side	Empty	10-09-09
M	1	8	Front-to-back	Empty	10-09-09
N	1	9	Front-to-back	Empty	10-09-09
P	1	10	Front-to-back	Empty	10-09-09
Q	1	11	Front-to-back	Empty	10-09-09
R	1	12	Side-to-side	25 kg	15-09-09
S	1	12	Side-to-side	50 kg	15-09-09
T	1	12	Front-to-back	50 kg	15-09-09
U	1	13	Front-to-back	50 kg	15-09-09
V	1	13	Front-to-back	50 kg	15-09-09
W	1	14	Front-to-back	50 kg	15-09-09
X	1	15	Front-to-back	50 kg	15-09-09
Y	1	14	Front-to-back	25 kg	15-09-09
Z	1	14	Front-to-back	Empty	15-09-09